An investigation into the cytotoxic properties of isatin-derived compounds: potential for use in targeted cancer therapy

Kara Lea Vine
University of Wollongong

An Investigation into the Cytotoxic Properties of Isatin-Derived Compounds: Potential for use in Targeted Cancer Therapy

A thesis submitted in fulfillment of the requirements for the award of the degree

DOCTOR OF PHILOSOPHY

From

School of Biological Sciences

UNIVERSITY OF WOLLONGONG

By

Kara Lea Vine, B.Biotech (Hons)

2007

Declaration

The work described in this thesis does not contain any material that has been submitted for the award of any higher degree in this or any other University and to the best of my knowledge contains no material previously published or written by any other person, except where due reference is made in the text of this thesis.

Kara Lea Vine

14th September 2007

Acknowledgements

My sincere thanks to my supervisory 'committee' A. Prof. Marie Ranson, Prof. John Bremner, Dr. Kirsten Benkendorff and Prof. Stephen Pyne for your continued support and encouragement. You have all helped me on my PhD journey in so many ways, both on an academic and personal level and for this I am truly grateful. For helping me build fences and having a laugh along the way, I would also like to thank Dr. Julie Locke, for which without her synthetic skills, this thesis would not have been possible. Thank you also to Dr. Christopher Burns (Cytopia, Vic) and Dr. Laurent Meijer (CNS, France) for the compound screening and Dr. Renate Griffith (Newcastle University, NSW) for assistance with related work. A big thank you also to Dr. Larry Hick, Sister Sheena McGhee and Prof. Alistair Lochhead for running mass spectrometry samples, taking blood and help with histopathological analysis of tissue sections (in that order). Thank you to the University of Wollongong for financial support through a University Cancer Research grant and University Postgraduate Award (UPA).

For continued support in the lab and the start of new friendships I would also like to thank the Ranson (including Dave) and Bremner research groups (special thanks to Joey for running my MS samples). To Tamantha, Tracey and Laurel, thank you for all of your advice and help during the animal studies. To the 'Lay-dees' (Christine, Elise, Jill, Martina, Amanda, Carola, Anna) and Justin for your continued friendship, support and laughter, I couldn't have done it without you!

Thank you to my wonderful family for your patience, support and love. And last but not least, thank you to my loving and inspirational husband Shane, for your endless encouragement and belief in me. I made it here because of you!

Abstract

The increased incidence of multidrug resistance (MDR) and systemic toxicity to conventional chemotherapeutic agents suggests that alternative avenues need to be explored in the hope of finding new and effective treatments for metastatic disease. Considering natural products have made enormous contributions to many of the anticancer agents used clinically today, the cytotoxic molluscan metabolite tyrindoleninone (**1**) and its oxidative artifact, 6-bromoisatin (**5**), were initially used as templates for drug design in this study. Structural modifications to the isatin scaffold afforded a total of 51 isatin-based analogues, 21 of which were new. Cytotoxicity screening of the compounds against a panel of heamatological and epithelial-derived cancer cell lines *in vitro*, found the di- and tri-bromoisatins to be the most potent, with activity observed in the low micromolar range. Interestingly compound activity was enhanced by up to a factor of 22 after *N*-alkyl and *N*-arylalkylation, highlighting the importance of N1 substitution for cytotoxic activity. 5,7-Dibromo-*N*-(*p*-methylbenzyl)-isatin (**39**) was the most active compound overall and exhibited an IC_{50} value of 490 nM against U937 and Jurkat leukemic cell lines, after 24 h. 5,7-Dibromo-*N*-(*p*-trifluoro-methylbenzyl)isatin (**54**) was also of interest, considering the potent cell killing ability displayed against a metastatic breast adenocarcinoma (MDA-MB-231) cell line. Investigation into the molecular mode of action of the *N*-alkylisatin series of compounds found the *p*-trifluoromethylbenzyl derivative (**54**), together with 9 other representative molecules to destabilise microtubules and induce morphological cell shape changes *via* inhibition of tubulin polymerisation. This resulted in cell cycle arrest at G2/M and activation of the effector caspases 3 and 7, ultimately resulting in apoptotic

cell death.

Further investigations into the pharmacological profile of compound **54** *in vivo*, found it to be moderately efficacious (43% reduction in tumour size compared to vehicle control treated mice) in a human breast carcinoma xenograft mouse model. Although histopathological analysis of the bone marrow *in situ* after acute dosing found only mild haematopoietic suppression, analysis of biodistribution *via* SPECT imaging found large amounts of activity also in the gut and liver.

In an effort to reduce non-target organ up-take and thus increase accumulation of drug in the tumour, the *N*-benzylisatin **54** was derivatised so as to contain an acid labile imine linker and was conjugated to the targeting protein PAI-2 (a naturally occurring inhibitor of the urokinase plasminogen activation system) *via* amide bond formation with free lysine residues. The conjugate was found to contain an average of 4 molecules of **54** per protein molecule without affecting PAI-2 activity. Hydrolytic stability of the PAI-2-cytotoxin conjugate at pH 5-7 as determined by UV/Vis spectrophotometry, was directly correlated with the lack of activity observed *in vitro*, suggesting a need to investigate cleavable linker systems with enhanced lability in the future. Despite this, PAI-2 conjugated to the cytotoxin 5-FUdr through a succinate linker system, showed enhanced and selective uPA-mediated cytotoxicity, in two different breast cancer cell lines which varied in their expression levels of uPA and its receptor. This suggests that PAI-2-cytotoxin based therapies hold potential, in the future, as new therapeutic agents for targeted therapy of uPA positive malignancies, with limited side effects.

Abbreviations

ATP	adenosine triphosphate
CDK	cyclin-dependant kinase
d	doublet
DCC	dicyclohexylcarbodiimide
dd	doublet of doublets
ddd	doublet of doublets of doublets
DMF	*N*,*N*-dimethylformamide
DMSO	dimethyl sulfoxide
DNA	deoxyribose nucleic acid
dt	doublet of triplets
EDTA	ethylenediaminetriacetic acid
EI	electron impact
ESI	electrospray ionisation
EtOH	ethanol
FCS	foetal calf serum
HPLC	high performance liquid chromatography
HR	high resolution
HRMS	high resolution mass spectrometry
Hz	Hertz
i.v.	intravenous
J	coupling constant
LDP	ligand-directed prodrug
Lit.	literature
LR	low resolution
m	multiplet
m.p.	melting point
m/z	mass to charge ratio
MDR	multi-drug resistance

MeOH	methanol
MS	mass spectrometry
MTD	maximum tolerated dose
MTS	3-(4,5-dimethylthiazol-2-yl)-5-(3-carboymethoxyphenyl)-2-(4-sulfophenyl)-2*H*-tetrazolium, inner salt
NHS	*N*-hydroxysuccinamide
NMR	nuclear magnetic resonance
OD	optical density
p.i.	post injection
PAI-2	plasminogen activator inhibitor type 2
PBS	phosphate buffered saline
PI	propidium iodide
ppm	parts per million
R_f	retention factor
RME	receptor mediated endocytosis
RPMI-1640	Roswell Park Memorial Institute
RT	room temperature
s	singlet
SAR	structure activity relationship
SD	standard deviation
SDS-PAGE	sodium dodecyl sulfate polyacrylamide gel electrophoresis
SEM	standard error of the mean
td	triplet of doublets
THF	tetrahydrofuran
TLC	thin layer chromatography
uPA	urokinase-type plasminogen activator
UV/Vis	ultraviolet/visible spectrum
δ	chemical shift in ppm downfield form TMS

Units Used

mol	mole (6.022×10^{23} particles)
MW	molecular weight: mass of 1 mole (g/ mole)
Da	Dalton: unit of molecular weight (g/mol)
g	gram
k	kilo (10^{3})
m	milli (10^{-3})
µ	micro (10^{-6})
n	nano (10^{-9})
L	Litre
M	Molar: concentration mole/L
v/v	concentration expressed as volume ratio
m	metre
h	hour
min	minutes
sec	seconds
°C	degrees Celsius
K	Kelvin
rpm	revolutions per minute
$\times g$	gravity force of rotation

Table of Contents

List of Tables

List of Figures

List of Schemes

List of Thesis Publications and Conference Abstracts

1) Vine, K. L., Locke, J. M., Ranson, M., Benkendorff, K., Pyne, S. G. and Bremner, J. B. (2007) *In vitro* Cytotoxicity Evaluation of Some Substituted Isatin Derivatives. *Bioorg. Med. Chem.*, **15**, *2*, 931-8.

2) Vine, K. L., Locke, J. M., Ranson, M., Pyne, S. G. and Bremner, J. B. (2007) An Investigation into the Cytotoxicity and Mode of Action of Some Novel *N*-alkyl Substituted Isatins *J. Med. Chem.*, **50**, *21*, 5109-77.

3) Julie M. Locke, Kara L. Vine, Marie Ranson, Stephen G. Pyne, and John B. Bremner. The Serendipitous Synthesis of 6-Hydroxyisatins. The 21st International Congress for Heterocyclic Chemistry, Sydney, NSW, AUSTRALIA, July 15-20th 2007.

4) Lidia Matesic, John B. Bremner, Stephen G. Pyne, Julie M. Locke, Marie Ranson and Kara L. Vine. Isatin Derivatives as Novel Anti-Cancer Agents. The 21st International Congress for Heterocyclic Chemistry, Sydney, NSW, AUSTRALIA, July 15-20th 2007

5) Kara L. Vine, Julie M. Locke, John B. Bremner, Stephen G. Pyne and Marie Ranson. *N*-alkylisatins: Potent Anti-Cancer Agents. RACI Drug Design Amongst the Vines, Hunter Valley, NSW, AUSTRALIA, Dec 3-7th 2006.

6) Kara L. Vine, Julie M. Locke, John B. Bremner, Stephen G. Pyne and Marie Ranson. Substituted Isatins as Small Molecule Anti-Cancer Agents. Inaugural HMRI Cancer Conference, New Therapeutics, Newcastle, NSW, AUSTRALIA, Sept 20-22nd 2006.

7) Kara L. Vine, Julie M. Locke, John B. Bremner, Stephen G. Pyne and Marie Ranson. Substituted Isatins as Small Molecule Anti-Cancer Agents RACI Natural

Products Group Symposium, University of Wollongong, NSW, AUSTRALIA, Sept 29th, 2006.

8) Kara L. Vine, Marie Ranson and Kirsten Benkendorff. Cytotoxic Activity of Indole Derivatives from the Egg Masses of Marine Muricid Molluscs. Indirubin the Red Shade of Indigo, Les Eyzies-de-Tayac, FRANCE, April 8-13th 2006.

9) Kara L. Vine, John B. Bremner, Stephen G. Pyne, Kirsten Benkendorff and Marie Ranson. A Cytotoxic Marine Natural Product as a Novel Anti-Tumour Agent and Potential for use in Targeted Cancer Therapy. Inaugural HMRI Cancer Conference, New Therapeutics, Newcastle, NSW, AUSTRALIA, Oct 4-6th 2004

10) Kara L. Vine, Marie Ranson and Kirsten Benkendorff. Cures from the Deep: The Cytotoxicity of Indole Derivatives from the Egg Masses of the Marine Mollusc *Dicathais Orbita*. Australian Health Management Group Medical Research Week Symposium, Wollongong, NSW, AUSTRALIA, 4th June, 2004.

CHAPTER 1

Drug Design and Development: Advances in the Area of Targeted Cancer Therapy

CHAPTER 1

Drug Design and Development: Advances in the Area of Targeted Cancer Therapy

1.1 General Introduction

Cancer is a disease related to abnormal cell proliferation and metastases and is one of the major causes of death in the developed nations. In Australia, cancer accounts for 31% of male and 26% of female mortalities and since 1991, over 65,000 new cases of cancer were diagnosed (AIHW, 2004). Although most tumours are treated with cytotoxic chemotherapies that were discovered over 20 years ago, only a small subset of cancers including Hodgkin's lymphoma, testicular cancer, acute lymphoid leukemia and non-Hodgkin's lymphoma are routinely cured using these agents (Abeloff *et al*., 2000). This is because the majority of cancer chemotherapeutics in clinical use owe what little selectivity they have to the higher proliferation rates of cancer cells, which often leads to increased toxicities against normal tissues that also show enhanced proliferation rates, such as the bone marrow, gastrointestinal (GI) tract and hair follicles (Kaelin, 2005). Side effects that occur as a result of toxicity to normal tissues mean that anticancer chemotherapeutics are often administered at sub-optimal doses, which eventually leads to the failure of therapy (DeVita, 1997; Foote, 1998). Therapeutic failure is also enhanced by the emergence of multi-drug resistance (MDR) (Nooter and Stoter, 1996; Ling, 1997; Gottesman *et al.*, 2002) and thus highlights the need for the development of new and effective antineoplastic agents with minimal side effects. Efforts to improve cancer treatment have involved reassessing structures from natural

product resources in an attempt to generate novel compound leads with enhanced and selective anticancer activity (Grabley and Thiericke, 1999; Demain and Zhang, 2005). More recently, identification of rational biochemical targets has allowed the design of anticancer agents ranging from small molecule inhibitors to larger antibody/ ligand-directed prodrugs that appropriately affect these targets (Allen, 2002; Szekeres and Novotny, 2002; Imai and Takaoka, 2006). These agents have shown much therapeutic potential in the treatment of a variety of malignancies, with a number of targeted therapies recently being approved by the US Food and Drug Administration (FDA). Despite this, the development of small molecule inhibitors and ligand-based targeted therapies, both synthetic and from natural product resources, still requires further optimisation, as very few drugs that enter preclinical trials are ever approved for clinical use (Rothenberg *et al.*, 2003).

This chapter will provide an overview of the current developments in the area of anticancer drug design, with a focus on the development of marine natural products, small molecule inhibitors and ligand-based drug delivery of relevance to this study. The project rationale and objectives are also discussed.

1.2 The Molecular Biology of Cancer: a Disease of Deregulated Proliferation and Cell Death

Cancer describes a range of diseases in which abnormal cells proliferate and spread out of control (Bertram, 2000). Under normal circumstances, cells grow and multiply in an

orderly fashion to form organs and tissues that have a specific function. Occasionally, however, cells multiply in an uncontrolled manner after being affected by a carcinogen, or after developing from a random genetic mutation, and form a mass known as a tumour or neoplasm that has no physiological function. Although tumours can be benign or malignant, benign tumours do not invade other tissues or spread to other parts of the body. Malignant tumours however, have the ability to grow in an uncontrolled way and can invade and spread to other parts of the body, a process referred to as metastasis (Rang, 1999; Figure 1.1). Invasion occurs when cancer cells push between and break through other surrounding cell and tissue barriers and subsequently degrade

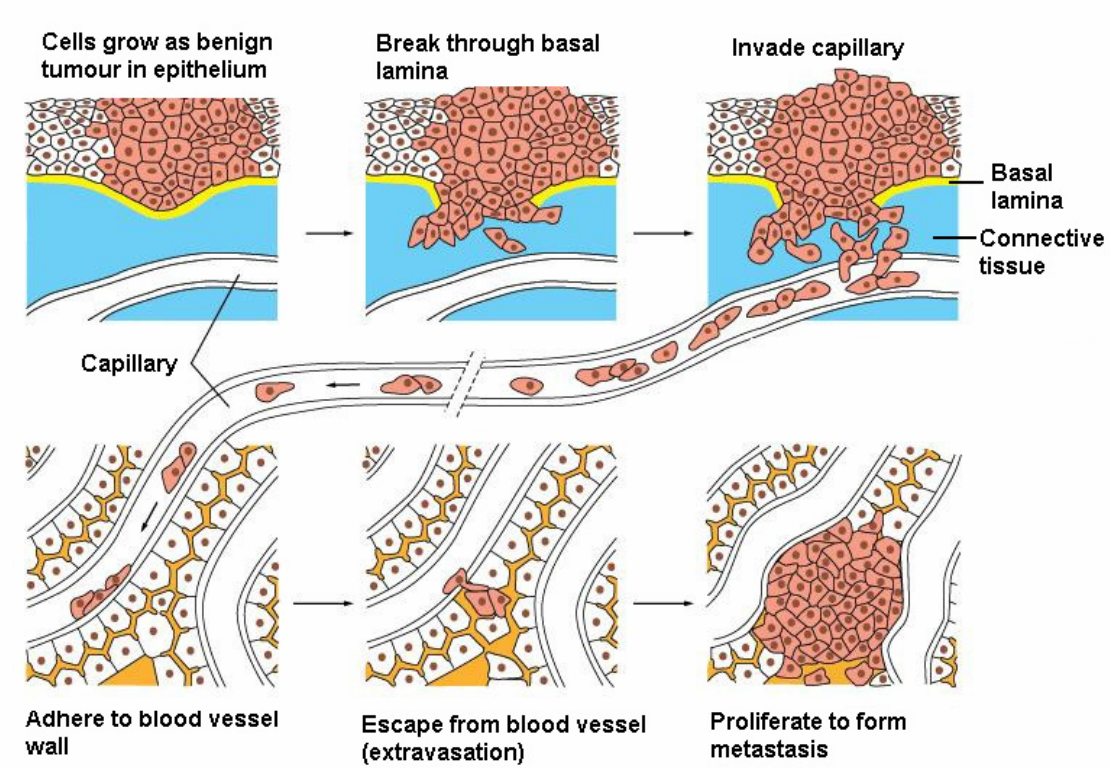

Figure 1.1 A schematic representation of the development of a benign tumour into a metastatic malignant tumour through degradation of the extracellular matrix (ECM). Adapted from Alberts, *et al*. 2002.

the components of the extracellular matrix (ECM) including the basal lamina (Alberts, *et al*. 2002). After gaining access to the blood and lymphatic vessels, cancer cells are then carried to distant sites around the body whereby they have the ability to start a new tumour or secondary cancer and begin invading again. Although tumours are diverse and heterogeneous in nature, they all share the ability to proliferate beyond the constraints that limit the growth of normal tissue (Bertram, 2000). Changes in the regulation of a number of key pathways that control cell proliferation (i.e. the cell cycle) and cell survival (i.e. apoptosis) are responsible for the establishment of all tumours (Evan and Vousden, 2001). These include oncogenic transformations and the loss of tumour suppressor gene function as well as alterations in signal transduction pathways that often lead to increased proliferation in response to external/ mitogenic signals. As such, tumour-associated mutations in many of these pathways result in the alteration of the basic regulatory mechanisms that control the mammalian cell cycle.

1.2.1 The Cell Cycle

The cell cycle contains four major, sequential phases (Figure 1.2) which consist of: 1) the gap phase (G1), where the cell prepares for DNA replication, 2) the synthesis (S) and replication stage, where the cell generates an exact copy of its DNA, 3) a second gap phase (G2), where the cell prepares for the division process and 4) the mitosis phase (M), where the cell divides into two daughter cells (de Carcer *et al.*, 2007). Unless stimulated by mitogens (i.e. growth factors/ chemical signals), most cells in the body are not actively replicating and therefore remain out of the cell cycle in a state of

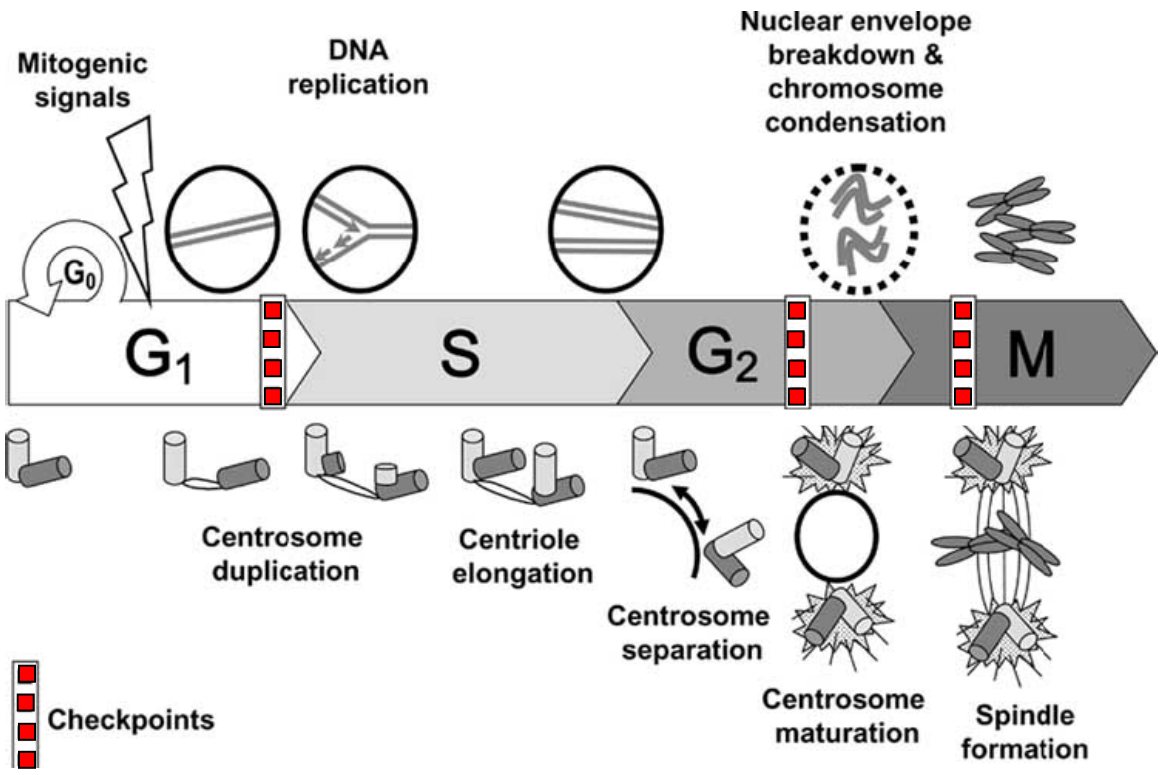

Figure 1.2 Phases of the mammalian cell cycle and associated checkpoints. DNA replication and chromosome segregation are tightly coupled to the centrosome duplication cycle. The major cell cycle checkpoints, the DNA damage checkpoint (acting in G1 and G2) and the spindle assembly checkpoint (during M phase) are indicated in red. Adapted from de Cárcer *et al*., 2007.

quiescence (G0 phase). When they are cycling, certain checkpoints prevent normal cells from entering into a new phase until they have successfully completed the previous one (Hartwell and Weinert, 1989). Major checkpoints include the G1 checkpoint, the DNA damage checkpoints (G2/M) as well as a mitotic spindle checkpoint which occurs during M phase (McDonald and El-Deiry, 2000, Figure 1.2). In non-cancerous cells, each phase of the cell cycle is governed by a large and diverse array of protein families, whereby progress through the cell cycle depends on a fine balance between various

positive and negative regulatory protein signals (Karp and Broder, 1995). Positive regulatory forces involve growth factors, as well as a series of cyclins and cyclin dependent kinases (CDKs). CDKs are activated by phosphorylation and binding of specific cyclin activators. Cyclins are proteins whose levels fluctuate in the different phases of the cell cycle and when the levels increase, form stable complexes with CDKs allowing their activation through conformational change (Malumbres and Barbacid, 2001). When cyclin protein levels decrease upon degradation, CDKs lose their activity and are unable to phosphorylate their targets until the next turn of the cell cycle is initiated. Various cyclins (A, B, D and E) activate distinct CDK subtypes that function at different stages of the cell cycle (Figure 1.3). For example activation of CDK2 by cyclin E is associated with progression from G1 into S (Sherr and Roberts, 1999), while cyclin A mediates CDK1-stimulated G2/M transition (Norbury and Nurse, 1992; Bartek *et al.*, 2001). In particular the D-type cyclins are important integrators of mitogenic signaling as their synthesis is one of the main end points of the RAS/RAF/MAPK pathway (Malumbres and Pellicer, 1998), a signal-transduction pathway that is crucial in cell cycle progression, mediated by a variety of growth factors.

Concomitantly, the action of various CDKs is modulated by a series of negative regulatory forces, which bind to CDKs and inhibit their action (Figure 1.3). These proteins, termed cyclin dependent kinase inhibitors (CKIs), are encoded by various genes such as the p53 gene and the retinoblastoma (Rb) gene which constitute two superbreaks in the cell cycle (Malumbres and Barbacid, 2001). The Rb gene is

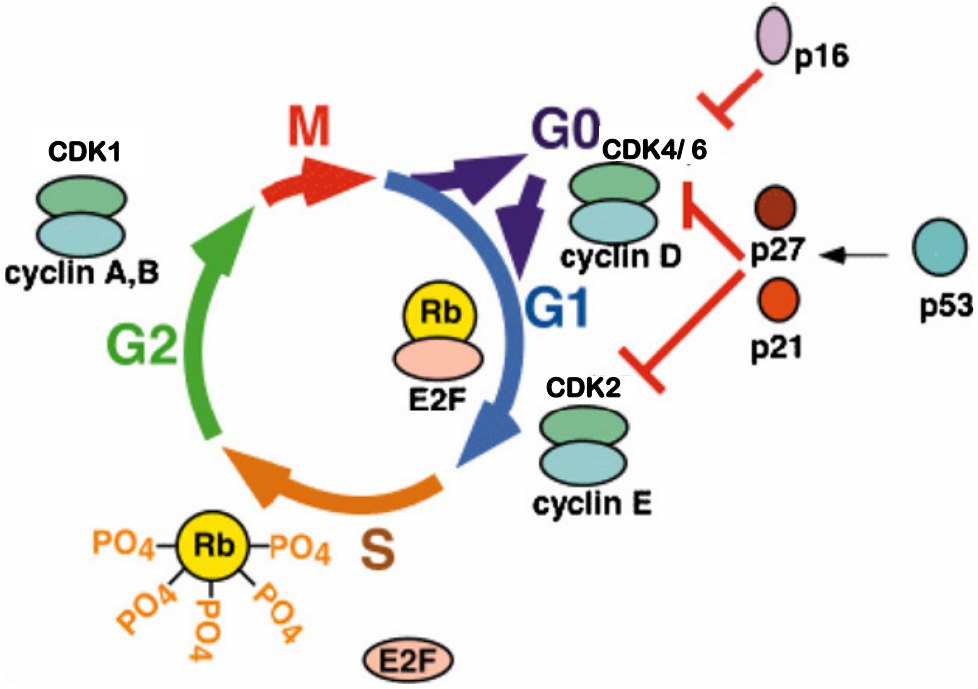

Figure 1.3 Phases of the cell cycle in a non-cancerous cell and their corresponding regulatory components. Cyclins are synthesised with their associated catalytic subunits, the cyclin dependent kinases (CDKs), whereby different cyclins drive the phases of the cell cycle: cyclin D and E for the G1 and early S phases, cyclin A for the S and G2 phases and cyclin B for the late G2 phase. The transition from the G1 phase to the S phase requires phosphorylation of the product of the retinoblastoma (Rb) gene, which is mediated by complexion of cyclin D and CDK4 or CDK6. Normal control of the cell cycle requires a balance between CDK activators (cyclins) and inhibitors (p16, p27, p21). P53 tumour suppressor gene can inhibit cell growth by producing a protein that blocks the cell cycle. Adapted from Voorzanger-Rousselot and Garnero (2007).

responsible for arresting cells in G0 and early G1 by repressing E2F, a transcriptional activator associated with the transcription of genes necessary for G1 to S-phase transition (Harbour and Dean, 2000). Such arrest is usually initiated upon the induction of DNA damage, whereby inhibitors halt the cell cycle at checkpoint 1, allowing for repair. If however repair fails, cell death is usually initiated *via* a process known as apoptosis (see Section 1.2.2).

1.2.1.1 Cell Cycle Mutations in Cancer

Molecular analysis of human tumours has shown that cell-cycle regulators such as CDKs and CKIs are frequently mutated in human neoplasias (Sherr, 2000). Specifically, alterations include the overexpression of cyclins (primarily D1 and E1) and CDKs (primarily CDK4 and CDK6, Table 1.1), as well as loss of CKI (e.g. p15, p16 and p27) and Rb tumour suppressor gene expression. Tumour-associated changes in the expression of these regulators frequently result from chromosome alteration or inactivation. Miscoding mutations in CDK4 and CDK6, resulting in the loss of p16 binding, have also been identified. However, these are generally of lower frequency (Wolfel *et al.*, 1995; Easton *et al.*, 1998). Mutations involving G1 checkpoint associated

Table 1.1 Overexpression of the cell cycle kinases as detected by mRNA expression profiles in different tumour types. Table sourced from de Cárcer *et al.*, 2007.

Please see print copy for Figure.

proteins often contribute to uncontrolled tumour proliferation; the two major aberrant pathways being the p53 and Rb pathways (Figure 1.3). Similarly, the overexpression of the DNA damage checkpoint kinases (e.g. CHK1 and WEE1) and the mitotic kinases (e.g. CDK1 and AURA/B) have been associated with a vast number of tumour types (Table 1.1). Recently, a new cell-cycle inhibitory protein that enhances WEE1-dependent phosphorylation of CDK2, coined Cables, has been reported to be inactivated in 50–60% of primary colon and head and neck tumours (Wu *et al.*, 2001). Interestingly, mutations in the E2F family of transcription factors have not yet been observed in any human tumours.

Mutations in cell-cycle regulators that do not affect cell growth or cell proliferation have also been identified. These mutations appear in molecules that are involved in the control of sister-chromatid separation during mitosis, and are likely to induce aneuploidy as well as other chromosomal alterations, that contribute to the transformed phenotype (de Carcer *et al.*, 2007). The identification of these and other aberrant cell cycle pathways has thus provided new targets for exploitation in the development of new cancer therapeutics. Specific targets and their associated small molecule inhibitors will be discussed in more detail in Section 1.5.1.

1.2.2 Apoptosis

Cancer is characterised not only by uncontrolled proliferation but also cell immortality. Over the years it has become apparent that programmed cell death (apoptosis) is at least, if not more, critical to the understanding of tumourigenesis than the deregulation of

cellular proliferation (Bold *et al.,* 1997). In normal cells, apoptosis is intimately involved in development and homeostasis and includes a series of morphological alterations that are distinct from necrosis. These include cell shrinkage, plasma and nuclear compaction, chromatin condensation, and production of membrane enclosed particles containing intracellular material called apoptotic bodies (Bold *et al.,* 1997).

There are two distinct pathways which can lead to apoptosis, the intrinsic pathway and the extrinsic pathway (Figure 1.4), both of which have been linked to the development of a variety of malignancies upon deregulation. Activation of the intrinsic pathway due to stresses such as hypoxia and direct DNA damage is regulated by the Bcl-2 family of proteins. This family includes 25 proteins (Reed, 2002) comprising of anti-apoptotic molecules such as Bcl-X_L and pro-apoptotic molecules such as Bax and Bid (Fulda and Debatin, 2003). The function of these proteins is to regulate the release of the enzyme cytochrome c which in turn stimulates the activity of a family of intracellular cysteine proteases (caspases), whose function is to rapidly degrade cellular organelles and chromatin. Mechanistically, pro-apoptotic Bcl-2 proteins become inserted into the outer mitochondrial membrane, leading to the release of cytochrome c from the intermembranous space in the mitochondria. The cytochrome c molecules are then able to recruit caspase-9 through apoptosis protease-activating factor-1 (Apaf-1) to activate other caspases which carry out the apoptotic response (Karp, 2005).

Conversely, the extrinsic pathway is triggered by tumour necrosis factor (TNF), an

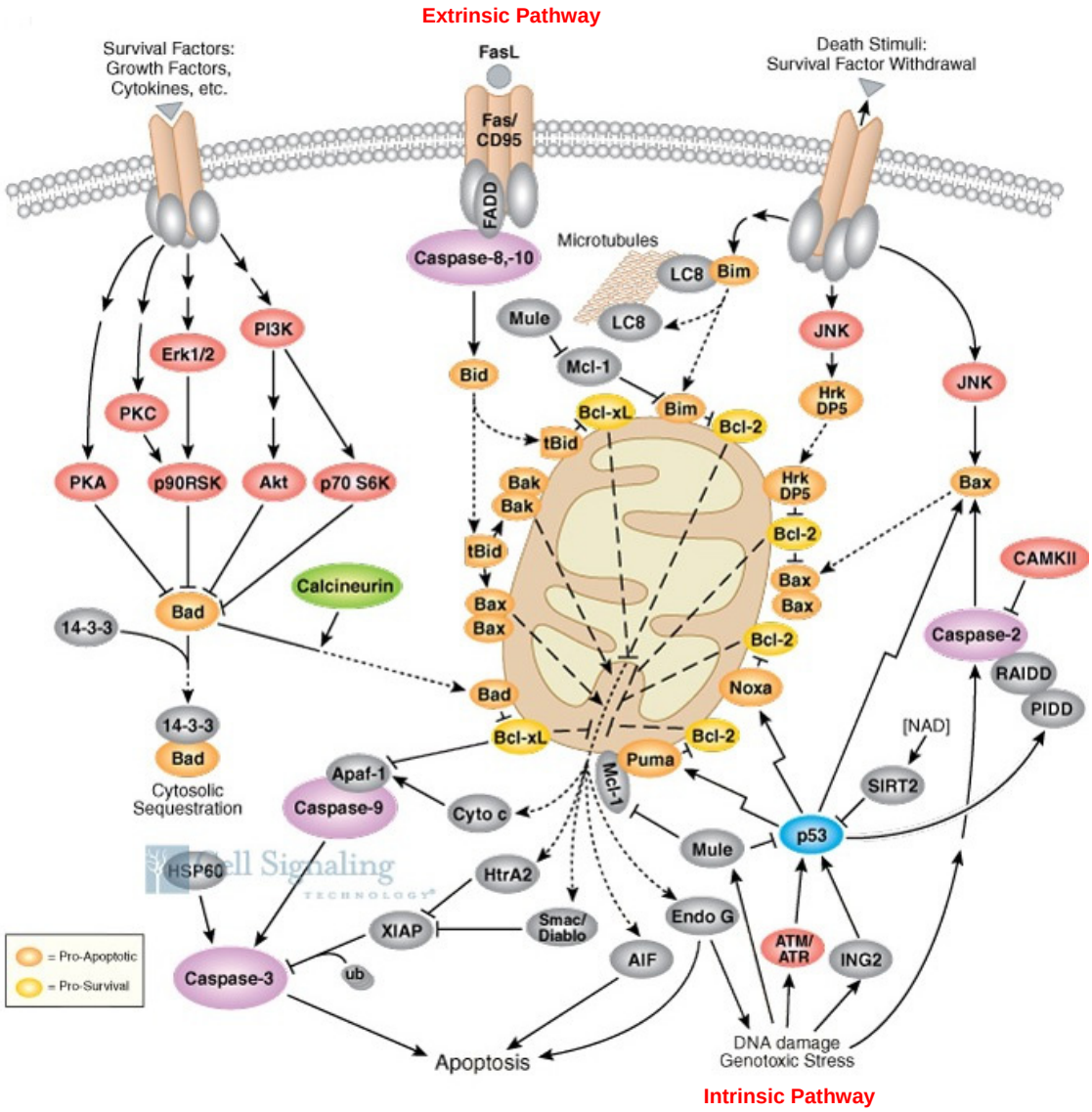

Figure 1.4 Molecular pathways involved in apoptosis. Two major apoptotic pathways are illustrated: one activated *via* death receptor activation (extrinsic) and the other by stress-inducing stimuli (intrinsic). Triggering of cell surface death receptors of the tumour necrosis factor (TNF) receptor superfamily in the extrinsic pathway, results in rapid activation of the initiator caspase 8 after its recruitment to a trimerised receptor-ligand complex. In the intrinsic pathway, stress-induced apoptosis results in perturbation of mitochondria and release of proteins from the inter-mitochondrial membrane space. The release of cytochrome c, from mitochondria is regulated in part by Bcl-2 family members, with anti-apoptotic (Bcl-2/ Bcl-X_L/Mcl1) and pro-apoptotic (Bax, Bak and tBid) members inhibiting or promoting the release, respectively. Adapted from Pattabhiraman (2003).

extracellular ligand, binding to the TNF receptor apoptosis-inducing ligand (TRAIL) on the plasma membrane (Karp, 2005; Ricci and Zong, 2006). TRAIL death receptors recruit Fas-associating death domain-containing protein (FADD) which in turn recruits caspase-8 and caspase-10. Adding these caspases to the complex containing the cellular receptor and FADD leads to auto-proteolytic cleavage. Activation of effector caspases by activated caspase-8 and -10 is then sufficient to invoke apoptosis (Ricci and Zong, 2006).

1.2.2.1 Apoptotic Aberrations in Cancer

Suppression of apoptosis is one of the major acquired attributes of cancer cells (Evan and Vousden, 2001). Mutations in apoptotic signaling pathways such as the expression of the survival factor insulin-like growth factor (IGF) (Yu and Rohan, 2000), activating mutations of Akt, a serine/threonine kinase that induces a strong survival signal (Datta *et al.*, 1999; Stambolic *et al.*, 1999; Bonneau and Longy, 2000) and loss of the suppressor of Akt, PTEN, function (Bonneau and Longy, 2000) have been identified in many tumour types. The anti-apoptotic oncoproteins Bcl-2 and Bcl-xL, which exert their principal effects through stabilisation of the mitochondrion, have also been found to be overexpressed in several cancer types (Table 1.2). Recent analyses have indicated that loss of Apaf-1 is a relatively frequent event, especially in malignant melanoma and is most likely responsible for resistance to apoptosis (Soengas *et al.*, 2001). In most cases, over-expression of the Bcl-2 and Bcl-xL oncoproteins is caused by structural gene modifications such as frameshift mutations which inactivate Bax and is associated with some forms of colon cancer (Fulda and Debatin, 2003).

Table 1.2 The annual incidence of human cancers and their corresponding percentages of Bcl-2 overexpression. Adapted from Zhang (2002).

Types of Cancer	New Incidences*	Bcl-2 Overexpression
Hormone-refractory prostate cancer	66,000	90-100%
Malignant melanoma	48,000	90%
Estrogen-receptor-positive breast cancer	96,000	80-90%
Non-Hodgkin's lymphoma	58,000	50%
Colon cancer	97,000	30-50%
Chronic lymphocytic leukemia (CLL)	12,000	25-50%

* US incidences reported per annum.

Another potent driving force involved in the suppression of apoptosis in tumour cells is the deregulation of the oncoprotein transcription factor Myc, which has a coupled relationship in both cell proliferation and cell death (Evan and Vousden, 2001). In addition to its well documented growth-promoting property, c-Myc is reported to be a powerful inducer of apoptosis, especially under conditions of stress, genotoxic damage or depleted survival factors (Askew *et al.*, 1991). Aberrations in expression of the *c-Myc* gene have found constitutively activated c-Myc in IL-3-dependent myeloid cell lines to suppress cell cycle arrest and accelerate apoptosis (Askew *et al.*, 1991). Most, if not all, types of human malignancies have been reported to have amplifications and/or some form of overexpression of this gene (Nesbit *et al.*, 1999), although the frequency of these alterations varies greatly among different reports.

In contrast to genetic mutations, resulting in the overexpression of gene products, Fas/FasL signaling is now also thought to play an important role in carcinogenesis, tumour outgrowth, and metastasis (Owen-Schaub *et al.*, 2000). A novel mechanism by

which cancer cells avoid FAS- and TRAIL-mediated apoptosis has been discovered, which involves the synthesis of decoy receptors to which the ligands bind without inducing apoptosis (Pitti *et al.*, 1998; Ashkenazi and Dixit, 1999; Marsters *et al.*, 1999) allowing the continuation of neoplastic cell growth. The understanding of apoptosis *via* the discovery of such mechanisms has thus provided the basis for which novel targeted therapies can be developed. For detailed reviews concerning cancer therapies aimed at targeting apoptotic pathways see Zhang, (2002) and Ghobrial *et al.,* (2005).

1. 3 Current Treatment Strategies: Promises and Pitfalls

1.3.1 Conventional Chemotherapy and Systemic Toxicity

Conventional cancer treatments such as cytotoxic chemotherapy (e.g. anti-metabolites, alkylating agents, topoisomerase inhibitors) and radiation therapy have been developed based upon the observation that malignant cells divide at a greater rate than the normal cells. For example, ionising radiation induces DNA damage that, upon multiple cell divisions, may lead to errors in transcription and translation resulting in cell death (Rydberg, 2001). Similarly, cytotoxic chemotherapy may interrupt microtubule formation that is essential for mitotic events that ultimately affect cell survival (Marchetti *et al.*, 2002). This is true for many haematopoietic malignancies, however, as little as 5% of some solid tumours actually consist of rapidly proliferating, and therefore, susceptible cells (Rang *et al.*, 1999). As a result, only a small subset of cancers such as Hodgkin's lymphoma, testicular cancer, acute lymphoid leukemia and non-Hodgkin's lymphoma are routinely cured using these agents (Abeloff and Armitage, 2004). This is primarily because therapies that are directed against rapidly

proliferating cells result in the death of normal tissues that also show enhanced proliferation rates, such as the bone marrow, gastrointestinal (GI) tract and hair follicles (Kaelin, 2005). Side effects such as nausea, vomiting, alopecia, liver and kidney damage and occasionally more serious affects including neutropenia and cardiotoxicity means that anticancer chemotherapeutics are often administered at sub-optimal doses, which eventually leads to the failure of therapy (DeVita, 1997; Foote, 1998).

1.3.2 The Emergence of Multi-Drug Resistance (MDR)

The development of drug resistance is also a major obstacle in patients receiving prolonged chemotherapeutic treatment. Clinical resistance to anticancer agents can occur at the time of presentation, as well as during the course of treatment and after relapse (Quesada *et al.*, 1996). Although a number of different resistance mechanisms have been described, such as insufficient activation of the drug, utilisation of alternate metabolic pathways, mutations in the p53 gene and over expression of the Bcl-2 gene family, the most intensely studied has been the decreased accumulation of drugs in cells, which is the leading cause of multi-drug resistance (Gottesman *et al.*, 2002). Such resistance is characterised by a failure to respond to a variety of chemotherapeutic agents, many of which are structurally dissimilar and do not share a common intracellular target (Rang *et al.*, 1999). The mechanism responsible for MDR in mammalian cells involves the overexpression of a 170 kDa cell surface, energy dependant plasma membrane glycoprotein (P-gp) encoded on the MDR1 gene (Bellamy, 1996). The physiological role of P-gp is thought to be in the protection of cells against environmental toxins and works by exporting drugs out of mammalian

cells, lowering the intracellular drug concentration below the toxic threshold (Gottesman and Pastan, 1993; Patel and Rothenberg, 1994) is therefore to find ways of overcoming drug resistance due to the expression of P-gp, which involves a search for clinically novel drugs that retain relatively good activity on MDR cells. However, the chemotherapy of cancer, as compared with that of bacterial disease, poses a difficult problem. Microorganisms are both quantitatively and qualitatively different from human cells, while, cancer cells and normal cells are so similar that it has proved difficult to find general, exploitable biochemical differences between them (Rang *et al.*, 1999). This is illustrated by the number of drugs selected for preclinical or clinical testing, based on their activity in experimental animal systems, that do not become clinically useful agents due to their severe or unpredictable toxicity towards normal cells, or because they lack any therapeutic advantage. The prevalence of MDR and systemic toxicity in association with currently administered cancer chemotherapies therefore suggests that alternative avenues need to be explored in the hope of finding new and effective therapeutic agents.

1.4 Revival of Natural Product Research

The use of natural products in the discovery of new medicines has been the single most successful strategy, primarily because the chemical diversity of natural products is greater than any other source. Between 1983 and 1995 as many as 60% of the approved drugs and drug application candidates for anti-infective and anticancer treatments were of natural product origin. In 1997, of the 42 new chemical entities that were submitted for approval by the FDA, 32 (76%) were natural products or derivatives thereof

(Grabley and Thiericke, 1999) and in 2000, 57% of all drugs in clinical trials for cancer were natural products or were based on natural product leads (Demain and Zhang, 2005). For reference purposes, a list of approved antitumour agents (up to the end of 2002) and their chemical origin is shown in Table 1.3. Such figures thus provide evidence for the importance of natural product research and its impact on drug discovery and development, in the area of cancer therapy.

In the past decade, research into natural products in the pharmaceutical industry has declined, owing to issues such as the development of high-throughput screening (HTS) against defined molecular targets and the development of combinatorial chemistry (Koehn and Carter, 2005). Consequently, many pharmaceutical companies have placed greater emphasis on high-throughput screening of mass-produced combinatorial libraries over natural product research. One problem however, is that the percentage of isolated or synthesised compounds that are showing biological activity is low, and the expected surge in productivity has not been as great as projected. For example, the number of new active substances (NASs), also known as new chemical entities (NCEs), has hit a 20 year low of 37 in 2001 and is still declining (Newman *et al.*, 2003). This is because combinatorial chemistry is limited to the rearrangement of known chemical structures, whereas completely novel chemical skeletons can only be found in nature. For this reason, many researchers are now turning back to natural products and investigating organisms from different niches that were previously inaccessible or unconsidered.

Table 1.3 All anticancer agents approved for clinical use by the FDA between the 1940s and 2002. Data modified from Newman *et al*., (2003).

Generic Name	Year Introduced	Source	Generic Name	Year Introduced	Source
alemtuzumab	2001	B	aminoglutethimide	1981	S
celmoleukin	1992	B	amsacrine	1987	S
denileukin diftitox	1999	B	arsenic trioxide	2000	S
interferon alfa2a	1986	B	bisantrene hydrochloride	1990	S
interferon, gamma-1a	1992	B	busulfan	Pre-1981	S
interleukin-2	1989	B	camostat mesylate	1985	S
OCT-43	1999	B	carboplatin	1986	S
pegaspargase	1994	B	carmustine	Pre-1981	S
rituximab	1997	B	chlorambucil	Pre-1981	S
tasonermin	1999	B	chlortrianisene	Pre-1981	S
teceleukin	1992	B	cis-diamminedichloro- platinum	Pre-1981	S
trastuzumab	1998	B	cyclophosphamide	Pre-1981	S
aclarubicin	1981	N	dacarbazine	Pre-1981	S
actinomycin D	Pre-1981	N	diethylstilbestrol	Pre-1981	S
angiotensin II	1994	N	flutamide	1983	S
arglabin	1999	N	fotemustine	1989	S
asparaginase	Pre-1981	N	heptaplatin/SK-2053R	1999	S
BEC	1989	N	hexamethylmelamine	Pre-1981	S
bleomycin	Pre-1981	N	hydroxyurea	Pre-1981	S
daunomycin	Pre-1981	N	ifosfamide	Pre-1981	S

B: Biological, N: Natural product, ND: Natural product derivative, S: Synthetic, S*: Synthetic based on a pharmacophore from a natural product, V: Vaccine, NM: Natural Product Mimic

Table 1.3 continued from page 19

Generic Name	Year Introduced	Source	Generic Name	Year Introduced	Source
doxorubicin	Pre-1981	N	levamisole	Pre-1981	S
masoprocol	1992	N	lobaplatin	1998	S
mithramycin	Pre-1981	N	lomustine	Pre-1981	S
mitomycin C	Pre-1981	N	lonidamine	1987	S
paclitaxel	1993	N	mechlorethanamine	Pre-1981	S
pentostatin	1992	N	melphalan	Pre-1981	S
peplomycin	1981	N	mitotane	Pre-1981	S
solamargine	1987	N	mustine hydrochloride		S
streptozocin	Pre-1981	N	nedaplatin	1995	S
testosterone	Pre-1981	N	nilutamide	1987	S
vinblastine	Pre-1981	N	nimustine hydrochloride	Pre-1981	S
vincristine	Pre-1981	N	oxaliplatin	1996	S
alitretinoin	1999	ND	pipobroman	Pre-1981	S
amrubicin hydrochloride	2002	ND	porfimer sodium	1993	S
cladribine	1993	ND	procarbazine	Pre-1981	S
cytarabine ocfosfate	1993	ND	ranimustine	1987	S
docetaxel	1995	ND	sobuzoxane	1994	S
dromostanolone	Pre-1981	ND	thiotepa	Pre-1981	S
elliptinium acetate	1983	ND	triethylenemelamine	Pre-1981	S
epirubicin hydrochloride	1984	ND	uracil mustard	Pre-1981	S
estramustine	Pre-1981	ND	zoledronic acid	2000	S

B: Biological, N: Natural product, ND: Natural product derivative, S: Synthetic, S*: Synthetic based on a pharmacophore from a natural product, V: Vaccine, NM: Natural Product Mimic

Table 1.3 continued from page 20

Generic Name	Year Introduced	Source	Generic Name	Year Introduced	Source
ethinyl estradiol	Pre-1981	ND	aminoglutethimide	Pre-1981	S*
etoposide	Pre-1981	ND	capecitabine	1998	S*
etoposide phosphatea	1996	ND	carmofur	1981	S*
exemestane	1999	ND	cytosine arabinoside	Pre-1981	S*
fluoxymesterone	Pre-1981	ND	doxifluridine	1987	S*
formestane	1993	ND	enocitabine	1983	S*
fulvestrant	2002	ND	floxuridine	Pre-1981	S*
gemtuzumab ozogamicin	2000	ND	fludarabine phosphate	1991	S*
hydroxyprogesterone	Pre-1981	ND	fluorouracil	Pre-1981	S*
idarubicin hydrochloride	1990	ND	gemcitabine hydrochloride	1995	S*
irinotecan hydrochloride	1994	ND	goserelin acetate	Pre-1981	S*
medroxyprogesterone acetate	Pre-1981	ND	leuprolide	Pre-1981	S*
megesterol acetate	Pre-1981	ND	mercaptopurine	Pre-1981	S*
methylprednisolone	Pre-1981	ND	methotrexate	Pre-1981	S*
methyltestosterone	Pre-1981	ND	mitoxantrone hydrochloride	1984	S*
miltefosine	1993	ND	tamoxifen	Pre-1981	S*
mitobronitol	1991	ND	thioguanine	Pre-1981	S*
pirarubicin	1988	ND	bexarotene	2000	S*/NM
prednisolone	Pre-1981	ND	raltitrexed	1996	S*/NM
prednisone	Pre-1981	ND	temozolomide	1999	S*/NM
teniposide	1989	ND	anastrozole	1995	S/NM

B: Biological, N: Natural product, ND: Natural product derivative, S: Synthetic, S*: Synthetic based on a pharmacophore from a natural product, V: Vaccine, NM: Natural Product Mimic

Table 1.3 continued from page 21

Generic Name	Year Introduced	Source	Generic Name	Year Introduced	Source
topotecan hydrochloride	1996	ND	camostat mesylate	1985	S/NM
testolactone	Pre-1981	ND	bicalutamide	1995	S/NM
triamcinolone	Pre-1981	ND	fadrozole hydrochloride	1995	S/NM
triptorelin	1986	ND	gefitinib	2002	S/NM
valrubicin	1999	ND	imatinib mesilate	2001	S/NM
vindesine		ND	letrazole	1996	S/NM
vinorelbine	1989	ND	toremifene	1989	S/NM
zinostatin stimalamer	1994	ND	bcg live	1990	V
			melanoma theraccine	2001	V

B: Biological, N: Natural product, ND: Natural product derivative, S: Synthetic, S*: Synthetic based on a pharmacophore from a natural product, V: Vaccine, NM: Natural Product Mimic

1.4.1 The Marine Environment as a Source of Novel Anticancer Agents

In the past, scientists have commonly exploited microorganisms and plants from terrestrial habitats to isolate many of the bioactive compounds we use today (Aszalos, 1981). For example, vinblastine and vincristine, initially isolated from the Madagascar periwinkle plant, *Catharanthus roseus*, were first introduced in the late 1960s and have made enormous contributions to the long term regressions and cures of childhood leukemia, testicular teratoma and Hodgkin's disease (Mann, 2002). Until the mid-1960s, however, investigation of natural products from marine organisms was essentially non-existent (Mann, 2002). This is most likely due to the fact that the marine environment lacks an ethnobotanical history and because of this, there is difficulty associated with identifying suitable organisms for study, which in contrast to terrestrial organisms are harder to collect. Nevertheless, over the past 30 years, approximately 10,000 new structures have been identified from marine microorganisms, seaweeds, sponges, soft corals, and marine invertebrates, such as bryozoans, echinoderms, molluscs and ascidians (Faulkner, 2000; Faulkner, 2001). In addition, more than 300 patents have been issued covering potential anticancer agents from the sea (Mann, 2002). But as yet, no marine natural product has been licensed for clinical use as an anticancer agent (Nuijen *et al.*, 2000). Despite this, over a dozen compounds derived from marine sources are in various stages of pre-clinical and clinical trials (Newman and Cragg, 2005, Table 1.4).

One of the most promising anticancer agents from marine organisms is bryostatin, which was originally isolated from the tunicate *Bugula neritina*, and has activity against

a range of cancers. Analogues based on the basic skeleton of bryostatin have been synthesised to further explore structure activity relationships (SARs) and recently a series of much simplified structures with potent *in vitro* antitumour activity have been reported (Wender *et al.*, 1998; Wender and Lippa, 2000). One particular analogue, bryostatin 1, is being evaluated in approximately 50 Phase I and Phase II clinical trials against melanoma, leukemias, lymphomas, and cancers of the breast, prostate, lung,

Table 1.4 Status of selected marine-derived compounds in clinical and preclinical trials as of December 2003. Adapted from Simmons *et al.*, (2005).

Name	**Source (organism)**	**Status**
Bryostatin 1	*Bugula neritina* (tunicate)	phase II
TZT-1027	Synthetic derivative of dolastatin (mollusc)	phase II
Ecteinascidin 743	*Ecteinascidia turbinate* (tunicate)	phase III
Aplidine	*Aplidium albicans* (tunicate)	phase II
E7389	*Lissodendoryx sp.* (sponge)	phase I
Discodermolide	*Discodermia dissolute* (sponge)	phase I
Kahalalide F	*Elysia rufescens/ Bryopsis sp.* (mollusc)	Phase II
ES-285 (Spisulosine)	*Spisula polynyma* (mollusc)	Phase I
HTI-286	*Cymblastella sp.* (sponge)	Phase I
KRN-7000	*Agelas mauritianus* (sponge)	Phase I
Laulimalide	*Cacospongia mycofijiensis* (sponge)	preclinical
Cauacin A	*Lyngbya majuscule* (cyanobacteria)	preclinical
Vitilevuamide	*Didemnum cucliferum* (tunicate)	preclinical
Diazonamide	*Diazona angulata* (tunicate)	preclinical
Eleutherobin	*Eleutherobia sp.* (soft coral)	preclinical
Sarcodictyin	*Sarcodictyon roseum* (soft coral)	preclinical

kidney, cervix, ovary, oesophagus and stomach. So far, there have been no complete remissions, but some patients have experienced disease stabilisation for almost two years (Mann, 2002), which suggests that the new analogues may offer greater bioavailability, potency and selectivity. Two classes of structurally similar marine natural products from soft coral are also of interest. These are the sarcodictyins from the Mediterranean coral *Sarcodictyon roseum* (Pietra, 1997) and eleutherobin from coral (*Eleutherobia* sp.) found off the coast of Western Australia in 1994 (Fenical, 1997). These compounds have taxol-like activity, with eleutherobin showing up to 50 times more potency than taxol itself against a range of cancer cell lines *in vitro* (Mann, 2002).

The proportion of natural products isolated from different marine phyla can be seen in Figure 1.5, where it can be observed that approximately one third of all marine natural products are isolated from Porifera (sponges). This is most likely due to their sessile nature, making them easier to collect. In addition, the sessile, benthic nature of sponges also provides strong selective pressure for the synthesis of a variety of bioactive defense products (Carte, 1996). Despite this, it should not be assumed that some taxa are richer in bioactive compounds than others. Some believe that the current phyletic break down of active resources reflects biases in the research field, where some phyla have been frequently targeted (for example sponges) while others have not (de Vries and Hall, 1994). Investigation into natural products isolated from molluscan resources accounts for less than 11%, however it is maintained that the potential for this phyla to produce beneficial bioactive compounds is greater than expected. This is firstly because

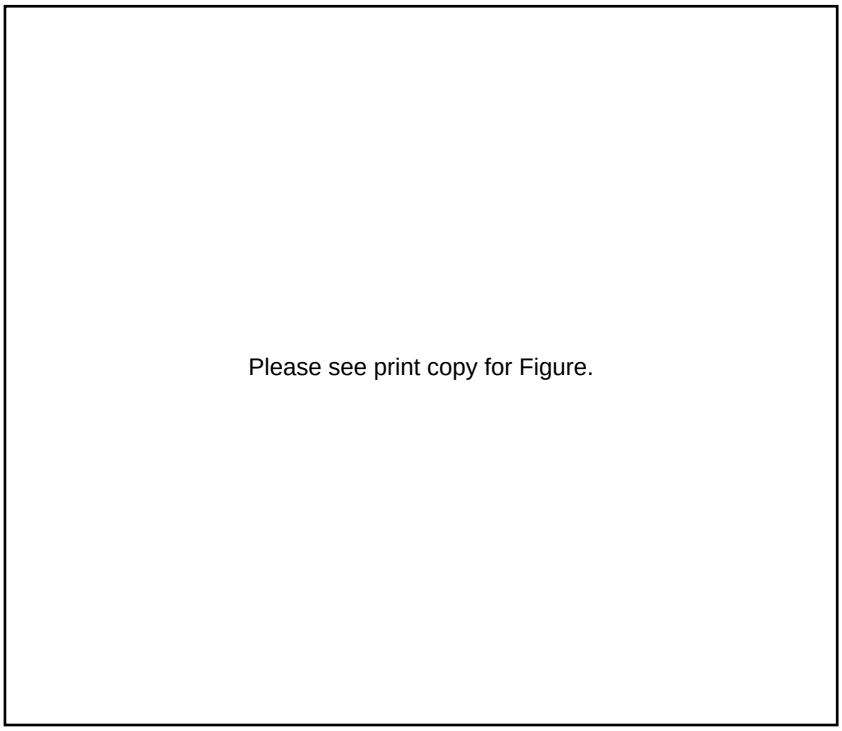

Figure 1.5 The percentage of marine natural products isolated from various phyla. Almost one third of reported marine natural products are derived from the sea sponge (Porifera), while Arthropoda, Brachiopoda, Euglenophycota and Nematoda are all less then 1% and therefore have not been depicted. Pie chart courtesy of Jaspers (1998).

molluscs are the second largest animal phylum on earth and encapsulate an enormous diversity of species and secondly there still remains a great diversity of molluscan natural products that have been structurally elucidated but never tested for biological activity. For example, less than 160 of the 585 molluscan metabolites reviewed in a book chapter by Alam and Thomson in 1998 appear to have been tested in any bioassays (Alam and Thomson, 1998). So there is great potential for discovering new antitumour drug leads by screening natural products that have already been described in the literature.

1.4.1.1 Cytotoxic Molecules from Marine Molluscs and their Egg Masses

Indigo and indirubin (Figure 1.6) have been identified in purple secretions from marine molluscs belonging to the Muricidae family of gastropods (Cooksey, 2001; Naegel and Cooksey, 2002; Meijer *et al.*, 2003) amongst other sources (Adachi *et al.*, 2001; MacNeil *et al.*, 2001; Maugard *et al.*, 2001). These compounds are based on the simple heterocycle, indole and have been used for centuries as dyestuffs for clothing and war paint (Maugard *et al.*, 2001). More recently, indirubins have been identified as the major active ingredient of the traditional Chinese medical remedy known as Danggui Lomghui Wan, used for over 30 years to treat chronic myelogenous leukemia (Chen and Xie, 1984; Xiao *et al.*, 2002). Investigation into the mode of action of this class of compounds found indirubins to be inhibitors of several CDKs, STATs (signal transduced and activator of transcription) as well as GSK-3 (glycogen synthase kinase-3, Meijer *et al.*, 2003). Potent and selective *in vitro* activity displayed by the indirubins

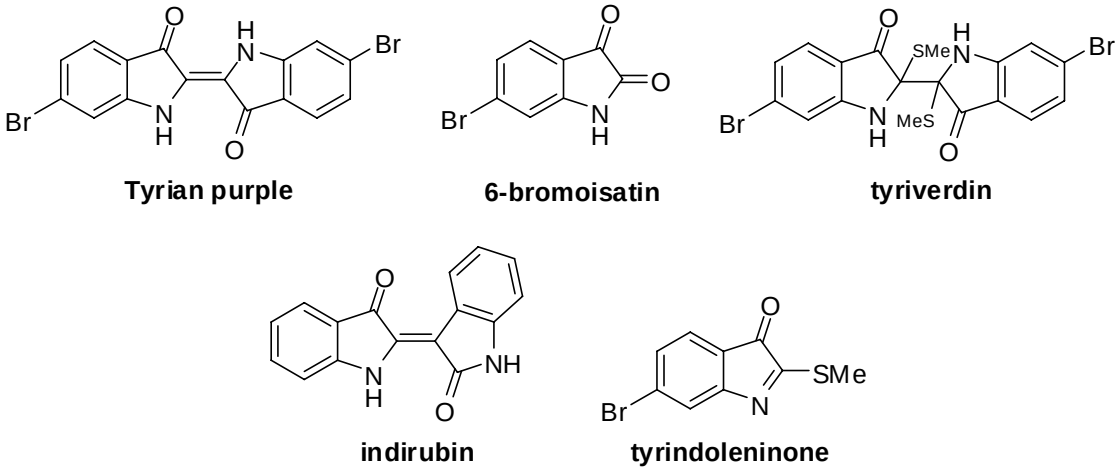

Figure 1.6 Examples of the brominated and non-brominated compounds present in the hypobranchial gland and egg masses of Muricidae molluscs.

has prompted further *in vivo* assessment and has found the structural analogue, 5-methyl-indirubin, to show promising anticancer activity in patient derived lung, renal and prostate xenograft mouse models (Fiebig and Schuler, 2006). Poor solubility and absorption as well as gastrointestinal tract problems (Wang and Mencher, 2006) however, have slowed their path to development.

In addition to containing the biologically active pigment indirubin, the hypobranchial glands and egg masses of muricid molluscs have also been found to contain the structural isomer of indirubin, Tyrian purple, along with other brominated and non-brominated analogues (Figure 1.6, Benkendorff *et al.*, 2000; Benkendorff *et al.*, 2001; Cooksey, 2001; Naegel and Cooksey, 2002), which are proposed to play a defensive role during embryonic development (Benkendorff *et al.*, 2000; Westley *et al.*, 2006). Recent studies have demonstrated that a brominated precursor to Tyrian purple, 6-bromo-2-methylthio-3*H*-indol-3-one (tyrindoleninone) has anticancer activity (Vine, 2002). Investigations into the cytotoxic activity of tyrindoleninone prepared from chloroform extracts of *Dicathais orbita* egg masses, have revealed greater specificity towards cancer cells than untransformed, human mononuclear cells *in vitro* (Vine, 2002). This apparent selectivity for tumour cells thus highlights this indole derivative as a potentially useful lead for anticancer drug development. However, complete chemical synthesis of the marine natural product has not been reported to date.

Other independent studies have also reported the presence of biologically active substances in the egg masses of opisthobranch molluscs (Kamiya *et al.*, 1986; Roesener

and Scheuer, 1986) For example, Ulapualide A and B, macrolides from nudibranch egg masses, have been reported to show antitumour activity in a L1210 leukemia cell line (Roesener and Scheuer, 1986). Recent mode of action investigations has found Ulapualide A to play a role in actin-depolymerisation which is thought to be responsible for its potent antiproliferative affect *in vitro* (Vincent *et al.*, 2007).

1.4.2 Obstacles in the Prevention of Marine Natural Products as Drugs

Despite, the potent anticancer activity displayed by compounds isolated from the egg masses of marine molluscs, there are two potential obstacles that may prevent the development of marine natural products as drugs. The first is that most bioactive marine metabolites prove to be highly toxic. For example, didemnin B from a Caribbean tunicate proceeded to phase II clinical trials before hepatotoxicity prevented further development as an antitumour agent (Rinehart, 2000). Providing enough material is available, modification of the parent compound could potentially reduce the toxicity. However, the supply issue is another serious problem, inhibiting the development of most marine natural products. Typically, the yields from the organism itself are quite low, often less than one thousandth of the wet weight (Fuestani, 2000). One way to overcome the lack of selectivity observed with certain highly potent, cytotoxic natural products for efficacious treatment of cancer is to use monoclonal antibody (mAb) delivery through conjugate formation. For example, calicheamicin is a potent DNA damaging agent produced by *Micromonospora echinospora* (Lee *et al.*, 1993). Although it is 100-1,000 times more potent than conventionally used therapeutic agents (Koehn and Carter, 2005), calicheamicin itself lacks the therapeutic index required for systemic

administration. The potency of calicheamicin has therefore been harnessed by immunoconjugation, using a chemical modification followed by linkage to a monoclonal antibody (mAb) that specifically binds to the CD33 cell surface antigen present on acute myeloid leukemia (AML) cells. After internalisation into lysosomal vesicles, the conjugate is engineered to release calicheamicin, which migrates to the nucleus, cleaves DNA and results in cell death (Hamann *et al.*, 2002; Damle and Frost, 2003). The calicheamicin-mAb conjugate, or Mylotarg as it is now known commercially (Figure 1.7), was approved by the US FDA in 2000 for the treatment of

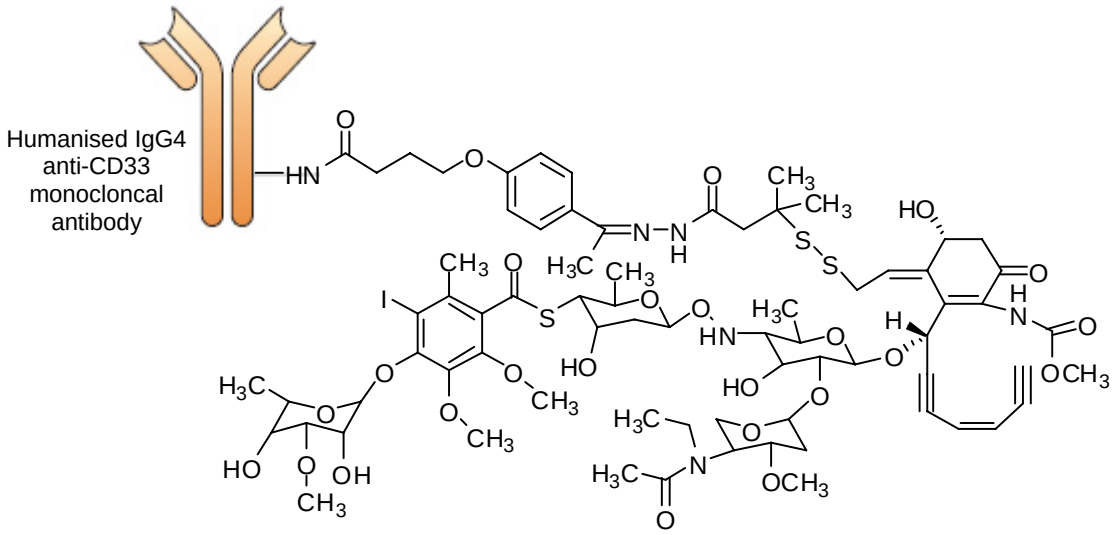

Figure 1.7 Structure of gemtuzumab ozogamicin (Mylotarg). The potent DNA damaging agent calicheamicin was conjugated to a humanised monoclonal antibody (mAb) that specifically binds to the CD33 cell surface antigen present on acute myeloid leukemia (AML) cells. Mylotarg was approved by the US FDA in 2000 for the treatment of CD33 positive relapsed AML and was the first targeted chemotherapy agent using monoclonal antibody technology.

CD33 positive relapsed AML and was the first targeted chemotherapy agent using mAb technology. The therapeutic advantages of other ligand-targeted therapeutics will be discussed further in Section 1.5.2.

1.5 Targeted Cancer Therapy

Advances in the understanding of aberrant signaling pathways in various types of cancer cells has meant that many pivotal regulators of malignant behaviour have emerged as candidates for molecular target-based cancer therapy. Such strategies have improved the management of many cancer types (Hanahan and Weinberg, 2000) with a recent surge in compounds being approved for clinical use (Imai and Takaoka, 2006). A crucial challenge in the development of targeted agents however, is to choose a suitable approach. The two main approaches discussed in the remaining sections of this chapter are small molecule inhibitors and mAb/ ligand- directed prodrug therapies.

1.5.1 Small Molecule Inhibitors

1.5.1.1 Targeting Cell Signaling Pathways and their Receptors

Receptor tyrosine kinases (RTKs) and non-RTKs are crucial mediators in signaling pathways of cell proliferation, differentiation, migration, new blood vessel formation (angiogenesis) and cell-cycle regulation (Baselga, 2006), many of which are deregulated during tumourigenesis (Gschwind *et al.*, 2004) (Figure 1.8). Most small molecule inhibitors of tyrosine kinases are ATP mimetics and therefore hit a variety of

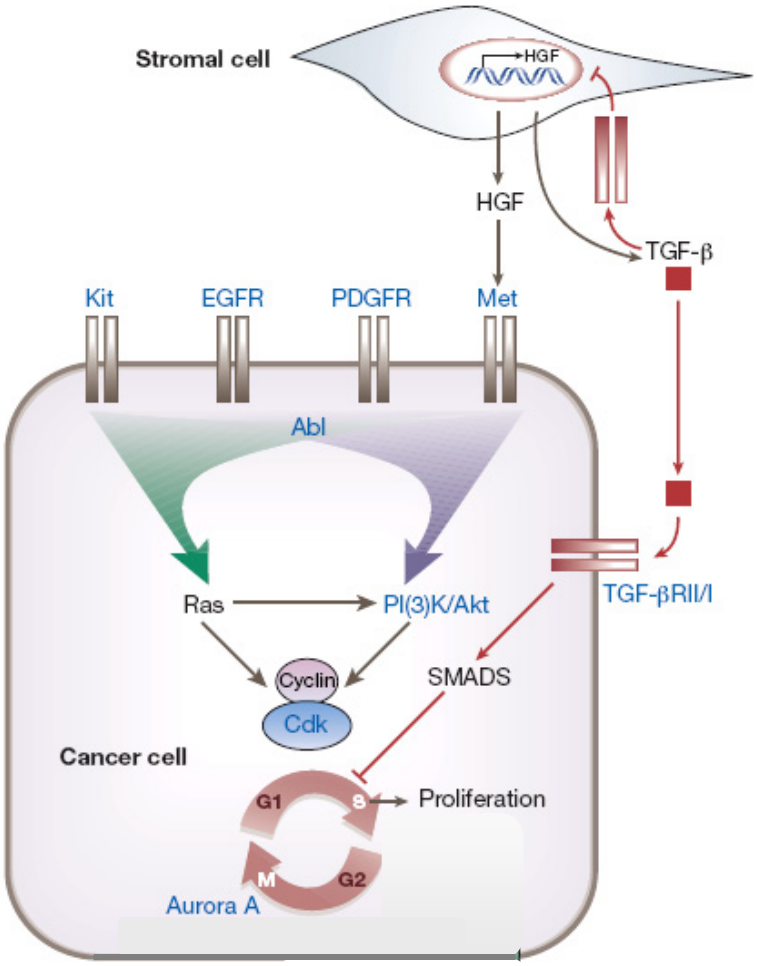

Figure 1.8 Cancer pathways for exploitation in targeted therapy. Multiple signaling pathways are deregulated in cancer cells owing to specific alterations in oncogenes or tumour suppressor genes which stimulate tumour cell proliferation, often by promoting G1/S cell-cycle progression. Signals from the tumour microenvironment, including stromal fibroblasts can also positively or negatively effect cancer cell proliferation. The inhibition of growth-promoting pathways by therapy aimed at specific genetic alterations found in cancer, offers a new therapeutic approach. The major kinases targeted for therapy are depicted in blue. KIT: stem-cell factor receptor (SCFR), EGFR: epidermal growth factor receptor, PDGFR: platelet-derived growth factor receptor, Met: membrane receptor for hepatocyte growth factor (HGF), TGF-β: transforming growth factor beta. Adapted from Sawyers (2004).

targets. For example, imatinib mesylate (Gleevec), one of the first successful, clinically used small molecule inhibitors, inactivates the kinase activity of the BCR-ABL fusion

protein (Druker, 2002; Druker, 2004) by binding in the ATP binding pocket and has proven highly efficacious in the treatment of patients with Philadelphia chromosome-positive CML (O'Dwyer *et al.*, 2003). Imatinib also inhibits KIT (a stem-cell factor receptor (SCFR)), which is essential to the pathogenesis of metastatic gastrointestinal stromal tumours (GISTs), as well as the platelet-derived growth factor receptors (PDGFRα and PDGFRβ), which play key roles in the pathogenesis of PDGF associated tumours such as glioblastoma (Buchdunger *et al.*, 2002).

In the wake of imatinib therapy, many other ATP mimetics that target oncogenic RTKs have also been developed (Table 1.5). For example, gefitinib (Iressa) and erlotinib (Tarceva) both selectively inhibit the epidermal growth factor receptor (EGFR) (Minna and Dowell, 2005) and are efficacious against EGFR-expressing cancers such as non-small-cell lung cancer (NSCLC) and head and neck squamous-cell carcinoma (HNSCC) (Tabel 1.5). Cancer cell adhesion, invasion and neovascularisation pathways have also been targeted *via* the use of small molecules that inhibit SRC kinase or matrix metalloproteinases (MMPs) and the vascular endothelial growth factor RTK (VEGFR). Of interest is the new small molecule, sorafenib (Nexavar), which is known to exert its inhibitory effect not only on different isoforms of Raf serine kinase but also various RTKs such as VEGFR, EGFR and PDGFR (Arora and Scholar, 2005). This dual-action kinase inhibitor therefore shows broad-spectrum antitumour activity by inhibiting both tumour proliferation and angiogenesis (Marx, 2005). Another new anti-angiogenesis

Table 1.5 FDA approved small molecule inhibitors and their corresponding molecular targets.

Drug	Target	Disease Type	Cancer Type
Imatinib mesylate (Gleevec)	TKs (BCR-ABL, KIT, PDGFR)	GIST and CML	Solid and haematological
Gefitinib (Iressa)	TK (EGFR)	NSCLC	Solid
Erlotinib (Tarceva)	TK (EGFR)	NSCLC and pancreatic cancer	Solid
Sunitinib (Sutent)	TKs (VEGFR, PDGFR, KIT, FLT3)	GIST and renal cancer	Solid
Sorafenib (Nexavar)	Kinases (B-Raf, VEGFR2, EGFR, PDGFR)	Renal cancer	Solid
Bortezomib (Velcade)	28S protease	Multiple myeloma	Haematological

Drugs are shown as generic names with trade names in parentheses. TK: tyrosine kinase; PDGFR: platelet-derived growth factor receptor, EGFR: epidermal growth factor receptor, VEGFR: vascular endothelial growth factor receptor, FLT3: Fms-like tyrosine kinase 3, GIST: gastrointestinal stromal tumour, CML: chronic myeloid leukemia, NSCLC: non-small-cell lung cancer.

small molecule drug, sunitinib malate (Sutent), is also a multi-targeted tyrosine kinase inhibitor of VEGFR, PDGFR, KIT and Fms-like tyrosine kinase 3 (FLT3) (Marx, 2005) (Table 1.5) Interestingly, Sutent is used for the treatment of advanced renal cell carcinoma (RCC) and gastrointestinal stromal tumours (GIST), only when treatment with imatinib fails.

1.5.1.2 Problems Associated with Small Molecule Targeted Therapies

Imatinib not only exemplifies the successful development of the small molecule, targeted therapy approach, but also illustrates that molecular resistance is still a potential problem. Relapse after initial response to imatinib is common in advanced

CML, and occurs primarily through target resistance, a process by which there is an expansion of clonal cells carrying either amplifications or mutations of the target kinase (Hingorani and Tuveson, 2003). To date mutations in at least 17 positions scattered through the ABL kinase domain have been associated with resistance to imatinib (Carlomagno and Santoro, 2005). Another problem associated with the use of small molecule targeted therapies is to identify patients for which the targeted treatment will be effective. For example, when gefitinib was tested in patients with non-small-cell lung cancer (NSCLC), only patients whose tumours contained the specific mutations actually responded to the treatment (Argiris *et al.*, 2006). To solve this problem, new drugs are being designed or combined with existing ones in combination therapy to target the tumour more effectively (Imai and Takaoka, 2006). One such example is the ligand-directed prodrug approach.

1.5.2 Ligand-Directed Prodrug Therapies

The use of mAb and other ligands as targeting moieties to increase the selective toxicity of cancer chemotherapeutics is now a rapidly growing area of research, with several targeted mAb already in clinical use (Table 1.6). The basic principle that underlies ligand-targeted therapy, over small molecule targeted inhibitors, is that the delivery of an antineoplastic drug to cancer cells can be selectively increased by associating the drug with a molecule that binds to receptors that are uniquely expressed or overexpressed on the target cells. This therefore allows specific delivery and binding of the drug to cancer cells and depending on the targeting ligand, internalisation *via*

Table 1.6 FDA approved monoclonal antibodies (mAb) and their corresponding molecular targets.

Drug	Toxin Attached	Target	Disease Type	Cancer Type	Year Approved
cetuximab (Erbitux)	none	EGFR	CRC and HNSCC	solid	2004
trastuzumab (Herceptin)	none	ERBB2	Breast cancer	solid	1998
bevacizumab (Avastin)	none	VEGF	CRC	solid	2004
rituximab (Rituxan)	none	CD20	B-cell lymphoma	haemato-logical	1997
ibritumomab tiuxetan (Zevalin)	Yttrium-90	CD20	B-cell lymphoma	haemato-logical	2002
tositumomab-I131 (Bexxar)	Iodine-131	CD20	B-cell lymphoma	haemato-logical	2003
gemtuzumab ozogamicin (Mylotarg)	Caliche-amicin	CD33	AML	haemato-logical	2000
alemtuzumab (Campath)	none	CD52	B-cell CLL	haemato-logical	2001

Agents are shown as generic names with trade names in parentheses. CLL: chronic lymphocytic leukaemia, CML: chronic myeloid leukemia, CRC: colorectal cancer, EGFR: epidermal growth factor receptor, NSCLC: non-small-cell lung cancer, HNSCC: head and neck squamous-cell carcinoma, VEGFR: vascular endothelial growth factor receptor.

receptor mediated endocytosis (RME) (Allen, 2002; Schrama *et al.*, 2006). In the early development phase of ligand-directed prodrug (LDP) therapy, it was believed that the tumour specificity of anticancer drugs could be improved just by linking the drugs directly to antibodies *via* amide bonds. Thus, several clinically used anticancer agents such as methotrexate, daunorubicin, vinblastine, mitomycin C, idarubicin and *N*-acetyl melphalan were linked *via* non-cleavable bonds to a number of murine mAbs (Hurwitz *et al.*, 1985; Pietersz, 1990; Pietersz and Krauer, 1994). Typically an average of 4-8 drug molecules were linked per antibody molecule, but in most cases, the conjugates lacked potency and were less cytotoxic than the unconjugated drugs themselves. Further

attempts were made to increase conjugate activity by linking a larger number of drug molecules to the antibody. But these molecules also showed reduced activity *in vitro* due to impaired receptor binding affinity (Chari, 1998). As a result, over the past decade, the significance of the chemical link between the drug and the carrier molecule in relation to its pharmacological activity has been readdressed. Now, LDPs are generally being linked to their corresponding molecular carrier through a spacer molecule which incorporates a predetermined cleavage point. This allows the bound drug to be released only at a specific location. Since the vast majority of receptor targeted drugs are delivered through the endocytic pathway, many linkers have been explored over the last decade based on their ability to be cleaved in endosomal and lysosomal compartments. The two major types of linkers that have been investigated in some detail include acid-cleavable bonds (Mueller *et al.*, 1990; Kratz *et al.*, 1999) and peptide bonds that can be cleaved by lysosomal enzymes (Subr *et al.*, 1990; Duncan and Spreafico, 1994). Both types of linkers exploit the cellular uptake mechanism for macromolecules (i.e. endocytosis) which allows the LDP to be cleaved and released specifically in intracellular cancer cell compartments and therefore exert its cytotoxic effect (Figure 1.9).

1.5.2.1 Acid-Labile Linker Systems

According to Dyba and colleagues (2004), the design of acid labile linkers useful for receptor mediated drug delivery is defined by the condition that the linker should be stable at physiological pH, but hydrolyse when the pH is decreased by approximately

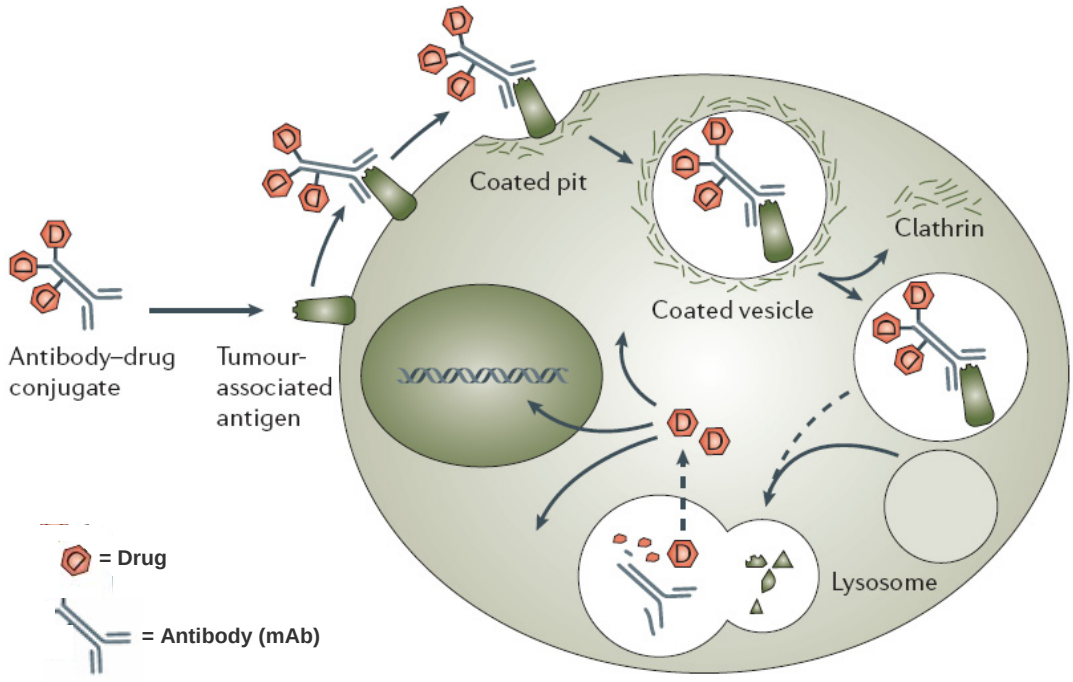

Figure 1.9 Internalisation of a ligand–drug conjugate, using a mAb as the ligand example. The cytotoxin conjugate binds to the specific tumour associated antigen and is internalised. Uptake of antibodies predominantly occurs *via* the clathrin-mediated endocytosis pathway. After binding the respective antigen associated with coated pits, antibody– drug conjugates will be readily endocytosed, from where they transit through several stages of transport and endosomal vesicles and finally end up in a lysosome. There, linkers and antibody will be cleaved releasing the cytotoxic agent which, after exit from the lysosomal compartment, exerts its cytotoxic effect. Adapted from Schrama *et al*., (2006).

one pH unit (Dyba *et al.*, 2004) This is based on the fact that after endocytosis, a significant drop in pH takes place, from a physiological pH (7.2-7.4) in the extracellular space, to pH 6.0-6.8 in the endosomes and pH 4.5-5.5 in the primary and secondary lysosomes (Bach *et al.*, 1999; Kratz *et al.*, 1999; Marsh, 2001). As a result, many acid-labile linkers that exploit the acidic environment of the endosomes and lysosomes have been designed and described in the literature (Kratz *et al.*, 1999).

1.5.2.1a Ligand-Directed Prodrugs Containing cis-Aconityl Linkers

One of the first acid-labile linkers to be reported was a *cis*-aconityl spacer (Figure 1.10a) between daunomycin and a series of macromolecular carriers in 1981 (Shen and Ryser, 1981). Here the hydrolysis half-life of the linker was reported to be less than 3 h at pH 4.0 but more than 96 h at pH 7.0. Shen and Ryser (1981) then demonstrated the importance of the acid-sensitive nature of the *cis*-aconityl bond for biological activity, by comparing the inhibitory effect of a poly-D-lysine daunorubicin conjugate with an analogous conjugate that did not contain an acid-sensitive spacer, *in vitro*. Consequently, the proliferation of leukemic cells treated with the daunorubicin conjugate that contained the *cis*-aconityl bond was significantly inhibited, while cells that were treated with the non-cleavable *N*-maleyl spacer were not (Shen and Ryser, 1981). One year later, a more successful method of conjugating doxorubicin to carrier molecules was developed and involved the use of an acid-labile hydrazone linker (Laguzza *et al.*, 1989; Greenfield *et al.*, 1990) (Figure 1.10b).

1.5.2.1b Ligand-Directed Prodrugs Containing Carboxylic Hydrazone Linkers

In general, doxorubicin prodrugs containing hydrazone linkages have shown *in vitro* toxicity similar to free doxorubicin against lymphoma cell lines, but have been twice as efficient in releasing doxorubicin than their *cis*-aconityl analogues (Dyba *et al.*, 2004). As a result, acid-sensitive hydrazone linkers have been used to connect a range of drugs including paclitaxel, doxorubicin, streptomycin, 5-fluorouridine, chlorambucil and vinblastine to various carrier molecules (Kratz *et al.*, 1999) and are the most extensively

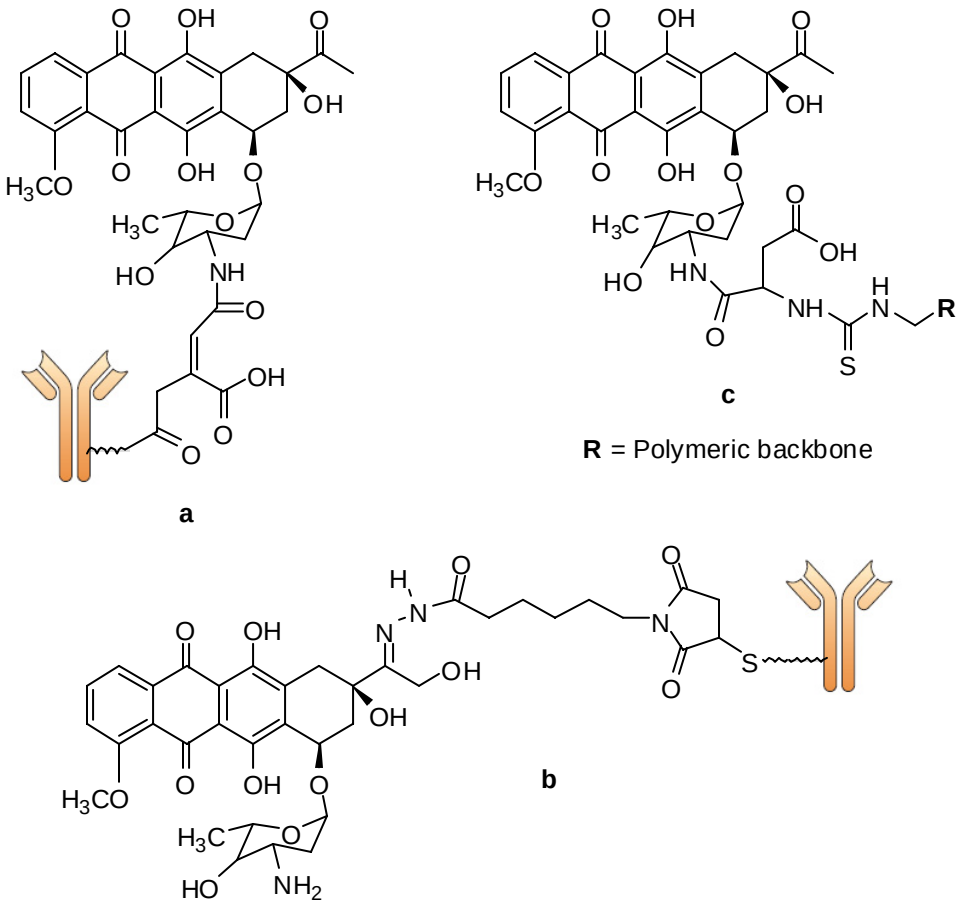

Figure 1.10 Structures of representative acid-labile drug conjugates: a) *cis*-aconitate linked daunorubicin conjugate, b) hydrazone-linked doxorubicin conjugate and c) daunorubicin conjugate containing a thiourea link.

studied acid-labile linker to date. For example, paclitaxel and doxorubicin conjugates containing hydrazone bonds to polyethylene glycol (PEG) carriers have shown good stability at pH 7.4, with less then 10% free drug released after 48 h. Reasonable cleavage times at pH 4.0-5.0 have also been reported, with half lives ranging from 28 h for paclitaxel to 2 h for doxorubicin (Rodrigues *et al.,* 1999a; Rodrigues *et al.,* 1999b; Rodrigues *et al.,* 2003). However, *in vitro* experiments against many tumour cell lines have shown a 2 to 40 fold decrease in activity when compared to the free drug

(Rodrigues *et al.,* 1999a). Despite this, a hydrazone linker has been used successfully in the targeted drug, gentuzumab ozogamicin (Mylotarg, Figure 1.7), designed for the treatment of acute myeloid leukemia (Sievers *et al.*, 1999). In spite of the slow hydrolysis of the hydrazone linker in plasma, it still appears to be the most effective among acid-labile linkers and can be particularly useful for the attachment of toxins with relatively low potency, to the ligands of surface receptors that are expressed at relatively high densities on cancer cells.

1.5.2.1c Esters

Because of their hydrolytic sensitivity and high risk of enzymatic cleavage in circulation, ester linkers are generally not used in the construction of prodrugs (Dyba *et al.*, 2004). An example of the lability of esters is illustrated in a paper by Guo and colleagues (2001), whereby gemcitabine conjugated to a peripheral benzodiazepine receptor ligand connected through a succinic acid moiety was used to target brain cancer. It was shown that the prodrug with the ester bond between gemcitabine and succinic acid was unstable in serum with a half life of approximately 5 minutes. Similarly, taxol connected to octo-arginine amide derivatives through an ester bond, was liberated at pH 7.4, with a half life of between 1 and 21 minutes (Kirschberg *et al.*, 2003). Other reports on the instability of ester bonds in circulation have also been published (See review by Dyba *et al.,* 2004). However, a study involving the use of 5-FUdr conjugated to a murine anti-Ly-2.1 mAb through an ester-based succinate linker has shown promising results *in vitro* (Goerlach *et al.*, 1991).

1.5.2.1d Other Acid-Labile Linkers

Other acid-sensitive bonds that have been studied in some depth include trityl, silyl ether, phosphamide and thiocarbamoyl (Figure 1.10c) linkers (Chari, 1998), but these will not be discussed in further detail, as they are beyond the scope of this thesis. Surprisingly, ligand-directed prodrugs containing imine bonds, that from a chemical viewpoint are classic examples of acid sensitive linkers (Hermanson, 1996), have been investigated in only a few cases (Kratz *et al.,* 1999).

1.5.2.2 Lysosomally Degradable Linkers

In addition to the acidic environment, LDPs that are internalised and delivered to lysosomes are also exposed to many lysosomal proteases (Dyba *et al.,* 2004). As a result, peptide linkers have been designed to contain specific sequences that are recognised by lysosomal proteases (such as cathepsin B and D), which release the cytotoxin after internalisation and cleavage. Cathepsin D is one of the most abundant lysosomal aspartic proteases and cleaves between two hydrophobic (preferably aromatic) residues and requires at least a pentapeptide substrate for cleavage (Authier *et al.*, 2002). Despite this, examples of LDPs containing shorter peptide linkers have shown promising activity *in vitro* and *in vivo*. These include, for example, a *N*-(2-hydroxypropyl)methacrylamide copolymer and a cyclic transferrin receptor nanopeptide conjugated to doxorubicin through a Gly-Phe-Leu-Gly linker (Seymour *et al.*, 1991; Schatzlein *et al.*, 2001). The LDP containing the *N*-(2-hydroxypropyl)methacrylamide copolymer aimed at the hepatocyte galactose receptor allowed the use of doxorubicin at doses that were 5 times greater than that of free drug, without detectable cardiotoxicity

(Hopewel *et al.*, 2001). A simple Gly-Gly-Gly spacer between a camptothecin analogue and a carboxymethyl dextran polymer has also proved useful as a lysosomal degradable linker (Harada *et al.*, 2000; Okuno *et al.*, 2000). The conjugate showed a steady release of the camptothecin analogue *in vivo*, which proved to be active against MX-1 human mammary xenograft tumours (Harada *et al.*, 2001).

In addition to containing an appropriate linking system that is capable of specific cleavage and cytotoxin release, the success of LDP therapies also depends upon a correctly chosen, tumour specific carrier molecule.

1.5.2.3 Carrier Molecules

1.5.2.3a Antibodies

Several types of targeting agents have been employed to direct cytotoxic moieties to cancer cells, such as antibodies, cytokines, growth factors and soluble receptors (for comprehensive reviews see Allen, 2002; Luo and Prestwich, 2002; Fracasso *et al.*, 2004). The most frequently used however, have been mAb because of their selective targeting properties in a variety of human malignancies (Fracasso *et al.*, 2004, Table 1.6). For example, mAbs have been used to target the epidermal growth factor (EGF) family of receptors (reviewed in Imai and Takaoka, 2006), as well as a variety of cell surface antigens on haematopoietic cells (Frankel *et al.*, 2003) and have been shown to be cytotoxic to cancer cells on their own, or when conjugated to clinically used drugs, bacterial/ plant toxins and radionuclides. For example the anti-CD20 mAb rituximab (Rituxan), has revolutionised lymphoma treatment (Maloney *et al.*, 1997), while the

entirely humanised mAb Trastuzumab (Herceptin) has provided new prospects for the treatment of breast cancer and is the first clinically approved mAb against an ErbB family member (ERBB2) (Carter *et al.*, 1992). Herceptin has also been reported to exhibit excellent antitumour activity, particularly when combined with the cytotoxic agents doxorubicin and paclitaxel (Cragg and Glennie, 2004) and has been approved for the treatment of patients with metastatic breast cancer who carry an increased *ERBB2* copy number.

Despite the success of a handful of FDA approved, mAb-based targeted therapies (Table 1.6), the disadvantages of using mAbs as targeting ligands for LDP therapy often outweigh their advantages. One of the problems associated with the use of antibodies in targeted cancer therapy is that mAbs that are directed to differentiation antigens on the cell surface of tumour cells are also directed to and taken up by normal cells that express the same antigens. In fact, according to Fracasso and colleagues (2004), unique tumour specific antigens have not yet been identified for most human tumours. Other problems that arise with the use of mAb drug conjugates include poor penetration into tumours due to their relatively large molecular size (Imai and Takaoka, 2006). Although this can be overcome by utilising truncated mAb fragments which have been shown to penetrate tumours more readily than the full-length mAb, another downfall is that their smaller size means that they are sometimes cleared from the circulation too quickly (Imai and Takaoka, 2006). One last and relatively major problem associated with the use of mAbs as targeting ligands, is that they are usually of mouse origin and are therefore immunogenic in humans. To counter this, (in addition to humanisation),

naturally existing ligands have been identified for LDP therapy and include cytokines (Ogata *et al.*, 1989; Walz *et al.*, 1989; Hoogenboom *et al.*, 1991; Chadwick *et al.*, 1993; Gould *et al.*, 1998) and growth factors (Banker *et al.*, 1989; Hirota *et al.*, 1989; Masui *et al.*, 1989; Di Massimo *et al.*, 1997; Chandler *et al.*, 1998). One naturally occurring serum protein that shows promise for targeted drug delivery and has been relatively unexplored to date, is the plasminogen activator inhibitor type 2 (PAI-2), a key regulator of the urokinase plasminogen activation system.

1.5.2.3b PAI-2 and the Urokinase Plasminogen Activation System

The urokinase plasminogen activation system is an extracellular proteolytic cascade mechanism that is involved in a range of cellular processes, including matrix degradation, fibrinolysis and a number of other regulatory proteolytic events (Andreasen *et al.*, 2000). The system is transiently active under normal physiological conditions and is involved in, for example, wound healing and angiogenesis (Andreasen *et al.*, 2000), but is constitutively active under pathological conditions such as cancer (Andreasen *et al.*, 1997). Recently, a large body of experimental and clinical evidence has indicated that the inappropriate over expression and activation of this system is strongly associated with tumor invasion and metastasis (Jankun, 1994; Berger, 2002a; Weigelt *et al.*, 2005). The urokinase plasminogen activation system is therefore an attractive and relatively new target for LDP therapy.

In this system the urokinase plasminogen activator (uPA) binds to its specific receptor (uPAR) and converts cell surface bound plasminogen into the serine protease plasmin

(Andreasen *et al.*, 1997; Ranson and Andronicos, 2003), which promotes tissue degradation and remodeling of the local extracellular environment (Andreasen *et al.*, 1997). Generally, uPA is secreted as a pro-enzyme (pro-uPA), with very low intrinsic activity (Nielsen *et al.*, 1982; Petersen *et al.*, 1988). Proteolytic activation of pro-uPA to the active two-chain uPA molecule is catalysed by plasmin as well as a variety of other proteases with trypsin-like specificity (Frenette *et al.*, 1997; List *et al.*, 2000). The fact that plasmin can efficiently activate pro-uPA highlights the strong positive feedback mechanism which is exploited by a variety of malignancies, including breast, lung, endometrial (Dear and Medcalf, 1995), gastrointestinal, pancreatic and colorectal cancers (Berger, 2002b).

The proteolytic activity of uPA is tightly regulated by the plasminogen activator inhibitors type 1 and type 2 (PAI-1 and PAI-2), which bind with strong affinity to soluble and receptor bound uPA (Ellis *et al.*, 1990; Kruithof *et al.*, 1995; Andreasen *et al.*, 1997; Al-Ejeh *et al.*, 2004). Although both proteins belong to the serine protease inhibitor (serpin) superfamily (Silverman *et al.*, 2001), they are functionally quite different, as their role in breast cancer invasion and metastasis are somewhat contrasting. For example, clinical studies show that uPA and PAI-1 co-expression has level one evidence as a prognostic marker of progression in early breast cancer (Duffy, 2004; Weigelt *et al.*, 2005) and is therefore associated with a poor clinical outcome (Foekens *et al.,* 1995b). In contrast, high tumour PAI-2 expression has been related to prolonged overall survival (Duffy, 2004; Duffy and Duggan, 2004). Furthermore, a number of other observations using *in vitro* and *in vivo* models have shown PAI-2 to

reduce tumour growth, invasion and metastasis *via* inactivation of cell surface uPA (Foekens *et al.,* 1995a; Kruithof *et al.,* 1995; Smith *et al.,* 2007).

To this end, the urokinase plasminogen activation system is an appealing target for the design of both small molecule inhibitors and LDPs. For example, cell invasion and metastasis could be inhibited by a small molecule antagonist that interferes with the catalytic activity of uPA, thus preventing uPA from binding to its receptor (Romer *et al.*, 2004). Or, of relevance to this study, by exploiting the uPA receptor through the binding of the inhibitors PAI-1 and PAI-2, to deliver cytotoxic agents into tumour cells. This latter strategy is achievable because both PAI-1 and PAI-2 can be internalised into cells through interactions with endocytosis receptors of the lipoprotein receptor family, such as low density lipoprotein receptor related protein (LRP) and very low density lipoprotein receptor (VLDLr) (Herz *et al.*, 1992; Kounnas *et al.*, 1993; Argraves *et al.*, 1995; Croucher *et al.*, 2006). Upon PAI-1 and PAI-2 inhibition of uPAR-bound uPA a covalent complex is formed, ultimately resulting in endocytosis (Nykjaer *et al.*, 1994; Croucher *et al.*, 2006).

Previously, PAI-1 has been exploited to deliver cytotoxic agents, such as the A-chain cholera toxin to cancer cells (Jankun, 1992), but the targeting ability of PAI-2 has not yet been extensively studied. In terms of targeting ability, PAI-2 has numerous advantages over PAI-1. Firstly, it is stable *in vitro* and *in vivo* and does not revert to an inactive form compared to PAI-1 (Ranson *et al.,* 2002b). Like PAI-1, PAI-2 is a protein of human origin and therefore does not cause an immunogenic response. Additionally,

abnormally elevated levels of PAI-2 in the plasma of women in late pregnancy (Astedt *et al.*, 1998) are not associated with toxicity, indicating that the administration of high concentrations of PAI-2 is unlikely to cause adverse side effects. To date, the only successful targeting of a toxin conjugated to PAI-2 has involved the use of the α-emitting radiolabelled isotope ^{213}Bismuth (Li *et al.,* 2002; Ranson *et al.,* 2002a; Allen *et al.,* 2003; Stutchbury *et al.,* 2007) and as yet, no small molecule, organic cytotoxins have been investigated. This suggests that known or novel cytotoxins conjugated to PAI-2 may be a new strategy to target and eradicate uPA positive metastases with minimal side effects, as localisation studies indicate that quiescent, normal and benign tissues do not express significant levels of cell surface uPA. The clinical application of PAI-2 targeted therapies could therefore be substantial.

1.6 Rationale and Project Objectives

The increased incidence of multidrug resistance (MDR) and systemic toxicity to conventional chemotherapeutic agents suggests that alternative avenues need to be explored in the hope of finding new and effective treatments for metastatic disease. Natural products have made enormous contributions to many of the anticancer agents used clinically today and as a result, the cytotoxic molluscan metabolite tyrindoleninone (**1**) as well its oxidative artifact 6-bromoisatin (**5**), were initially used as templates for drug design. Both small molecule inhibitors and LDPs have also shown much therapeutic potential in the treatment of a variety of malignancies, yet their development still requires further optimisation, as very few drugs that enter preclinical trials are ever approved for clinical use.

The specific aims of this study were therefore:

1. to synthesise the natural product (**1**) and derivatives thereof, as well as analogues of 6-bromoisatin (**5**), for cytotoxicity and SAR assessment.
2. to investigate the biological mode of action of the most active compounds using both cell-based and cell-independent approaches.
3. to determine the dose tolerance, biodistribution and efficacy of the most active, cytotoxic compound in a relevant human xenograft mouse model. And finally
4. to derivatise the cytotoxin (and for comparison, the commercial anticancer agent 2′-deoxy-5-fluorouridine (5-FUdr)) for conjugation to the targeting ligand PAI-2 and assess the cytotoxicity and targeting ability of each small molecule, organic cytotoxin conjugate *in vitro*.

CHAPTER 2

General Materials and Methods

CHAPTER 2

General Materials and Methods

This chapter contains the general materials and methods for experimental procedures used throughout this thesis. Other chapter-specific materials and methods are described in the corresponding chapters.

2.1 Materials

2.1.1 Chemicals

All organic solvents used were AR grade and either obtained from Unichrom (APS Ltd., USA) or Sigma-Aldrich (Sigma-Aldrich Chemicals MO, USA). Buffers and reagents are described in corresponding chapters.

2.1.2 Cells Lines and Culture Reagents

The human lymphoma (U937), leukemic (Jurkat), breast carcinoma (MDA-MB-231 and MCF-7), prostate carcinoma (PC-3), colorectal carcinoma (HCT-116) and melanoma (A-375) cell lines were all obtained from American Type Culture Collection (ATCC, VA, USA) distributed by Cryosite, NSW, Australia. RPMI-1640 was purchased from Gibco™ (Invitrogen Life Technologies, NSW, Australia). Foetal calf serum (FCS) was obtained from MultiSer™ (ThermoTrace, VIC, Australia). Sodium bicarbonate was purchased from Univar Analytical Reagents (Ajax Chemicals, Australia.). Trypsin-

EDTA solution and propidium iodide (PI) were purchased from Sigma-Aldrich (MO, USA). Lymphoprep™ was obtained from Pharmacia (Biotech, Australia) and the CellTiter 96® AQueous One Solution Cell Proliferation Assay and Apo-ONE® Homogeneous Caspase-3/7 Assay were purchased from Promega Co. (Madison, WI, USA).

2.2 General Organic Chemistry Methods

Dichloromethane (DCM) was LR grade and distilled before use. The term petroleum spirit (pet. spirit) refers to pet. spirit with the boiling range of 40-60 °C. When necessary, the purification of solvents and starting materials was carried out using standard procedures. Organic solvents were dried with anhydrous sodium sulfate and removed under reduced pressure (*in vacuo*) by a Büchi rotary evaporator. All solvent mixtures were v/v. NMR spectra were measured at 300 MHz (^{1}H NMR) and 75 MHz (^{13}C NMR) on a Varian Unity-300 spectrometer or at 500 MHz (^{1}H NMR) and 126 MHz (^{13}C NMR) on a Varian Inova-500 spectrometer with a probe temperature of 298K. The NMR spectra were referenced to the residual solvent peak of the solvent, as stated in the individual procedures. Hydrogen and carbon assignments were made using standard NOE, DEPT, gCOSY, gHSQC and gHMBC spectroscopic techniques. Low resolution EI mass spectra (LR EIMS) were determined on a Shimadzu QP5050 spectrometer. High resolution EI mass spectra (HR EIMS) were determined on VG Autospec spectrometer operating at 70 eV with a source temperature of 250 °C and were referenced with PFK. Melting points were determined on a Reichert melting point

apparatus and are uncorrected. Chromatography using Merck Kieselgel 60 silica gel (230-400 mesh) was performed under medium pressure as described by (Still *et al.*, 1978). Preparative thin layer chromatography (PTLC) was performed on either Merck Silica gel 60 F_{254} or Alumina F_{254} on aluminium sheets and the compounds were detected by examination under ultraviolet (UV) light and/ or iodine vapour.

2.3 General Cell and Protein Analysis Methods

2.3.1 Cell Lines and Tissue Culture

2.3.1.1 Human Cancer Cells

Cell lines were routinely cultured at 37 ºC in a Heracell incubator (Kendro Laboratory Products, Langenselbold, Germany) in 95% humidified atmosphere, containing 5% CO_2. Cells were grown in culture media (10.4 g/L RPMI-1640 with 2 mM L-glutamine and 2 g/L $NaHCO_3$) supplemented with 5% (v/v) foetal calf serum (FCS), and routinely passaged at confluency for up to 20 passages. Adherent cell lines were detached using sterile trypsin-EDTA, washed with culture media and centrifuged at 1500 rpm (514 × *g*) for 5 min at room temperature (RT) before reseeding. Cell lines were routinely tested for Mycoplasma.

All cell experiments were performed using cells in exponential growth, passaged 48 h before without change of media. Adherent cells were detached prior to experiments with sterile 1 × phosphate buffered saline (PBS) containing 5 mM EDTA (pH 7.4). Detached

cells and suspension cell lines were centrifuged at 1500 rpm (514 × *g*) for 5 min at RT. Cell viability and cell number were assessed by the trypan blue exclusion method and viable cells counted with the aid of a hemocytometer.

2.3.1.2 Untransformed Human Cells

2.3.1.2a Blood Collection

Samples of human blood were collected by a clinical nurse (Department of Biomedical Sciences, University of Wollongong) using standard procedures (Human ethics No. 46). Typically, peripheral blood was drawn into a $21G^{11/2}$ syringe and deposited into sterile tubes coated with EDTA. All blood samples were used on the day of collection.

2.3.1.2b Isolation of Human Mononuclear Cells (MNC): Density Centrifugation

Lymphoprep™ (Pharmacia Biotech, Australia, 7 mL) was carefully layered beneath fresh, human, peripheral blood (10 mL) that had been diluted 1:2 in PBS (pH 7.4). The preparation was then centrifuged (Heraeus megafuge) at 1800 rpm (800 × *g*) for 20 min at RT. After centrifugation the top diluted plasma layer was carefully removed and discarded. The opaque layer, at the interface, containing mononuclear cells (MNC) was collected and placed into a sterile tube. Collected cells were then washed twice with PBS by centrifugation at 1800 rpm (800 × *g*) for 30 min at RT and the supernatant discarded. Pelleted cells were finally resuspended in 2 mL of complete media RPMI-1640 supplemented with 5% FCS.

2.3.2 Cell Viability Assays

2.3.2.1 MTS Assay

The ability of test compounds to alter cellular proliferation or induce cytotoxicity was measured using the colourimetric CellTiter 96® AQueous One Solution Cell Proliferation Assay, (MTS assay). The CellTiter 96® AQueous One Solution Reagent contains the tetrazolium compound (3-(4,5-dimethylthiazol-2-yl)-5-(3-carboxymeth-oxyphenyl)-2-(4-sulfophenyl)-2*H*-tetrazolium, inner salt, MTS) which is bio-reduced by dehydrogenase enzymes in metabolically active cells into a coloured formazan product (Figure 2.1). The quantity of formazan produced is directly proportional to the number of living cells in culture.

The MTS cell proliferation assay was performed in 96-well microplates, as described previously (Cory *et al.*, 1991). Briefly, cells (1.0×10^4) in a total volume of 90 μL of complete media were seeded into 96-well microtitre plates and incubated for 24 h (37 ºC, 95% humidity, 5% CO_2) prior to the addition of test compounds. Test compounds were made up fresh on the day of testing in dimethyl sulfoxide (DMSO, 100%) at a final concentration of 4 mg/mL and diluted in complete media to give a final DMSO concentration of 25%. Compounds of various concentrations (10 μL) were then added in triplicate to the wells of a 96-well microtitre plate, containing cells, to give a final volume of 100 μL. Solvent controls containing 2.5% DMSO and background controls containing test compounds, but no cells, were also prepared. Cells were incubated for a further 24 h (37 ºC, 95% humidity, 5% CO_2). The MTS assay substrate

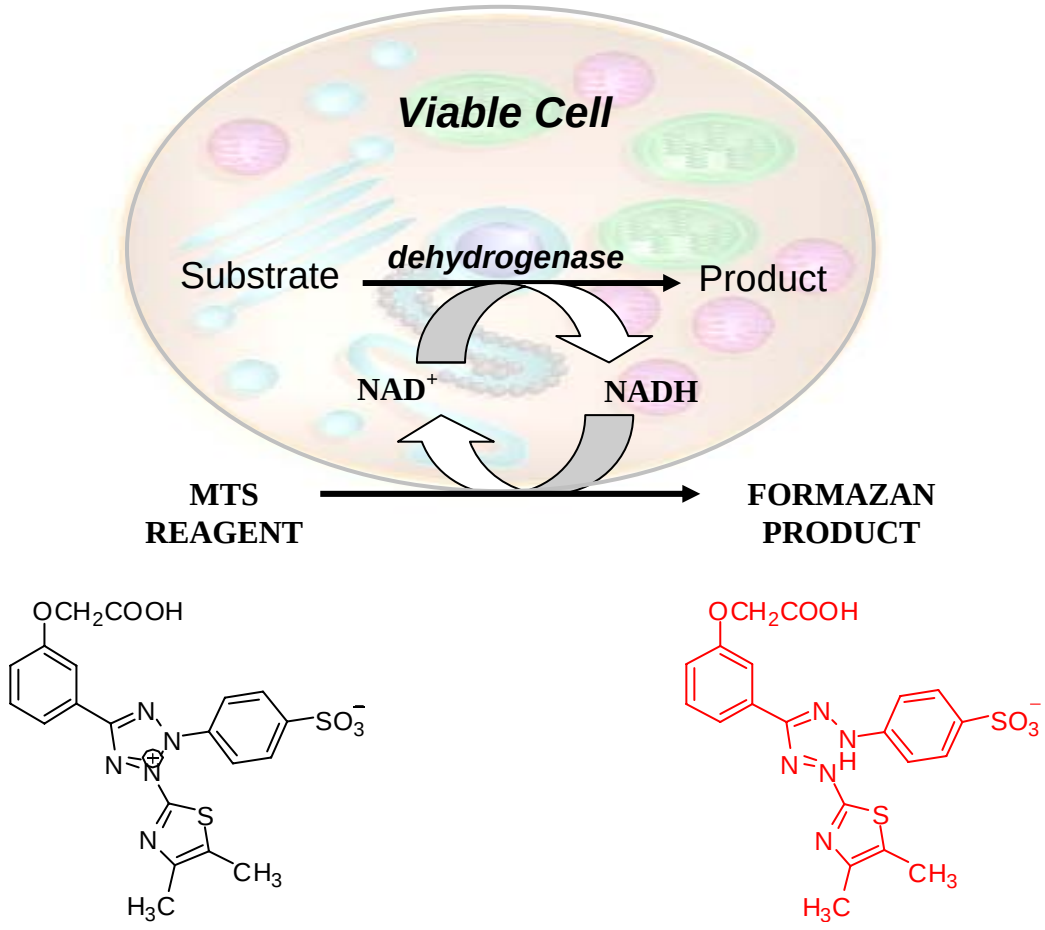

Figure 2.1 Cellular conversion of the CellTiter 96 Aqueous One Solution Cell Proliferation Assay Reagent. MTS tetrazolium [3-(4,5-dimethylthiazol-2-yl)-5-(3-carboymethoxyphenyl)-2-(4-sulfophenyl)-2*H*-tetrazolium, inner salt] is actively bioreduced to the red coloured formazan product by viable cells. Adapted from Promega Technical Bulletin (2006).

(20 µL) was then added to each well and cells incubated for 3 h to allow colour development. The absorbance at 490 nm was measured using the Spectromax® 250 UV plate reader (Molecular Devices, USA) utilising Softmax Pro® software. All cell

proliferation assays were performed using the number of cells which fell in the linear range.

2.3.2.2 Propidium Iodide (PI) Staining and Flow Cytometry

Loss of membrane integrity in cell populations was measured by flow cytometry using the fluorescent nuclear stain, propidium iodide (PI). Cells were harvested by centrifugation (1700 rpm) in a Beckman Coulter GS-6R centrifuge (USA) for 5 min at 4 ºC in a microplate carrier, washed with ice cold 0.22 μm filtered PBS (pH 7.4) and then resuspended at a cell density of 1.0×10^6 cells/mL. PI at 1 mg/mL was added to the cell suspension to give a final concentration of 5 μg/mL, just prior to analysis by a FACSort Flow Cytometer (Becton Dickinson, USA). Loss of membrane integrity was measured as a large increase in cell associated red fluorescence (FL2), and granularity (SSC) and a decrease in size (FSC). Viable cell populations were gated in control samples and the percentage of viable cells to non-viable cells calculated for treated samples.

2.3.3 Apoptosis Detection Systems

2.3.3.1 Caspase-3/7 Assay

Induction of apoptosis and activation of caspases can result from a variety of stimuli including chemotherapeutic agents, which bring about systemic structural disassembly of dying cells. The activation of effector caspases 3 and 7 was determined in Jurkat cells

after incubation with test compound or 2 μM staurosporine (positive control) using the Apo-ONE Homogeneous Caspase-3/7 Assay kit and was performed using a modification to that described previously (Carrasco *et al.*, 2003). Briefly, cells (2.0×10^4) in a total volume of 90 μL of complete media were seeded into 96-well microtitre plates and increasing concentrations of test compound added. After 5 h incubation (37 ºC, 95% humidity, 5% CO_2), 50 μL of supernatant was taken from each well and transferred to a black 96-well plate (Greiner Bio-One, Interpath Aust.) and an equivalent volume of caspase reagent added. The reagent was made up fresh by diluting the substrate 1:100 with the buffer. Cells were then mixed at 300-500 rpm for 1 h at room temperature. The caspase-3/7 substrate rhodamine 110, *bis*-(N-CBZ-L-aspartyl-L-glutamyl-L-valyl-L-aspartic acid amide) Z-DEVD-R110, exists as a profluorescent substrate, whereupon cleavage and removal of the DEVD peptides by caspase-3/7 activity, becomes intensely fluorescent (Figure 2.2). The amount of fluorescent product

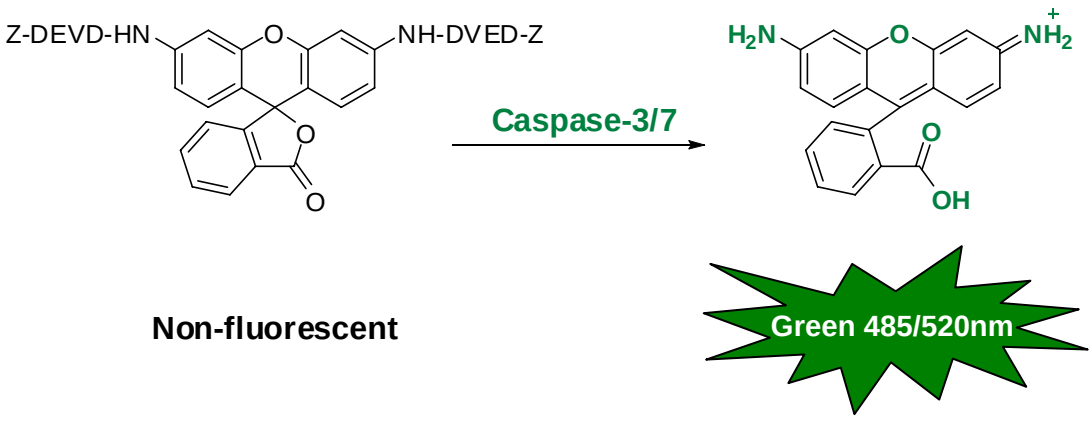

Figure 2.2 Cleavage of the non-fluorescent Caspase substrate Z-DEVD-R110 by Caspase-3/7 to create the fluorescent Rhodamine 110. Adapted from Promega Technical Bulletin (2006).

generated is proportional to the amount of caspase-3/7 cleavage activity in the sample. The fluorescence was measured using the FLUOstar fluorescence plate reader (BMG Labtech) at an excitation wavelength of 485 nm and an emission wavelength of 520 nm.

2.3.4 Protein Analysis methods

2.3.4.1 Protein Concentration Assay

The BioRad® DC protein concentration assay kit was used to determine the concentration of various protein samples against bovine serum albumin (BSA) standards. Aliquots (5 µL) of BSA standards ranging from 0-2 mg/mL and protein samples were added to the wells of a 96-well microtitre plate in duplicate. For each well, 25 µL of Reagent A and 200 µL of Reagent B were added and mixed by manual pipetting. The plate was incubated for 15 min at RT for maximal colour development and the absorbance measured at 750 nm using the Spectromax® 250 UV plate reader (Molecular Devices, USA). A standard curve was generated using the Softmax Pro® software to calculate protein concentration.

2.3.4.2 Sodium Dodecyl Sulfate –Polyacrylamide Gel Electrophoresis (SDS-PAGE)

Gel preparation for SDS-PAGE was based on the method described by (Laemmli, 1970). Unless otherwise stated, PAGE was performed using gels composed of 4% stacking gel [4% v/v of 40% acrylamide, 126 mM Tris-HCl pH 6.8, 0.1% w/v sodium dodecyl sulfate (SDS), 0.1% TEMED and 0.05% w/v ammonium persulfate (APS)] and

12% resolving gel (12% v/v of 40% acrylamide, 0.1% w/v SDS, 375 mM Tris-HCl pH 8.8, 0.1% TEMED and 0.05% w/v APS). Protein samples (~2 μg) were prepared in a final volume of 20 μL of PBS (pH 7.4) and denatured prior to loading by boiling for 5 min with 5 μL of 5 × non-reducing sample buffer (60 mM Tris-HCl, 2% w/v SDS, 10% v/v glycerol, 0.01% w/v bromophenol blue). Samples (25 μL) and commercial molecular weight markers (15 μL) were fractionated by electrophoresis for 1 h at 120 V, or until the dye front had reached the bottom of the gel, in running buffer (3.03 g/L Tris, 14.4 g/L glycine and 1 g/L SDS). Gels were stained by placing in Coomassie blue stain (0.1% w/v Brilliant Blue R250, 40% v/v methanol and 10% v/v glacial acetic acid) and microwaving on high for 1 min, then cooling to RT with rocking. Gels were destained by placing in destain buffer (40% methanol and 10% glacial acetic acid) and microwaving on high for 1 min, then cooling to RT with rocking. Gels were then placed in a final destain (10% glacial acetic acid and 4% glycerol) and destained overnight with rocking. The molecular masses of the proteins were calculated from a standard curve generated from the log MW of the protein standards versus their distance migrated on the gel.

CHAPTER 3

From Tyrindoleninone to Isatin: synthesis and *in vitro* cytotoxicity evaluation of some substituted isatin derivatives

Adult Muricid molluscs *Dicathais orbita*, amongst freshly laid egg capsules, Towradgi, NSW, Australia, 2004.

CHAPTER 3

From Tyrindoleninone to Isatin: synthesis and *in vitro* cytotoxicity evaluation of some substituted isatin derivatives

3.1 Introduction

A variety of halogenated marine compounds have been found to exhibit cytotoxic and antineoplastic activity (Teeyapant *et al.*, 1993; Yamada, 2000; Nagle *et al.*, 2004) yet a large number still remain uninvestigated. Recently, the cytotoxic activity of tyrindoleninone (6-bromo-2-methylthio-3*H*-indol-3-one, **1**) a brominated precursor to Tyrian purple (**2**), isolated from the egg masses of the Australian mollusc *Dicathais orbita* (Figure 3.1), was reported (Vine, 2002). Investigations into the cytotoxicity of **1** revealed greater specificity towards cancer cells (IC_{50} 4 μM) than freshly isolated, human, mononuclear cells (MNC) (IC_{50} 195 μM), *in vitro*. Although this highlights **1** to be a potential lead for anticancer drug development in the future, attempts to synthesise this compound, *de novo*, have been unsuccessful to date, despite the reported synthesis of halogenated analogues (Baker and Duke, 1972; Duke, 1974).

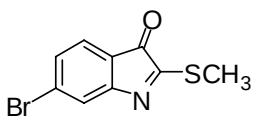

1

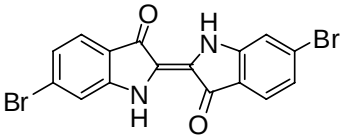

2

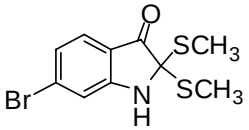

3

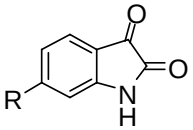

4 R = H
5 R = Br

Figure 3.1 Adult Muricid molluscs *Dicathais orbita*, amongst freshly laid egg capsules, Towradgi, NSW, Australia, 2004.

3.1.1 Reported Syntheses of Tyrindoleninone Derivatives

The reaction of 4-, 5- and 7-bromoisatin with phosphorus pentachloride (PCl_5) to produce 2-methythioindoleninone analogues of **1** (Scheme 3.1) has been reported to proceed with little difficulty (Baker and Duke, 1972). In 1973 Baker and Duke reported the partial synthesis of **1** by decomposition of 6-bromo-2,2-dimethylthio-indoleninone (**3**), obtained from the hypobranchial glands of *D. orbita* in refluxing toluene. Complete synthesis of **1** from 6-bromoisatin (**5**) however, has not been described using this method and the lack of solubility of **5**, in a range of solvents, is predicted to be the primary cause (Duke, 1974). The instability of the intermediates has also been problematic and in most cases substituted '2-chloroindoleninones' are not fully characterised or purified as they readily hydrolyse (Moriconi and Murray, 1964;

Cornforth *et al.*, 1996) or decompose completely on standing overnight (Grimshaw and Begley, 1974). In addition, Baker and Duke (1972) report the instability of the final product (**1**), stating that the red spot on TLC (alumina, benzene) decomposed in air and light to form the purple compound, **2**. These observations were further supported by Benkendorff (1999). This is not surprising as the indoleninone nucleus is highly reactive and susceptible to oxidation and nucleophilic attack at C2. As a result, indoleninone has not been isolated, although it has been proposed as an intermediate in the production of indigotin (Baker and Duke, 1972).

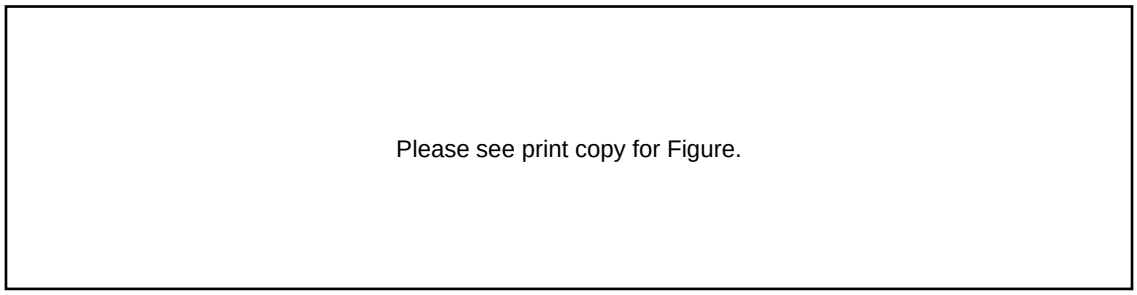

Scheme 3.1 Method of synthesis of tyrindoleninone derivatives from isatin as reported by Baker and Duke (1972).*

3.1.2 Isatins as Anticancer Agents

Looking to other less reactive, biologically active compounds in the egg masses of the muricid *D. orbita,* we find 6-bromoisatin (**5**), a major decomposition product formed through the oxidation of tyriverdin and tyrindoleninone (Benkendorff *et al.*, 2001). It has been established that **5** also has anticancer activity against a human lymphoma cell line (IC_{50} 0.02 mg/mL), but was not as active as **1** (Vine, 2002). This is not altogether surprising as isatin (**4**) itself, an endogenous compound identified in many organisms,

* N.B. The 2-(2,2-dichloro-2,3-dihydro-3-oxoindol-1-yl)-3*H*-indol-3-one intermediate is described by Cornforth *et. al.*,1996.

possesses a wide range of biological activities, including anxiogenic (Bhattacharya and Chakraborti, 1998), sedative and anticonvulsant effects (McIntyre and Norman, 1990). Isatin has also been described to act as a potent antagonist on atrial natriuretic peptide (ANP) receptors *in vitro* (Bhattacharya *et al.,* 1988) and is the most potent monoamine oxidase (MAO) inhibitor *in vitro* reported to date (Glover, 1998). In particular, halogenated derivatives derived from isatin have been reported to exhibit anticancer activity (Eshba and Salama, 1985). For example, 5-bromo-3-*o*-nitrophenyl isatin hydrazone (Figure 3.2a) was found to be active intramuscularly against Walker carcinoma-256 (Pajouhesh *et al.,* 1983) and a series of 5-bromo-(2-oxo-3indolinyl)thiazolidine-2,4-diones (Figure 3.2b) substituted by various Mannich bases were found to exhibit antileukaemic activity against P388 lymphocytic leukaemia in mice (Eshba and Salama, 1985). Recently, SU11248 (Sutent), a 5-fluoro-3-substituted-2-oxoindole (Figure 3.2c) was approved by the US FDA for the treatment of gastrointestinal stromal tumors (GIST) (Prenen *et al.*, 2006) and advanced renal-cell carcinoma (Motzer *et al.*, 2006).

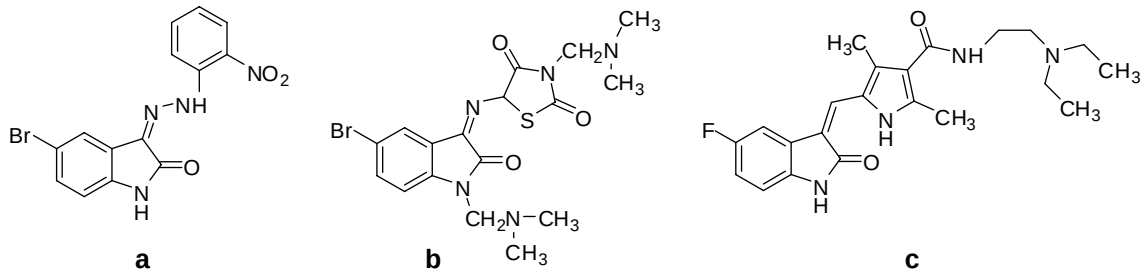

Figure 3.2 Some halogenated derivatives of isatin with reported anticancer activity.

3.1.3 Rationale and Aims

Based on previous studies (Vine, 2002), the synthesis of the natural product (**1**) and its analogues were investigated with the view of obtaining sufficient material for cytotoxicity assessment. The aims of the current study were therefore to synthesise a derivative of the natural product, 2-methylthioindoleninone (**29c**) from isatin (**4**) based on the method of Baker and Duke (1972) and compare the cytotoxicity to that of **1**. Secondly, to successfully synthesise **1**, through methylation of the thioamide intermediate using Lawesson's reagent and confirm its activity against the human monocyte-like, histiocytic lymphoma cell line, U937.

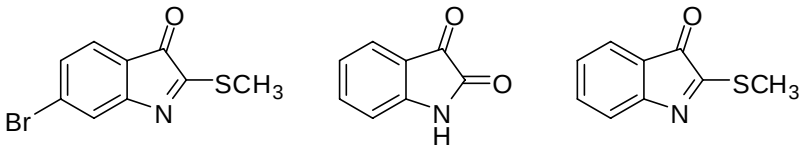

1 **4** **29c**

In a parallel study, a range of stable analogues based on the isatin scaffold were synthesised or obtained commercially (Figure 3.3). By screening for cytotoxic activity against a panel of cancer cell lines, aspects of the structure activity relationship (SAR) were also determined. Since it is proposed that some isatins inhibit cell proliferation and promote apoptosis (Cane *et al.*, 2000), the ability of selected isatins from those synthesised to activate effector caspases 3 and 7 and to inhibit cyclin dependent kinase 2 (CDK2) was also investigated to determine a possible mode of action.

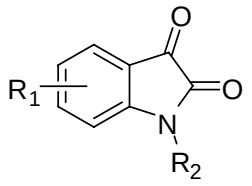

4 R_1 = H, R_2 = H
5 R_1 = 6Br, R_2 = H
6 R_1 = 4Br, R_2 = H
7 R_1 = 5Br, R_2 = H
8 R_1 = 7Br, R_2 = H
9 R_1 = 5F, R_2 = H
10 R_1 = 5I, R_2 = H
11 R_1 = 5NO_2, R_2 = H
12 R_1 = 5OCH_3, R_2 = H
23 R_1 = H, R_2 = CH_3

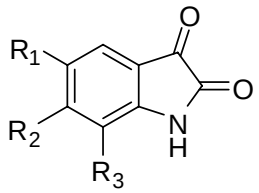

13 R_1 = Br, R_2 = H, R_3 = Br
14 R_1 = Br, R_2 = Br, R_3 = H
15c R_1 = I, R_2 = H, R_3 = I
16 R_1 = Br, R_2 = H, R_3 = NO_2
17 R_1 = NO_2, R_2 = Br, R_3 = H
18 R_1 = NO_2, R_2 = H, R_3 = Br
19 R_1 = Br, R_2 = Br, R_3 = Br

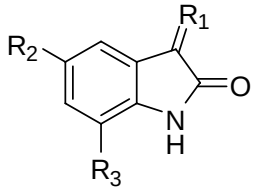

20 R_1 = N-C_6H_5, R_2 = H, R_3 = H
21 R_1 = N-C_6H_5, R_2 = Br, R_3 = Br
22 R_1 = N-NHC_6H_5, R_2 = Br, R_3 = Br

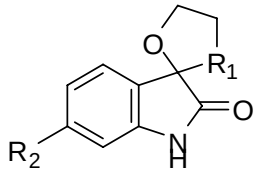

24 R_1 = O, R_2 = H
25 R_1 = O, R_2 = Br
26 R_1 = S, R_2 = H

Figure 3.3 Chemical structures of the isatin-based compounds **4-26** that were screened for cytotoxic activity in this study.

3.2 Materials and Methods

3.2.1 General

Phosphorus pentachloride (PCl_5) was purchased from Sigma-Aldrich. 4-Bromoisatin (**6**), 6-bromoisatin (**5**), and 7-bromoisatin (**8**) were purchased from Butt Park Ltd, UK. 5-Iodoisatin (**10**) (98%) and 5-fluoroisatin (**9**) (98%) were obtained from Alfa Aesar. 5-Methoxyisatin (**12**) was purchased from the Tokyo Kasei Kogyo Co. Ltd. Isatin (**4**)

(98%), 5-bromoisatin (**7**) (90%) was obtained from Sigma-Aldrich. Compound **7** was purified by successive crystallisations from absolute ethanol and the purity confirmed using ^{1}H NMR spectroscopy and melting point. 5,7-Dibromoisatin (**13**), 5,6-dibromoisatin (**14**), 5,6,7-tribromoisatin (**19**), 3-(phenylimino)-2-indolinone (**20**), 5,7-dibromo-3-(phenylimino)-2-indolinone (**21**), isatin-3-phenylhydrazone (**22**), *N*-methylisatin (**23**), spiro[1,3-dioxolane-2,3′-[3*H*]-indol]-2′(1′*H*)-one (**24**), 6′-bromo-spiro[1,3-dioxolane-2,3′-[3*H*]in-dol]-2′(1′*H*)-one (**25**) and spiro[3*H*-indole-3,2′-[1,3]oxathiolan]-2(1′*H*)-one (**26**), were supplied by Dr. Julie M. Locke, Postdoctoral Research Fellow, Department of Chemistry, University of Wollongong. Reactions were monitored using thin layer chromatography (TLC) on aluminum backed pre-coated silica gel 60 F_{254} plates (E Merck). In general isatins are highly coloured and were visible on a TLC plate; colourless compounds were detected using UV light (λ365 nm or λ254 nm) and/or iodine vapor. Flash chromatography (Still *et al.*, 1978) was carried out using Merck silica gel 60 (230-400 mesh) with the solvent system indicated in the individual procedures. All solvent ratios are quoted as vol/vol (v/v). Solvents were removed by rotary evaporation under vacuum using a Büchi rotary evaporator. Full characterisation data is included for known compounds where this data is incompletely reported in the literature. For details on MS, NMR spectra and ^{1}H and ^{13}C NMR assignments see Chapter 2 Materials and Methods, Section 2.2.

3.2.2 Chemical Synthesis

3.2.2.1 Attempted Synthesis of 2-methylthioindoleninone (29c)

The attempted synthesis of **29c** was carried out according to Scheme 3.2.

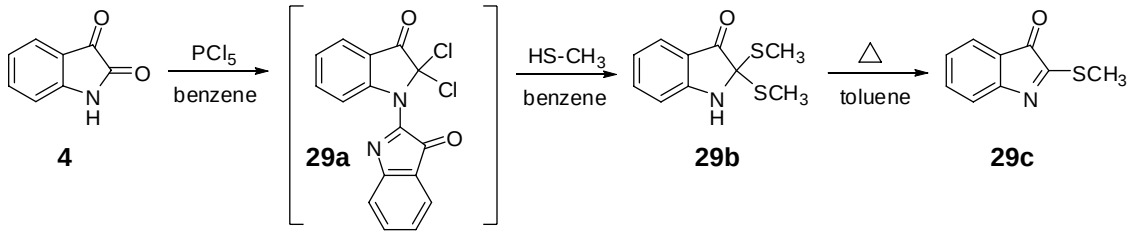

Scheme 3.2 Proposed method for the synthesis of 2-methylthioindoleninone (**29c**) based on the method reported by Baker and Duke (1972).

*2-(2,2-Dichloro-2,3-dihydro-3-oxoindol-1-yl)-3H-indol-3-one (**29a**)*

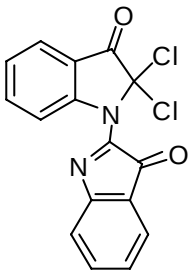

29a

The synthesis of 2-(2,2-dichloro-2,3-dihydro-3-oxoindol-1-yl)-3*H*-indol-3-one (**29a**) was modified from the method reported by Baker and Duke (1972). To isatin (**4**, 2.0 g, 14 mmol) was added anhydrous benzene (60 mL) and phosphorus pentachloride (2.6 g, 12 mmol). The mixture was heated at reflux for 6 h, then evaporated to dryness and the residue crystallised from benzene (60 mL) to give crude **29a** as red-brown crystals (0.063 g, 2.8 %), Rf 0.7 (alumina, benzene). Because of the instability of this intermediate, compound **29a** was used in the proceeding reaction without further characterisation.

*Attempted synthesis of 2,2-dimethylthioindolin-3-one (**29b**)*

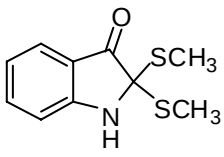

29b

The synthesis of 2, 2-dimethylthioindolin-3-one (**29b**) was modified from the method reported by Baker and Duke (1972). To crude **29a** (5.0 g) in benzene (70 mL), sodium thiomethoxide in HCl/ diethyl ether (8 mL, 10%) was added. After stirring at room temperature (15 min) the solution

was evaporated to give only the starting material **4** as evidenced by TLC (R_f 0.43, silica, 9:1 DCM/methanol). None of the product (**29b**) could be detected.

3.2.2.2 Attempted Synthesis of Tyrindoleninone (1) and Brominated Derivatives

The attempted synthesis of tyrindoleninone (**1**) from 6-bromoisatin (**5**) and brominated derivatives of **1** from 4-bromoisatin (**6**) and 5-bromoisatin (**7**) was carried out by Dr. Julie Locke using the general method described by Baker and Duke (1972). Results are discussed in Section 3.3.1.

3.2.2.3 Attempted Synthesis of Tyrindoleninone (1) *via* Methylation of a Thioamide Intermediate

The attempted synthesis of tyrindoleninone (**1**) *via* this novel method (Scheme 3.3) was performed by Dr. Julie Locke and results are discussed in Section 3.3.1.

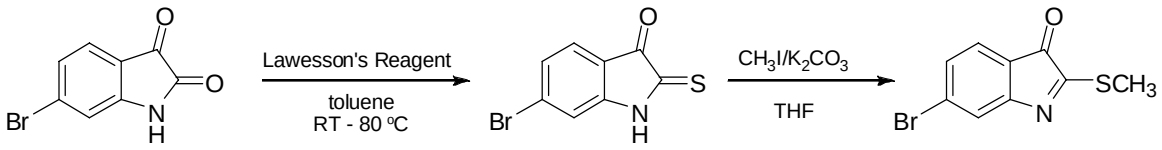

Scheme 3.3 Proposed method for the synthesis of tyrindoleninone (**1**).

3.2.2.4 Synthesis of Substituted Isatin Derivatives

*5-Nitroisatin **(11)***

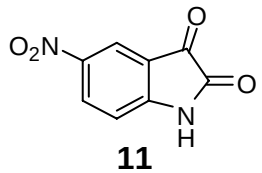

11

Nitration of isatin was based on a reported general method (Calvary *et al.*, 1925). A solution of isatin (**4**, 500 mg, 3.4 mmol) in conc. H_2SO_4 (3.2 mL) was added dropwise to a solution of KNO_3 (344 mg, 3.4 mmol) in conc. sulfuric acid (3.8 mL) over a period of 1 h whilst maintaining the temperature between 0 and 4 °C. The reaction mixture was then poured into 25 mL of ice water and the precipitate collected and washed with water. The crude 5-nitroisatin was purified by flash chromatography eluting with DCM:MeOH (98:2). The product was a bright yellow/orange solid (350 mg, 47%), mp 252-254 °C (lit. 254-255 °C, (Calvary *et al.*, 1925)), R_f 0.49 (silica, DCM:MeOH, 98:2). ^{1}H NMR (DMSO-d_6, 500 MHz) δ 7.07 (d, J = 9 Hz, 1H, H7), 8.18 (d, J = 2 Hz, 1H, H4), 8.78 (dd, J = 2, 9 Hz, 1H, H6), 10.92 (br s, 1H, NH). ^{13}C NMR (DMSO-d_6, 126 MHz) δ 113.2, 118.8, 120.3, 133.8, 143.3, 156.0, 160.6, 183.1. LREI-MS *m/z* 192 ($[M]^+$).

*5-Bromo-7-nitroisatin **(16)***

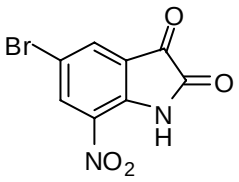

16

5-Bromo-7-nitroisatin (**16**) was prepared from 5-bromoisatin (**7**, 1.0 g, 4.4 mmol) using a previously reported method (Polychronopoulos *et al.*, 2004), with the only modification being the use of KNO_3 in the place of $NaNO_3$. The crude product was purified using flash chromatography. The crude mixture was adsorbed on to silica to load and eluted with DCM to yield **16** as a bright yellow solid (703 mg, 59%), mp 246-248 °C (lit. 244-245 °C (Sawicki *et al.*, 1959)), R_f 0.25 (DCM: MeOH, 98:2). ^{1}H NMR

(DMSO-d_6, 500 MHz) δ 8.11 (s, 1H, H4), 8.42 (s, 1H, H6), 11.82 (s, 1H, NH). ^{13}C NMR (DMSO-d_6, 126 MHz) δ 113.9, 124.0, 133.1, 133.2 (C4), 133.3 (C6), 144.8, 160.3 (C2), 180.9 (C3). LREI-MS *m/z* 270/272 ($[M]^+/[M+2]^+$).

*6-Bromo-5-nitroisatin (**17**)*

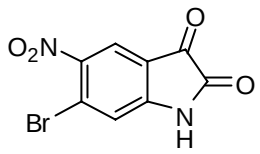

17

This di-substituted isatin was synthesised from 6-bromoisatin (**5**, 100 mg, 0.4 mmol) using the method for the preparation of **16** (Polychronopoulos *et al.*, 2004). Pure **17** was isolated from the crude reaction mixture by flash chromatography by adsorbing the crude product onto silica to load the sample and then eluting with DCM. The product **17** was obtained as a bright yellow solid (80 mg, 67%), mp 251-253 °C, R_f 0.33 (DCM: MeOH, 9:1). ^{1}H NMR (DMSO-d_6, 300 MHz) δ 7.29 (s, 1H, H7), 8.15 (s, 1H, H4), 11.57 (s, 1H, NH). ^{13}C NMR (DMSO-d_6, 75 MHz) δ 117.2 (C7), 117.5, 121.8 (C4), 123.6, 144.4, 153.0, 159.7 (C2), 181.7 (C3). HREI-MS *m/z* calcd for $[M+2]^+$ $C_8H_3{}^{81}BrN_2O_4$: 271.9256; found 271.9262.

*7-Bromo-5-nitroisatin (**18**)*

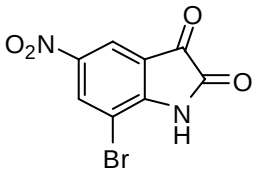

18

7-Bromo-5-nitroisatin (**18**) was synthesised using the method for the preparation of **16** (Polychronopoulos *et al.*, 2004). To a solution of KNO_3 (44.7 mg, 0.44 mmol) in conc. H_2SO_4 (760 µL) was added drop wise a solution of 7-bromoisatin (100 mg, 0.44 mmol) in conc. H_2SO_4 (640 µL) for a period of 1 h at 0 °C. The reaction mixture was then poured onto ice (5 mL) and the precipitate collected *via* filtration and washed with

water. Pure **18** was isolated from the crude mixture by flash chromatography. The crude product was adsorbed onto silica to load and eluted with DCM. The product **18**, was a bright yellow solid (71 mg, 60%), mp 215-217 °C, R_f 0.19 (DCM: MeOH, 98:2). ^{1}H NMR (DMSO-*d6*, 500 MHz) δ 8.18 (d, *J* = 2 Hz, 1H, H4), 8.62 (d, *J* = 2 Hz, 1H, H6), 11.94 (s, 1H, NH). ^{13}C NMR (DMSO-*d6*, 126 MHz) δ 105.1, 117.8 (C4), 118.9, 120.5, 135.5 (C6), 143.6, 161.2 (C2), 182.9 (C3). HREI-MS *m/z* calcd for $[M+2]^+$ $C_8H_3{}^{81}BrN_2O_4$: 271.9256; found 271.9253.

*5'-Iodo-spiro[1,3-dioxolane-2,3'-[3H]indol]-2'(1'H)-one (**15a**)*

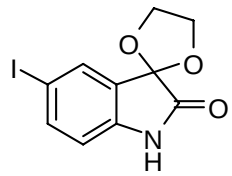

15a

This compound was prepared from 5-iodoisatin (**10**) in accordance with the literature method (Rajopadhye and Popp, 1988). The crude product was partially purified by flash chromatography (9:1 - 7:3 pet. spirit/ethyl acetate) and the resulting yellow solid was crystallised from ethanol to afford **15a** as a colourless solid (0.68 g, 43%), mp172-174 °C (lit. 173-175 °C (Rajopadhye and Popp, 1988)), R_f 0.35 (DCM: MeOH, 95:5). ^{1}H NMR (CD_3OD, 500 MHz) δ 4.28 (AA'BB' m, B signal, 2H, $H4_B$ and $H5_B$), 4.43 (AA'BB' m, A signal, 2H, $H4_A$ and $H5_A$), 4.86 (br s, 1H, NH), 6.66 (d, *J* = 8 Hz, 1H, H7'), 7.59 (d, *J* = 8, 2 Hz, 1H, H4'), 7.64 (dd, 1H, *J* = 2, 8 Hz, H6'). ^{13}C NMR (CD_3OD, 126 MHz) δ 66.0 (C4, C5), 84.4, 102.0, 112.7, 127.6, 133.8, 140.3, 142.6, 175.3. LREI-MS *m/z* 317 ($[M]^+$).

*5,7'-Diiodo-spiro[1,3-dioxolane-2,3'-[3H]indol]-2'(1'H)-one (**15b**)*

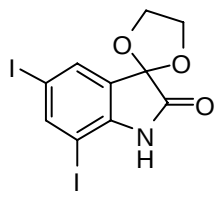

15b

This compound was prepared using the method of (Bass, 1971). 5'-Iodo-spiro[1,3-dioxolane-2,3'-[*3H*]indol]-2'(*1'H*)-one (**15a**) (200 mg, 0.63 mmol) was heated at reflux in methanol (20 mL) with ICl (213 mg, 1.31 mmol) for 5 h. After cooling, the reaction mixture was poured into water and extracted with diethyl ether. The combined ether extracts were dried over $MgSO_4$, filtered and the diethyl ether removed by rotary evaporation. The crude product was purified using flash chromatography (DCM). The identity of the colourless product (53 mg, 19%), R_f 0.22 (DCM) was confirmed as **15b** on the basis of LREI-MS *m/z* 443 ($[M]^+$). The compound was then used without additional characterisation

*5,7-Diiodoisatin (**15c**)*

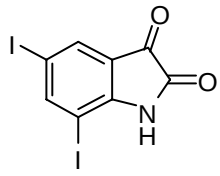

15c

The spiroketal (**15b**, 11 mg, 0.02 mmol) was heated at reflux in a mixture of HCl:AcOH (3:1, 4 mL) for 40 min. The resulting bright orange solution was poured onto ice water (5 mL) and the precipitate collected and washed with water. Compound **15c** was obtained as a bright red solid (8 mg, quant.), mp 259-260 °C (lit. 261-263 °C (Sumpter and Amundsen, 1932)), R_f 0.57 (DCM). ^{1}H NMR (DMSO-d_6, 500 MHz) δ 7.70 (d, *J* = 2 Hz, 1H,), 8.21 (d, *J* = 2 Hz, 1H), 11.10 (br s, 1H, NH). LREI-MS *m/z* 399 ($[M]^+$).

3.2.3 Biological Activity

3.2.3.1 *In vitro* Cytotoxicity Evaluation of Isatin Derivatives

3.2.3.1a Initial Screen

The cytotoxic activity of the synthesised isatin derivatives described in this chapter were previously unknown, therefore all compounds were initially screened for activity against the human monocyte-like, histiocytic lymphoma cell line (U937). Cytotoxicity was determined using the CellTiter 96 Aqueous One Solution Cell Proliferation Assay (MTS), in 96-well microplates, as described in Chapter 2, Materials and Methods, Section 2.3.2.1. Test compounds were incubated with U937 cells at various concentrations ranging from 0 -150 μg/mL for 24 h before the cytotoxic activity was determined spectrophotometrically. Results for each compound are reported as the concentration (μM) required to inhibit the metabolic activity of 50% of the cell population (IC_{50}) in comparison to DMSO, vehicle-treated control cells. These values were calculated from sigmoidal dose response curves using the variable slope parameter, generated from GraphPad Prism V. 4.02 software (GraphPad Software Inc.).

3.2.3.1b Panel Screening

Only compounds that gave an IC_{50} value of 12 μM or less in the initial screen were considered active and were further evaluated against a panel of 5 human cancer cell lines. Cell lines in this screen consisted of MCF-7 and MDA-MB-231 (breast), HCT-116 (colorectal), PC-3 (prostate) and Jurkat (leukemia). *In vitro* testing was carried out in 96-well microplates as described in Section 3.2.3.1a.

3.2.3.2 Investigations into Cancer Cell Specificity

Since **1** has been reported to display a 50 fold greater cytotoxic effect on U937 cells than PBL (Vine, 2002), **7** was further investigated for its ability to exhibit cancer cell selectivity. Freshly isolated, human PBLs were prepared as described in Chapter 2, Materials and Methods, Section 2.3.1.2 and subjected to treatment with increasing concentrations of **7** and incubated for 24 h as described in Section 3.2.3.1a. The IC_{50} value was then compared to that observed for U937 cells and the overall selectivity expressed as a fold increase over U937 treated cells.

3.2.3.3 Preliminary Mode of Action Studies

It has been proposed that some isatins inhibit cancer cell proliferation and as a result promote apoptosis through activation of the caspase signaling cascade (Cane *et al.,* 2000). As part of a preliminary mode of action study the ability of selected isatins to inhibit cellular proliferation, promote apoptosis and inhibit cyclin dependant kinase 2 (CDK2) was investigated.

3.2.3.3a Inhibition of Cellular Proliferation

The ability of **19** to inhibit cancer cell proliferation was determined on U937 cells after treatment with increasing concentrations of the isatin over time. Cells were prepared as described in Section 3.2.3.1a and incubated with **19** for either: 0, 24, 48 or 72 h. Dose response curves were generated using GraphPad Prism V. 4.02 software and treatment groups assessed for their ability to inhibit proliferation by comparison to control populations over time. Differentiation between cytotoxic and antiproliferative activity

was confirmed by staining with the cell-impermanent dye propidium iodide (PI). Briefly, cells were prepared as described above, then stained with 1 mg/mL PI (final concentration 10 μg/mL) and assessed for cell associated fluorescence with a 488 nm excitation laser on a Leica DM IL inverted contrasting fluorescence microscope.

3.2.3.3b Activation of Apoptotic Caspases

The activation of effector caspases 3 and 7 was determined in Jurkat cells after incubation with test compound or 2 μM staurosporine (positive control) using the Apo-ONE Homogeneous Caspase-3/7 Assay as described in Materials and Methods 2.3.3.1.

3.2.3.3c CDK2 Inhibition Assay

Since a number of structurally related isatins have been reported to be potent inhibitors of CDKs, the ability of **13** to inhibit the activity of CDK2 was investigated. Inhibition studies were performed by Dr Yuzhu Cheng and Lan-Zhen Wang of the Northern Institute for Cancer Research (NICR), Medical School, University of Newcastle upon Tyne, using an assay established by (Havlicek *et al.*, 1997). Briefly, radiolabelled [^{32}P] ATP was added to buffered **13** (dissolved in 1% DMSO) and incubated at 30 °C for 10 min. After incubation the assay mixture was spotted onto phosphocellulose filter paper, allowed to dry for 20-30 sec and then transferred to stirring 1% phosphoric acid to dilute the phosphate substrate, thereby terminating the reaction. The filters were washed a further 5-6 times, and dried, before being placed on a scintillation counter. The amount of [^{32}P] incorporated into histone was measured by counting the number of disintegrations per minute. This gave the value of pmol enzyme activity. Control

assays were also carried out in 1% DMSO, allowing the percentage inhibition to be calculated, the control was classed as having a 100% activity. The IC_{50} value for **13** was determined by plotting percent inhibition values against inhibitor concentration.

3.3 Results and Discussion

3.3.1 Chemistry

The complete chemical synthesis of the marine natural product tyrindoleninone (**1**) has not been reported to date and there is still a need for a synthetically pure product for biological assessment. Previously, cytotoxic activity had only been reported for a mixture of **1** and a common phthalate ester, 1,2-benzenedicarboxylic acid, bis(2-ethylhexyl) ester (**30**) (a common plasticizer), which could not be separated without decomposition of **1** (Vine, 2002). The aim of this study was therefore to synthesise a non-brominated derivative of **1**, namely 2-methylthioindoleninone (**29c**) in a model reaction and then **1**, for cytotoxicity evaluation. The synthesis of 2-(2,2-dichloro-2,3-dihydro-3-oxoindol-1-yl)-3*H*-indol-3-one (**29a**) was the first intermediate produced in the multi-step synthesis towards the production of 2-methythioindoleninone (**29c**). Although **29a** was first obtained in 1879, its structure was only recently elucidated (Cornforth *et al.*, 1996).

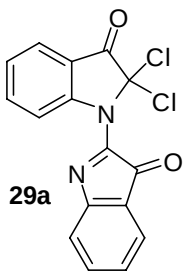

29a

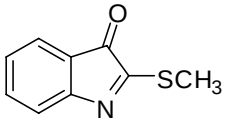

29c

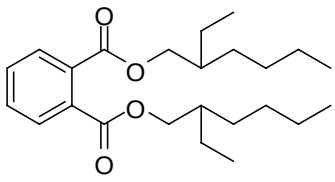

30

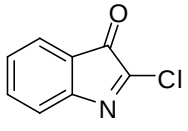

31

Many investigators have pointed out that **29a** resists purification by conventional techniques and is hydrolysed (Moriconi and Murray, 1964) or decomposed (Grimshaw and Begley, 1974) completely on standing overnight. As a result, reactions reported over a period of 115 years in 40 papers and 4 patents have described the structure of **29a** simply as 2-chloroindoleninone (**31**). Using the method described by Baker and Duke (1972), Cornforth *et al*., (1996) formed a benzene solvate of **29a** decreasing its sensitivity to moist air and under dry conditions obtained satisfactory ^{1}H and ^{13}C NMR spectra showing the presence of 8 different hydrogens and 16 different carbons. The ^{1}H NMR spectrum in $CDCl_3$ obtained in the current study was consistent with this data, although trace amounts of isatin were also present. In addition, the LREI-MS spectrum of **29a** showed an isotopic pattern consistent with the di-chlorinated product (*m/z* 331/333/335 $[M]^+/[M+2]^+/[M+4]^+$ (Cornforth *et al*., (1996)). Yields were extremely low however (2.8%), due to the unstable nature of the product in air and light. Due its instability, compound **29a** was not purified prior to the next step towards the production of **29b**. Instead crude **29a** was reacted with 10% sodium thiomethoxide in HCl/ diethyl ether (to produce methanethiol *in situ*) in an effort to produce the di-thiomethylated product. However, TLC analysis of the reaction mixture after solvent evaporation revealed only the original starting material **4**. Similarly brominated derivatives of **29c** were not obtained even when using a one pot method, due to hydrolysis of the di-methylthioisatin(s) back to the starting material, (Dr Julie Locke, per. com.).

Considering the problems associated with the reactivity of **29c** and the brominated derivatives thereof, **1** was not pursued using this method. Instead, it was envisioned that

the synthesis of **1** could be accomplished *via* a novel, two step pathway, of which, the proposed retrosynthetic scheme is shown below (Scheme 3.4). The reaction of the starting material, **5**, with Lawesson's reagent was predicted to give the thiolactam (or cyclic thioamide) which could then be reacted with methyl iodide, in the presence of base, to form **1**.

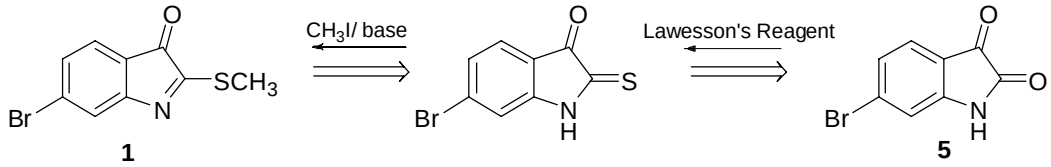

Scheme 3.4 A retrosynthetic scheme for the synthesis of tyrindoleninone (**1**) *via* the thiolactam.

A model reaction performed by Julie Locke with **5** showed that it was possible to form the thioamide by reaction with Lawesson's reagent in toluene, but it was somewhat unstable. In light of this, the reaction of the thioamide with methyl iodide in the presence of a base (K_2CO_3) was carried out in a one-pot manner by Julie Locke, but unfortunately this reaction proved unsuccessful, as no **1** could be detected. In a model study to improve the stability of the intermediate thiolactam, isatin (**4**) was protected as a ketal **24**, and then the reaction with Lawesson's reagent was performed (Scheme 3.5). The ketal-protected thiolactam **32** had improved stability; however it was only obtained in poor yield and further steps to the synthesis of **29c** were therefore not investigated. The thioamide method was also not pursued as difficulty was likely to be encountered in removing the ketal group while maintaining the integrity of the product (**29c**).

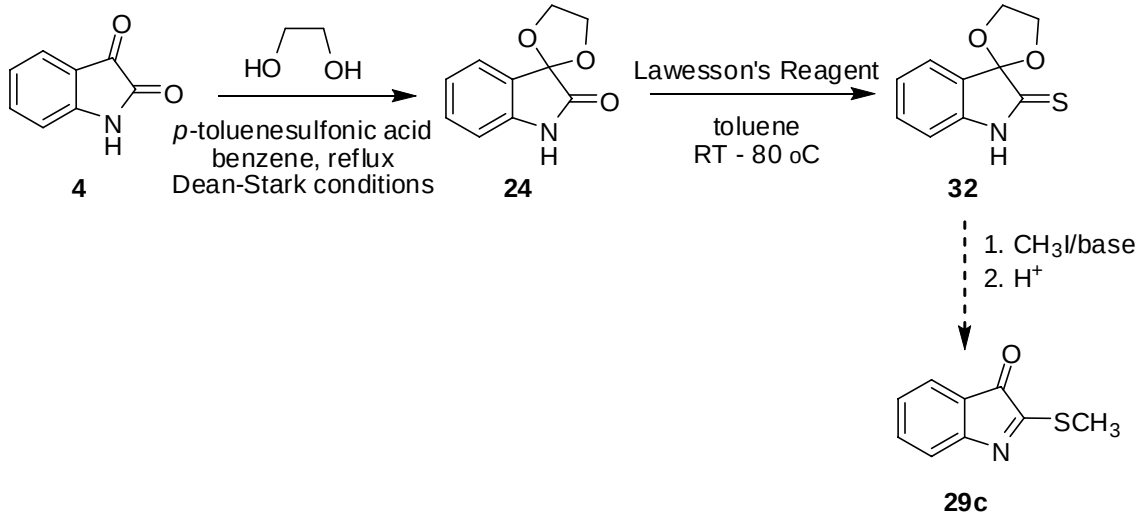

Scheme 3.5 A proposed, novel method for the synthesis of 2-methylthioindoleninone (**29c**).

Looking to other less reactive, yet biologically active compounds in the egg masses of *D. orbita,* our focus turned to 6-bromoisatin (**5**). Since it has been established that **5** also possesses anticancer activity (Vine, 2002), a range of stable analogues based on the isatin (**4**) scaffold were synthesised. All compounds except, **14** and **19** (Table 3.1, Section 3.3.2) were commercially available or prepared using literature procedures. Compounds **16**, **17** and **18** were synthesised using a general method for the nitration of isatins from the analogous bromoisatin (Polychronopoulos *et al.*, 2004) and were obtained as bright orange solids in moderate yields. Identification of known compound **16** was achieved by ^{1}H and ^{13}C NMR spectroscopy (Appendix 1, Figure A1.4 and Figure A1.5, respectively) and LREI MS spectrometry. LREI MS found *m/z* 270/272 ($[M]^+/[M+2]^+$, Appendix 1, Figure A1.6). The previously unreported compounds **17** and **18** were similarly characterised using HREI-MS. *m/z* values calculated for **17** and **18**

$[M+2]^+$, $C_8H_3{}^{81}BrN_2O_4$ were 271.9256 (found 271.9262), and $C_8H_3{}^{81}BrN_2O_4$, 271.9256; (found 271.9253) respectively (Appendix 1, Figure A1.12). Since the benzene ring of **4** is activated towards electrophilic attack at positions 5 and 7, the pattern of substitution for compounds **16** and **18** (Figure 3.3) was further confirmed using the magnitude of the coupling constant between H4 and H6. A *meta* coupling constant of 2 Hz was apparent in each case.

Halogenation of the isatin molecule generally follows a standard substitution pattern: firstly, substitution at the 5-position preferentially occurs and secondly, when there is excess reagent available, 5,7-disubstituted products are obtained. This is routinely observed for dichloro- and dibromo- substituted isatins however diiodoisatins can not be prepared by direct halogenation procedures. In 1932 a method was devised by Sumpter and Amundsen for the synthesis of 5,7-diiodoisatin (**15c**) from 5,7,5',7'-tetraiodoindigo (Sumpter and Amundsen, 1932), but only modest yields were obtained. As a result, **15c** was made *via* the ketal intermediate **15a** to improve the reactivity of **10** towards further iodination (Scheme 3.6). Using a modification to the procedure previously reported by

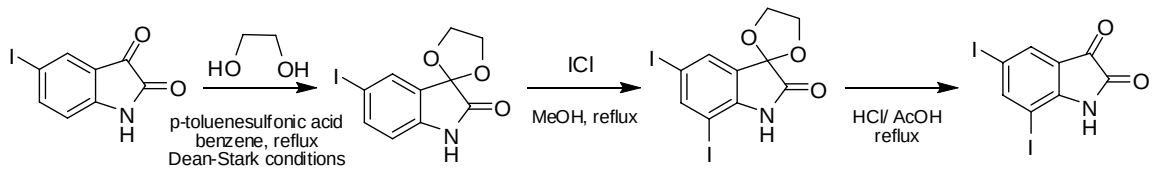

Scheme 3.6 Synthesis of **15c**.

Bass (1971), moderate yields of **15c** were obtained.

The imines **20** and **21** were found to be mixtures of *E*- and *Z*-isomers. The ^{1}H NMR spectrum (DMSO-d_6) of the isatin imine **20** showed only a trace of the minor isomer and assignment of signals for this isomer was not possible. However the ^{1}H NMR spectrum (DMSO-d_6) of the dibrominated derivative **21** showed clearly resolved signals for a 4:1 mixture of *E/Z*-isomers. The major isomer was assigned the *E* stereochemistry based on the following evidence. The signal from H4 of the *E*-isomer (6.32 ppm) was markedly shifted upfield relative to the H4 signal of both the parent dibromoisatin **13** (7.63 ppm) and the minor *Z*-isomer (7.68 ppm). In contrast, the chemical shifts of H4 and H6 of the *Z*-isomer showed little difference in chemical shift to that for the parent isatin. The signal from H4 in *(E)*-**21** is presumably shifted upfield due to interaction with the ring current of the phenyl substituent shielding this proton. The major isomer also exhibited a weak NOE correlation between H4 and H2′. The observed NOE enhancement is only possible for the *E*-isomer. This has also recently been described for a range of 3-substituted indolin-2-ones, whereby formation of the *E*-isomer was predominant in virtually all cases (Abadi *et al.*, 2006).

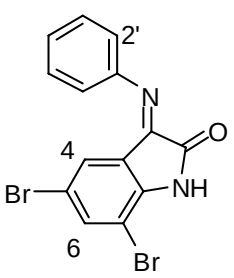

(*E*)-21

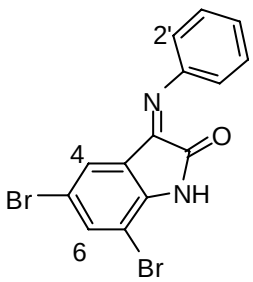

(*Z*)-21

3.3.2 Biological Activity

The *in vitro* cytotoxic activities of compounds **4-26** were determined initially against the human monocyte-like, histiocytic lymphoma cell line (U937) and are reported as IC_{50} values in Table 3.1. The toxicity of derivatives varied with structural modification, but only **19** was as active as previous estimates for **1** (Vine, 2002). Introduction of electron withdrawing groups at positions 5, 6 and 7 greatly increased activity from that of isatin (**4**), with substitution at the 5-position being most favourable. This is not surprising, as C5 substitution has previously been associated with increased biological activity for a range of indole-based compounds (Cane *et al.*, 2000; Lee *et al.*, 2001), including indirubin, a potent inhibitor of cyclin dependent kinases (CDKs) (Hoessel *et al.*, 1999) and glycogen synthase kinase 3 (GSK3) (Meijer *et al.*, 2003). Halogenation yielded the most active compounds, with di- (**13**, **14**, **15c**) and tri-substitution (**19**) increasing activity up to >100 fold from the parent molecule **4**. A comparison of the cytotoxicity (IC_{50}) of compounds **4-23** with their corresponding, calculated Log*P* (cLog*P*) values (Table 3.1) found a moderate correlation (R^2 = 0.5669, P = 0.0003) using the Pearson correlation algorithm (GraphPad Prism V 4.02) indicating that 57% of the variance in the data is accounted for by lipophilicity .

Preliminary investigation into the biological mode of action of the most active compound **19**, found it to be antiproliferative at low concentrations and cytotoxic at higher concentrations (Figure 3.4), which was further confirmed by PI staining (Figure 3.5). This effect was evident within the first 24 h of treatment, and subsequent incubation periods (up to 72 h) did not enhance the activity of **19** any further. Activation

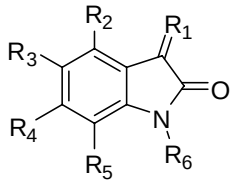

4 - 23

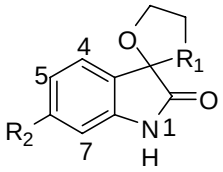

24 - 26

Table 3.1 Cytotoxicity IC_{50} (μM) of isatin derivatives **4-26** on U937[a] cells as calculated from dose response curves.[b]

Compound	R_1	R_2	R_3	R_4	R_5	R_6	cLog*P*[c]	IC_{50} (μM)[d]
4	O	H	H	H	H	H	0.828	565
5	O	H	H	Br	H	H	1.69	74.8
6	O	Br	H	H	H	H	1.69	214
7	O	H	Br	H	H	H	1.69	64.5
8	O	H	H	H	Br	H	1.69	83.0
9	O	H	F	H	H	H	0.971	98.4
10	O	H	I	H	H	H	1.95	53.4
11	O	H	NO_2	H	H	H	0.571	132
12	O	H	OCH_3	H	H	H	0.747	420
13	O	H	Br	H	Br	H	2.55	10.5
14	O	H	Br	Br	H	H	2.35	11.6
15c	O	H	I	H	I	H	3.07	7.85
16	O	H	Br	H	NO_2	H	1.43	257
17	O	H	NO_2	Br	H	H	1.23	17.1
18	O	H	NO_2	H	Br	H	1.43	>369
19	O	H	Br	Br	Br	H	3.02	6.76
20	N-C_6H_5	H	H	H	H	H	2.65	76.5
21	N-C_6H_5	H	Br	H	Br	H	4.38	13.7
22	N-NHC_6H_5	H	H	H	H	H	2.47	>211
23	O	H	H	H	H	CH_3	0.564	238
24	O	H	-	-	-	-	0.429	NA[e]
25	O	Br	-	-	-	-	1.55	NA[e]
26	S	H	-	-	-	-	0.888	NA[e]
staurosporine								2.00

[a] U937: human monocyte-like, histiocytic lymphoma.
[b] Sigmoidal dose response curves (variable slope) were generated using GraphPad Prism V. 4.02 (GraphPad Software Inc.).
[c] CLogP values were calculated using ChemDraw Ultra V. 8.0 (CambridgeSoft Corporation).
[d] Values are the mean of triplicates of at least two independent experiments.
[e] NA= not active at the highest concentration tested (100 μg/mL).

of effector caspases 3 and 7 after treatment with **19** was dose dependent in Jurkat cells, with maximum activity detected at 8 μM after 5 h (Figure 3.6). This was equivalent to the activity observed for staurosporine (positive control) at 2 μM, a potent, broad spectrum protein kinase inhibitor. A range of isatin-based molecules have also been reported to display antiproliferative (Juranic *et al.*, 1999; Natarajan *et al.*, 2004) and proapoptotic activity *in vitro* (Igosheva *et al.*, 2005). Mechanistically, isatin itself is proposed to inhibit cell proliferation *via* interaction with extracellular signal related protein kinases (ERKs), thereby promoting apoptosis (Cane *et al.,* 2000). The oxindoles, for example 3,3-diaryloxindoles, reduce cell growth *via* Ca^{2+}-mediated inhibition of translation initiation (Natarajan *et al.,* 2004).

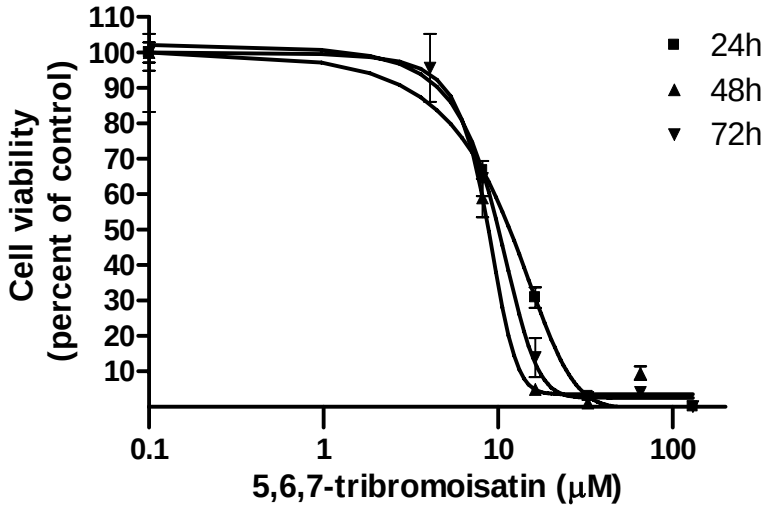

Figure 3.4 Viability of U937 cells after treatment with increasing concentrations of 5,6,7-tribromoisatin (**19**) over time. Briefly, cells were incubated for 24 h, 48 h or 72 h at 37 °C (95% humidity, 5% CO_2) with increasing concentrations of **19**, then analysed for a change in metabolic activity and expressed as percent viability in reference to the DMSO control. Each data point is a mean of triplicates ± SE of one representative experiment.

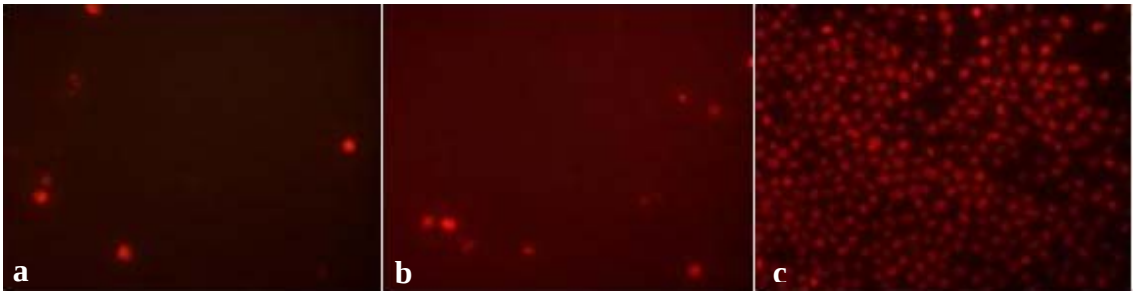

Figure 3.5 Cell associated fluorescence of U937 cells after treatment with a) 2.5% DMSO (control), b) 4 μM (1.56 μg/mL) or c) 130 μM (50 μg/mL) of 5,6,7-tribromoisaitn (**19**) for 24 h. Cells were stained with 1 mg/mL PI (final concentration 10 μg/mL) and assessed for fluorescence with a 488nm excitation laser viewed at 40 × magnification on a Leica DM IL inverted contrasting fluorescence microscope.

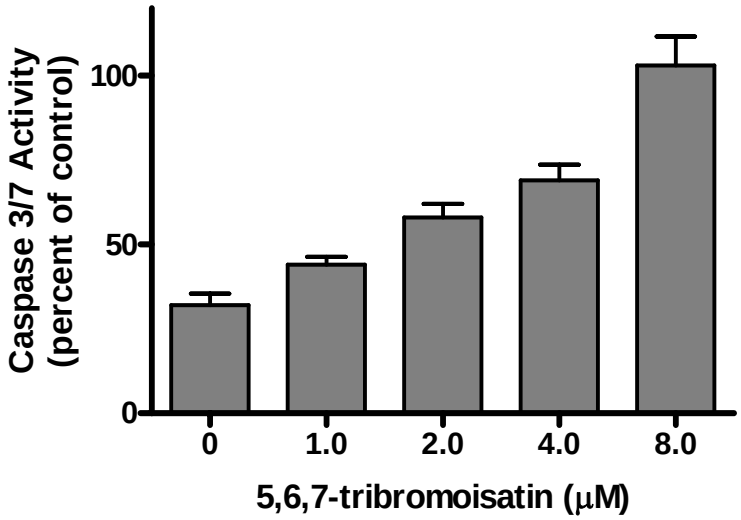

Figure 3.6 Activation of caspases 3 and 7 in Jurkat cells after treatment with various concentrations of 5,6,7-tribromoisatin (**19**). Cells were treated with increasing concentrations of **19** or staurosporine (2 μM) for 5 h. Values are normalised to staurosporine (positive control). Data are means ± SE of one representative experiment performed in triplicate.

Formation of the spiroketals **24** (R_1 = O, R_2 = H) and **25** (R_1 = O, R_2 = Br) and the spirothioketal **26** (R_1 = S, R_2 = H) at C3 did not enhance activity relative to that of **4**. As only mild activity was observed for compounds **24**, **25** and **26** at the highest concentration tested (100 μg/mL), IC_{50} values were not determined (Figure 3.7). Similarly, imine bond formation at C3 gave the hydrazone **22** (R_1 = N-NH-Ph); which showed no activity at the highest concentration tested (50 μg/mL, 210 μM, Table 3.1). Formation of the imine **20** (R_1 = N-Ph) however, increased activity against U937 cells by a factor of 13.5 (Figure 3.7). Di-bromination of **20** to form **21** enhanced activity by a further 18% but **21** was not as active as the ketone analogue **13**. This is interesting as many C3 substituted isatins have been found to selectively target and inhibit PTKs at submicromolar concentrations in cell based assays (Sun *et al.*, 1998; Fong *et al.*, 1999). Molecular modeling studies have shown that the oxindole core occupies a site where the adenine of ATP binds, while substituents at C3 of various isatins, for example SU5416, contact residues in the hinge region of growth factor receptors (Fong *et al*., 1999). The *in vitro* activity of isatins **13**, **14**, **15c** and **19** at low micromolar concentrations and the ability of **19** to arrest cellular proliferation and promote apoptosis suggests that these compounds may in fact share common interactions with ATP binding pockets associated with receptors of growth factors or even other protein kinases.

In light of this, **13** was investigated for its ability to inhibit cyclin dependent kinase 2 (CDK2), a key regulator of the cell cycle, and was found to cause 44% inhibition at 100 μM (Dr. Yuzhu Chen and colleagues, per. com.). Comparison of this data with *in*

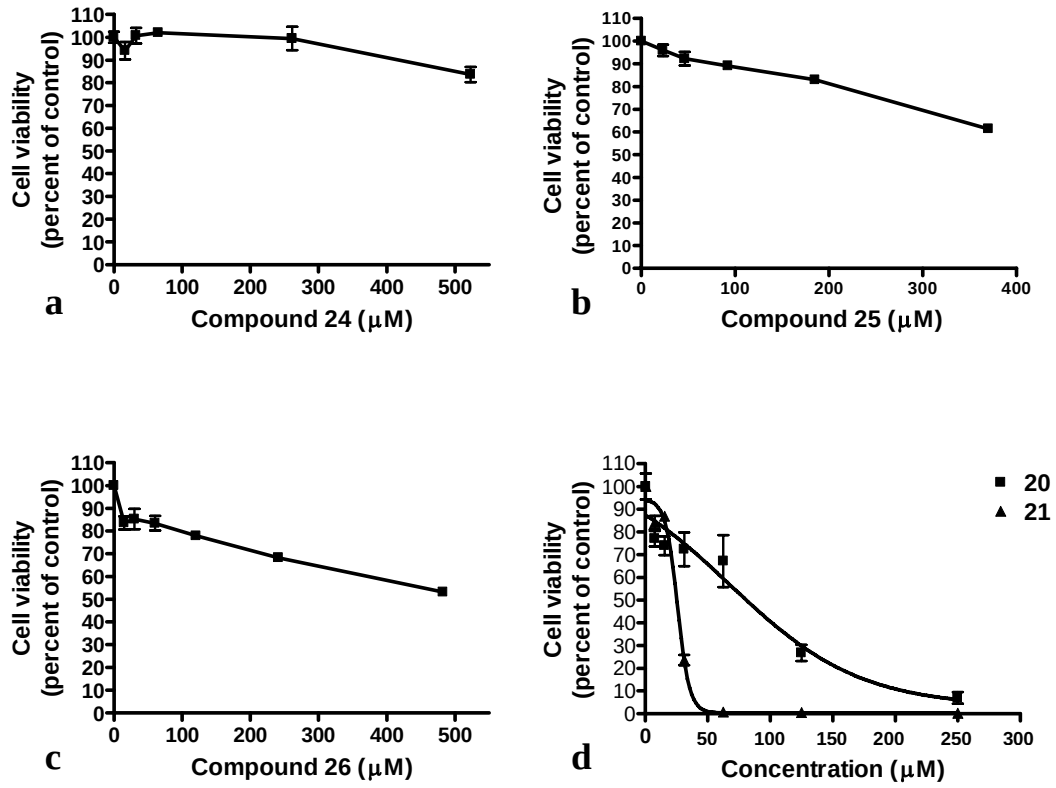

Figure 3.7 Viability of U937 cells after treatment with increasing concentrations of a) spiro[1,3-dioxolane-2,3'-[3*H]*indol]-2'(1'*H*)-one (**24**), b) 6'-bromospiro[1,3-dioxolane-2,3'-[3*H*]indol]-2'(1'*H*)-one (**25**), c) spiro[3*H*-indole-3,2' [1,3]oxathiolan]-2(1*H*)-one (**26**) and d) 3-(phenylimino)-2-indolinone (**20**) and 5,7-dibromo-3-(phenylimino)-2-indolinone (**21**). Briefly, cells were incubated for 24 h at 37 °C (95% humidity, 5% CO_2) with increasing concentrations of test compound, then analysed for a change in metabolic activity and expressed as percent viability in reference to the DMSO control. Each data point is a mean of triplicates ± SE.

vitro cytotoxicity of **13** in U937 cells (IC_{50} 10.5 μM), suggests that it does not directly interact with CDK2. This does not rule out interactions with other CDKs however, as a number of different inhibitors show potent selectivity based on the structural differences that exist at the protein's catalytic site (Hirai *et al.*, 2005). The hydrophobic nature of amino acids lining ATP binding cavities of kinases may also explain the higher cell-

based activity observed for di- and tri- halogenated isatins in comparison to unsubstituted compounds (Table 3.1). Such an effect has similarly been described for 3-substituted-2-oxoindole analogues upon binding to CDK5/p25 and GSK/3β (Abadi *et al.,* 2006). Furthermore, methylation of **4** at N1 to form **23** increased activity by almost 50% (Table 3.1). This supports the hypothesis that substituted isatins **4-23** may act on other CDKs or PTKs as the NH amide of the oxindole ring system of various isatins is found to be important for binding to the carbonyl backbone of amino acids in the ATP binding pocket of growth factors PDGF and VEGF (Sun *et al.,* 1998) as well as CDK2 (Bramson *et al.*, 2001).

Investigation into the cellular specificity of the mono-brominated isatin (**7**) found it to be >10 times more active towards the U937 lymphoma cell line (IC_{50} 64.5 μM) than the freshly-isolated, human peripheral blood lymphocytes (PBL) (IC_{50} >663 μM) (Figure 3.8). Although not as selective as **1** (Vine, 2002), **7** showed similar activity to a structurally related, *N*-alkylated isatin which demonstrated a 12 fold increase in activity towards tumor cells over freshly-isolated PBLs (Nguyen and Wells, 2003).

Finally, four of the most active isatins (**13**, **14**, **15c** and **19**), determined in the initial cell line screen, were selected for further testing against a panel of human leukemic, breast, prostate and colorectal cancer cell lines (Table 3.2). IC_{50} values generated from dose response curves indicated that Jurkat cells were the most sensitive to treatment, while PC-3 cells, in general, were the least responsive over all (Figure 3.9, Table 3.2). This was contrary to the results obtained for 5,7-dichloroisatin in the NCI (developmental

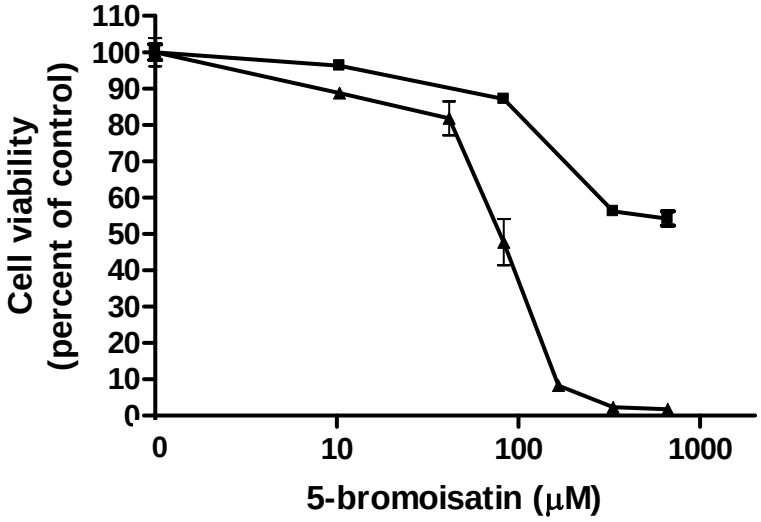

Figure 3.8 Viability of U937 cells (▲) and freshly isolated, human peripheral blood lymphocytes (PBL) (■) after treatment with 5-bromoisatin (**7**). Briefly, cells were incubated for 24 h at 37 °C (95% humidity, 5% CO_2) with increasing concentrations of **7**, then analysed for a change in metabolic activity and expressed as percent viability in reference to the DMSO control. Each data point is a mean of triplicates ± SE of one representative experiment.

Table 3.2 Cytotoxicity of di- and tri-substituted isatin derivatives (**13**, **14**, **15c** and **19**) against various cancer cell lines as determined by dose response curves.[a]

	IC_{50} (μM)[b]				
Compound	Jurkat[c]	MDA-MB-231[d]	MCF-7[e]	PC-3[f]	HCT-116[g]
13	14.3	42.3	31.3	101	24.6
14	20.2	41.7	20.2	41.0	37.3
15c	20.9	41.8	18.4	71.9	24.0
19	5.80	21.8	13.3	25.9	15.9

[a]Sigmoidal dose response curves (variable slope) were generated using GraphPad Prism V. 4.02 (GraphPad Software Inc.).
[b]Values are the mean of triplicates of at least two independent experiments.
[c]Jurkat: human leukemic T- cell.
[d]MDA-MB-231: human mammary gland adenocarcinoma (metastatic).
[e]MCF-7: human mammary gland adenocarcinoma (non-metastatic).
[f]PC-3: human prostate adenocarcinoma.
[g]HCT-116: human colorectal carcinoma.

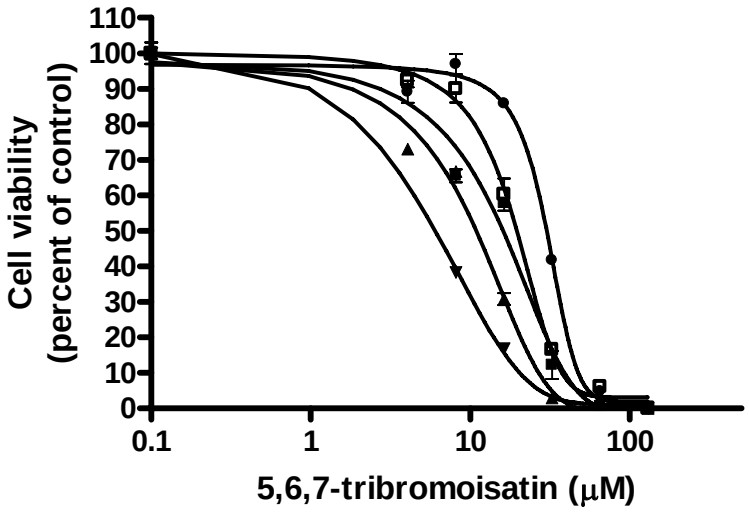

Figure 3.9 Viability of U937 (▲), Jurkat (▼), HCT-116 (■), MDA-MB-231 (□) and PC-3 (●) cells after treatment with 5,6,7-tribromoisatin (**19**). Briefly, cells were incubated for 24 h at 37 °C (95% humidity, 5% CO_2) with increasing concentrations of **19**, then analysed for a change in metabolic activity and expressed as percent viability in reference to the DMSO control. Each data point is a mean of triplicates ± SE of one representative experiment.

therapeutics program) 60 cell line screen, which showed little difference in activity between HCT-116 (IC_{50} 79.4 μM), PC-3 (IC_{50} 100 μM), MCF-7 (IC_{50} 79.4 μM) and MDA-MB-231 (IC_{50} 100 μM) cell lines, even after a 48 h incubation period (Table 3.3). Overall, activity was lower than that obtained for our structurally related, brominated compound **13**.

3.4 Conclusions

Despite various synthetic approaches, tyrindoleninone (**1**) could not be obtained for biological testing due to the reactive nature of the indoleninone ring. As a result, a range

Table 3.3 IC_{50} (μM) mean graph for 5,7-dichloroisatin courtesy of NCI cancer screen, 2005. Average IC_{50} over all cell lines is 82 μM.

Cell Panel	Cell Line	Log I C_{50}
Leukemia	CCRF-CEM	-4.0
	HL-60(TB)	-4.0
	K-562	-4.0
	MOLT-4	-4.0
	SR	-4.0
Non-Small Cell Lung	A549/ATCC	-4.2
	EKVX	-4.2
	HOP-62	-4.1
	HOP-92	-4.0
	NCI-H226	-4.0
	NCI-H23	-4.0
	NCI-H322M	-4.0
	NCI-H460	-4.0
Colon	COLO 205	-4.0
	HCC-2998	-4.0
	HCT-116	-4.1
	HCT-15	-4.0
	HT29	-4.0
	KM12	-4.0
	SW-620	-4.0
Central Nervous System	SF-295	-4.2
	SF-539	-4.2
	SNB-19	-4.0
	SNB-75	-4.0
	U251	-4.0
Melanoma	LOX IMVI	-4.1
	MALME-3M	-4.5
	M14	-4.1
	SK-MEL-2	-4.2
	SK-MEL-28	-4.2
	SK-MEL-5	-4.3
	UACC-257	-4.2
	UACC-62	-4.2
Ovarian	IGROV1	-4.0
	OVCAR-3	-4.0
	OVCAR-4	-4.2
	OVCAR-5	-4.1
	OVCAR-8	-4.0
	SK-OV-3	-4.0
Renal	786-0	-4.0
	A498	-4.0
	ACHN	-4.0
	CAKI-1	-4.2
	RXF 393	-4.2
	SN12C	-4.2
	TK-10	-4.0
	UO-31	-4.0
Prostate	PC-3	-4.0
Breast	MCF7	-4.1
	NCI/ADR-RES	-4.0
	MDA-MB-231/ATCC	-4.0
	HS 578T	-4.1
	MDA-MB-435	-4.4
	MDA-N	-4.3
	BT-549	-4.2

of stable isatin derivatives were synthesised (or obtained) resulting in the generation of two new compounds (**18** and **19**). Cytotoxicity screening revealed **19** to be the most active compound across all cell lines and resulted in the initiation of apoptosis in Jurkat cells after 5 h. A preliminary cyclin dependent kinase activity assay assessing the inhibitory ability of **13** suggests CDK2 is not the primary target. However the structural similarity it shares with other isatins that competitively bind at ATP catalytic sites suggests the molecular mode of action may be *via* inhibition of growth factor receptors or other protein kinases. Compound **7** was found to be selective for cancer cells over normal human cells, indicating that structural modification of di- and tri-substituted isatins may lead to new derivatives with enhanced and selective anticancer activity.

CHAPTER 4

An Investigation into the Cytotoxicity and Mode of Action of Some *N*-alkyl Substituted Isatins

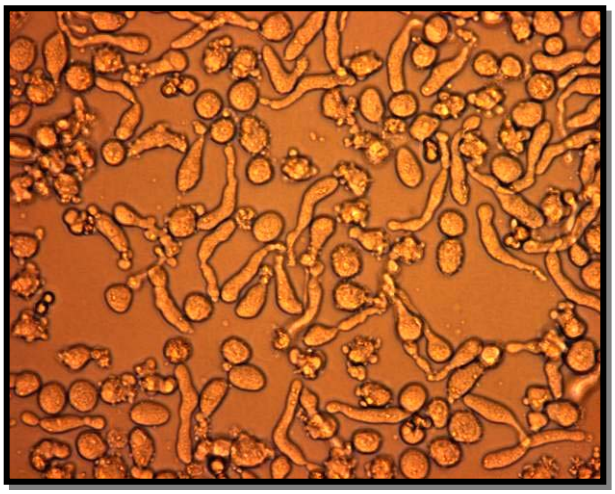

The effect of a 24 h treatment with 5,7-dibromo-*N*-(*p*-iodobenzyl)isatin (**53**) on the morphology of U937 cells. Image viewed at 1000 × magnification

CHAPTER 4

An Investigation into the Cytotoxicity and Mode of Action of Some *N*-alkyl Substituted Isatins

4.1 Introduction

The isatin molecule (1*H*-indole-2,3-dione) is a versatile moiety, of which its analogues have been described to display diverse types of biological activities (Pandeya *et al.*, 2005), including anticancer (Cane *et al.*, 2000; Vine *et al.*, 2007). The synthetic flexibility of isatin has led to the synthesis of a variety of substituted derivatives. However, the susceptibility of isatin to attack by nucleophiles at C3 (Figure 4.1) has resulted in the generation of a large number of 3-substituted isatins in particular. This is reflected by the large proportion of biologically active 3-substituted indolin-2-ones reported in the literature. For example a variety of 1*H*-indole-2,3-dione 3-phenylhydrazones (Figure 4.2a) and 3-(anilinomethylene)-1,3- dihydro-2*H*-indol-2-ones

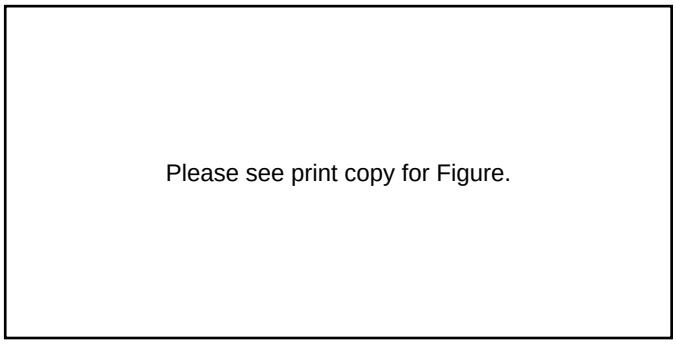

Figure 4.1 The reactivity of isatin. Isatin will primarily react at three different sites, namely *via* aromatic substitution at C5, *N*-alkylation and carbonyl reactions at C3. If the system carries electron withdrawing groups on the benzene ring or at the nitrogen, attack at C2 can also occur (da Silva *et al.*, 2001).

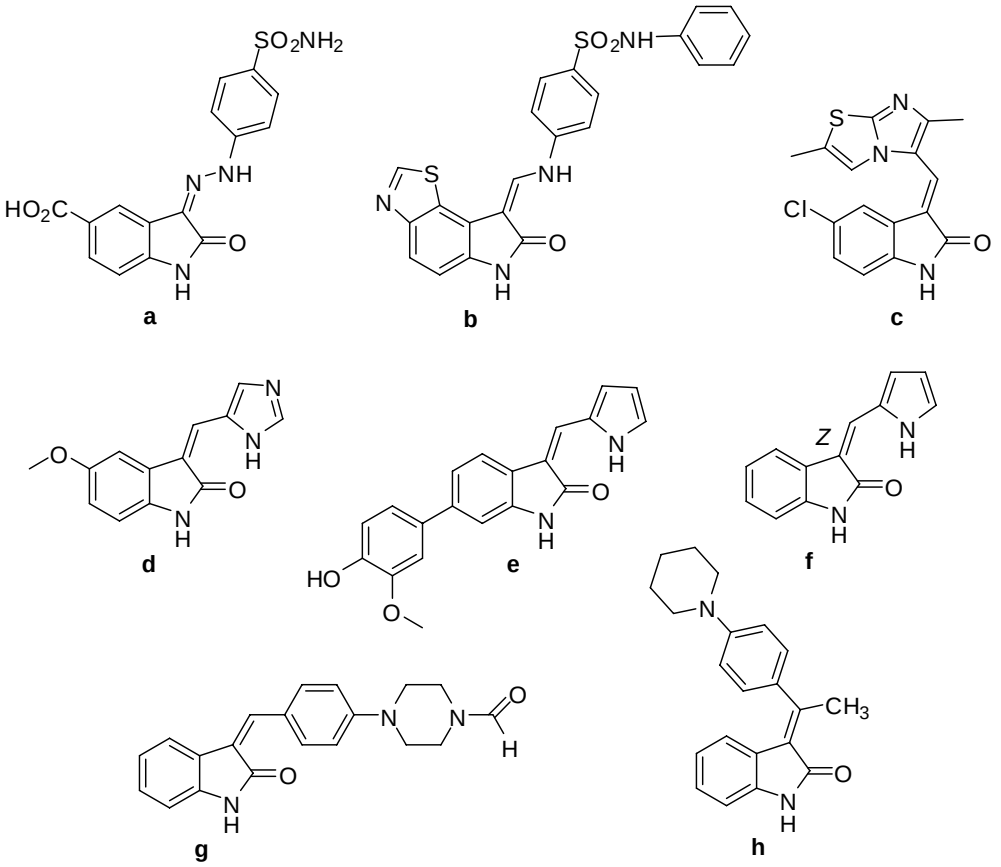

Figure 4.2 Examples of some 3-substituted indolin-2-ones with reported anticancer activity.

(Figure 4.2b) have been shown to slow cancer cell cycle progression *via* inhibition of cyclin dependant kinase 2 (CDK2, Bramson *et al.*, 2001). Similarly, an array of 3-(5-imidazo[2,1-b]ylmethylene)-2-indolinones (Figure 4.2c and d) and [6-(4-hydroxy-3-methoxyphenyl)-3-(1*H*-pyrrol-2-ylmethylene)-1,3-dihydroind-ol-2-one, A-432411] (Figure 4.2e) inhibit tubulin polymerisation in a range of cancer cell lines, leading to cell cycle arrest at G2/M and eventual cell death (Andreani *et al.*, 2005; Chen *et al.*, 2005). Furthermore, 3-substituted indolin-2-ones have been designed and synthesised as a novel class of tyrosine kinase inhibitors which exhibit selectivity toward different

receptor tyrosine kinases (RTKs). In 1998, Sun and colleagues reported 3-[(five-membered heteroaryl ring)methylidenyl]indolin-2-ones (Figure 4.2f) to be highly specific against the VEGF (*Flk-1*) RTK and 3-(substituted benzylidenyl)indolin-2-ones containing bulky groups in the phenyl ring at the C3 position (Figure 4.2g-h) showed high selectivity toward the EGF and Her-2 RTKs (Sun *et al.*, 1998). Despite a large proportion of anticancer research being devoted to this chemical class, it should not be assumed that 3-substituted isatins are richer in bioactivity than other substituted 1*H*-indole-2,3-diones. *N*-alkylated indoles have also been reported to exhibit anticancer activity (Bacher *et al*., 2001; Nguyen and Wells, 2003; Liu *et al*., 2003), though little has been reported on the antineoplastic activity of di- or tri-halogenated *N*-alkyl* isatins.

4.1.2 Anticancer Activity of N-Alkylated Indoles

The ability of *N*-alkyated indoles to act as anticancer agents has only recently been discovered, despite the plethora of information available on the biological activity of structurally related compounds. In 2001, D-24851 (*N*-(pyrindin-4-yl)-[1-(4-chlorobenz-yl)indol-3-yl]-glyoxyl-amide, Figure 4.3a) was found to block cell cycle progression in a variety of malignant cell lines including those derived from the prostate, brain, breast, pancreas and colon (Bacher *et al*., 2001). A structurally related compound (Figure 4.3b), was then described two years later to activate caspases in a cytochrome c-dependent manner and induce apoptosis in cancer cell lines but not normal cells (Nguyen and

* For simplicity, the term *N*-alkyl also includes *N*-arylalkyl isatins in this thesis.

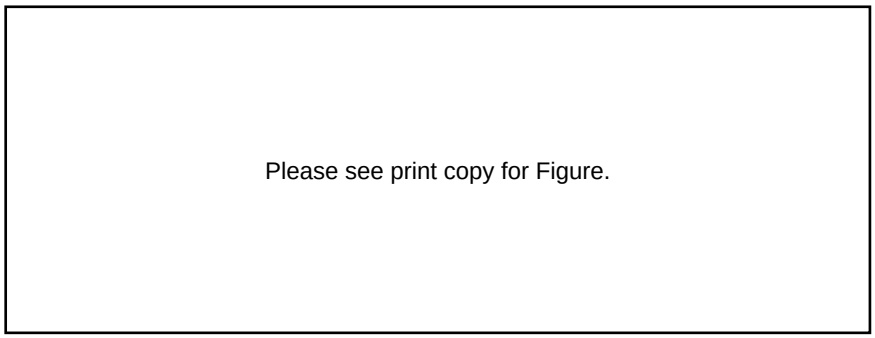

Figure 4.3 Examples of recently reported *N*-alkylated indoles with anticancer activity (Bacher *et al*., 2001; Nguyen and Wells, 2003; Liu *et al*., 2003).

Wells, 2003). Subsequently, Liu and colleagues identified a class of isatin *O*-acyl oximes (Figure 4.3c) that selectivity inhibited neuronal ubiquitin C-terminal hydrolase (UCH-L1) in a H1299 lung cancer cell line which is proposed to be linked to tumour progression upon upregulation (Liu *et al.*, 2003). Very few studies however (Cane *et al*., 2000; Liu *et al*., 2003; Pandeya *et al*., 2005) have described SARs attributable to modifications to the benzene ring of isatin. This is interesting considering that the introduction of electron withdrawing groups to the benzene ring has been shown to be associated with increased biological activity for a range of indole-based compounds (Cane *et al*., 2000; Lee *et al*., 2001, Vine *et al*., 2007), including indirubin (Ribas *et al*., 2006).

4.1.3 Rationale and Aims

Due to the reactivity of isatin, a large proportion of structural derivatives that have been previously investigated are based on modifications at positions 2 and 3 and fewer

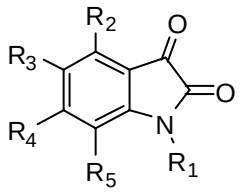

Table 4.1 Chemical structures of the *N*-alkylated isatins (compounds **33-60**) that were screened for cytotoxic activity in this study.

	R_1	R_2	R_3	R_4	R_5		R_1	R_2	R_3	R_4	R_5
33	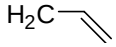	H	Br	H	Br	**47**	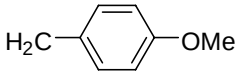	H	Br	Br	Br
34	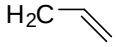	H	Br	Br	H	**48**	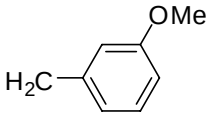	H	Br	H	Br
35	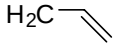	H	Br	Br	Br	**49**		H	Br	H	Br
36	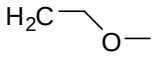	H	Br	H	Br	**50**	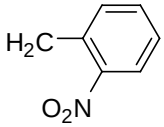	H	Br	H	Br
37	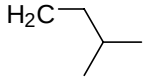	H	Br	H	Br	**51**	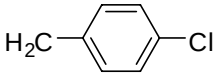	H	Br	H	Br
38	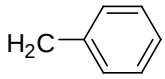	H	Br	H	Br	**52**	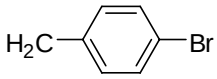	H	Br	H	Br
39	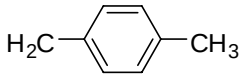	H	Br	H	Br	**53**	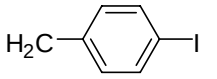	H	Br	H	Br
40	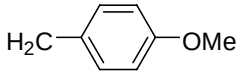	H	H	H	H	**54**	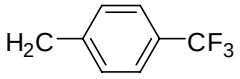	H	Br	H	Br
41	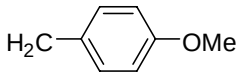	Br	H	H	H	**55**	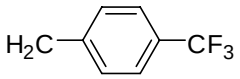	H	H	Br	H
42	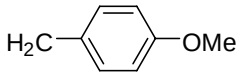	H	Br	H	H	**56**	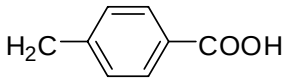	H	Br	H	Br
43	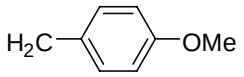	H	H	Br	H	**57**	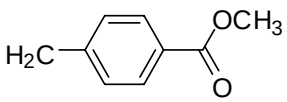	H	Br	H	Br
44	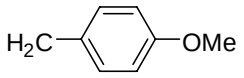	H	H	H	Br	**58**	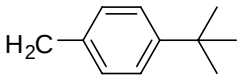	H	Br	H	Br
45	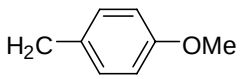	H	Br	H	Br	**59**	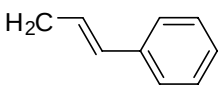	H	Br	H	Br
46	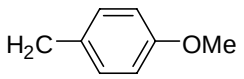	H	Br	Br	H	**60**	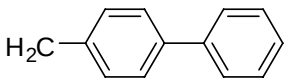	H	Br	H	Br

derivatives have been synthesised *via* alkylation at N1. In addition, little is known about the anticancer activity of *N*-alkylated isatins in comparison to C3 substituted indolin-2-ones. The aim of this study was therefore to screen a range of *N*-alkylated and *N*-arylalkylated isatins (**33-60**, Table 4.1) varying in chain length and substituent position, including substitution on the benzene ring of the isatin moiety, for cytotoxicity against a panel of cancer cell lines and to determine the SAR. A further aim was to investigate the mode of action using a range of cell-based and cell-independent approaches.

4.2 Materials and Methods

4.2.1 General

All *N*-alkyl isatins (**33-60**) were supplied by Dr. Julie M. Locke, Postdoctoral Research Fellow, Department of Chemistry, University of Wollongong. Tubulin Tracker™ Green Reagent was obtained from Molecular Probes (Invitrogen Aust. Pty Ltd, Australia) and the Tubulin Polymerisation Assay from Cytoskeleton Inc. (Jomar Diagnostics, Australia). The Diff-Quik® staining kit was purchased from Lab Aids (Sydney, NSW Aust.) and propidium iodide from Sigma-Aldrich (St Louis, MO, USA). Light and fluorescence microscopy images were obtained using a Leica DC500 12-megapixel high-performance FireWire camera system and the accompanying Leica IM50 image manager software (Leica Microsystems AG, Heerbrugg, Germany).

4.2.2 Chemical Synthesis

4.2.2.1 General Method for the Alkylation of Isatin

Alkylation of the isatins was carried out by Dr. Julie Locke using a general method based on that of Garden *et al*., (1998) (Scheme 4.1). The appropriate isatin (1 equiv.) was taken up in anhydrous DMF (~ 1 mL per 0.1 mmol of isatin) and cooled on ice with stirring. Solid K_2CO_3 (1.4 equiv.) or Cs_2CO_3 (1.4 equiv.) was added in one portion and the dark-coloured suspension was brought to RT and stirred for a further 2 h. The appropriate benzyl halide (1.1 equiv.) and KI (0.2 equiv.) were added and the reaction mixture stirred at 80 °C for 5 - 16 h, until all the isatin starting material had been consumed (as evidenced by TLC analysis). The reaction mixture was then added to aqueous HCl (0.5 M) and extracted with ethyl acetate (1 × 50 mL). The ethyl acetate layer was washed with brine and dried over $MgSO_4$. The solvent was removed and the crude product was purified using flash column chromatography (silica gel) with isocratic elution with DCM. Compounds **33-60** were fully characterised using ^{1}H and ^{13}C NMR spectroscopic and MS spectrometric procedures. Compound purities were assigned ≥95% on the basis of RP HPLC analysis as well as ^{1}H NMR and ^{13}C NMR spectral analysis.

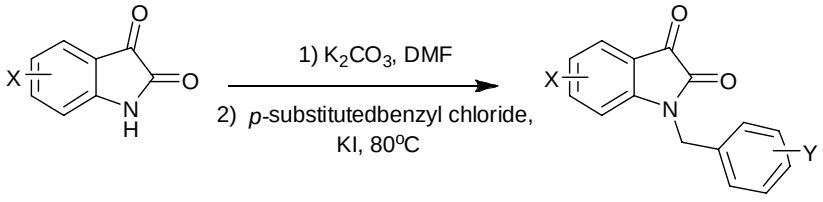

Scheme 4.1 General method for the *N*-alkylation of isatin

4.2.3 Biological Activity and SAR Studies

4.2.3.1 *In vitro* Cytotoxicity Evaluation of *N*-alkyl Isatin Derivatives

The cytotoxic activities of the synthesised *N*-alkyl isatin derivatives described in this chapter were unknown, therefore all compounds were screened for activity against human lymphoma (U937), leukemic (Jurkat), breast carcinoma (MDA-MB-231, and MCF-7), prostate carcinoma (PC-3), colorectal carcinoma (HCT-116) and melanoma (A375) cancer cell lines and freshly prepared human peripheral blood lymphocytes (PBL) *in vitro*. Cytotoxicity was determined using the CellTiter 96 AQueous One Solution Cell Proliferation Assay (MTS), in 96-well microplates, as described in Chapter 2, Materials and Methods, Section 2.3.2.1. Test compounds were incubated with different cell lines at increasing concentrations ranging from 0-100 μg/mL for 24 h (unless stated otherwise) prior to the addition of MTS reagent. Cytotoxic activity was then determined spectrophotometerically at 490 nm. Results for each compound are reported as the concentration (μM) required to inhibit the metabolic activity of 50% of the cell population (IC_{50}) in comparison to vehicle-treated (DMSO) control cells. These values were calculated from logarithmic sigmoidal dose response curves using the variable slope parameter, generated from GraphPad Prism V. 4.02 software (GraphPad Software Inc.).

4.2.4.2 Investigations into Cancer Cell Specificity

The ability of compound **54** to demonstrate cancer cell specificity was investigated by comparison to normal, non-transformed human cells. Briefly, freshly isolated, human PBL were prepared as described in Chapter 2, Materials and Methods, Section 2.3.1.2

and subjected to treatment with increasing concentrations of **54** and incubated for 24 h as described in Section 3.2.3.1a. The IC_{50} value was then compared to that observed for U937 cells and the overall selectivity expressed as a fold increase over U937 treated cells.

4.2.4 Mode of Action Studies

4.2.4.1 Apoptosis Investigations

4.2.4.1a Whole Cell Staining: Propidium Iodide (PI)

Because of the fundamental differences that exist between apoptotic and necrotic cell death pathways (Kroemer *et al*., 1998), it is possible to use a cell impermanent, nuclear-binding dye such as propidium iodide (PI) to distinguish between apoptotic and necrotic populations (Vitale *et al*., 1993). In this study, U937 cells were prepared as described in Section 4.2.3.1 and incubated with either a high (e.g. 50 µg/mL) or low (e.g. 0.39 µg/mL) concentration of test compound for 24 h. Cells were then stained with PI (final concentration 10 µg/mL) and fluorescence visualised immediately on a Leica DM IL inverted contrasting fluorescence microscope (Leitz Wetzlar, Germany) using a 488 nm excitation laser.

4.2.4.1b Activation of Apoptotic Caspases

The activation of effector caspases 3 and 7 was determined in Jurkat cells after incubation with test compound or 2 µM staurosporine (positive control) using the Apo-ONE Homogeneous Caspase-3/7 Assay as described in Chapter 2, Materials and

Methods, Section 2.3.3.1. Cells were incubated at 37 ºC (95% humidity, 5% CO_2) with test compound for 5 h prior to the addition of Caspase-3/7 reagent, or up to 8 h in the case of time course experiments.

4.2.4.1c Nuclear Staining: Diff-Quik®

Nuclei in treated and untreated cell populations were fixed and stained with Diff-Quik® Stain Set 64851, a proprietary brand of a Romanowsky stain. The Romanowsky group of stains are defined as being the black precipitate formed from the addition of aqueous solutions of methylene blue and eosin, dissolved in methanol. The stain class was originally designed to incorporate cytoplasmic (pink) staining with nuclear (blue) staining and fixation as a single step for smears and thin films of tissue (Skipper and DeStephano, 1989). Briefly, U937 cells (~1.0×10^5) were treated with 0.39 μg/mL 5,7-dibromo-*N*-(*p*-iodobenzyl)isatin (**53**) in DMSO for 24 h then mounted onto glass slides by cytocentrifugation (1000 rpm, 5 min) using a Cytospin 2 (Shandon Inc. Pittsburgh, PA). Cells were then stained with Diff-Quik® as per manufacturers instructions.

4.2.4.2 Cell Cycle Arrest

Flow cytometry analysis of cellular DNA content was performed using a modification to the method described previously (Chen *et al*., 2003). Briefly, cells (2.0×10^4) were harvested by centrifugation (1500 rpm, 5 min) and fixed with ice-cold ethanol (70%) for 30 min to overnight at -20 °C. The ethanol was then removed by centrifugation and cells were stained with PI master mix (100 μg/mL RNase A, 40 μg/mL PI, PBS pH 7.4) for 30 min at 37 °C. DNA content was then measured using a Becton Dickinson BD™

LSR II FACSort flow cytometer (BD Biosciences, USA) and the proportion of cells in G0/G1, S and G2/M phases of cell cycle were calculated on the basis of DNA distribution histograms using FlowJo software (V7.1, Tree Star Inc., USA).

4.2.4.3 Analysis of Cell Morphology using Light Microscopy

Cells were prepared as described in Section 4.2.3.1 and incubated at 37 ºC (95% humidity, 5% CO_2) with increasing concentrations of test compounds (i.e. **37**, **39**, **46**, **53**, **58** and **59**) for 24 h (unless stated otherwise). Changes in cellular morphology, in reference to DMSO controls were then noted after viewing samples under a Leica DM IL inverted light microscope (Leitz Wetzlar, Germany).

4.2.4.4 Effect on Tubulin Polymerisation

4.2.4.4a Tubulin Polymerisation Assay

The tubulin polymerisation assay is a one step, fluorescence-based procedure for determining the effects of compounds on tubulin polymerisation (Bonne *et al*., 1985). It uses neuronal tubulin, which generates a polymerisation curve representing the three phases of microtubule formation; namely: nucleation, growth and steady state equilibrium. Compounds that interact with tubulin will often alter one or more of the characteristic phases of polymerisation. For example, Figure 4.4 shows the effect of adding the anti-mitotic drug paclitaxel and the microtubule destabilising drug vinblastine to the standard polymerisation reaction. Addition of paclitaxel at a concentration of 3 μM eliminates the nucleation phase and enhances the V_{max} of the growth phase. Thus, one application of this assay is the identification of novel anti-

mitotics. A second application is the detection of destabilising agents, for example, addition of vinblastine at a final concentration of 3 μM, causes a drastic decrease in V_{max} (Figure 4.4) and reduction in final polymer mass. Compounds **39**, **54**, **59** and **60** were tested for their anti-mitotic ability in reference to vinblastine sulfate and paclitaxel positive controls in a fluorescent based Tubulin Polymerisation Assay adapted from the method described by Bonne *et al*., (1985). Briefly, 50 μL tubulin reaction mix (2 mg/mL purified bovine brain tubulin in 80 mM PIPES pH 6.9, 2.0 mM $MgCl_2$, 0.5 mM EGTA, 1.0 mM GTP and 20% glycerol was added to duplicate wells of a half area 96-well black plate containing 5 μL of either vehicle control, paclitaxel, vinblastine sulfate or compounds **39**, **54**, **59** and **60** all at a final concentration of 3 μM or 10 μM. The rate

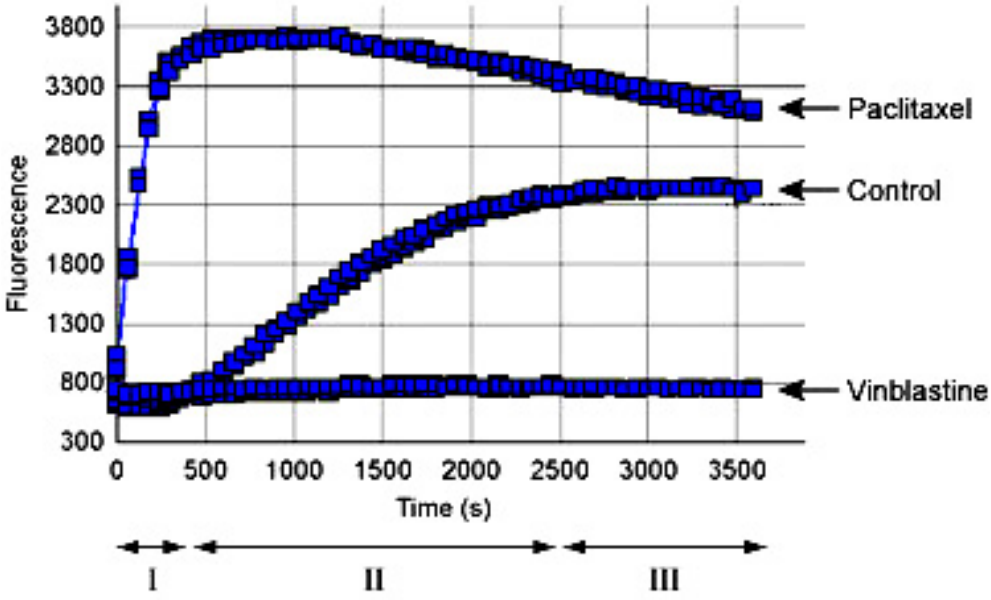

Figure 4.4 Measurement of tubulin polymerisation using the fluorescence based tubulin polymerisation assay. The three Phases of tubulin polymerisation are marked for the control polymerisation curve; I: nucleation, II: growth and III: steady state equilibrium. Addition of 3 μM paclitaxel induces tubulin stabilisation, while addition of 3 μM vinblastine causes tubulin destabilisation. Adapted from Cytoskeleton Inc. Technical Bulletin, 2006.

of polymerisation was followed for 1 h at 37 °C using an excitation wavelength of 360 ±10 nm and the fluorescence was collected at 440 ±10 nm.

4.2.4.4b Live Cell Staining with Tubulin Tracker ™ Green

Tubulin Tracker™ Green (Oregon Green® 488 taxol bis-acetate) reagent is an uncharged, non-fluorescent compound that easily passes through the plasma membrane of live cells to bind to polymerised tubulin. Once inside the cell, the lipophilic blocking group is cleaved by nonspecific esterases, resulting in a green-fluorescent, charged form which absorbs and emits optimally at 494 nm and 522 nm respectively, which can be visualised using a standard FITC filter. U937 cells (2.2×10^5 cells/ mL, 90 μL) were seeded into the wells of a 96-well microtitre plate and incubated for 24 h (37 ºC, 95% humidity, 5% CO_2) prior to the addition of test compound. Compound **54** (10 μL) was then added to the cells at a concentration that induced the greatest amount of morphological change (as determined from light microscopy experiments, Section 4.2.4.1) and were incubated for a further 24 h. Control samples were also prepared by incubating cells with either 2 μM vinblastine sulfate salt (positive control) or 2.5% DMSO (negative control) for 24 h. Cells were then stained with freshly prepared TubulinTracker™ Green reagent at a final concentration of 250 nM for 0.5 h (37 ºC, 95% humidity, 5% CO_2) as per manufacturers instructions. Stained cells were washed once with Dulbecco's PBS and fluorescence visualised by confocal microscopy. Confocal laser scanning microscopy images were acquired using a Leica TCS SP system with a UV 63 × 1.32 NA oil PALPO immersion objective lens (Leica,

Heidelberg, Germany). Cells were excited using the 488 nm spectral line of the Argon ion laser and fluorescence collected at 500-540 nm.

4.2.4.5 Kinase Inhibitory Assays

4.2.4.5a CDK5, GSK3 and DYRK1A

The inhibitory activity of the *N*-alkylisatins **39**, **45**, **48**, **54**, **59** and **60** against glycogen synthase kinase 3 (GSK-3), cyclin dependant kinase 5 (CDK5) and dual-specificity tyrosine-phosphorylation regulated kinase 1A (DYRK1A) were determined by Olivia Lozach in collaboration with Dr Laurent Meijer at the CNRS Station Biologique (Roscoff, France). Assays were carried out according to the method described by Leclerc *et al*., (2001).

4.2.4.5b JAK1, JAK2 and c-FMS

The inhibitory activity of the *N*-alkylisatins **39**, **45**, **48**, **54**, **59** and **60** against the Janus protein tyrosine kinase 1 (JAK1) and 2 (JAK2), and colony-stimulating factor-1 receptor (c-FMS/ CSF-1-R) were carried out by Dr. Christopher Burns and colleagues at Cytopia Research Pty Ltd. (Melbourne, Australia). Kinase assays were performed in 384 well Optiplates using the Alphascreen™ Protein Tyrosine Kinase kit (PerkinElmer Life and Analytical Sciences Inc., MA, USA), as per manufacturers instructions. The biotinylated peptide biotin-EGPWLEEEEEAYGWM-DF-NH_2 for c-FMS and JAKs (final concentration 1-5 mM) was used as the substrate. Affinity purified PTK domain (1.5 mg) was used in the presence of 50 mM HEPES, pH 7.5, 10 mM $MgCl_2$, 150 mM NaCl and 1 mM-10 mM ATP. In the Alphascreen assay (see Figure 4.5 for schematic

representation), the Alphascreen phosphotyrosine acceptor beads followed by streptavidin donor beads were added under subdued light. Inhibitors were added to the assays 15 min prior to the addition of ATP. Inhibitors were added in aqueous DMSO, with DMSO concentrations never exceeding 1%. The Alphascreen plates were then read on a Packard Fusion *Alpha* at the specified wavelength. Data is reported as n = 2, referring to 2 separate assays run at different times. For cell based assays, the growth factor dependent myelomonocytic cell line BaF3 was transfected with either pTELJAK2 or pTELJAK3 and the cells selected for factor independent growth. BaF3 TEL/JAK cells were cultured in DMEM 10% Tet-System Approved FBS (without

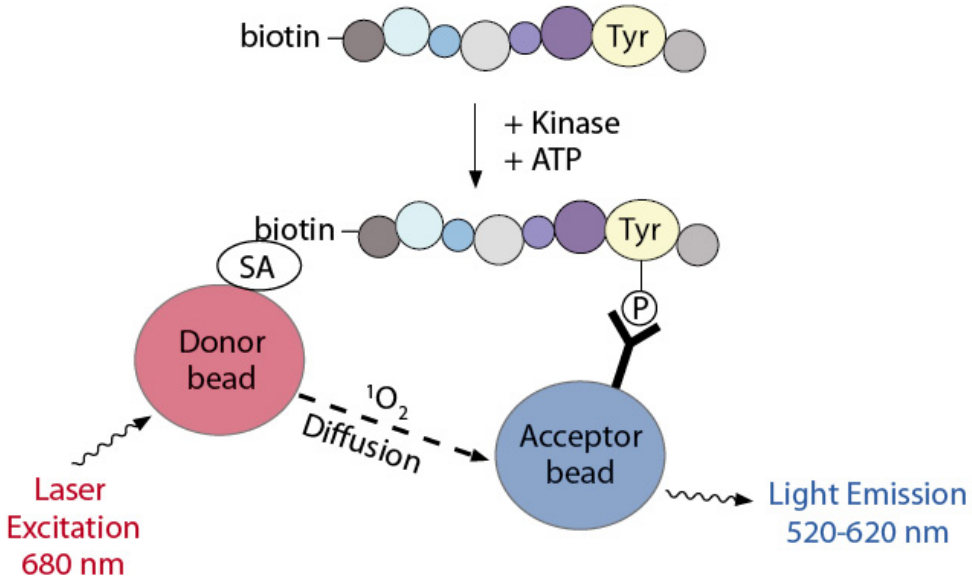

Figure 4.5 Principle for the AlphaScreen™ assay. The AlphaScreen™ assay is based on a sandwich assay principle. After tyrosine kinase phosphorylation, a biotinylated polypeptide substrate is sandwiched between a streptavidin (SA)-coated Donor bead and an anti-phosphotyrosine antibody conjugated Acceptor bead. Phosphorylation of the polypeptide by the tyrosine kinase results in an increase in the luminescence signal in the range of 520-620 nm.

WEHI 3B conditioned medium). All cells were grown at 37 °C in 5% CO_2. Cell suspensions were prepared by harvesting cells in later log phase growth from culture and were diluted into growth medium to 1.1 × the final concentration (from 5.0×10^4 cell/mL to 2.0×10^4 cell/mL, depending on the cell line). The *N*-alkylisatins **39**, **45**, **48**, **54**, **59** and **60** were added (10 μL, 10 × the final concentration) to a flat bottom 96-well plate. The cellular suspension (90 μL per well) was then added and the plate incubated for 40 h at 37 ºC, 5% CO_2. MTT (20 μL per well, 5 mg/mL in PBS) was added and the plates were returned to the incubator for a further 6 h. Lysis buffer (100 μL per well, 10% SDS, 0.01N HCl) was added and the plate stored in the incubator overnight. The plates are then read at 590 nm.

4.3 Results and Discussion

4.3.1 Cytotoxic Activity and SAR Studies

As part of an ongoing effort to identify potent inhibitors of cancer cell proliferation, *N*-alkylated analogues of the isatin moiety (with and without substituents) were investigated for cytotoxicity against a range of cancer cell types. A structure activity-based selection process was used to identify several crucial structural requirements needed to enhance cytotoxicity, which were determined initially against three human cancer cell lines (U937, Jurkat and MCF-7, Table 4.2). The general trend observed amongst the 3 cancer cell populations indicated that:

1. Introduction of an aromatic ring with a one carbon atom linker at N1 (e.g. compound **38**) enhanced biological activity from that of allyl, 2'-methoxyethyl and 3'-methylbutyl *N*-substituted isatins (**33-37**), by at least a factor of 2 when

comparing the 5,7-dibrominated series. No significant change in activity was observed for compounds tested against the MCF-7 cell line.

2. Introduction of electron withdrawing groups such as $-NO_2$ were favoured in the *para* (**49**) position over the *ortho* (**50**) orientation, however no significant difference in activity was observed for *para* (**45**) or *meta* (**48**) substituted $-OCH_3$ groups.
3. Introduction of a bromine atom at C5 and C7 or C5, C6 and C7 for the *N*-(*p*-methoxybenzyl)isatin series of compounds (**45** and **47**), substantially increased biological activity in comparison to the non- (**40**) or mono-substituted (**41-44**) *N*-alkyl isatins (Figure 4.6). In both the *N*-allyl and *N*-(*p*-methoxybenzyl)isatin series, tri-bromination always led to the most active compound.
4. Increasing the carbon chain length from 1 (**38**) to 3 (**59**) resulted in no significant difference in activity against all 3 cancer cell lines tested.

Focusing on the most active compounds in the 5,7-dibromo-*N*-alkylisatin series, 9 were found to exhibit IC_{50} values in the sub-micromolar range against at least one cancer cell line (Table 4.2). 5,7-Dibromo-*N*-(*p*-methylbenzyl)isatin, (**39**) was the most active compound against two malignant haematological cell lines, inhibiting 50% of the metabolic activity and hence cellular proliferation in both U937 and Jurkat cells at a concentration of 0.49 μM (Table 4.2). This was 22 times more potent than the unsubstituted 5,7-dibromoisatin (**13**, Vine *et al*., 2007), thus emphasising the value of

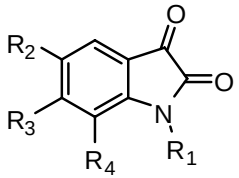

Table 4.2 Cytotoxicity of isatin derivatives **33-60** on U937[a], Jurkat [b] and MCF-7 [c] cells as calculated from dose response curves.[d]

Compound	R_1	R_2	R_3	R_4	IC_{50} (μM) [d]		
					U937	Jurkat	MCF-7
33	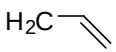	Br	H	Br	6.67	NT[f]	NT[f]
34	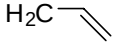	Br	Br	H	4.93	5.07	6.96
35	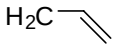	Br	Br	Br	2.36	0.71	2.29
36	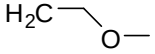	Br	H	Br	3.44	8.95	6.67
37	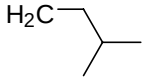	Br	H	Br	2.40	3.47	7.49
38	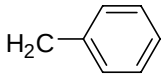	Br	H	Br	1.14	1.14	7.09
39		Br	H	Br	0.49	0.49	11.0
45	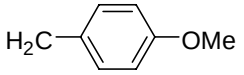	Br	H	Br	1.83	0.59	5.18
46	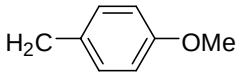	Br	Br	H	12.4	6.82	10.6
47	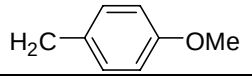	Br	Br	Br	1.19	0.50	4.17

Table 4.2 continued from page 113

Compound	R_1	R_2	R_3	R_4	IC_{50} (μM) [e]		
					U937	Jurkat	MCF-7
48	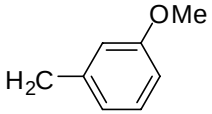	Br	H	Br	1.76	2.00	2.35
49		Br	H	Br	0.89	0.89	4.32
50	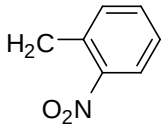	Br	H	Br	2.27	NT[f]	3.18
51	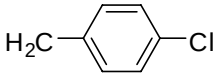	Br	H	Br	0.98	0.50	3.87
52	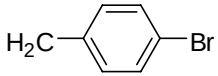	Br	H	Br	0.63	0.63	5.27
53	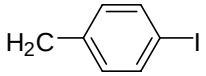	Br	H	Br	2.30	0.58	4.22
54		Br	H	Br	0.80	0.69	7.13
55	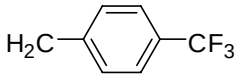	H	Br	H	5.21	5.21	NT[f]
56	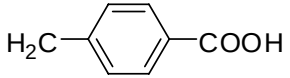	Br	H	Br	>14.2	>14.2	>14.2
57	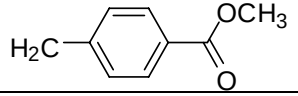	Br	H	Br	1.19	1.19	9.05

Table 4.2 continued from page 114

Compound	R_1	R_2	R_3	R_4	IC_{50} (μM) [e]		
					U937	Jurkat	MCF-7
58	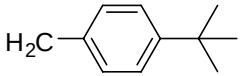	Br	H	Br	1.13	0.66	2.64
59	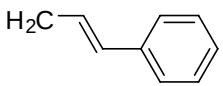	Br	H	Br	2.37	1.42	7.81
60	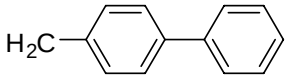	Br	H	Br	0.76	0.74	4.88
vinblastine					6.88	NT[f]	NT[f]
5-FU					>48.05[g]	NT[f]	NT[f]

[a] U937: human monocyte-like, histiocytic lymphoma cell line.
[b] Jurkat: human leukemic T-cell line
[c] MCF-7: human epithelial, mammary gland adenocarcinoma (non-metastatic) cell line.
[d] Sigmoidal dose response curves (variable slope) were generated using GraphPad Prism V. 4.02 (GraphPad Software Inc.).
[e] Values are the mean of triplicates of at least two independent experiments.
[f] NT = not tested
[g] U937 cells were incubated with increasing concentrations of 5-fluorouracil (5-FU) for 72 h. See Appendix 2 (Figure A2.1) for a comparison of 5-FU and *N*-alkylisatin cytotoxicity.

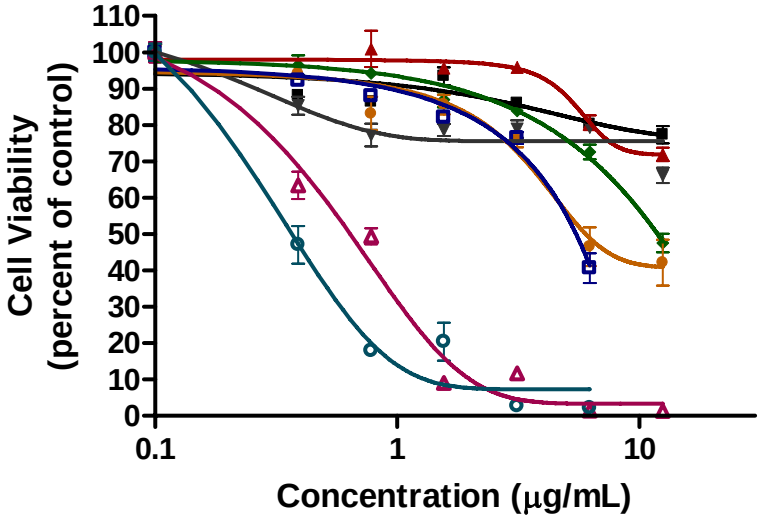

Figure 4.6 Viability of U937 cells after treatment with different concentrations of ■) *N*-(*p*-methoxybenzyl)isatin (**40**), ▲) 4-bromo-*N*-(*p*-methoxybenzyl)isatin (**41**), ▼) 5-bromo-*N*-(*p*-methoxybenzyl)isatin (**42**), ♦) 6-bromo-*N*-(*p*-methoxybenzyl)isatin (**43**), ●) 7-bromo-*N*-(*p*-methoxybenzyl)isatin (**44**), ∆) 5,7-dibromo-*N*-(*p*-methoxybenzyl)isatin (**45**), □) 5,6-dibromo-*N*-(*p*-methoxybenzyl)isatin (**46**), ○) 5,6,7-tribromo-*N*-(*p*-methoxybenzyl)isatin (**47**). Briefly, cells were incubated for 24 h at 37 °C (95% humidity, 5% CO_2) with increasing concentrations of test compound, then analysed for a change in metabolic activity and expressed as percent viability in reference to the DMSO control. Each data point is a mean of triplicates ± SE.

N1 substitution for cytotoxic activity. In addition, compound **39** was >22 times more selective for leukemic (Jurkat) and lymphoma (U937) cancer cell lines than the MCF-7 breast adenocarcinoma cell line (Table 4.2). Five other *N*-alkylisatins (**49**, **51**, **52**, **54** and **60**) also demonstrated a similar pattern of specificity, but none were as potent as **39**. This effect may be due in part to the expression of the anti-apoptotic Bcl-2 group of proteins that have been identified in MCF-7 cells, of which Bcl-2 and Bcl-XL expression specifically have been correlated with resistance and poor response to chemotherapy (Piche *et al*., 1998). Clinically, increased levels of Bcl-2 and Bcl-XL are

also associated with a poor response to chemo- and radiotherapy (Campos *et al*., 1993; Sakakura *et al*., 1996; Zhang *et al*., 2000), whereas increased levels of Bax are correlated with a good response (Zhang *et al*., 2000). For example, docetaxel sensitises MCF-7 cells to chemotherapy induced apoptosis through its ability to phosphorylate and inactivate Bcl-2 (Berchem *et al*., 1999). Similarly, doxorubicin causes a decrease in Bcl-2 expression and an increase in Bax expression (Leung *et al*., 1999). Etoposide and 4-hydroperoxycyclophosphamide both increase pro-apoptotic Bax levels (Leung *et al*., 1999; Gibson *et al.*, 1999) and when used in combination, reduce Bcl-2 expression and increase Bax levels more than either agent alone (Gibson *et al.*, 1999). Future studies may therefore involve synthesising structural analogues of the most active compounds against MCF-7 cells (**35**, **48** and **58**, Table 4.2), with the aim of increasing cytotoxicity and correlating it with the expression levels of Bcl-2 and Bax.

Interestingly, activity was abrogated in all 3 cancer cells lines when a carboxylic acid was substituted at the *para* position of the aromatic ring (**56**, Table 4.2). Such a decrease in activity was not correlated with electronic (σ) or steric effects (Es), hydrophobicity (c Log*P*) or localised hydrophobicity at the *p*-substituent (π) (Table 4.3). Considering that the pKa of benzoic acid is 4.2 (Merck Index, 2006), it is hypothesised that the carboxylic acid of **56** is deprotonated upon addition to the cell culture media (pH *ca* 7.4) and forms the carboxylate anion, resulting in the lipophilicity of the molecule being significantly reduced (Table 4.3). This implies that the *p*-substituent may play an important role in the cytotoxicity of the *N*-alkylisatins, but the large variety

Table 4.3 Physiochemical properties[a] of selected *N*-alkylisatins.

Compound	Substituent	c Log*P*	π	σ_p	E_s	IC_{50} (μM) Jurkat
38	-H	4.29	0.00	0.00	0.00	1.10
39	$-CH_3$	4.79	0.56	-0.17	-1.20	0.49
49	$-NO_2$	4.04	-0.80	0.78	-0.50	0.89
51	-Cl	4.18	1.10	0.23	-0.50	0.50
52	-Br	5.16	0.86	0.23	-2.50	0.63
53	-I	5.42	1.10	0.18	-0.90	0.58
54	$-CF_3$	5.18	0.88	0.54	-1.10	0.69
56	-COOH	4.04	-0.16	0.45	-1.40	>14.20
	$-COO^-$	1.80				>14.20
58	$-C(CH_3)_3$	6.12			-1.70	0.66
60	-Ph	6.18	2.00	-0.01	-3.80	0.74
Correlation Coefficient (*R*)[b]		**0.09** (*P* = 0.82)	**0.45** (*P* = 0.27)	**-0.31** (*P* = 0.46)	**-0.09** (*P* = 0.83)	

[a]c Log*P* values were calculated using ChemDraw Ultra V. 8.0 (CambridgeSoft Corporation). Other physiochemical constants were obtained from Hansch and Leo, (1979).
[b]The correlation coefficient (*R*) was calculated using the Pearson correlation test (GraphPad Prism V 4.0).

of groups that can be substituted at this position suggests that there is no highly specific binding interaction occurring in this region. Alternatively, carboxylate anion formation may reduce cell uptake and hence cytotoxicity.

The cytotoxicity of the most active compounds (i.e. IC_{50} < 1 μM) determined in the initial cell line screen, were subsequently tested against a panel of 4 additional adherent cancer cell lines (PC-3, MDA-MB-231, HCT-116 and A-375; Table 4.4) and one normal, non-transformed human cell line suspension (PBL; Figure 4.8). Of the 9 compounds tested, four exhibited activity in the sub-micromolar range (**52**, **54**, **58** and **60**, Table 4.4) against at least one cell line. HCT-116 cells were the most susceptible to

Table 4.4. Cytotoxicity of selected *N*-alkyl isatins against various cancer cell lines as determined by dose response curves.[a]

	IC_{50} (μM)[b]			
Compound	**PC-3[c]**	**MDA-MB-231[d]**	**HCT-116[e]**	**A375[f]**
39	4.57	1.91	1.22	2.00
45	3.50	5.29	2.59	4.66
49	NT[g]	2.75	2.70	2.50
51	2.17	2.77	1.84	1.68
52	3.44	1.90	0.53	1.22
53	10.9	2.92	3.36	2.40
54	1.17	0.54	0.84	1.25
58	3.06	0.98	1.66	0.89
60	3.42	2.06	0.83	1.19

[a] Sigmoidal dose response curves (variable slope) were generated using GraphPad Prism V. 4.02 (GraphPad Software Inc.).
[b] Values are the mean of triplicates of at least two independent experiments.
[c] PC-3: human prostate adenocarcinoma cell line.
[d] MDA-MB-231: human epithelial, mammary gland carcinoma (metastatic) cell line.
[e] HCT-116: human colorectal carcinoma cell line.
[f] A375: human malignant melanoma cell line.
[g] NT = Not tested.

treatment, with an average IC_{50} value of 1.7 μM (±1.0). Of those tested against this cell line, compound **52** was the most active, displaying an IC_{50} value of 0.53 μM. Conversely, PC-3 cells were the least susceptible to treatment overall, displaying an average IC_{50} value of 2.7 μM (±1.0, Table 4.4). Interestingly, cancer cell line selectivity was observed for compound **54** which exhibited greater than 5 times more activity towards the lymphoma and leukemic cell lines than the freshly-isolated, human peripheral blood lymphocytes (Figure 4.8). In all cases, treatment was more efficacious against the Jurkat (average IC_{50} 0.6 ± 0.1) and U937 (average IC_{50} 1.1 ± 0.6) cell lines over any of the epithelial derived cell lines. This is promising considering the lack of effective and non-toxic drugs available for the treatment of MDR lymphoid

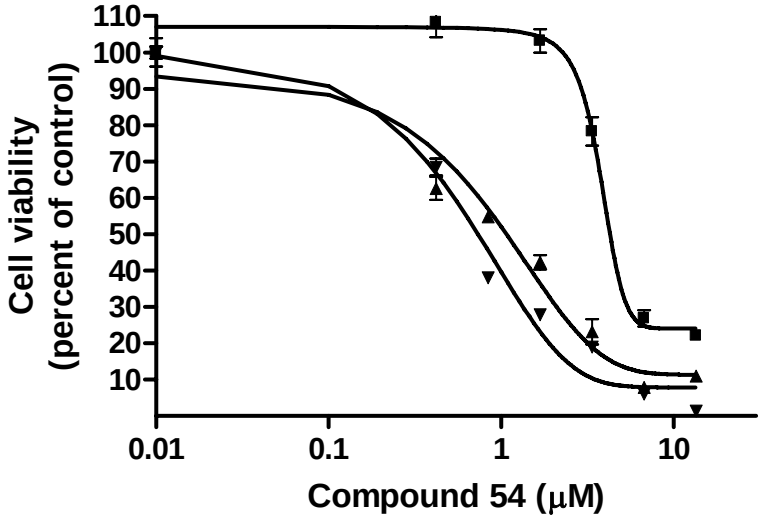

Figure 4.8 Cancer cell selectivity. Increasing concentrations of 5,7-dibromo-*N*-(*p*-trifluoromethylbenzyl)isatin (**54**) were incubated with either ■) freshly isolated, non-transformed, human peripheral blood lymphocytes (PBL), ▲) human monocyte-like, histiocytic lymphoma cells (U937) or ▼) human leukemic T-cells (Jurkat) for 24 h at 37 °C (95% humidity, 5% CO_2). Cells were then analysed for a change in metabolic activity and expressed as percent viability in reference to the DMSO control. Each data point is a mean of triplicates ± SE.

malignancies such as B-cell chronic lymphocytic leukemia (B-CLL), acute myelocytic leukemia, multiple myeloma and non-Hodgkin's lymphoma (Newcomb, 1995; Drénou *et al*., 1997; Nooter and Sonneveld, 2004).

4.3.2 Mode of Action Investigations

4.3.2.1 Apoptosis and Cell Cycle Arrest

Apoptosis plays a pivotal role in the cytotoxic activity of most chemotherapeutic drugs (Nguyen and Wells, 2003). Since it is known that several *N*-alkylindole derivatives can

induce G2/M arrest (Bacher *et al*., 2001; Bramson *et al*., 2001; Andreani *et al*., 2005) and apoptosis (Nguyen and Wells, 2003) in certain cancer cell lines, the effect of the most potent *N*-alkylisatins on the activation of the effector caspases 3 and 7 and cell cycle progression was investigated in an attempt to investigate the molecular mode of action. The isatins **35** and **45** were chosen as representative molecules for evaluation and were found to activate caspase 3 and 7 in a dose dependant manner in Jurkat cells, with maximum activity detected at 2 μM after 5 h (Figure 4.9a and b, respectively). Compound **54** was also found to activate caspase 3 and 7 in a dose (Figure 4.9c) and time (Appendix 2, Figure A2.2) dependant manner. At 3.3 μM the activity of compound **54** was comparable to that of the staurosporine positive control. Unlike staurosporine however, **54** exhibited a caspase activation trend in U937 cells similar to that seen in the Jurkat cell line, while only minimal caspase activity was observed in PBLs (Figure 4.9d). This compares closely with cytotoxicity data (Figure 4.8) whereby a decrease in the viability of cells correlates to an increase in the activation of effector caspases 3 and 7 and hence apoptosis. Such an effect was further supported by the appearance of fragmented nuclei in morphologically altered U937 cells after treatment with compound **53** at an equivalent concentration (Figure 4.10). Furthermore, U937 cells treated with compounds **39** and **54** at a concentration of 0.5 μM, exhibited an increase in the accumulation of cells in G2/M, in comparison to vehicle control treated cells (Figure 4.11, panels G and H). This effect was both dose and time-dependent, whereby mitotic arrest was most apparent after 24 h. At higher concentrations (i.e. 2 μM and 1 μM), cells treated with compounds **39** and **54** (respectively) showed an increase in S phase and

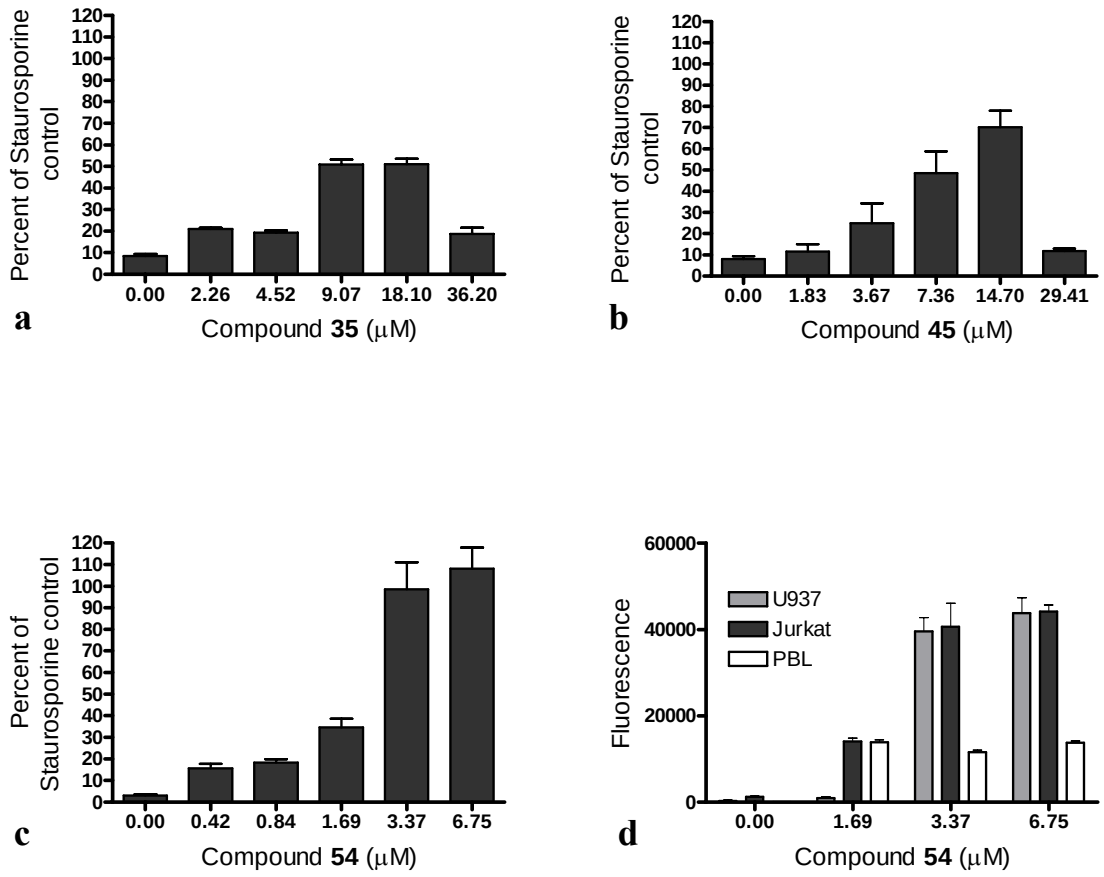

Figure 4.9 Activation of the effector caspases 3 and 7 in Jurkat, U937 and PBL cells after treatment with various *N*-alkylisatins. Jurkat cells were exposed to increasing concentrations of either a) *N*-allyl-(5,6,7-tribromo)isatin (**35**), b) 5,7-dibromo-*N*-(*p*-methoxybenzyl)isatin (**45**), or c) 5,7-dibromo-*N*-(*p*-trifluoromethylbenzyl)isatin (**54**) for 5 h at 37°C and values were normalised to a staurosporine (positive control). d) Jurkat, U937 and PBL cells were exposed to 3 concentrations of compound **54** for 5 h at 37°C. Cells were then incubated with the Caspase-3/7 reagent for 1 h at room temperature and fluorescence measured at an excitation wavelength of 485 nm and 520 nm emission. Data are means ± SE of one representative experiment performed in triplicate.

sub-G1 peak distribution (Figure 4.11, panels I and K). Although not observed in vinblastine treated cells, this latter effect was consistent with the induction of apoptosis.

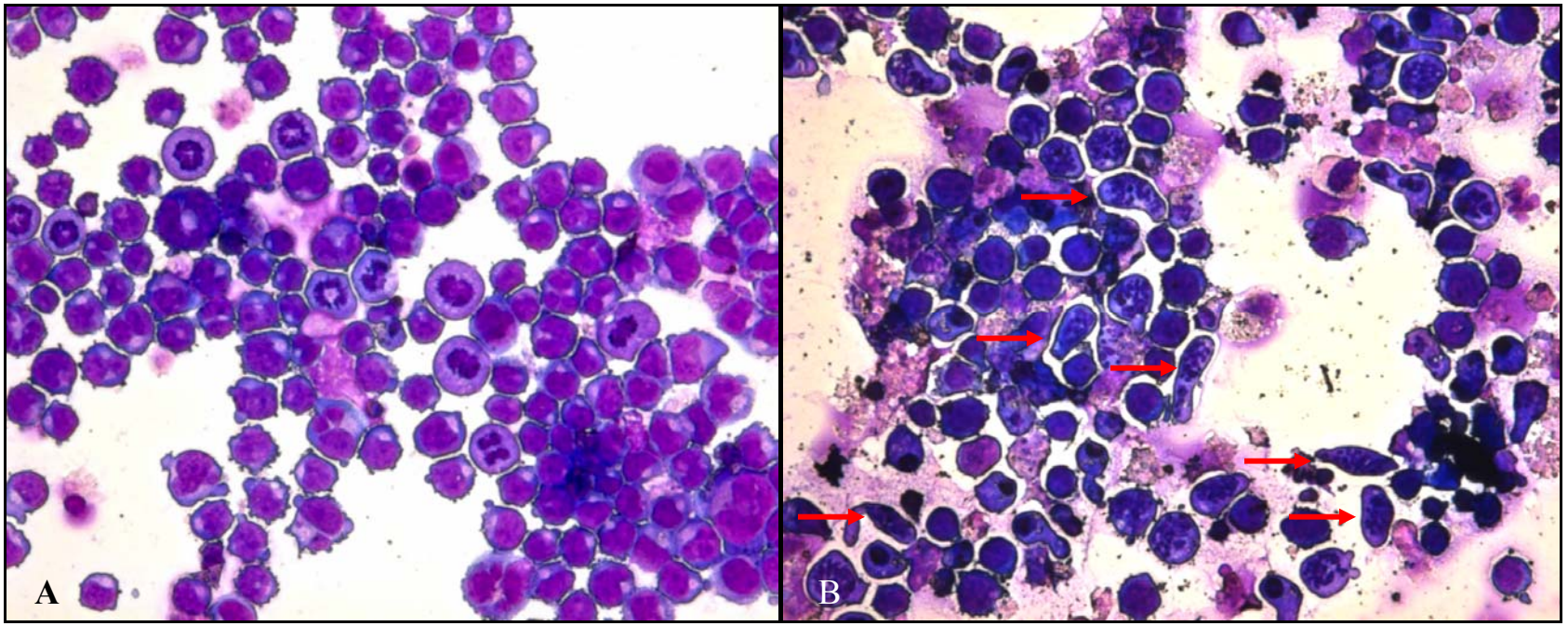

Figure 4.10 Morphological evaluation of nuclei stained with Diff Quik™ after 24 h of treatment. Briefly, U937 cells were treated with either A) DMSO vehicle control or B) 5,7-dibromo-*N*-(*p*-iodobenzyl)isatin (**53**) at 0.39 µg/mL. Treatment dose was based on the concentration that induced the greatest amount of morphological change in U937 cells at 24 h. Red arrows indicate morphologically altered cells containing fragmented nuclei. Magnification × 1000.

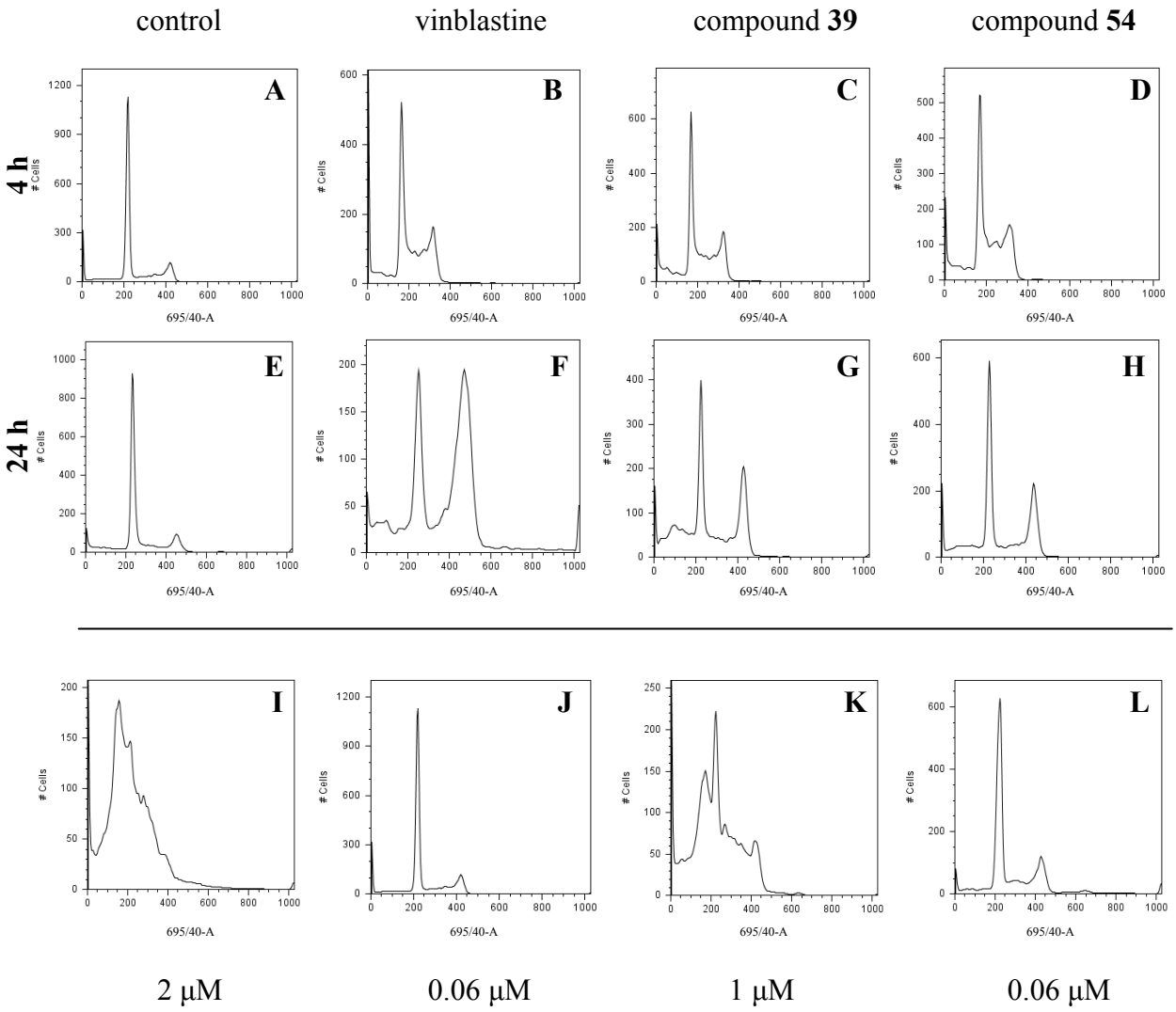

Figure 4.11 The effect of *N*-alkylisatins **39** and **54** on the cell cycle. U937 cells were treated with either A) and E) DMSO vehicle control, B) and F) 0.5 μM vinblastine sulfate, C) and G) 0.5 μM 5,7-dibromo-*N*-(*p*-methylbenzyl)isatin (**39**) or D) and H) 0.5 μM 5,7-dibromo-*N*-(*p*-trifluoromethylbenzyl)isatin (**54**) for 4 h (upper panels) or 24 h (lower panels). Cells were then ethanol fixed, stained with propidium iodide and analysed for DNA distribution by FACS. Cell cycle arrest was additionally determined after treatment with high and low concentrations of compounds **39** (panels I and J) and **54** (panels K and L) for 24 h.

2.3.2.2 Morphological Investigations

In addition to their potent cytotoxicity, various *N*-alkylisatins were also found to dramatically alter lymphocyte morphology. Within 5 h of treatment with compounds **39**, **53** and **59** a sub-population of U937 cells developed an elongated formation as well as irregular membrane protrusions, of which the latter appeared to be consistent with an apoptotic response (Kroemer *et al*., 1998; Figures 4.12c, 4.13c and 4.14c). After 24 h the elongated morphology was more pronounced, but only at lower concentrations (Figures 4.12d, 4.3d and 4.14d). Higher concentrations resulted in the accumulation of cellular debris and compromised membranes, indicative of necrotic cell death (Figures 4.12b, 4.13b and 4.14b) which was further confirmed by PI staining (Appendix 2, Figure A2.3). An analogous effect has also been reported for the benzylamide sulindac derivatives CP461 and CP248, whereby examination of WSU-CLL cells after an 18 h treatment revealed a marked affect on cell shape (Moon and Lerner, 2002). Interestingly, the structurally similar parent compounds, sulindac sulfide and sulindac sulfone, currently being studied as chemo-preventatives in patients with familial adenomatous polyposis (FAP, Van Stolk *et al*., 2000), did not. A change in leukemic T-cell morphology was also noted after treatment with compound **53** (Figure 4.15) but was not as obvious as that observed in the monocyte cell line (Figure 4.13). This effect is further exemplified in Figure 4.16 whereby the appearance of cellular elongation and apoptotic morphology is reduced in Jurkat cells, but cytotoxicity is not (Table 4.2). Morphological alterations were also seen in vinblastine and paclitaxel treated cells (Figure 4.17a and b), but not in 5-fluorouracil (Figure 4.17c) or staurosporine (Appendix 2, Figure A2.4) treated cells suggesting that *N*-alkylisatins may either disrupt

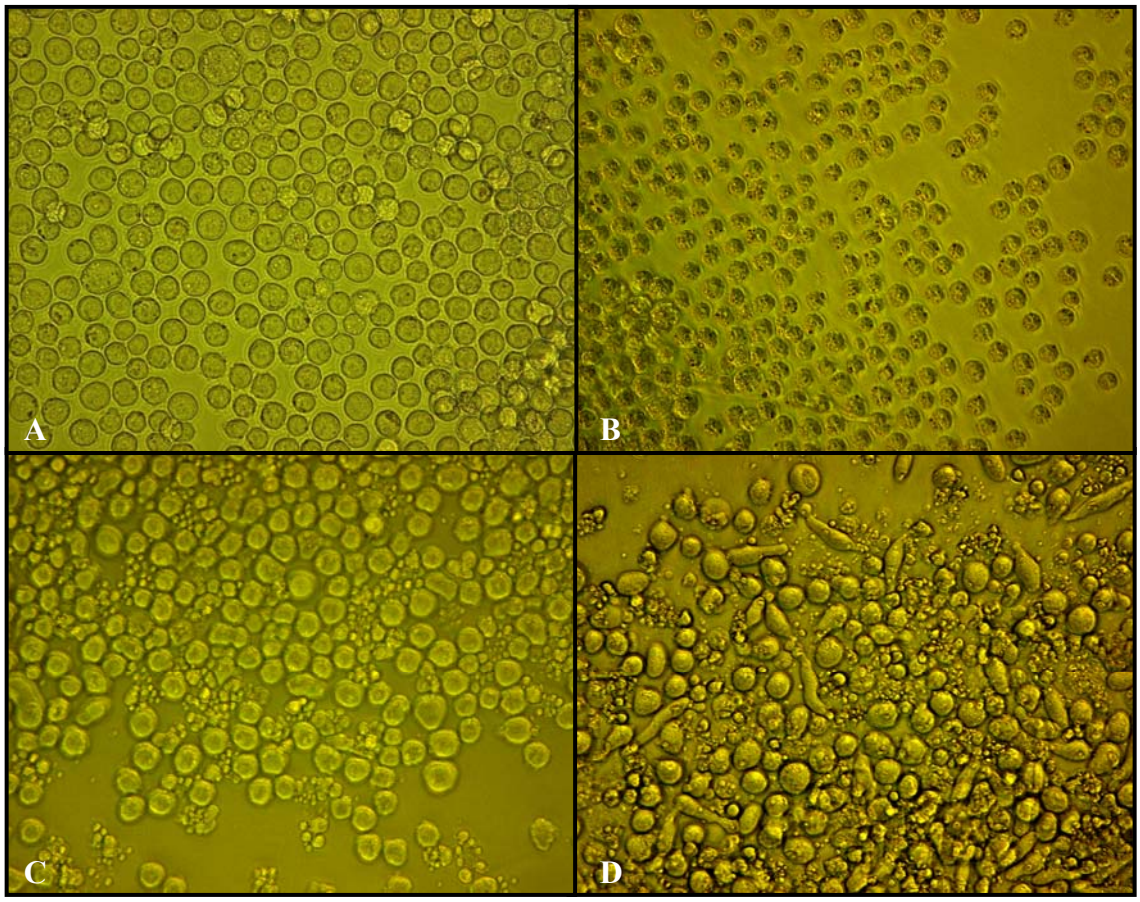

Figure 4.12 Morphological effects of compound 5,7-dibromo-*N*-(*p*-methylbenzyl)isatin (**39**) on U937 cells. Briefly cells (1.0×10^4) were prepared as described in Section 4.3.2.1 and incubated with either A) DMSO vehicle control for 24 h, B) compound **39** at 12.5 µg/mL for 5 h, C) compound **39** at 0.39 µg/mL for 5 h or D) compound **39** at 0.39 µg/mL for 24 h. Images were obtained by brightfield microscopy on an inverted light microscope using a Leica DC500 12-megapixel high-performance FireWire camera system. Images were viewed at 1000 × magnification.

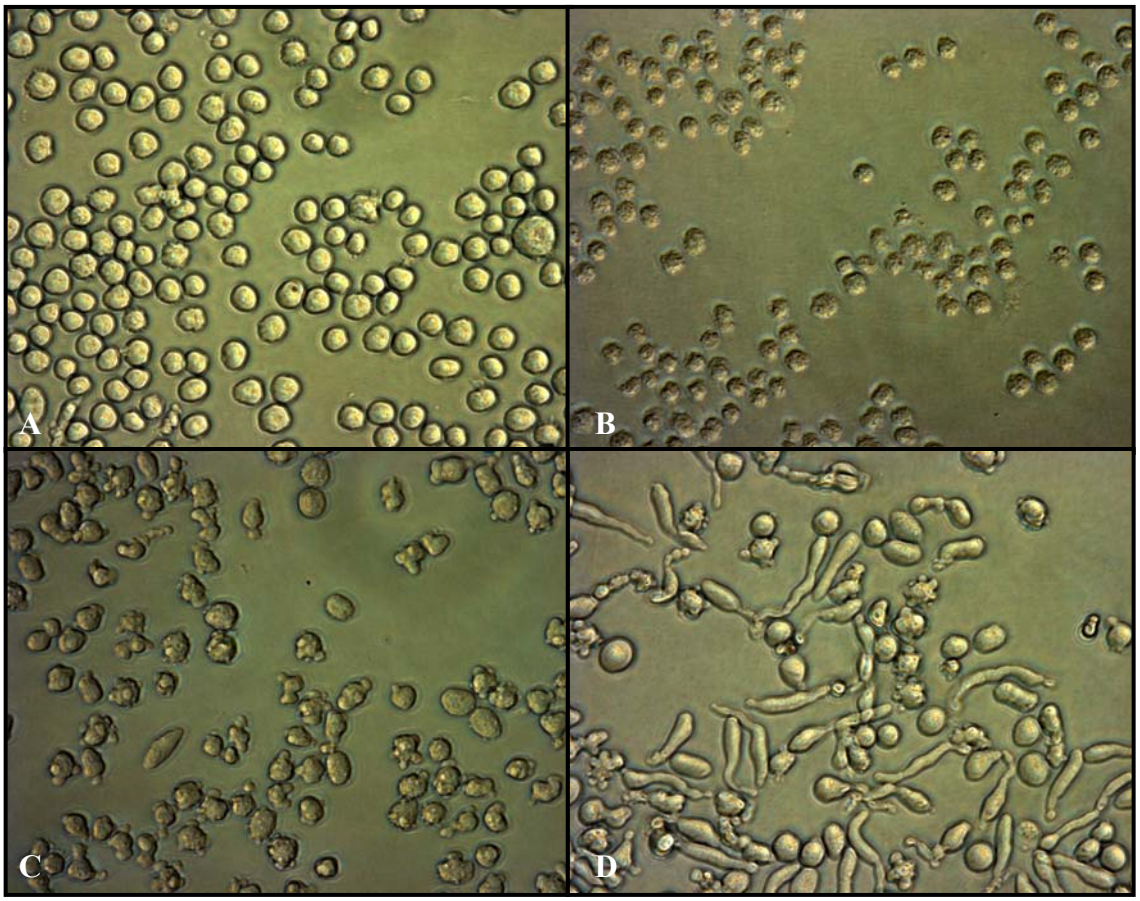

Figure 4.13 Morphological effects of compound 5,7-dibromo-*N*-(*p*-iodobenzyl)isatin (**53**) on U937 cells. Briefly cells (1.0×10^4) were prepared as described in Section 4.3.2.1 and incubated with either A) DMSO vehicle control for 24 h, B) compound **53** at 12.5 µg/mL for 5 h, C) compound **53** at 0.39 µg/mL for 5 h or D) compound **53** at 0.39 µg/mL for 24 h. Images were obtained by brightfield microscopy on an inverted light microscope using a Leica DC500 12-megapixel high-performance FireWire camera system. Images were viewed at 1000 × magnification.

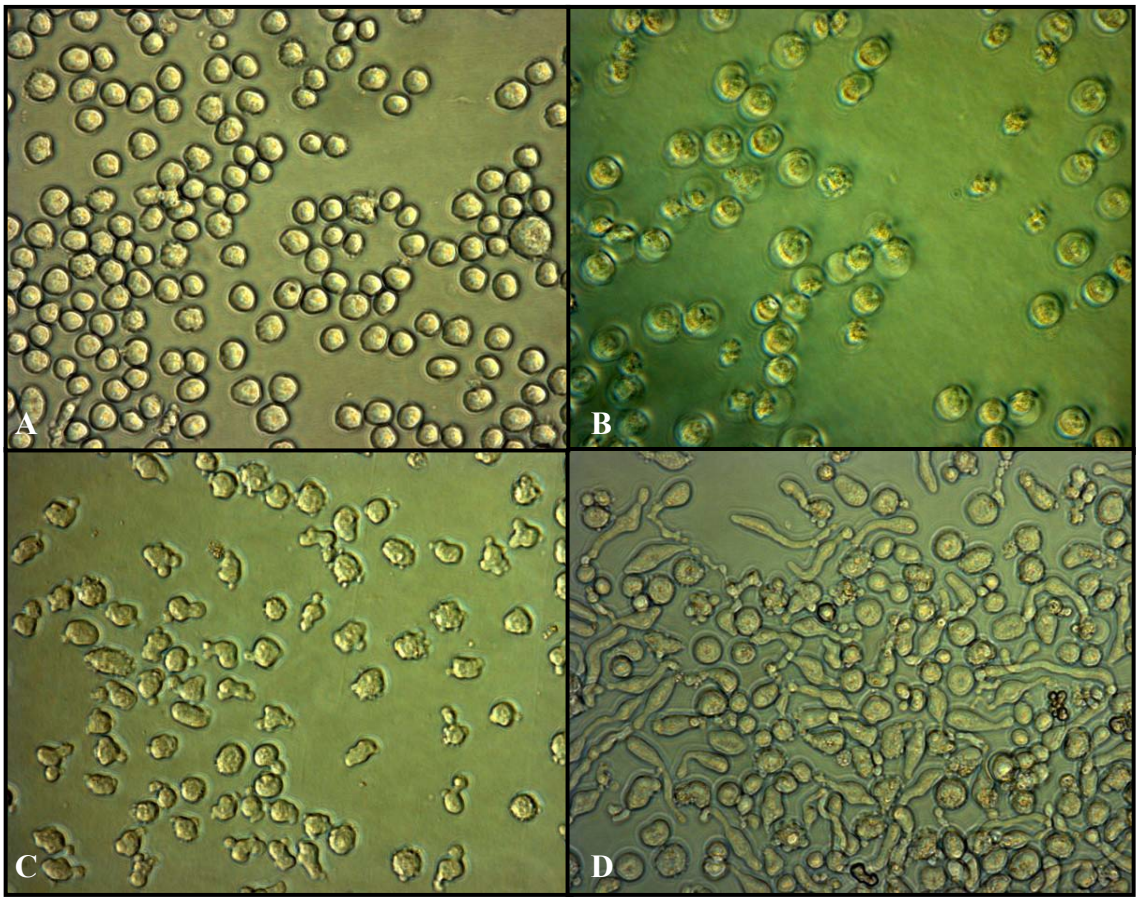

Figure 4.14 Morphological effects of compound 5,7-dibromo-*N*-(cinnamyl)isatin (**59**) onU937 cells. Briefly cells (1.0×10^4) were prepared as described in Section 4.3.2.1 and incubated with either A) DMSO vehicle control for 24 h, B) compound **59** at 12.5 µg/mL for 5 h, C) compound **59** at 0.39 µg/mL for 5 h or D) compound **59** at 0.39 µg/mL for 24 h. Images were obtained by brightfield microscopy on an inverted light microscope using a Leica DC500 12-megapixel high-performance FireWire camera system. Images were viewed at 1000 × magnification.

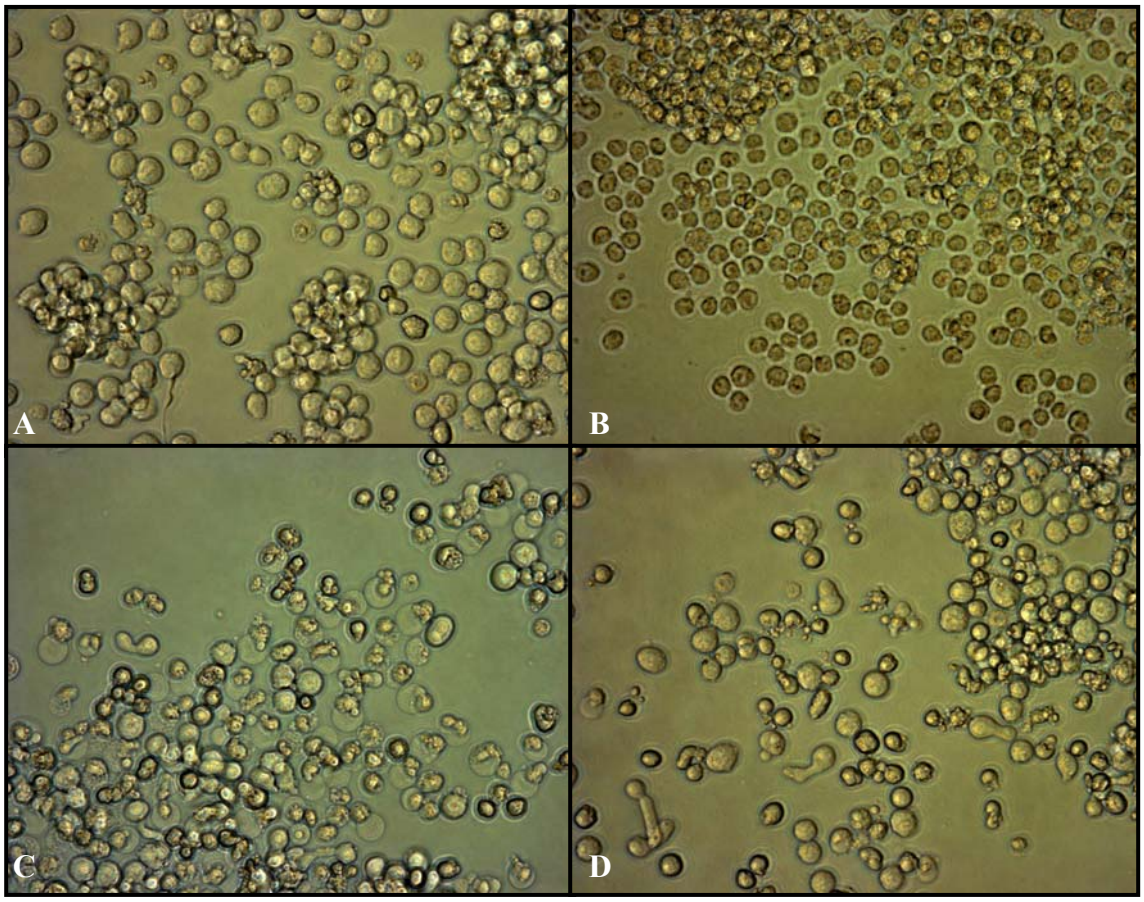

Figure 4.15 Morphological effects of compound 5,7-dibromo-*N*-(*p*-iodobenzyl)isatin (**53**) on Jurkat T-cells. Briefly cells (1.0×10^4) were prepared as described in Section 4.3.2.1 and incubated with either A) DMSO vehicle control for 24 h, B) compound **53** at 12.5 µg/mL for 5 h, C) compound **53** at 0.39 µg/mL for 5 h or D) compound **53** at 0.39 µg/mL for 24 h. Images were obtained by brightfield microscopy on an inverted light microscope using a Leica DC500 12-megapixel high-performance FireWire camera system. Images were viewed at 1000 × magnification.

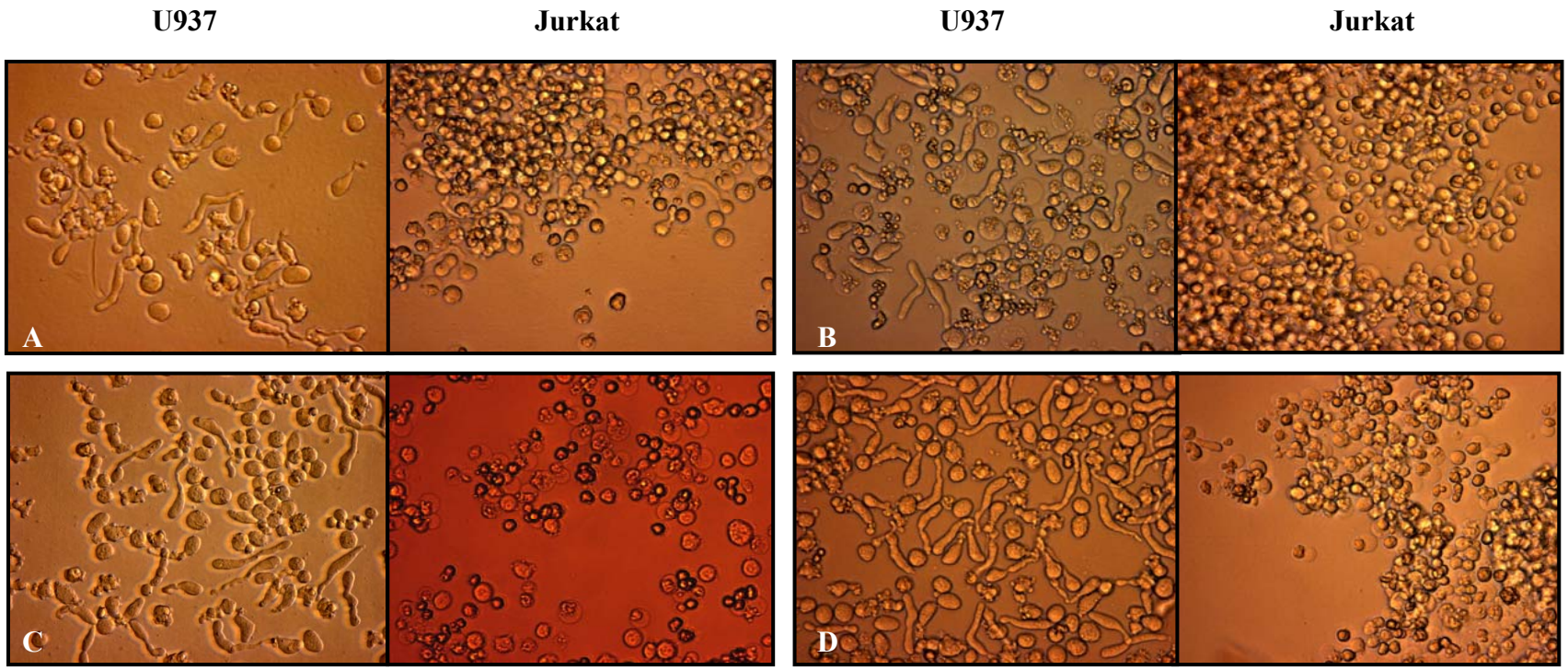

Figure 4.16 A comparison of the morphological effects exhibited by U937 (left panels) and Jurkat (right panels) cells after treatment with 0.39 μg/mL of: A) 5,7-dibromo-*N*-(isopentyl)isatin (**37**), B) 5,7-dibromo-*N*-(*p*-*tert*-butylbenzyl)isatin (**58**), C) 5,6-dibromo-*N*-(*p*-methoxybenzyl)isatin (**46**), and D) 5,7-dibromo-*N*-(cinnamyl)isatin (**59**) for 24 h. Images were obtained by brightfield microscopy on an inverted light microscope using a Leica DC500 12-megapixel high-performance FireWire camera system. Images were viewed at 1000 × magnification.

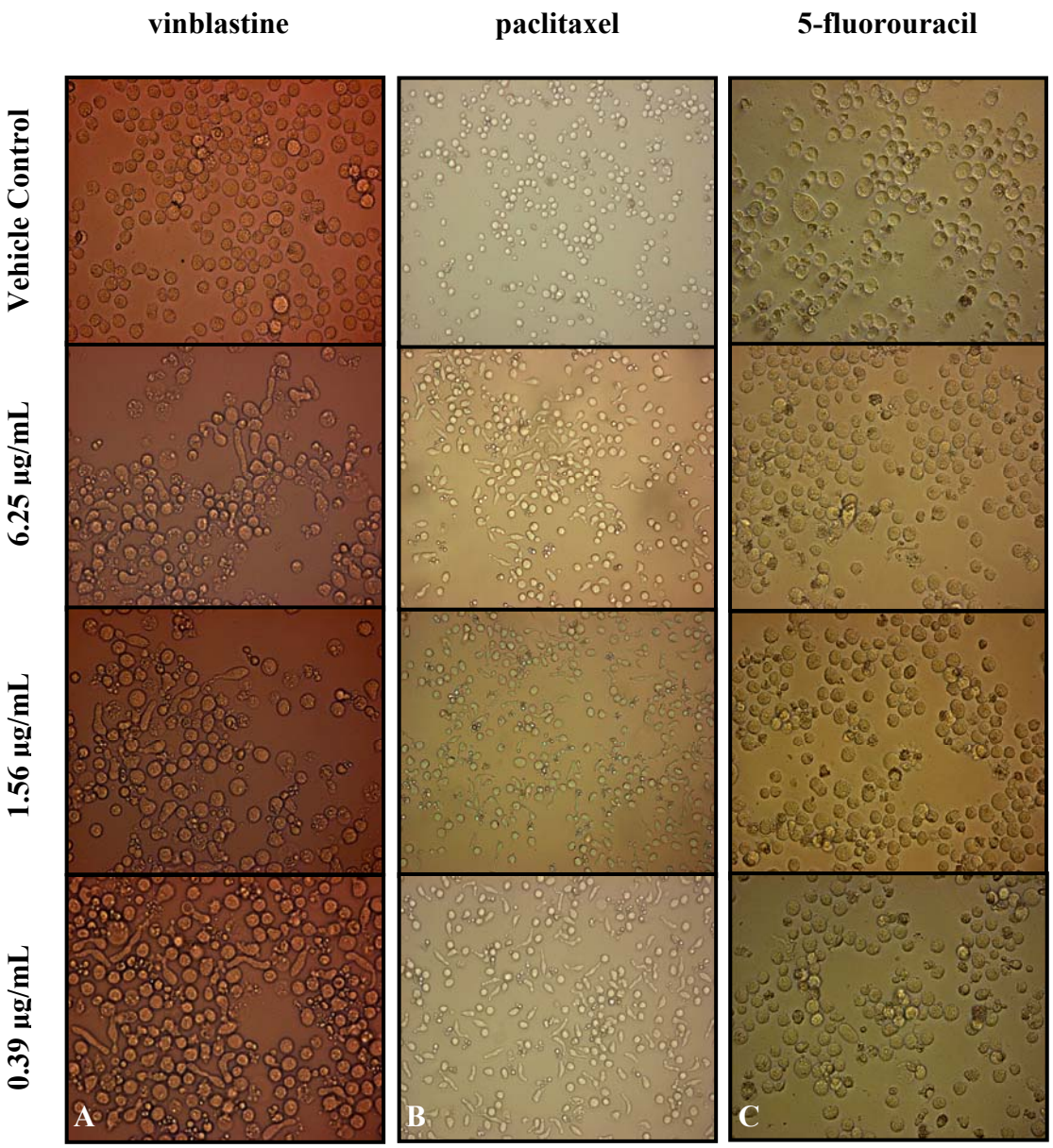

Figure 4.17 The morphological effects of the commercial anticancer agents vinblastine, paclitaxel and 5-fluorouracil on the U937 cell line. Cells were prepared as described in Chapter 2 Materials and Methods, Section 2.3.2.1, then treated with different concentrations of either A) vinblastine sulfate salt, B) paclitaxel or C) 5-fluorouracil for 24 h. Images were obtained by brightfield microscopy on an inverted light microscope using a Leica DC500 12-megapixel high-performance FireWire camera system and were viewed at A) 1000 × magnification, B) 400 × magnification and C) 1000 × magnification.

or stabilise microtubles in a fashion similar to the *Vinca* alkaloids (Rai and Wolff, 1996) or taxanes (Schiff *et al*., 1979). The ability of various *N*-alkylisatins to inhibit microtubule polymerisation in the *in vitro* microtubule polymerisation assay was therefore investigated.

2.3.2.2 Effects on Tubulin Polymerisation and Microtubule Formation

The indole nucleus is the core structure of a large number of tubulin polymerisation inhibitors (Beckers *et al*., 2003; Brancale and Silvestri; Figure 4.18) for example, the 2-aroylindoles, D-64131 and D-68144, the 2-phenylindoles (for example **61**, Gastpar *et al*., 1998) and a range of heterocombretastatins (for example **62**, Medarde *et al*., 1998). Considering the large number of *N*-alkylisatins that showed potent cell-based activity and morphological change in this study, four different compounds, **39**, **54**, **59** and **60** were chosen as representative molecules to further investigate their ability to alter

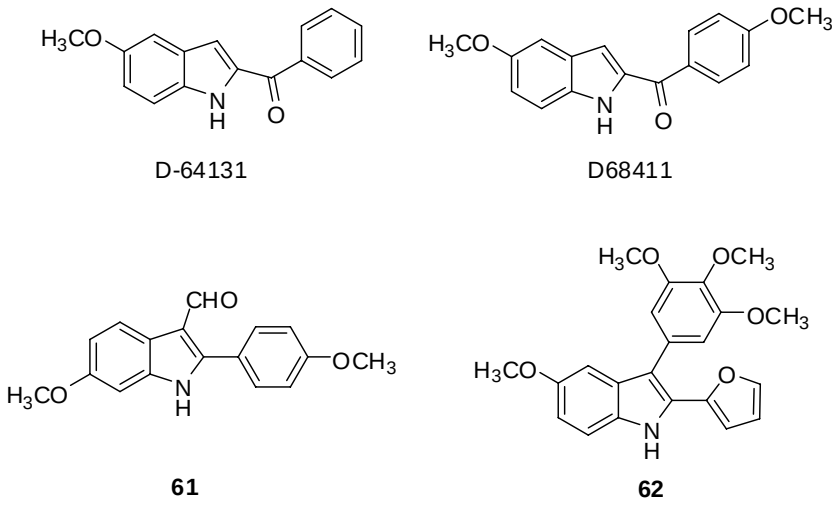

Figure 4.18 Examples of indole derivatives that inhibit tubulin polymerisation.

tubulin polymerisation in comparison to some well known tubulin interfering agents (Figure 4.19). As expected, the potent microtubule stabilising agent paclitaxel resulted in a dramatic increase in the rate of tubulin polymerisation at 10 μM, in comparison to the vehicle control, while vinblastine strongly inhibited microtubule formation at the

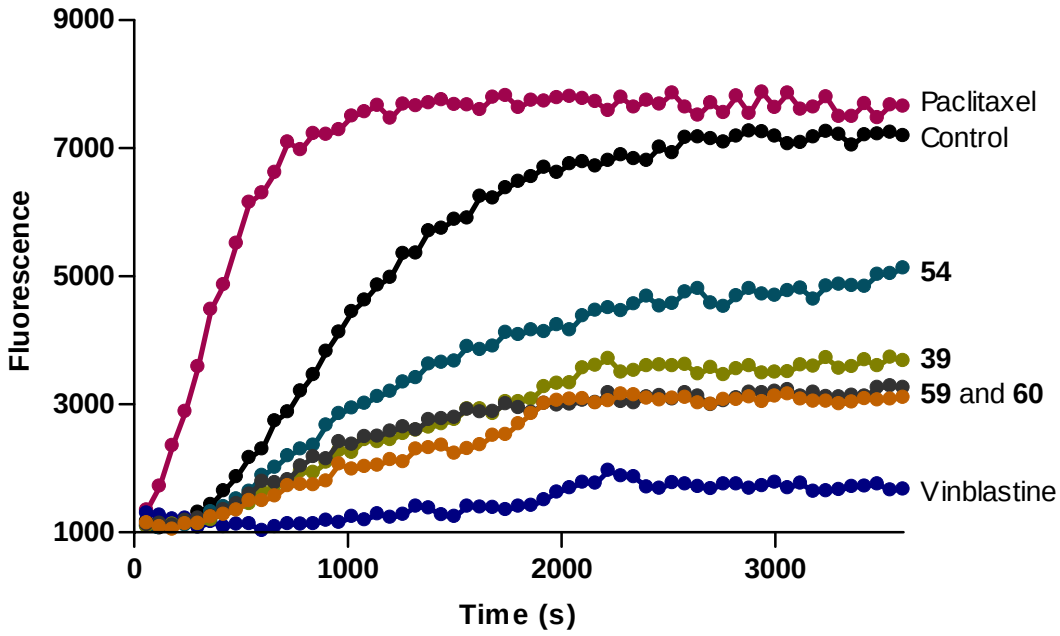

Figure 4.19 The effect of various *N*-alkylisatins and commercial anticancer agents on tubulin polymerisation as determined in the *in vitro* microtubule polymerisation assay. Purified bovine neuronal tubulin was used to assay for microtubule formation in the presence of either: ●) vehicle control, ●) paclitaxel 10 μM, ●) vinblastine sulfate salt 10 μM, ●) 5,7-dibromo-*N*-(*p*-methylbenzyl)isatin (**39**) 10 μM, ●) 5,7-dibromo-*N*-(*p*-trifluoromethylbenzyl) isatin (**54**) 10 μM, ●) 5,7-dibromo-*N*-(cinnamyl)isatin (**59**) 10 μM or ●) 5,7-dibromo-*N*-(*p*-phenylbenzyl)isatin (**60**) 10 μM at 37°C. A shift of the curve to the left of the control is indicative of an increase in polymerised tubulin and a shift to the right is indicative of a decrease in the rate of polymerisation. Changes in fluorescence were measured at an excitation wavelength of 360 ±10 nm and the fluorescence was collected at 440 ±10 nm. Data points are the means of duplicate experiments. SD bars were removed for clarity, and were always less than 12 % of the mean.

same molar concentration (Figure 4.19). This was greater than the effect seen at 3 μM (Appendix 2, Figure A2.5), indicating that the rate of microtubule stabilisation or destabilisation is dose-dependent. The *N*-alkylisatins **39**, **54**, **59** and **60** (Table 4.1) also strongly inhibited microtubule polymerisation at 10 μM, but did not destabilise microtubules as potently as vinblastine (Figure 4.19). This effect appeared to be independent of the nature of the *p*-substituent and size of the benzene carbon linker, since compounds **39**, **59** and **60** all inhibited microtubule polymerisation at a similar rate. By comparison, compound **54** was slightly less active, but considering its broad cell-line cytotoxicity (Table 4.3 and Table 4.4), suggests that cell death induced by direct microtubule destabilisation may not be its primary mechanism of action.

The role **54** played in the alteration of microtubule organisation in comparison to DMSO and vinblastine treated lymphoma cells was further investigated by direct fluorescence microscopy, using Tubulin Tracker Green (Figure 4.16). Compound **54** induced the accumulation of cells with fragmented microtubules, abnormal mitotic spindles, and reduced cell-associated fluorescence (Figure 4.20b, c and d, respectively). Cells treated with vinblastine, however, revealed highly fragmented microtubules at both high and low concentrations (Figure 4.20e and f, respectively). Considering compound **54** and *N*-alkylisatins in general are a collection of low molecular weight compounds that show no structural similarities to the *Vinca* alkaloids, it suggests that they may be interacting with tubulin in an entirely different manner. Recently, a structurally related indole-2-carboxylate (**63**), was reported to adopt an orientation

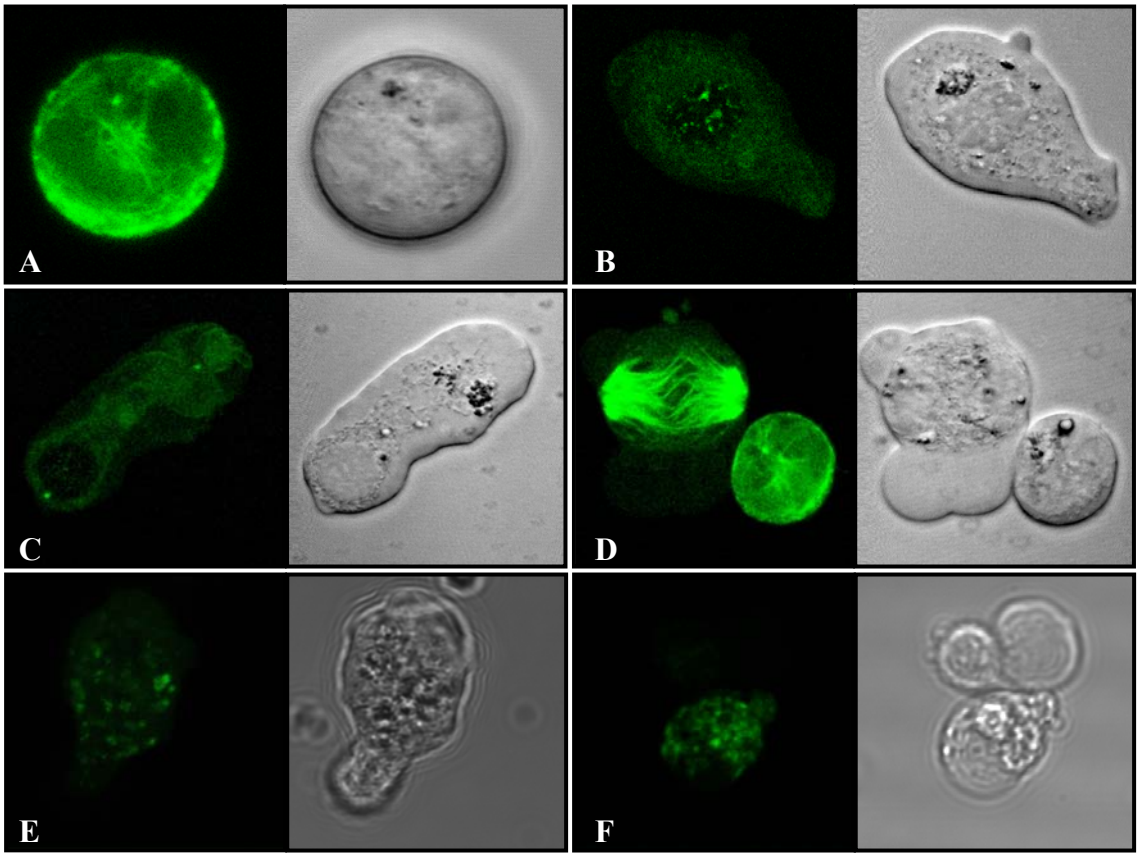

Figure 4.20 The effect of 5,7-dibromo-*N*-(*p*-trifluoromethylbenzyl) isatin (**54**) on the stability of microtubules in U937 cells. Treatment of cells with A) DMSO was used as the control. Cells were exposed to either B)-D) 0.78 μg/mL of compound **54** or E) 0.78 μg/mL or F) 0.20 μg/mL of the commercial anticancer agent vinblastine sulfate salt for 24 h. Microtubules were then visualised by direct fluorescence microscopy after incubation for 30 min with fluorescently labeled taxol (Tubulin Tracker Green).

similar to that of a colchicine analogue (DAMA-colchicine), when docked into the colchicine binding site of tubulin (De Martino *et al*., 2004). Similarly, A-432411 a dihydroindol-2-one was found to compete strongly with [^{3}H]colchicine (IC_{50} 0.13 μM) in a competition-binding scintillation proximity assay (Chen *et al*., 2005). Conversely, D-24851 did not compete for the binding of either radiolabeled vincristine or colchicine

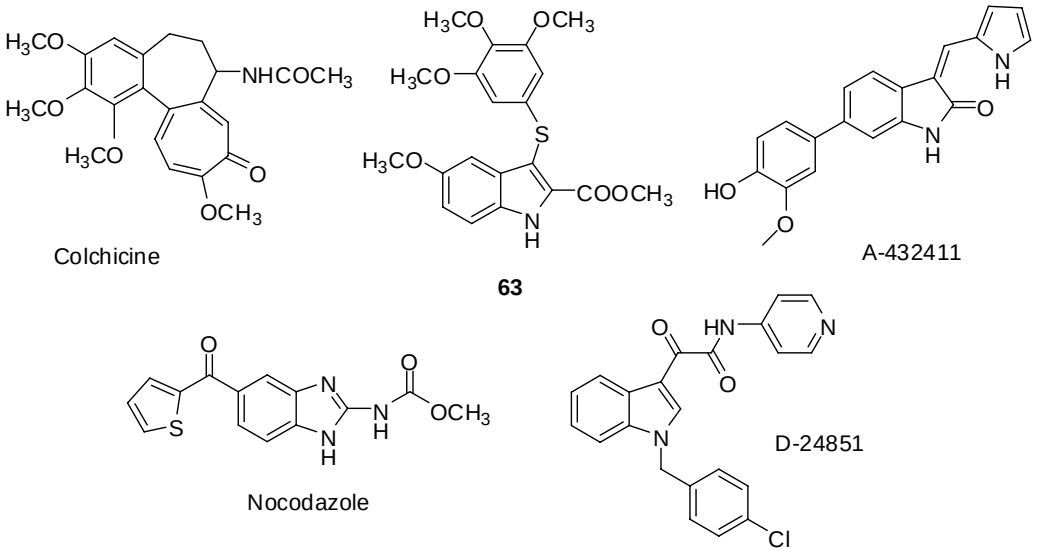

to tubulin (Bacher *et al*., 2001). This suggests that D-24851 may bind to a novel binding site on tubulin and induce inhibition of polymerisation. Since it is known that there are three major, well characterised binding sites on tubulin (Uppuluri *et al*., 1993; Rao *et al*., 1995; Rai and Wolff, 1996), it may be of interest to conduct future molecular modeling, docking and competition binding studies to verify the exact interactions occurring between the various *N*-alkylisatins (from this study) and tubulin, then correlate this with SAR data.

Alternatively, it is also possible that *N*-alkylisatin-induced microtubule disassembly is a secondary phenomenon, despite some characteristics resembling those induced by the destabilising agent vinblastine. For example, treatment of cells with the microtubule-dissociating agent nocodazole has been reported to result in Raf1 activation by Pak1, a kinase downstream of the small GTPases Rac/ Cdc42 (Zang *et al*., 2001). Activated Rac and Cdc42 induce cell shape changes at the plasma membrane by formation of

multimolecular focal complexes as well as lamellipodia and filopodia (Nobes and Hall, 1995). It may therefore be of interest in future studies to also determine whether various *N*-alkylisatins activate the Rac/ Cdc42/ Pak1/ Raf1 signaling pathway.

2.3.2.3 Inhibition of Protein Kinases

Considering the role that various kinases play in the regulation of the cell cycle together with the fact that a structural commonality exists between *N*-alkylisatins and variety of other known kinase inhibitors that induce G2/M arrest; the effect of six representative *N*-alkylisatins on the inhibitory activity of a range of kinases was investigated (Table 4.5). Looking at the direct inhibition of the enzymes DYRK1A, CDK5 and GSK3β, by the compounds **39**, **45**, **48**, **54**, **59** and **60** in the presence 15 μM ATP, it was found that none of the isatins inhibited enzyme activity even at the maximum concentration tested. This is interesting considering a range of small molecules based on the indole scaffold are known to inhibit the serine/threonine kinases GSK3 (Damiens *et al*., 2001; Leclerc *et al*., 2001) as well as CDK5 (Kent *et al*., 1999; Davis *et al*., 2001; Bramson *et al*., 2001; Lane *et al*., 2001) in the nanomolar range. Furthermore GSK3 is a core component of two pathways involved in cell fate determination and morphology, namely the Wnt and hedgehog pathways which, when deregulated, are both involved in several forms of human cancer (Doble and Woodgett, 2003). In these pathways, GSK3β is known to play a role in the dynamics of the mitotic spindle (Wakefield *et al*., 2003), whereby GSK3β directly phosphorylates several microtubule-associated proteins (MAPs) such as Tau, MAP1β and MAP2, involved in microtubule stabilisation (Goold

Table 4.5 Enzyme and cell based inhibitory activity of the representative *N*-alkylisatins **39**, **45**, **48**, **54**, **59** and **60** on serine/threonine kinases (CDK5 and GSK3) and tyrosine (DYRK1A, JAK1, JAK2 and c-FMS) kinases.

	IC_{50} (μM)							
	Enzyme						Cell[a]	
Compound	DYRK1A[b]	CDK5[c]	GSK3[d]	JAK1[e]	JAK2[f]	c-FMS[g]	Ba/F3-TJ2	Ba/F3-TJ3
39	> 10	> 10	> 10	>5	>5	>5	0.29	3.78
45	> 10	> 10	> 10	>5	>5	>5	<0.16	<0.16
48	> 10	> 10	> 10	>5	>5	>5	0.39	0.24
54	> 10	> 10	> 10	>5	>5	>5	0.29	<0.16
59	> 10	> 10	> 10	>5	>5	>5	0.17	<0.16
60	> 10	> 10	> 10	>5	>5	>5	1.07	0.79

[a] For cell based assays, the growth factor dependent myelomonocytic cell line BaF3 was transfected with either pTELJAK2 or pTELJAK3 and the cells selected for factor independent growth.
[b] DYRK1A: Dual-specificity tyrosine-phosphorylation regulated kinase 1A.
[c] CDK5: Cyclin dependent kinase 5.
[d] GSK3: Glycogen synthase kinase 3.
[e] JAK1: Janus protein tyrosine kinase 1.
[f] JAK2: Janus protein tyrosine kinase 2.
[g] c-FMS: Colony-stimulating factor-1 receptor.

and Gordon-Weeks, 2001). CDK5 and DYRK1A have also been implicated in the abnormal hyperphosphorylation of the microtubule-binding protein Tau, leading to cytoskeletal disruption (Imahori and Uchida, 1997; Mandelkow and Mandelkow, 1998).

The enzymatic activities of the JAK1, JAK2 and c-FMS kinases were also not altered by the *N*-alkylisatins **39**, **45**, **48**, **54**, **59** and **60**, even at the highest concentration tested (Table 4.5). This was further confirmed by cell based screening in the IL-3-independent, TEL-JAK2 and TEL-JAK3 mouse myeloid (Ba/F3), transfected cell lines, whereby all compounds were equipotent on both cell lines, with the exception of **39**. This indicates

that the cytotoxic effect is not likely to be occurring through the JAK signaling pathway. Together, these results thus suggest that despite the structural similarities that the representative *N*-alkylisatins share with known kinases inhibitors, tubulin may in fact be the primary target. Future investigations into the ability of this class of compounds to inhibit the mitotic and spindle assembly checkpoint kinases, for example CDK1, the aurora kinases, the polo-like kinases (PLK1) and BUB proteins would further support this theory.

4.4 Conclusions

N-Alkyl and arylalkyl isatins, in particular compounds **39**, **45**, **49**, **51**, **52**, **53**, **54**, **58** and **60** are novel synthetic cytotoxic agents with potent activity *in vitro*, some of which show >22 times greater selectivity for leukemic cells over the MCF-7, breast adenocarcinoma cell line. 5,7-Dibromo-*N*-(*p*-methylbenzyl)isatin (**39**) was the most active compound identified, exhibiting an IC_{50} value of 490 nM against two haematopoietic cell lines. Also of interest was 5,7-dibromo-*N*-(*p*-trifluoromethyl-benzyl)isatin (**54**), which exerted significant anticancer activity in a broad range of cancer cell lines but was the most active against the metastatic MDA-MB-231 mammary adenocarcinoma cell line (IC_{50} = 540 nM). Investigation into the molecular mode of action of the *N*-alkylisatins found the *p*-trifluoromethybenzyl derivative (**54**), together with the representative compounds **35**, **39**, **45**, **59** and **60**, to destabilise microtubules *via* inhibition of tubulin polymerisation, resulting in G2/M cell cycle arrest and apoptotic cell death. The potent cytotoxicity displayed by the *N*-alkylisatins in this study, compared to the commercial anticancer agents vinblastine, 5-FU and taxol,

together with the possibility of binding to a novel site on tubulin, suggest that the development of anticancer agents based on the *N*-alkylisatin scaffold may be beneficial in the treatment of paclitaxel and vincristine resistant tumours.

CHAPTER 5

A Preliminary *In vivo* Assessment of Some *N*-alkylisatins

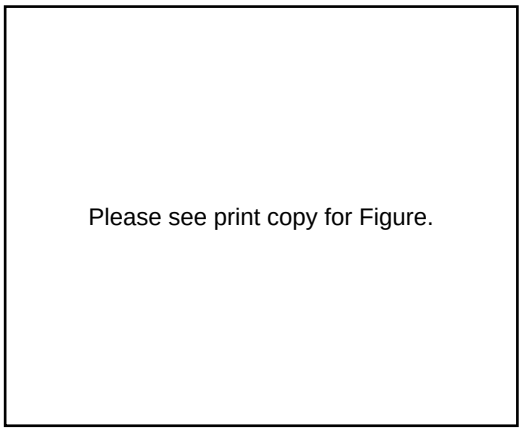

Athymic Balb/c (nu/nu) mouse used for human breast adenocarcinoma (MDA-MB-231) xenograft models

Photo courtesy of:
http://education.vetmed.vt.edu/Curriculum/VM8054/Labs/Lab13/NOTES/Nudemice.htm

CHAPTER 5

A Preliminary *In Vivo* Assessment of Some *N*-alkylisatins

5.1 Introduction

Compounds that interfere with the cell cycle have attracted much interest for the development of novel cancer chemotherapies (Jordan and Wilson, 1998). This is primarily because cancer cells, unlike normal cells, possess unlimited replicative potential and continue to divide without progressing into quiescence and senescence (Hayflick, 1997). This property of uncontrolled growth and division makes cancer cells extremely dependent upon microtubule dynamics and therefore vulnerable to antimitotic drugs that target microtubules (Jordan *et al*., 1998). In addition, proliferating endothelial cells that form neovasculature into the tumour are also sensitive to antimitotic agents (Tozer *et al*., 2002).

To date, several antimitotic drugs have successfully been used in the clinic for the treatment of cancer. These include the natural, plant-derived *Vinca* alkaloids, vincristine and vinblastine and the semi-synthetic derivative, vinorelbine, which are efficacious against haematologic cancers such as Hodgkin and non-Hodgkin lymphoma, as well as non-small cell lung carcinoma (Rowinsky and Donehower 1997; Jordan *et al*., 2004, Jackson *et al*., 2007). Paclitaxel and its semi-synthetic analogue, docetaxel have also been found to effectively treat many solid cancers arising from the ovary, breast, head

and neck and lung (Rowinsky, 1997). Despite this, the potential of antimitotic agents such as these is limited by the development of MDR (both acquired and intrinsic, Ferguson *et al*., 2005), neurotoxicity (Pace *et al*., 1997, Geldof *et al*., 1998), inadequate penetration of the drug into solid tumours (Baguley and Finlay, 1995) and in some cases lack of oral availability (Kavallaris *et al*., 2001). As a result, there has been great interest in identifying novel microtubule inhibitors that overcome various modes of resistance and have improved pharmacological profiles.

5.1.1 Efficacy of Synthetic, Small Molecule Tubulin Binders

A range of synthetic small molecules that bind to tubulin are currently being evaluated in preclinical and phase I clinical trials (Drukman and Kavallaris, 2002 and references therein; Figure 5.1). Among them are indole-based compounds that have been shown to both stabilise and destabilise microtubules (Brancale and Silvestri, 2007 and references therein). The 2-aroylindole, D-64131, for example was found to inhibit the proliferation of 12 out of 14 tumour cell lines with a mean IC_{50} value of 62 nM (Beckers *et al*., 2002), which is comparable with the potency of paclitaxel. *In vivo*, no signs of systemic toxicity were observed after peroral (PO) dosages of up to 400 mg/kg of D-64131. In experiments using human amelanoic melanoma MEXF 989 xenograft mouse models, D-64131 was also highly active with treatment resulting in a tumour growth delay of 23.4 days at 400 mg/kg (Beckers *et al*., 2002). Similarly, the anticancer activity of the indole A-289099 was evaluated in the syngeneic M5076 murine ovarian sarcoma flank tumour model (Tahir *et al*., 2003). When dosed once daily, from day 1-28, at the

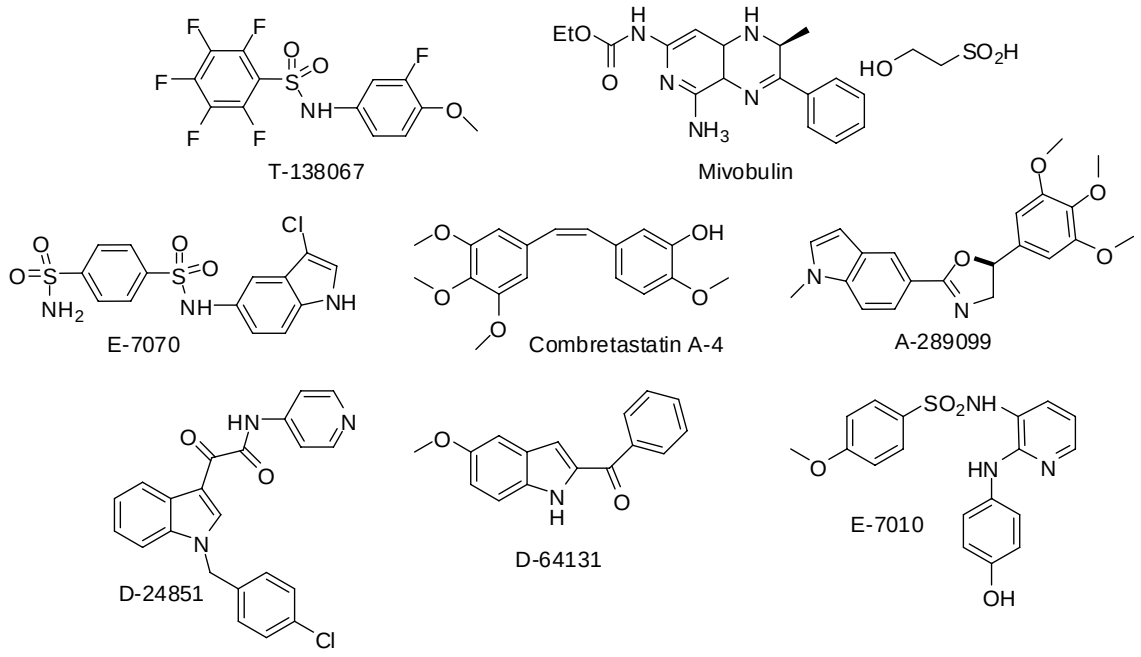

Figure 5.1 Examples of synthetic small molecule microtubule inhibitors in preclinical and clinical development.

maximum tolerated dose (MTD), A-289099 achieved a 206% increase in life span and a 28 day delay to 1 g tumour volume in mice. This efficacy is comparable to that of a previously reported antimitotic agent, E7010 (Koyanagi *et al*., 1994, Figure 5.1). Of particular interest to this study however, is the *N*-alkylated indole D-24851, which was found to be efficacious in a rat Yoshida AH13 sarcoma model and induced complete tumour regression and curative treatment of the animals, with no toxic side effects (Bacher *et al*., 2001). Preliminary results from these authors also stated that D-24851 inhibited tumour growth in mice transplanted with human PL-3 prostate carcinoma xenografts. This suggests that small, synthetic molecules have the potential to be

developed for cancer therapy, replacing or supplementing standard therapy regimens with tubulin-targeting drugs from natural sources.

5.1.2 Rationale and Aims

A critical step in any drug development program is the extrapolation of animal data for the purpose of predicting both efficacy and toxicity in humans (Voisin, 1990). Considering the potent activity of the *N*-alkylisatins *in vitro* against a variety of human tumour cell lines (Chapter 4), it was thus the aim of this study to determine the:

1. Dose tolerance of female outbred, Balb/c mice to a single administration of the *N*-alkylisatin **45**.
2. Acute toxicity of compound **54** in female outbred Balb/c mice by histopathological analysis of major organs.
3. Tumour growth delay of established tumours of the breast in an athymic xenograft mouse model in response to treatment with the *N*-alkylisatin **54**.
4. Biodistribution of two ^{123}I labeled *N*-alkylisatins (**67** and **68**) in two different animal models by means of single photon emission computed tomography (SPECT) imaging to further complement toxicity and efficacy findings.

5.2 Materials and Methods

5.2.1 General

Reactions were carried out using dried glassware and under an atmosphere of nitrogen. All solvents were AR grade except dichloromethane (DCM) which was LR grade and

distilled before use. 5,7-Dibromo-*N*-[4′-(tributylstannyl)benzyl]isatin (**66**) was supplied by Dr. Julie M. Locke, Postdoctoral Research Fellow, Department of Chemistry, University of Wollongong. The term petroleum spirit refers to petroleum spirit with the boiling range of 40 - 60 °C. When necessary, the purification of solvents and starting materials was carried out using standard procedures. Reactions were monitored using thin layer chromatography (TLC) on aluminum backed precoated silica gel 60 F_{254} plates (E. Merck). The *N*-alkylisatins are highly coloured and can usually be clearly seen on a TLC plate; colourless compounds were detected using UV light and/or iodine vapour. Flash chromatography (Still *et al*., 1978) was carried out using Merck silica gel 60 (230 - 400 mesh) with the solvent system indicated in the individual procedures. All solvent ratios are quoted as v/v. The ^{1}H and ^{13}C NMR spectra were acquired at 500 and 126 MHz respectively on a Varian Inova-500 spectrometer with a probe temperature of 298 K unless otherwise stated. All NMR spectra were referenced to the residual solvent peak (δ 7.26 or 77.0 ppm) in $CDCl_3$ solution. Hydrogen and carbon assignments were made using standard NOE, APT, gCOSY, gHSQC and gHMBC spectroscopic techniques. The ^{1}H and ^{13}C NMR spectra of some of the stannylated compounds exhibited minor signals from proton and carbon coupling to NMR active Sn isotopes (^{115}Sn, ^{117}Sn and ^{119}Sn), however only the major signals are quoted unless the minor signal were well resolved. Low resolution EI mass spectra (LREI-MS) were determined on a Shimadzu QP5050 spectrometer. High resolution EI mass spectra (HREI-MS) were determined on VG Autospec spectrometer operating at 70 eV with a source temperature of 250 °C and were referenced with PFK. Melting points were determined on a Reichert melting point apparatus and are uncorrected.

5.2.2 Chemical Synthesis

5.2.2.1 Attempted synthesis of 5-(tributylstannyl)isatin (64)

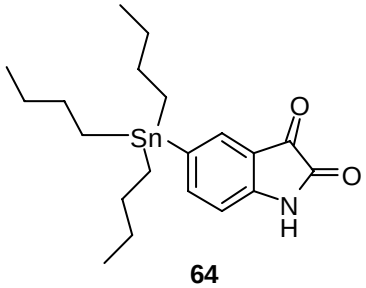

64

A solution of 5-bromoisatin (120 mg, 0.52 mmol), in dry toluene (40 mL), together with hexabutyldistannane (0.60 mL, 1.18 mmol) and tetrakis (triphenylphosphine)-palladium(0) (20 mg, 0.02 mmol) was heated at reflux under N_2. The reaction was followed by TLC analysis and after 48 h was found to give starting material **4** and a only a trace amount of product **64** (R_f 0.38, 95/5 DCM/MeOH, silica). LREI-MS *m/z* 437.14 ($[M]^+$)

5.2.2.2 Synthesis of *N*-(*p*-methoxybenzyl)-5-(tributylstannyl)isatin (65)

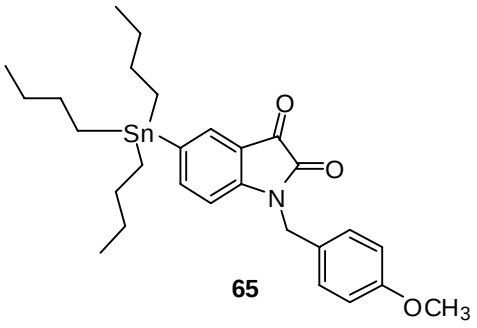

65

A mixture of 5-bromo-*N*-(*p*-methoxyphenyl)-isatin (90 mg, 0.26 mmol), hexabutyldistannane (0.30 mL, 0.59 mmol) and tetrakis(triphenylphosphine)palladium (10 mg, 0.01 mmol) in dry toluene (20 mL) was heated at reflux for 6.5 h under N_2. The solvent was removed at reduced pressure and the crude product was purified by flash chromatography, eluting with DCM, to afford the stannylated isatin (**65**) as a bright orange oil (60 mg, 41%), R_f 0.35 (DCM, silica). ^{1}H NMR δ 0.87 (d, *J* = 7 Hz, 9H, CH_3), 1.03 (m, 6H, CH_2), 1.30 (m, 6H, CH_2), 1.48 (m, 6H, CH_2), 3.78 (s, 3H, OCH_3), 4.84 (s, 2H, benzylic CH_2), 6.78 (d, *J* = 8 Hz, 1H, H7), 6.87 (d, *J* = 9 Hz, 2H,

phenyl ArH), 7.28 (d, *J* = 9 Hz, 2H, phenyl ArH), 7.54 (dd, *J* = 1, 8 Hz, 1H, H6), 7.66 (d, *J* = 1 Hz, 1H, H4). ^{13}C NMR δ 9.7, 13.6, 27.3, 28.9, 43.5, 55.3, 110.8, 114.3, 117.4, 126.7, 128.9, 132.6, 137.1, 146.2, 150.7, 158.2, 159.4, 183.9. LREI-MS *m/z* 557 ($[M]^+$); HREI-MS *m/z* calcd for $[M]^+$ $C_{28}H_{39}NO_3{}^{116}Sn$: 553.1940, found 553.1940.

5.2.2.3 Synthesis of 5,7-Dibromo-N-[4'-(tributylstannyl)benzyl]isatin (66)

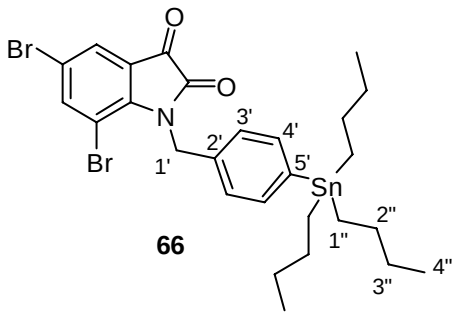

66

The synthesis of 5,7-dibromo-*N*-[4'-(tributyl-stannyl)benzyl]isatin (**66**) was a multi-step procedure carried out by Dr. Julie M. Locke, Postdoctoral Research Fellow, Department of Chemistry, University of Wollongong. 5,7-Dibromoisatin (100 mg, 0.33 mmol) and K_2CO_3 (63 mg, 0.46 mmol) were suspended in dry DMF (5 mL) and the mixture stirred at 0–5 °C for 30 min. 4-(Tributylstannyl)benzyl chloride (150 mg, 0.36 mmol) and KI (11 mg, 0.07 mmol) were added and the suspension stirred at 80 °C for 16 h. The reaction mixture was poured into HCl (0.5 M, 25 mL) and then extracted with ethyl acetate (1 × 25 mL) and the ethyl acetate layer washed with brine and dried over $MgSO_4$. The solvent was removed and the residue was purified using flash column chromatography, eluting with 1:1 DCM/pet spirit. The product was a bright red semi-solid that solidified on standing (97 mg, 43%), mp 111 – 113 °C, R_f 0.39 (1:1 DCM/pet spirit, silica). ^{1}H NMR δ 0.87 (t, *J* = 7 Hz, 9H, H4"), 1.03 (m, 6H, H1"), 1.31 (m, 6H, H3"), 1.52 (m, 6H, H2"), 5.39 (s, 2H, H1'), 7.19

(d, *J* = 8 Hz, 2H, H3'), 7.41 (d, *J* = 8 Hz, 2H, H4'), 7.71 (d, *J* = 2 Hz, 1H, H4), 7.81 (d, *J* = 2 Hz, 1H, H6). A minor signal at δ 7.41 (dd, *J* = 8, 37 Hz, H4') due to coupling of H4' with Sn was also observed. ^{13}C NMR δ 9.6 (C1"), 13.6 (C4"), 27.3 (C3"), 29.0 (C2"), 44.7 (C1'), 105.3, 117.1, 121.4, 125.9 (C3'), 127.5, 135.2, 136.9 (C4'), 141.6, 145.3, 146.8, 158.3 (C2), 181.3 (C3). LREI-MS *m/z* 570 ([M-C_8H_{18}]$^+$); HREI-MS *m/z* calcd for [M]$^+$ $C_{27}H_{35}{}^{81}Br_2NO_2{}^{118}Sn$: 685.001, found: 685.000.

5.2.2.4 Synthesis of *N*-(*p*-methoxybenzyl)-5-(^{123}I)iodoisatin (67)

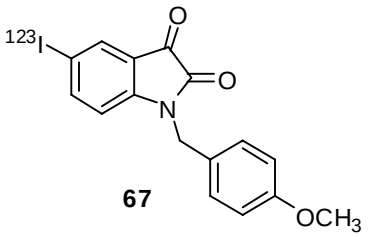

67

Method 1. To a solution of *N*-(*p*-methoxybenzyl)-5-(tributylstannyl)isatin (**65**) in EtOH (3.6 mM, 100 μL) was added 3.0 mCi of Na^{123}I in aqueous NaOH (20 mM, 5 μL), a solution of Chloramine-T in H_2O (3.6 mM, 100 μL) and 1M HCl (100 μL). The resulting mixture was then shaken for 5 min at RT and quenched with aqueous NaS_2O_5 (300 mM, 100 μL) and neutralised with aqueous $NaHCO_3$ (595 mM, 100 μL). To the reaction mixture, mobile phase (ACN/H_2O 65/35 + 0.01% TFA, 400 μL) was added and 2.6 mCi, (1 mL) was injected into a HPLC (Phenomenex Bondclone C18 300 × 7.8 mm, 2 mL/min 65/35 ACN/H_2O + 0.01% TFA). The spectra showed activity peaks at 9.8, 12 and 19.6 min, none of which corresponded to the iodo standard (*N*-(*p*-methoxybenzyl)-5-iodoisatin (**65**) at 13.2 min (Appendix 3, Figure A3.1).

Method 2. To a solution of *N*-(*p*-methoxybenzyl)-5-(tributylstannyl)isatin (**65**) in EtOH (3.6 mM, 100 μL) was added 3.3 mCi of Na^{123}I in aqueous NaOH (20 mM, 20 μL) and

peracetic acid solution (37%, 100 μL). The resulting mixture was then shaken for 5 min at RT and quenched with aqueous NaS_2O_5 (300 mM, 100 μL) and neutralised with aqueous $NaHCO_3$ (595 mM, 100 μL). To the reaction mixture, mobile phase (ACN/H_2O 65/35 + 0.01% TFA, 400 μL) was added and 2.2 mCi (1 mL) was injected into a HPLC (Phenomenex Bondclone C18 300 × 7.8 mm, 2 mL/min 65/35 ACN/H_2O + 0.01% TFA). The ^{123}I labeled product was collected at 14.8 min (1.0 mCi) in a glass vial which was then evaporated to dryness under high vacuum. Identity confirmation was done using a HPLC trace comparison with unlabeled *N*-(*p*-methoxybenzyl)-5-iodoisatin (**65**); retention time 14.8 min, radiochemical purity 37% (Phenomenex Bondclone C18 300 × 7.8 mm, 2 mL/min 65/35 ACN/H_2O + 0.01% TFA, UV 254 nm, Appendix 3, A3.2).

5.2.2.5 Synthesis of 5,7-dibromo-*N*-[4'-(^{123}I)iodobenzyl]isatin (68)

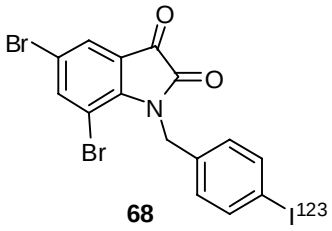

68

Method 1. To a solution of 5,7-dibromo-*N*-[4'-(tributylstannyl)-benzyl]isatin (**66**) in EtOH (2.9 mM, 100 μL) was added 4.0 mCi of $Na^{123}I$ in aqueous NaOH (20 mM, 15 μL) and peracetic acid solution (37%)/acetic acid (1:10 v/v, 100 μL). The resulting mixture was then shaken for 5 min at RT and quenched with aqueous NaS_2O_5 (300 mM, 100 μL) and neutralised with aqueous $NaHCO_3$ (595 mM, 100 μL). To the reaction mixture, mobile phase (ACN/H_2O 80/20 + 0.1% TFA, 300 μL) was added and 3.5 mCi (1 mL) was injected into a HPLC (Phenomenex Bondclone C18 300 × 7.8 mm 2 mL/min 80/20 ACN/H_2O + 0.1% TFA, UV 254 nm). The ^{123}I labeled product was collected at 13.3 min (1.3 mCi) in a glass vial which was then evaporated to dryness

under high vacuum. Identity confirmation was done by HPLC (Phenomenex Bondclone C18 300 × 7.8 mm 2 mL/min 80/20 ACN/H_2O + 0.1% TFA, UV 254 nm) comparison with unlabeled 5,7-dibromo-*N*-[4'-(iodo)benzyl]isatin (**66**); retention time 13.3 min, radiochemical purity 37% (Appendix 3, Figure A3.3).

Method 2. To a solution of 5,7-dibromo-N-[4'-(tributylstannyl)-benzyl]isatin (**66**) in EtOH (2.9 mM, 100 μL) was added 4.2 mCi of $Na^{123}I$ in aqueous NaOH (20 mM, 15 μL) and peracetic acid solution (37%)/acetic acid (1:1 v/v, 100 μL). The resulting mixture was shaken for 5 min at RT and then quenched with aqueous NaS_2O_5 (300 mM, 100 μL) and neutralised with aqueous $NaHCO_3$ (595 mM, 100 μL). To the reaction mixture, mobile phase (ACN/H_2O 80/20 + 0.1% TFA, 300 μL) was added and 3.8 mCi (1 mL) was injected into a HPLC (Phenomenex Bondclone C18 300 × 7.8 mm 2 mL/min 80/20 ACN/H_2O + 0.1% TFA, UV 254 nm). The ^{123}I labeled product was collected at 13.3 min (1.3 mCi) in a glass vial which was then evaporated to dryness under high vacuum. Identity confirmation was done by HPLC (Phenomenex Bondclone C18 300 × 7.8 mm 2 mL/min 80/20 ACN/H_2O + 0.1% TFA, UV 254 nm) comparison with unlabeled 5,7-dibromo-*N*-[4'-(iodo)benzyl]isatin (**66**); retention time 13.3 min, radiochemical purity 34%. The QC data indicated that there was no product breakdown in the mobile phase at RT after 2 h (Appendix 3, Figure A3.4).

5.2.3 In Vivo Studies

Animals were purchased aged 4-5 weeks old from the Animal Resources Centre (Canning Vale, WA, Australia) and experiments were conducted at the University of Wollongong with approval from the UOW AEC (ethics number AE03/07r05) and the

Australian Nuclear Science and Technology Organisation (ANSTO) in collaboration with Dr Andrew Katsifis and Dr Filomena Mattner with approval from ANSTO AEC (ethics number 195).

5.2.3.1 Preliminary Toxicological Assessment

5.2.3.1a Dose Tolerance

The tolerance of a single bolus administration of compound **45** was examined in female, 5-6 week old, outbred Balb/c mice and compared to control treatments. Mice were injected i.p. with either DMSO (control) or compound **45** (100 μL) using a dose-escalation protocol and the onset of dose limiting toxicity (defined as 15% loss of body weight and/or distressed behaviour, i.e. loss of activity or hunched posture) was noted. Animal weights were then compared to day 0 (first day of treatment) to determine percentage weight change. Mice were sacrificed at either -20% weight loss from day 0 or at the end of the observation period (day 34), whichever came first, by overdose of inhaled CO_2.

5.2.3.1b Acute Toxicity

Acute toxicity of a single bolus administration of compound **54** was investigated in female, 5-6 week old, outbred Balb/c mice and were compared to control treatments over a period of 3 and 5 days. Mice were injected i.p. with either 100% DMSO or 40 mg/kg of compound **54** (100 μL) and were monitored and weighed daily, up until the end of the observation period. The experimental endpoint was defined as described in the dose tolerance study, Section 5.2.3.2a. Animals were euthanised by inhaled CO_2,

dissected and major organs removed. Organs were weighed and visually inspected, before fixing for 24 h in 10% neutral-buffered formalin.

5.2.3.2 Tumour Models

5.2.3.2a Human Epithelial, Mammary Gland Adenocarcinoma (MDA-MB-231) Xenograft in Nude Mice

Human epithelial, mammary gland adenocarcinoma (MDA-MB-231) cells were routinely maintained in RPMI-1640 containing 5% FCS as described in Chapter 2, Materials and Methods, Section 2.3.1.1. On the day of inoculation, subconfluent cells were detached with 10 mL of sterile EDTA/ PBS (5 mM EDTA in Dulbecco's PBS without $CaCl_2$ and $MgCl_2$) for 5 min, at 37 ºC. The reaction was then stopped by incubating cells with 15 mL of Dulbecco's PBS containing $CaCl_2$ and $MgCl_2$. Cells were then pelleted by centrifugation (1700 rpm, 3 min), the supernatant discarded and resuspended in 20 mL of ice cold, sterile PBS for counting. Cells were prepared to a final concentration of 2.0×10^7 cells/mL (2.0×10^6 cells per 100 μL injection) and placed on ice. Cells were > 90% viable at the time of preparation (as determined by the trypan blue exclusion method). To establish orthotopic breast carcinoma xenografts, cells were injected into the left mammary fat pad of the first nipple of mice. A sample of remaining cells was found to be > 75% viable after all injections were complete.

5.2.3.2.b Human Amelanotic Melanoma (A375) Xenograft in Nude Mice

Female Balb/c (nu/nu) mice were injected sub-cutaneously (s.c.) into the left flank with A375 amelanotic melanoma cells (1.0×10^6) in 100 μL PBS (without Mg^{2+} and Ca^{2+})

by Paula Berghofer according to the protocol described in Appendix 3, Section A3.1. All cells were > 96% viable at the time of preparation. Tumour dimensions and animal weights were then recorded on days 7, 14, 21, 24, and 26 post tumour inoculation.

5.2.3.2.c Rat 13762 MAT B III Mammary Adenocarcinoma in F344 Fisher Rats

F344 Fisher rats were injected s.c. into the left flank with 13762 MAT B III mammary adenocarcinoma cells (1.0×10^6) in 100 μL PBS (without Mg^{2+} and Ca^{2+}) by Paula Berghofer (ANSTO, NSW) according to the protocol described in Appendix 3, Section A3.2. All cells were > 91% viable at the time of preparation. Tumour dimensions and animal weights were recorded on days 7 and 10 post tumour inoculation.

5.2.3.3 Tumour Growth Delay: Efficacy in a Human Mammary Tumour Model

Athymic, nude (nu/nu), 5-6 week old female Balb/c mice bearing early (non-palpable) mammary gland adenocarcinoma (MDA-MB-231) xenografts, underwent administration of compound **54** using a multiple fractionated dose administration schedule, similar to that described by Stutchbury *et al*., (2007). A multiple dose regimen was chosen over a single bolus dose considering that multiple dose schedules are routinely used for the administration of many clinically used chemotherapeutics (Simon and Norton, 2006). The total administered dose of **54** was calculated based on the highest single dose tolerated of a structurally related compound, **45** (Section 5.2.3.2a). Fourteen days post tumour inoculation, animals received either 100% DMSO or 5 mg/kg of compound **54** administered i.p. twice weekly for 2.5 weeks (total dose 25 mg/kg). Animals were monitored and weighed daily for 2.5 weeks, then twice weekly

after the final treatment. Once a tumour was measurable (approximately 5mm at longest diameter), it was measured twice-weekly using digital calipers along the x and y plane of the tumour. Tumour volume was determined using the formula volume = a × (b^2)/2, where a is the largest diameter and b is the smallest diameter (Carlsson *et al*., 1983). Antitumour assessment of treatments was determined by reduction in tumour growth rate compared to controls as determined by tumour volume and effect on overall survival. Efficacy experiment endpoints were defined as a tumour size of 15 × 15 mm along the longest axes or that impeded animal movement, and/or end of observation period. Animals were euthanised by inhaled CO_2, dissected and major organs and tumours removed. Tumours were observed macroscopically before being washed, weighed and fixed for 24 h in 10% neutral-buffered formalin. Major organs were visually inspected but not further processed.

5.2.3.4 Histopathology

Fixed tumours or major organs (i.e. lungs, heart, liver, spleen, kidneys, small intestine and bone) were embedded in paraffin and the tissues were sectioned and stained with hematoxylin and eosin (H&E) by accredited histopathologists at Southern IML Pathology Laboratories (Wollongong, Australia). Stained tumour sections were examined for evidence of necrosis while organs were assessed for any histopathological changes associated with drug treatment with the aid of Dr Alistair Lochhead, Southern IML Pathology.

5.2.3.5 Statistical Analyses

Combined tumour volumes and weight changes were compared using a paired T-test (GraphPad Prism V 4.02). Survival curves were analysed by the Kaplan-Meier log-rank test (GraphPad Prism V 4.02). *P* values < 0.05 were considered statistically significant.

5.2.3.6 Single Photon Emission Computed Tomography (SPECT) Imaging of Human Melanoma and Rat Mammary Tumour Models

For both models, the radiotracers **67** and **68** were prepared fresh on the day of imaging (as described in Section 5.2.2) and 100 μL (in 0.9% saline and 5% EtOH) injected *via* the tail vein. Between 35- 45 min post injection (p.i.), animals were anaesthetised using inhalant isoflurane with 200 mm/min oxygen via a nose cone fitted to the animal bed of the X-SPECT® SPECT/CT imaging system. Once the animal was no longer responsive to stimuli (pinching between toes) the animal was placed on the bed lying on its stomach and the bed driven into the imaging tunnel. The HRES (5" × 5") collimators were fitted and rotated to be horizontal above and below the animal, and moved in as close as possible to the animal without touching it (Head 1 was at 0° above animal). Acquisitions were taken to obtain images of the head and/or body at the time points indicated in Table 5.1 and Table 5.2. Afterwards, the animals were removed from anaesthetic, woken and observed for recovery between each imaging time point and had access to food and water. Animals were sacrificed by CO_2 suffocation followed by cervical dislocation at the last imaging time point.

Table 5.1 Protocol for SPECT imaging of radiotracer **67** and **68** in female Balb/c (nu/nu) melanoma xenografts.[a]

Time Point (Post Injection)	**Acquisition Type**	**Acquisition Time (min)**	**Camera Position**
40 – 60 min	Dynamic	20 4 frames (5 min per frame)	Above entire animal
3 - 3 h 15 min	Dynamic	15 3 frames (5 min per frame)	Above entire animal
6 h	Static	10	Above entire animal
24 h	Static	20	Above entire animal
48 h	Static	40	Above entire animal

[a] Mice were injected with 2 μCi/μL of either **67** or **68**, 27 days post tumour inoculation.

Table 5.2 Protocol for SPECT imaging of radiotracers **67** and **68** in F344 Fisher rats bearing 13762 MAT B III mammary adenocarcinoma.[a]

Time Point (Post Injection)	**Acquisition Type**	**Acquisition Time (min)**	**Camera Position**
45 – 60 min	Dynamic	15 3 frames (5 min per frame)	Lower body
1 h	Static	5	Head and upper body
3 h	Dynamic	15 3 frames (5 min per frame)	Lower body
3 h 20 min	Static	5	Head and upper body
6 h	Static	10	Lower body
6 h 15 min	Static	5	Head and upper body
24 h	Static	20	Lower body
48 h	Static	40	Lower body
72 h[b]	Static	40	Lower body

[a] Rats were injected with 5 μCi/μL of either **67** or **68**, 11 days post tumour cell inoculation.
[b] This additional time point was conducted on freshly euthanised rats.

5.3 Results and Discussion

5.3.1 Chemistry

The inclusion of radiohalogens into organic structures for SPECT can be achieved using many of the conventional processes of organic chemistry, such as the substitution of hydrogen from an aromatic system or addition across multiple bonds. But by far the most commonly used method is group displacement (Bolton, 2002). In this study, two different ^{123}I labeled analogues of isatin were prepared from their corresponding stannanes for animal imaging using this method. Firstly, *N*-(*p*-methoxybenzyl)-5-(tributylstannyl)isatin (**65**) was prepared in moderate yield (41%) from its halogenated precursor, 5-bromo-*N*-(*p*-methoxyphenyl)isatin, in a single-step reaction with bistributyltin (Scheme 5.1). The product was characterised by routine spectroscopic and analytical methods, with the HREI-MS spectrum exhibiting a distinctive isotopic pattern consistent with the stannylated product (Appendix 3, Figure A3.7). Interestingly, reaction of 5-bromoisatin under the same conditions yielded only trace amounts of

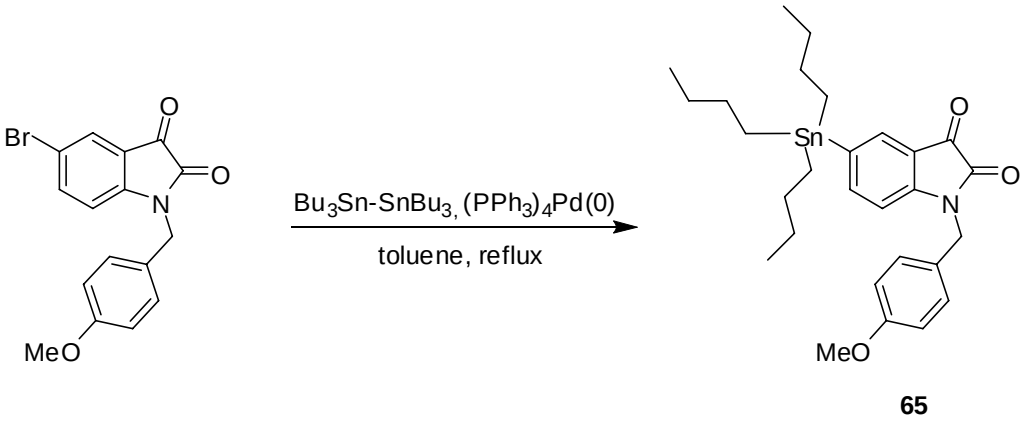

Scheme 5.1 Preparation of *N*-(*p*-methoxybenzyl)-5-(tributylstannyl)isatin (**65**)

product, even with long reaction times (i.e. > 45 h). Analysis of the HREI-MS showed isotopic patterns of Sn consistent with **64**, however other stannylated, higher molecular weight products were also present (Appendix 3, Figure A3.8). It is anticipated that the acidic nature of the amine at N1, as well as poor solubility of **64** in toluene may be responsible for the poor yield, considering the relatively short reaction time for the *N*-alkylated analogue (**65**). Conversely, the synthesis of 5,7-dibromo-*N*-[4'-(tributyl-stannyl)benzyl]isatin (**66**) was a multi-step procedure and was achieved through the reaction of 5,7-dibromoisatin with 4-(tributylstannyl)benzyl chloride (**69**) using a general method described for the *N*-alkylation of isatin (Garden *et al*., 1998). Since compound **69** was not commercially available, it was prepared from 4-bromobenzyl alcohol, by Dr. Julie Locke, in a two step synthesis in 71% yield (Scheme 5.2). A similar method has also been described for the preparation of *N*-1-substituted 5-pyrrolidinylsulfonyl isatins as a potential tool for the molecular imaging of caspases in apoptosis (Kopka *et al*., 2006). Similarly, the alkylation reagent was synthesised in two steps starting from the benzyl alcohol however the product, *p*-tributylstannylbenzyl mesylate was only obtained in an overall yield of 40% (Kopka *et al*., 2006). Despite

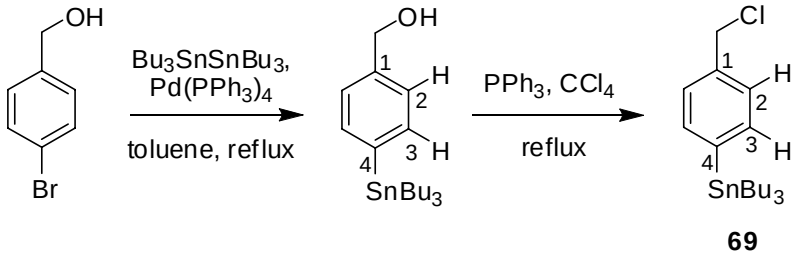

Scheme 5.2 Synthesis of 4-(tributylstannyl)benzyl chloride (**69**).

this, *N*-alkylation of isatin in this study with **69** or that described by Kopka *et al*., (2006) with the benzyl mesylate produced stannylated products in similar yields (*ca* 50%), suggesting that either reagent may be used to successfully prepare precursors ready for radioiodination.

The ^{123}I-labelled compounds **67** and **68** were next obtained from the corresponding tributylstannylated precursors by oxidative radioiodination using Na^{123}I in aqueous NaOH and peracetic acid as the oxidant (Scheme 5.3). Reaction of **65** for 5 min with Na^{123}I and 37% peracetic acid, gave **67** in a radiochemical yield of 37%. The identity of compound **67** was confirmed by HPLC analysis after co-injection of a sample spiked with cold 5-iodo-*N*-(*p*-methoxybenzyl)isatin (Appendix 3, Figure A3.2). Interestingly, the reaction of **65** with Na^{123}I and chloramine-T under the same conditions did not produce the radiolabeled product (**67**). Instead, the HPLC spectra showed activity peaks at 9.8, 12 and 19.6 min, none of which corresponded to the iodo standard at 13.2 min

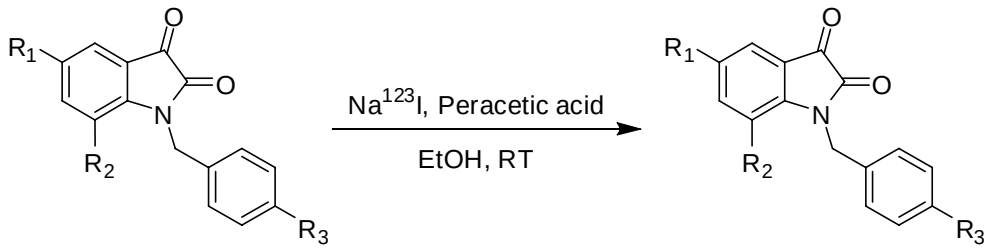

65 R_1=Bu_3Sn, R_2=H, R_3= OCH_3
66 R_1=Br, R_2=Br, R_3=Bu_3Sn

67 R_1=^{123}I, R_2=H, R_3= OCH_3
68 R_1=Br, R_2=Br, R_3= ^{123}I

Scheme 5.3 Synthesis of *N*-(*p*-methoxybenzyl)-5-(^{123}I)iodoisatin (**67**) and 5,7-dibromo-*N*-[4'-(^{123}I)iodobenzyl]isatin (**68**) by oxidative radiohalogenation.

(Appendix 3, Figure A3.1). Similarly, two separate reports have noted the superiority of peracetic acid over chloramine-T as an oxidizing agent in achieving iodination of an activated aromatic ring for some benzamide derivatives (Kung and Kung, 1989; Wang *et al*., 1998).

A similar radiochemical yield (36%) was also obtained for the second isatin **68**, after reaction of **66** with $Na^{123}I$ and peracetic acid: acetic acid (1:10, v/v). However unexpectedly, the yield did not increase after increasing the concentration of oxidant. Instead reaction of the HPLC purified precursor (**66**) with $Na^{123}I$ and peracetic acid: acetic acid (1:1, v/v) at RT for 5 min, found a radiochemical yield of just 34%. Despite this, collection of the active peak by HPLC for formulation found > 98% radiochemical purity and QC data indicated that there was no product breakdown in the mobile phase at RT after 2 h (Appendix 3, Figure A3.9). Future work may involve investigations into improving the overall radiochemical yield of compounds **67** and **68** by reducing the concentration of peracetic acid, increasing the reaction time or using alternative oxidants such as, hydrogen peroxide, sodium persulfate or *m*-choroperoxybenzoic acid.

5.3.2 In Vivo Studies

5.3.2.1 Toxicological Evaluation

To gain an understanding of the maximum dose of the representative *N*-alkylisatin **45** that could be tolerated for further *in vivo* efficacy studies, toxicity was investigated in mice over three dose ranges. Considering the maximum tolerated dose (MTD) of 5-FU

is *ca* 200 mg/kg in female balb/c mice (Dr Tamantha Stutchbury, Associate Research Fellow, UOW, per. com.), a starting dose of 25 mg/kg was calculated for **45** based on *in vitro* cytotoxicity data after comparison with the IC_{50} of 5-FU (Chapter 4, Section 4.3.1, Table 4.3). After a single bolus administration of compound **45** at 25 mg/kg, no significant toxicity was observed compared to DMSO treated animals, as defined by weight loss (Figure 5.2A) or change in animal behaviour. A small, acute weight loss of 5 – 10% from day 0 was observed in both the control and the 25 mg/kg cohorts; however this was quickly recovered by day 7 with mice in both treatment groups gaining weight thereafter. Despite percentage survival being 66.6% at the observation endpoint (day 33) for animals receiving 25 mg/kg of **45** (Figure 5.2B), the mortality of one individual at day 7 was not related to compound toxicity. This was confirmed by the lack of toxicity related behaviour as well as post mortem autopsy, with no macroscopic signs of organ degeneration noted (Dr Tracy Maddocks, Animal House Manager, UOW, per. com.). Conversely, two out of the four mice receiving the higher dose of 35 mg/kg died by day 4, while the remaining two showed an average increase in weight from day 6 up to day 23 (experimental endpoint). Although sufficient animal numbers were not used to determine the median lethal dose, the LD_{50} may be considered to be *ca* 35 mg/kg for this compound (Figure 5.2B). This is approximately 12 times more potent than the conventional chemotherapeutic agent vinblastine sulfate with a reported LD_{50} of 423 mg/kg after a single oral dose in mice (Todd, 1976). Despite this, vinblastine is still known to cause neurotoxicity (King and Boder, 1979; Geldorf *et al*., 1998) and thus re-emphasises the need for new and improved antimitotics

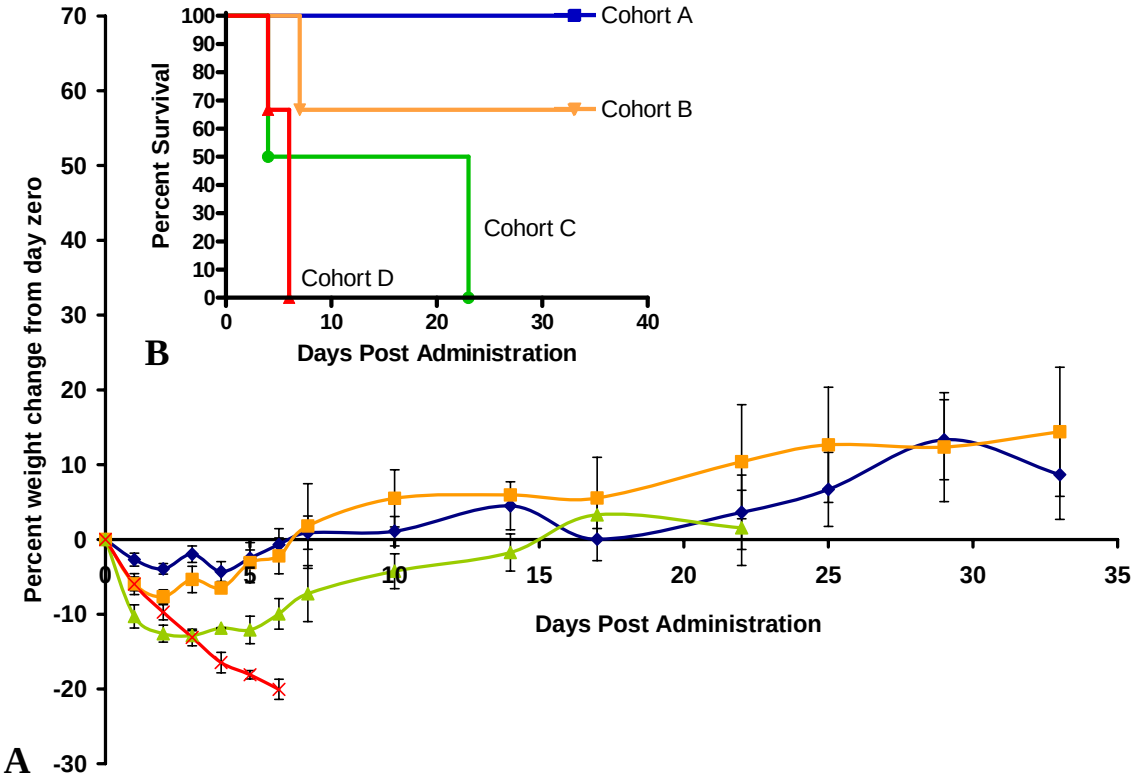

Figure 5.2 Average weight change from day zero and percent survival of mice treated with different concentrations of 5,7-dibromo-*N*-(*p*-methoxybenzyl)isatin (**45**). Female Balb/c mice were administered a single bolus dose of compound **45** at either ■ 25 mg/kg (Cohort B), ▲ 35 mg/kg (Cohort C) or x 50 mg/kg (Cohort D) and A) weights recorded and compared to weight change from day zero or B) percent survival determined using the Kaplan-Meier log rank test (GraphPad Prism V 4.0). Treatments were compared to ● vehicle control treated mice (Cohort A). Data points are the means of $n = 3 - 4 \pm$ SD.

with better tolerability. Finally, at the highest dose of compound **45** administered (i.e. 50 mg/kg), mice showed substantial acute weight loss, up to 13% by day 3, together with other signs of toxicity such as hunched posture and lack of activity and grooming. By day 6, 100% of mice that received the 50 mg/kg dose reached toxicity endpoint as defined by weight loss up to 20% from day 0 (Figure 5.2) and were therefore sacrificed.

In an effort to further assess the pharmaceutical potential of the *N*-alkylisatins and provide a preliminary identification of target organs of toxicity, acute toxicity studies in female 5-6 week old Balb/c mice were undertaken. Compound **54** was chosen for further toxicological evaluation over compound **45** due to its impressive *in vitro* activity against various epithelial derived cell lines (Chapter 4, Table 4.3 and Table 4.5), with the aim of using **54** for further *in vivo* efficacy assessment. Animals were injected i.p. with a single dose of compound **54** at 40 mg/kg and assessed for acute toxicity with regards to weight loss, excised organ weight and organ histopathology. Mice sacrificed 3 days post treatment showed an average weight loss of 12.5% from day 0 (Appendix 3, Figure A3.10) and a significant decrease in major organ weights ($P < 0.05$, $n = 4$ in all cases) compared to control mice (Figure 5.3). This effect was exacerbated in mice sacrificed on day 5 (Figure 5.3), despite an average increase in body weight from day 4. Analysis of hematoxylin and eosin (H & E) stained tissue preparations found mice treated with compound **54** showed large areas of liver necrosis (bland infarction), with some sub-capsular invasion of inflammatory cells (Figure 5.4B). This was observed in both 3 and 5 day treatment groups, however the effect was most severe in mice 5 days post administration of **54**. Despite the appearance of hepatotoxicity at this concentration, other antimitotics such as vincristine (known to be excreted primarily by the liver), have seldom been implicated as hepatotoxins and has only produced hepatotoxicity when used in combination with radiation (King and Perry, 2001). In addition, atrophic white pulp was prominent in the spleen of animals 3 and 5 days post administration of **54**. This is not surprising considering the potent *in vitro* activity of

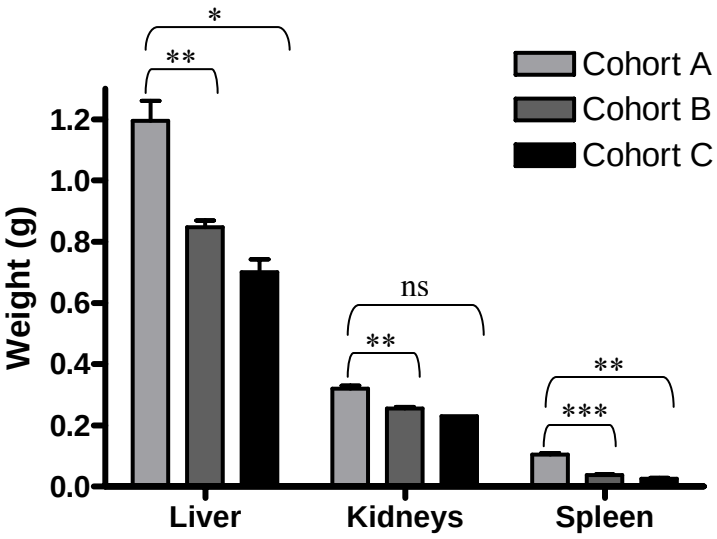

Figure 5.3 Acute toxicity organ profile of 5,7-dibromo-*N*-(*p*-trifluoromethylbenzyl)isatin (**54**) over time. A comparison of major organ weights for mice treated with either a single bolus i.p. administration of DMSO (cohort A), a single bolus i.p. administration of 40 mg/kg compound **54** and sacrificed 3 days post treatment (cohort B) or a single bolus i.p. administration of 40 mg/kg compound **54** and sacrificed 5 days post treatment (cohort C). Histograms are the means of $n = 2 – 4 \pm$ SE. The *P* value was calculated by comparing mean organ weight of the treated group with the mean organ weight of the vehicle-treated control group using an unpaired *t* test (two tailed). * P <0.05 significant, ** <0.01 highly significant, *** <0.001 extremely significant and ns: not significant.

compound **54** against Jurkat cells; a lymphoid derived cell line (Chapter 4, Table 4.3). Furthermore, brown deposits in the red pulp of the spleen were also noted (Figure 5.4E) and were later confirmed as iron-rich by pearl staining (Figure 5.4F), indicative of spleenic hemorrhaging (Dr Alistair Lochhead , Medical Director, Southern IML Pathology, Wollongong, per. com.). Interestingly, erythroid precursors have also been described to be susceptible to mitotic arrest by vincristine (Morse and Stohlman, 1966). In rats, binucleate erythroid precursors, nuclear fragmentation and remnants (Howell-

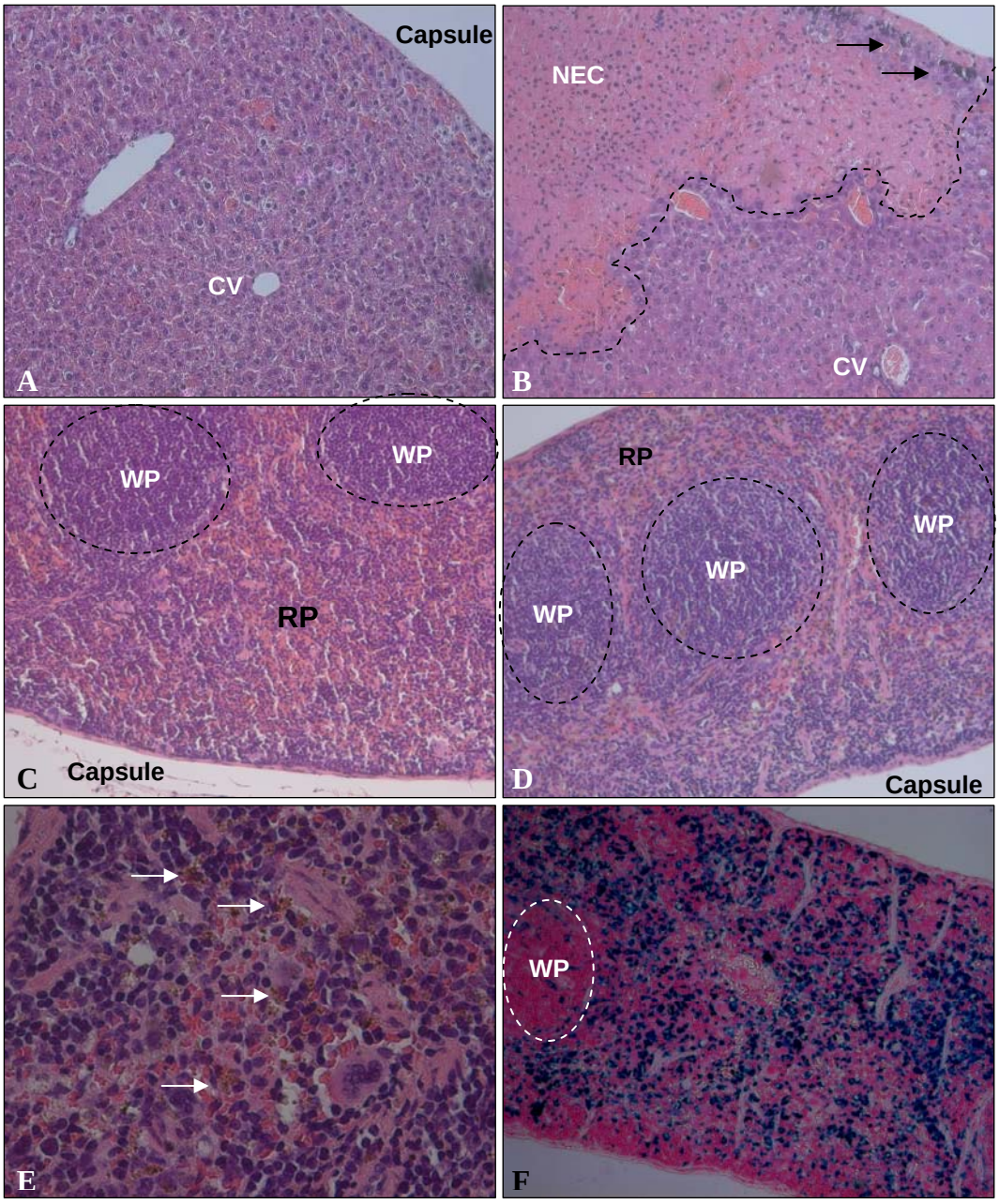

Figure 5.4 Hematoxylin and eosin (panels A- E) and pearl (panel F) stained tissue preparations used to assess acute toxicity in mice after treatment with 5,7-dibromo-*N*-(*p*-trifluoromethylbenzyl)isatin (**54**). A) Control liver showing hepatocytes arranged into radial patterns converging onto a central vein (CV), B) treated liver showing a large area of tissue necrosis (NEC), arrows indicate sub-capsular infiltration of inflammatory cells, C) control spleen showing red pulp (RP) consisting of blood sinuses, plasma cells and macrophages and ovoid areas of white pulp (WP) consisting of B and T cell regions, D) treated spleen showing atrophic areas of white pulp (WP), E) magnified view of treated spleen showing red deposits (arrows) and F) treated spleen showing iron-rich regions (blue staining).

Jolly bodies) have been reported one day after initiation of vincristine therapy (Morse and Stohlman, 1966), a phenomenon consistent with spleenic dysfunction. Conversely, histological analysis of the bone marrow *in situ* found only mild hematopoietic suppression (Figure 5.5B), suggesting some benefit of **54** over the conventional antimitotic agent vinblastine (Jackson *et al*., 2007). Finally, no histopathological changes were noted in the lungs, small intestine or kidneys, with the exception of one

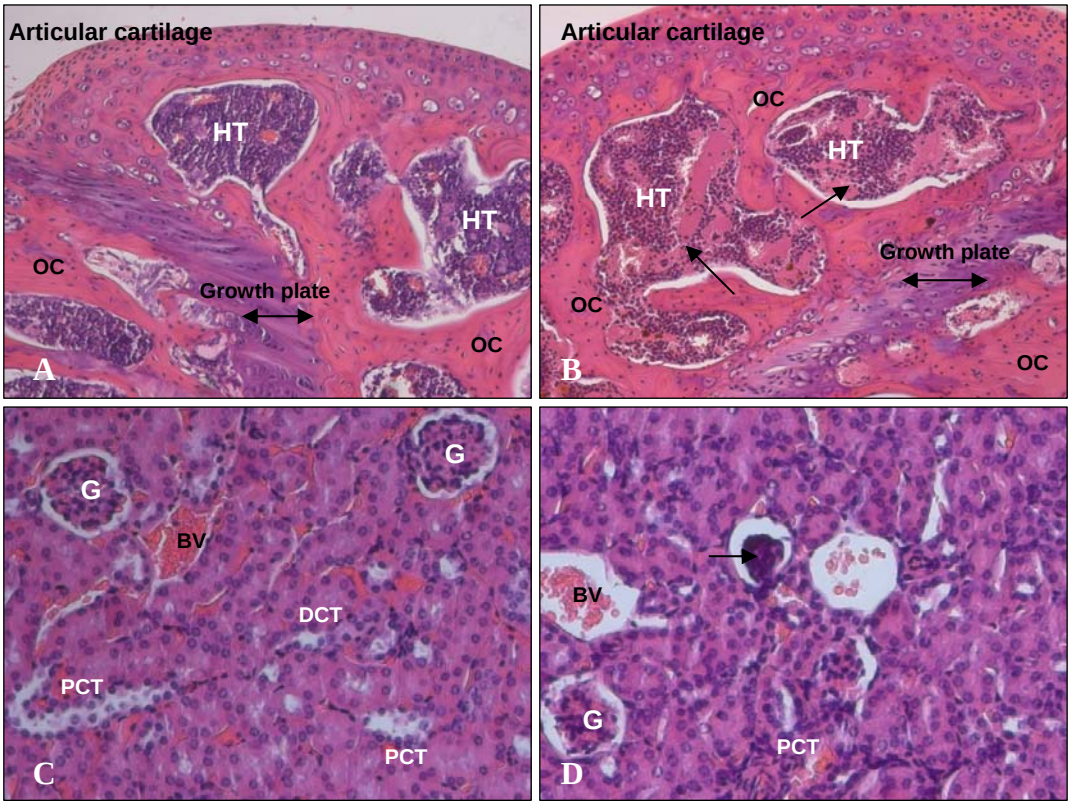

Figure 5.5 Hematoxylin and eosin (H & E) stained tissue preparations used to assess acute toxicity in mice after treatment with 5,7-dibromo-*N*-(*p*-trifluoromethylbenzyl)isatin (**54**). A) Control long bone (humerus) showing cancellous bone consisting of numerous osteocytes (OC) and hemopoietic tissue (HT) occupying the marrow cavities, B) treated long bone (humerus) showing hemopoietic suppression (black single-headed arrow), C) control renal cortex of kidney showing proximal convoluted tubules (PCT), distal convoluted tubules (DCT), blood vessels (BV) and scattered renal corpuscles consisting of glomeruli (G) and D) treated kidney showing atrophic glomeruli (arrow).

individual revealing atrophic glomeruli and chronic infiltration of inflammatory cells in the renal cortex 5 days post treatment (Figure 5.5D).

5.3.2.2 Evaluation of Efficacy in MDA-MB-231 Tumour Xenografts

Mouse models of cancer have consistently been used to qualify new anticancer drugs for study in human clinical trials. The most used models include transplantable murine tumours grown in syngeneic hosts and xenografts of human tumours grown in immunodeficient mice (Sausville, 2006). Many transplantable tumour therapy experiments however utilise ectopic, subcutaneous cancer cell implantation methods for ease of tumour measurement. But, the clinical predictability and response to certain anticancer drugs is questionable (Kerbel, 2003; Kelland, 2004). In this study, an orthotopic human tumour xenograft model bearing MDA-MB-231 breast adeno-carcinoma was used to assess the ability of compound **54** to inhibit solid tumour growth. This particular model was chosen based on its enhanced clinical relevance over ectopic murine/ human tumour models and because of the potent activity displayed by **54** against the MDA-MB-231 cancer cell line *in vitro* (IC_{50} 540 nM; Chapter 4, Table 4.5). A multiple fractionated dose schedule was used to deliver a total dose of 25 mg/kg of **54** (determined as the maximum dose tolerated from toxicology studies) to tumour bearing mice 14 days post implantation, when tumours were palpable but not yet measurable. A dose of 5 mg/kg was administered i.p. twice weekly for 2.5 weeks and by day 14 (the last day of treatment), the rate of tumour growth had decreased and the average tumour volume was significantly less ($P = 0.0386$, $n = 6$; Figure 5.6) than the control treatment cohort. By day 23, compound **54** had significantly reduced the average tumour volume

by almost 45% ($P = 0.0475$, $n = 6$) compared to control mice and showed a reduction in tumour size (in all individuals) from day 21, though this was not significant. Since the experimental endpoint was defined as a tumour size reaching 15 × 15 mm along the longest axes and tumours were to be prepared for histopathology, the observation period ended on day 23. However, it would have been of interest to determine tumour growth delay (GD) over an extended period of time and compare this with the GD properties of other antimitotics at the same concentration. One individual in the control cohort was

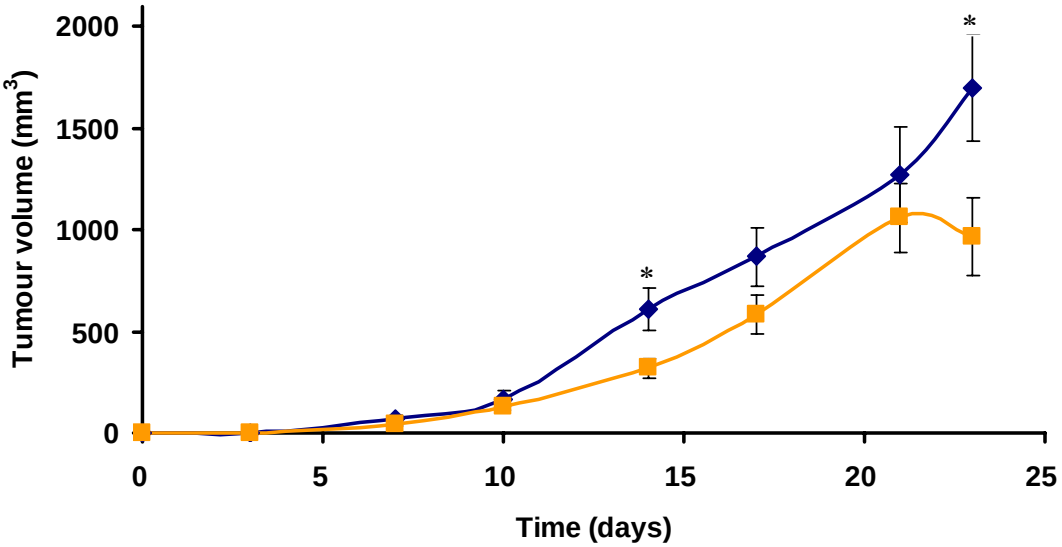

Figure 5.6 MDA-MB-231 cells (2.0×10^6) were implanted into the MFP of 5-6 week old female BALB/c *nu/nu* mice. Fourteen days post tumour implantation (denoted as day 0), animals received either ● 100% DMSO or ■ 5 mg/kg of compound **54**, administered i.p. twice weekly for 2.5 weeks (total dose 25 mg/kg). Tumour growth during the treatment period was monitored by measuring the tumour mass on the animals using digital calipers. Tumour volumes were calculated as described in Section 5.2.3.3. Data points are the means ($n = 5 – 6$), ± SE. The P value was calculated by comparing mean tumour size of the treated group with the mean tumour size of the vehicle-treated control group using the Student's t test (two tailed). * P <0.05 significant.

euthanised on day 18 due to tumour size impeding movement, but of importance, was that no systemic toxicity in terms of body weight loss (Figure 5.7) or behavioral changes such as hunched posture or lack of activity/grooming was observed for mice treated with this dose of **54**. Furthermore, a reduction in tumour associated vascularisation was observed by macroscopic analysis of tumours (Dr Tracy Maddocks, UOW, per. com.), which may also account for the decrease in tumour

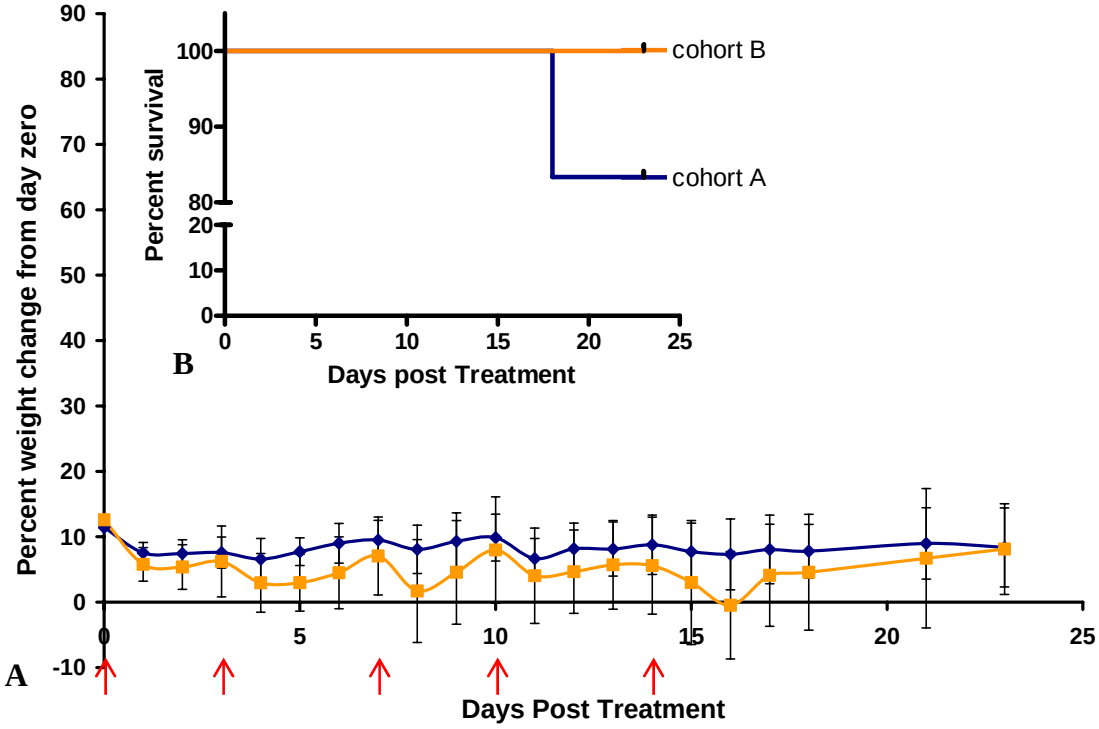

Figure 5.7 Average weight change from day zero and percent survival of mice treated with 5,7-dibromo-*N*-(*p*-trifluoromethylbenzyl)isatin (**54**). Tumoured mice were administered ■ 5 mg/kg of **54** (cohort B) or ● DMSO (cohort A) on the days indicated by red arrows and A) weights recorded and compared to weight change from day zero, or B) percent survival determined using the Kaplan-Meier log rank test (GraphPad Prism V 4.0). Data points are the means of $n = 6 \pm$ SD.

growth up to 9 days after the last treatment. It is known that endothelial cells that form neovasculature in the tumour are rapidly proliferating (Zetter, 1998) and recent studies have found they are also sensitive to antimitotic agents (Tozer *et al*., 2002). Furthermore, long-lasting inhibitory activity *in vivo* has been described for the structurally related VEGF receptor inhibitor SU5416; which was found to be efficacious in 3 different tumour xenograft models despite the fact that it has a short plasma half-life (Mendel *et al*., 2000). This suggests that together with its antimitotic ability, compound **54** may also act as an EGF receptor substrate, due to the structural similarities it shares with other known inhibitors that interact at the ATP binding site of VEGF, FGF and PDGF (Fong *et al*., 1999; Laird *et al*., 2000; Mendel *et al*., 2000).

Histopathological evaluation of the tumours after H & E staining found nearby skeletal muscle infiltrated by murine stromal cells, indicative of high grade malignant tumours (Figure 5.8A and B). Large areas of necrosis were also detected in both control and treatment groups (Figure 5.8C and D, respectively), but no difference in the extent of tissue damage due to treatment with **54** could be detected. A reduction in the amount of tumour associated blood vessels was also noted in the tumours of treated mice (data not shown), but further immunohistochemical staining for blood vessels with von Willebrand Factor (Factor VIII Related Antigen) and/or CD31 antibody (PECAM-1) would be necessary to support the proposed antiangiogenic effect (Horak *et al*., 1992). In addition, *in vitro* biochemical kinase assays screening for VEGF receptor inhibition together with molecular modeling studies would help to validate this hypothesis.

Despite structural similarity, compound **54** was not as efficacious as the structurally related microtubule inhibitor D-24851, which showed complete tumour regression in rats bearing Yoshida AH13 sarcomas. It should be noted that the difference in animal models selected for experimentation; as well as dose regimens can account for large variations in tumour responses. For example, D-24851 induced complete tumour regressions in the Yoshida AH13 rat sarcoma model, but was found to cause only

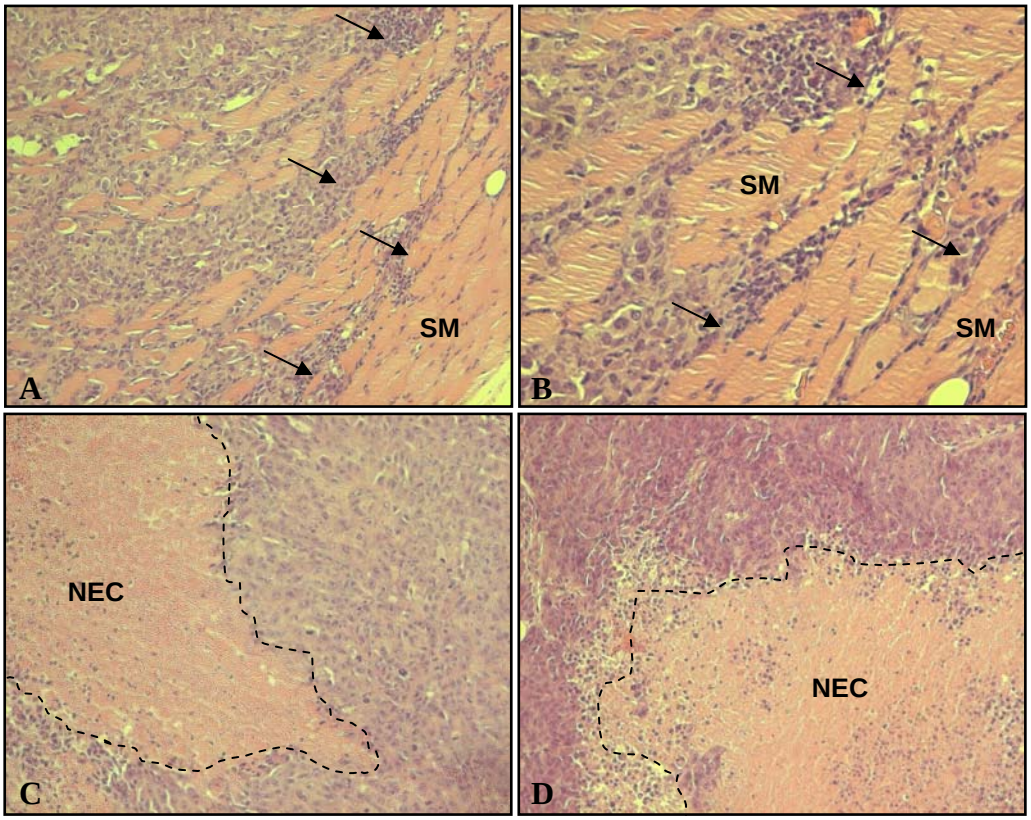

Figure 5.8 Hematoxylin and eosin (H & E) stained mammary MDA-MB-231 tumours excised from female Balb/c xenografts on day 23, after treatment with DMSO (panels A-C) or 5,7-dibromo-*N*-(*p*-trifluoromethyl-benzyl)isatin (**54**, panel D). A) Infiltration of murine stromal cells and human MDA-MB-231 cells (purple staining) into nearby skeletal muscle (SM, low magnification) and B) high magnification indicative of high grade malignant tumours. Arrows indicate direction of invasion. Tumours taken from mice treated with either C) DMSO (control) or D) **54** show large areas of necrosis (NEC).

modest inhibition of tumour growth in a more clinically relevant, human xenograft model bearing PL-3 prostate carcinoma (Bacher *et al*., 2001). In addition, a single bolus dose of D-24851 showed no antitumoural efficacy in mice while complete tumour cures were observed after treatment with 10 mg/kg/day for 2 weeks. A similar effect has also been reported for the indole SU5416, whereby i.p. administration of 25 mg/kg/day significantly inhibited A431 tumour growth by 51% in melanoma xenografts, but treatment with 25 mg/kg twice weekly did not (Mendel *et al*., 2000). This suggests that future studies involving variations to the dose schedule of **54** may lead to increased antitumour efficacy.

5.3.2.3 Single Photon Emission Computed Tomography (SPECT) Imaging

In addition to determining tumour growth delay in clinically relevant animal models, analysis of the biodistribution and blood clearance properties of potential drug candidates is also important. Advances in understanding the routes and times of excretion of molecules from the body, as well as the accumulation of compounds in target tissues, helps to demonstrate the appropriateness of the drug. For example, if compounds are cleared too quickly, they may lack the time in the body to penetrate the tumour and hence kill the cells. Similarly if compounds are widely dispersed, at higher concentrations they may inflict a large amount of non-specific damage. These factors can be determined using single photon emission computed tomography (SPECT) and augment traditional *in vivo* efficacy and toxicity studies (Cai and Chen, 2006).

It is already known that isatins can readily cross the blood brain barrier, targeting MAO in the brain (Crumeyrolle-Arias *et al.,* 2003) however, little is known about whole body biodistribution for cancer therapy. In this study, analysis of two different ^{123}I radiolabeled analogues of isatin, namely compound **67** and **68** were investigated in two different animal models using SPECT, to further assess their pharmaceutical potential. Compound **67** and **68** were first assessed in mouse xenografts bearing human A375 amelanotic melanomas. This model was chosen due to the potent activity displayed by the non-radiolabeled isatin 5,7-dibromo-*N*-(*p*-iodobenzyl)isatin (**53**), against the A375 cancer cell line *in vitro* (IC_{50} 2.4 μM, Chapter 4, Table 4.5). Analysis of radiotracer uptake over time found both ^{123}I compounds to be metabolised rapidly, with moderate activity detected in the thyroid within the first 40 min (Figure 5.9, panel A and B respectively). Some uptake of **67** in the gut was detected between 40 min and 6 h p.i. (Figure 5.9, panels C and E respectively) although a large proportion was excreted in the urine and feces (as evidenced by accumulation of activity in the bladder and large intestine) by 24 h (Figure 5.9, panel G). By 48 h, the remaining activity was localised in the thyroid (Figure 5.9, panel I). Conversely, the tissue distribution profile of compound **68** differed significantly, whereby the liver showed the greatest amount of radiotracer uptake. Activity was detected in both the liver and gut from as early as 40 min p.i., but only minimal fecal clearance was observed after 48 h (Figure 5.9, panel J). In both cases, no tumour uptake was observed at any of the imaging time points, despite the activity of the cold material against the A375 cell line *in vitro* (**53**, Chapter 4, Table 4.5). In addition, only minimal activity was detected in the brains of the animals, which

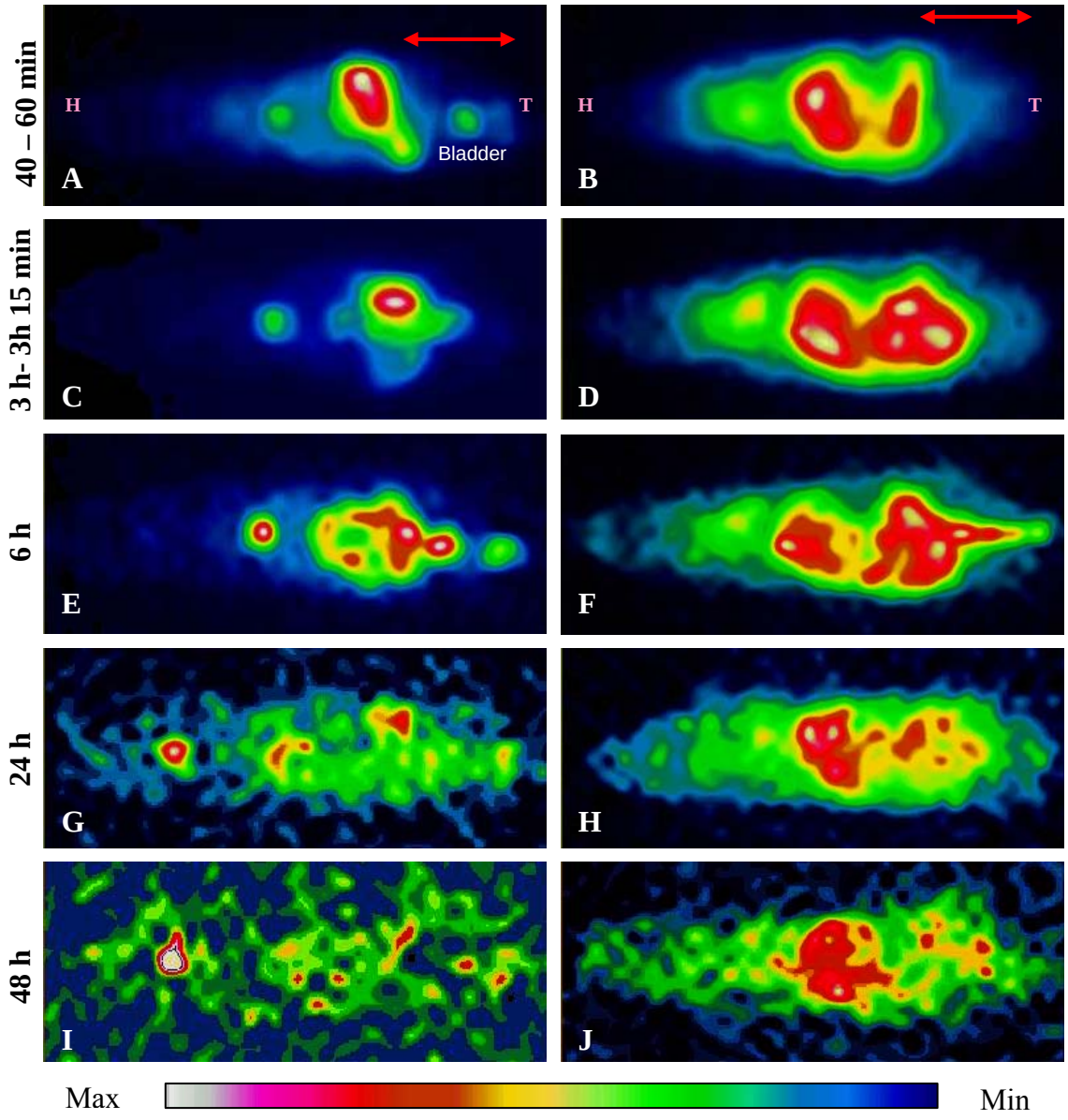

Figure 5.9 SPECT imaging of ^{123}I labeled compounds **67** (left panels) and **68** (right panels) in athymic female Balb/c (nu/nu) melanoma xenografts. Images were obtained at A and B) 40 - 60 min, C and D) 3 h - 3 h 15 min, E and F) 6 h, G and H) 24 h and I and J) 48 h post injection. Mice were injected *via* the tail vein with 100 µL of 2 µCi/µL radiotracer in 0.9% saline and 5% EtOH. H = head, T = tail. Red arrows indicate tumour region. Images are one representative animal from experiments performed in duplicate.

may be due to the differences in molecular weight and lipophilicity (Oldendorf, 1974; Levin, 1980) of the *N*-alkylisatins compared to unsubstituted isatin.

The tissue distribution patterns of compounds **67** and **68** were next assessed in a rat tumour model, bearing 13762 MAT B III mammary adenocarcinoma. Analysis of radiotracer uptake over time found both ^{123}I labeled compounds to accumulate in the major organs including the liver and gut (Figure 5.10), similar to that observed in the mouse xenograft model. Unlike the mouse model however, neither compound was found to accumulate in the thyroid and no activity was detected in the brains of F344 Fisher rats at any time point after i.v. administration (Appendix 3, Figure A3.11). Interestingly, the majority of compound **68** was cleared from the liver by 6 h, while a large proportion remained in the gut. This observation was further supported by a pilot biodistribution study in rats, whereby activity in the gut was 5 times greater than in the liver 72 h p.i. (Appendix 3, Figure A3.12). Furthermore, elevated levels of activity were detected in the tumours of animals over time, with maximum activity recorded at 48 h (Figure 5.10, panel I and J respectively). Despite the reduced cytotoxicity displayed by 5-iodo-*N*-(*p*-methoxybenzyl-isatin compared to 5,7-dibromo-*N*-(*p*-iodobenzyl)isatin (**53**) *in vitro* (IC_{50} >63μM and IC_{50} 2.4μM respectively) the ^{123}I labeled analogue (**67**) was shown to exhibit greater tumour uptake than **68** *in vivo*. This is further exemplified in Figure 5.11 and indicates that the most active compound *in vitro* may not always be the most viable compound pharmaceutically. In essence, the SPECT imaging profiles of the ^{123}I labeled compounds reconfirm both efficacy and toxicological findings, that

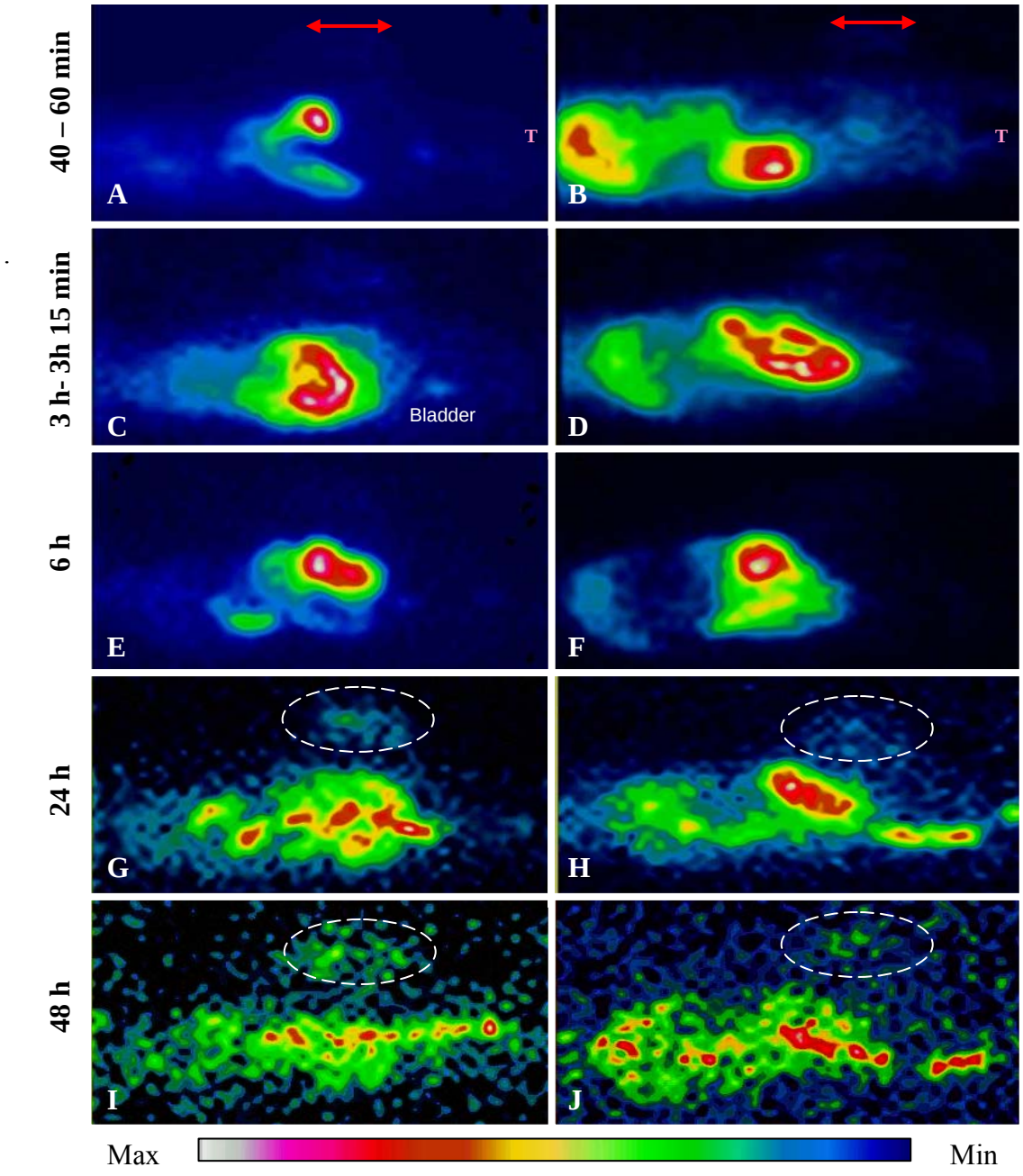

Figure 5.10 SPECT imaging of ^{123}I labeled compounds **67** (left panels) and **68** (right panels) in F344 Fisher rats bearing 13762 MAT B III mammary adenocarcinoma. Images were obtained at A and B) 40 - 60 min, C and D) 3 h - 3 h 15 min, E and F) 6 h, G and H) 24 h and I and J) 48 h post injection. Rats were injected *via* the tail vein with 100 µL of 5 µCi/µL radiotracer in 0.9% saline and 5% EtOH. T = tail. Red arrows indicate tumour region. Dashed circles represent detectable levels of radiotracer accumulated in tumour. Images are one representative animal from experiments performed in duplicate.

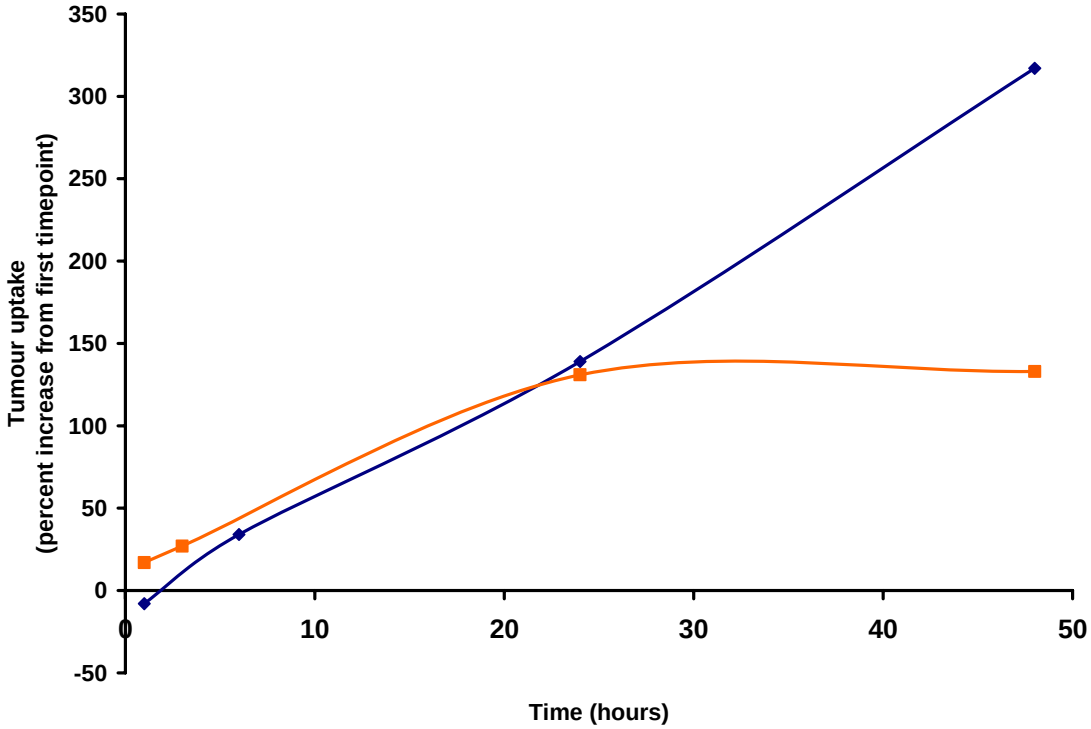

Figure 5.11 Tumour uptake (as measured by radioactive intensity) of ^{123}I labeled compounds in F344 Fisher rats bearing 13762 MAT B III mammary adenocarcinoma. Rats were treated with either ♦) *N*-(*p*-methoxybenzyl)-5-(^{123}I)iodoisatin (**67**) or ■) 5,7-dibromo-*N*-[4'-(^{123}I)iodobenzyl]isatin (**68**) and tumour uptake relative to skin (non-tumour tissue) uptake measured over time. Curves are representative of tumour uptake in one animal from duplicate experiments as imaging time points varied slightly between individuals.

1) *N*-alkylisatins can be taken up by the tumour and 2) non-target organs such as the liver and gut are also found to accumulate compound.

Finally, the fact that the *N*-alkylisatins **67** and **68** are taken up by and retained in the tumour over a period of 48 h (as evidenced by SPECT) may explain why tumour regression was observed in mouse xenografts 9 days after administration of **53**. The intestinal epithelium is one of the most rapidly proliferating tissues in the body

(Podolsky, 1993; Polk, 1999) and perhaps explains the elevated levels of ^{123}I *N*-alkylisatin accumulation in the gut. Furthermore, the EGF family, including EGF and transforming growth factor (TGF-) and their receptor (EGFR) play critical roles in intestinal epithelial proliferation (Podolsky, 1993; O'Loughlin, 1994; Stern *et al*., 2000). Considering the structural similarity that the *N*-alkylisatins share with other EGF receptor tyrosine kinase inhibitors (Kelloff *et al*., 1996; Sun *et al*., 1998; Fong *et al*., 1999), suggests that they too may be inhibitors of kinases involved in the EGF signal transduction pathway.

5.4 Conclusions

The antimitotic compound **54**, has proven to be efficacious in a human tumour xenograft mouse model bearing mammary MDA-MB-231 adenocarcinoma. In addition, when administered at a total dose of 25 mg/kg, **54** showed a significant reduction in tumour size without evidence of systemic toxicity. Analysis of biodistribution *via* SPECT imaging found moderate tumour uptake of both radioiodinated compounds (**67** and **68**) in a rat mammary carcinoma model 48 h p.i., although large amounts of activity were also detected in the gut and liver. To counter this, a prominent strategy may be to develop *N*-alkylisatin prodrugs conjugated to a moiety designed to cleave enzymatically or under acid conditions specifically in cancer cells. This strategy could then target the cytotoxins to receptor-enriched cancer cells, reaching higher therapeutic concentrations at tumour sites with lower systemic toxicity to other non-target organs, ultimately resulting in fewer side effects.

CHAPTER 6

A Preliminary Investigation into Targeted Drug Delivery *via* Receptor Mediated Endocytosis

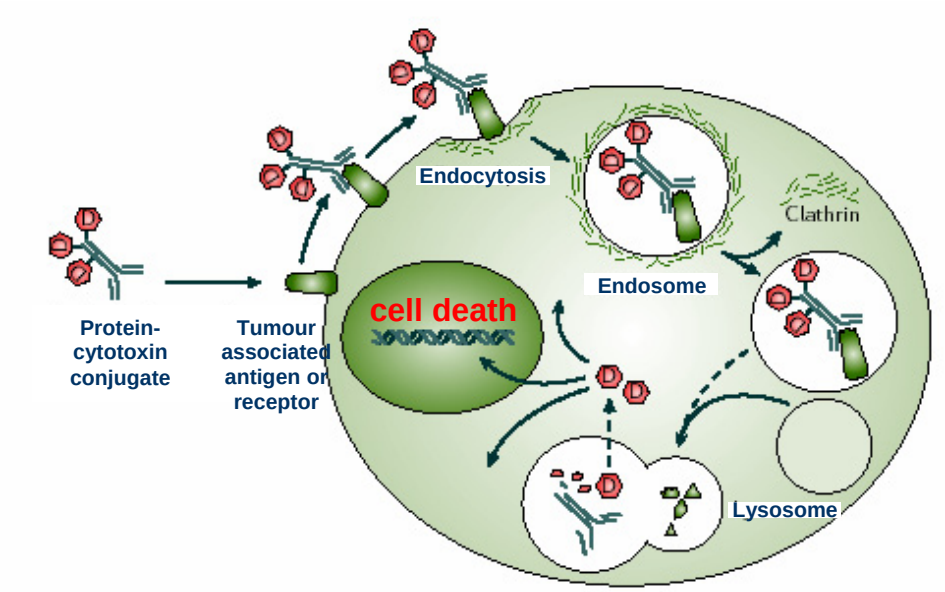

Internalisation of a protein-cytotoxin conjugate *via* receptor mediated endocytosis. Adapted from (Schrama *et al.*, 2006)

CHAPTER 6

A Preliminary Investigation into Targeted Drug Delivery *via* Receptor Mediated Endocytosis

6.1 Introduction

Antineoplastic agents have for many decades formed the basis of chemotherapeutic treatment for a variety of cancers. However one limitation of their use has been the administration of an effective dose that does not cause toxic side effects (Chabner *et al.*, 1984; Chabner and Roberts, 2005). The majority of cancer chemotherapeutics in clinical use, including doxorubicin, vincristine, 5-fluorouracil, paclitaxel and cyclophosphamide owe what little selectivity they have to the higher proliferation rates of cancer cells. But this can lead to increased toxicities against normal tissues that also show enhanced proliferation rates such as the bone marrow, GI tract and hair follicles (Kaelin, 2005). Side effects that occur as a result of toxicity to normal tissues mean that anticancer chemotherapeutics are often administered at sub-optimal doses, which eventually leads to the failure of therapy (DeVita, 1997; Foote, 1998). This can also be accompanied by the development of drug resistance and progression into metastatic disease.

One attractive strategy used to enhance the therapeutic index of cytotoxic drugs is to specifically deliver these agents to a defined target, keeping them as largely as possible away from healthy cells. The utilisation of cell-specific receptors to target particular cell

types, for example tumour cells, is an attractive concept because it offers the possibility of minimising non-selective toxic effects. There are, however, difficulties associated with the targeting approach. One difficulty is the identification of a suitable receptor that is present predominantly on cancerous cells and is in sufficient density. In addition, modifications to ligands must be tolerated without affecting receptor binding interactions. The fate of internalised ligand-receptor complexes also needs to be determined. Cytotoxic moieties that can be successfully derivatised so as to be employed in a targeting strategy also need to be identified. Despite these hurdles, many attempts are being made to explore the potential of specific and target-oriented delivery systems. One system that has received much interest over the past few years is ligand-receptor mediated delivery, due to the potential of site-specific targeting to ligand-specific sites with no immunogenic response (Vyas and Sihorkar, 2000; Vyas *et al.*, 2001; Schrama *et al.*, 2006).

6.1.1 Serum Proteins as Carriers in Drug Targeting Strategies

Naturally existing, serum proteins have received major attention in the area of drug targeting since these proteins are biodegradable, nontoxic, and non-immunogenic (Kratz and Beyer, 1998). Moreover, they can achieve site-specific targeting due to the high amounts of their receptors present on the cell surface (Brock, 1985; Vitols, 1991). For example, the efficient cellular uptake of transferrin and human serum albumin (HSA) have shown potential in the delivery of anticancer drugs, proteins, and therapeutic genes into primarily proliferating malignant cells that over-express transferrin and albumin receptors (Kratz and Beyer, 1998; Singh, 1999; Vyas and Sihorkar, 2000; Kircheis *et*

al., 2002). Chlorambucil when bound to transferrin through an acid-sensitive hydrazone bond exhibited an IC_{50} approximately 3-18 fold lower than that of chlorambucil alone (Beyer *et al.*, 1998). Preliminary toxicity studies in mice also showed that this conjugate can be administered at higher doses in comparison to unbound chlorambucil (Beyer *et al.*, 1998).

6.1.2 The uPA System in Drug Targeting Strategies

Several biochemical and biological characteristics of PAI-1 and PAI-2, (inhibitory serpins of the uPA system, See Chapter 1, Section 1.5.2.3b), also advocate their use as targeting agents. For example, PAI-1 conjugated to A-chain cholera toxin and modified PAI-1 conjugated to saporin have been used to target fibrosarcoma cells (Jankun, 1992) with moderate cytotoxicity. Furthermore, previous studies have described the conjugation of PAI-2 to the α–emitting radioisotope ^{213}Bismuth (^{213}Bi) *via* the metal chelator cDTPA. Studies have found that PAI-2-DTTA-^{213}Bi shows preferential targeting of metastatic breast cancer cells *in vitro* (Ranson *et al.*, 2002) and targets tumour xenografts and micrometastases *in vivo* (Li *et al.*, 2002; Allen *et al.*, 2003; Stutchbury *et al.*, 2007). Although the impressive activity of PAI-2-DTTA-^{213}Bi can be attributed to the efficient binding and rapid internalisation of PAI-2:uPA complexes (Al-Ejeh *et al.*, 2004), there are also some foreseeable limitations. Radioisotopes such as ^{213}Bi are very expensive and are associated with handling difficulties. In addition, ^{213}Bi has a very short half-life, less than 45 minutes (Hagemann, 1950), which complicates drug manufacture, delivery and quality control processes. Waste disposal of α-emitters can also be problematical.

6.1.2 Rationale and Aims

5-Fluorouracil (5-FU, in association with folinic acid) is used as a standard treatment for many carcinomas, including colorectal cancer in the adjuvant setting (Meyerhardt and Mayer, 2005). Although 5-FU is one of the most widely used chemotherapeutic agents in the clinic, response rates are still low and dose limiting toxicity is still problematical (Meyerhardt and Mayer, 2005). Previously, the targeting of 5-FUdr (a cytotoxic metabolite of 5-FU) has been described through the use of monoclonal antibodies (mAb). However, delivery of the immunoconjugate to the tumour was reported to be inefficient, resulting in only a fraction of the dose entering the tumour (Goerlach *et al.*, 1991). Considering previous reports on the ability of PAI-2-DTTA-^{213}Bi to preferentially target metastatic breast cancer cells *in vitro* (Ranson *et al.*, 2002) and tumour xenografts and micrometastates *in vivo* (Li *et al.*, 2002; Allen *et al.*, 2003; Stutchbury *et al.*, 2007), it was anticipated that by linking a derivatised version of 5-FUdr to PAI-2, the cytotoxin could also be specifically delivered to and concentrated within uPA expressing tumour cells (Scheme 6.1). The principal aims of this study were therefore to assess the targeting ability of 5-FUdr conjugated to PAI-2 in a proof of concept study. Specifically the aims of this section were to:

1. Conjugate 2′-deoxy-5-fluorouridine (5-FUdr), a potent metabolite of the clinically used anticancer agent 5-FU, to PAI-2.
2. Optimise the method of conjugation of 5-FUdr to PAI-2 (i.e. maximise the number of cytotoxins incorporated into the protein without compromising activity or binding ability).

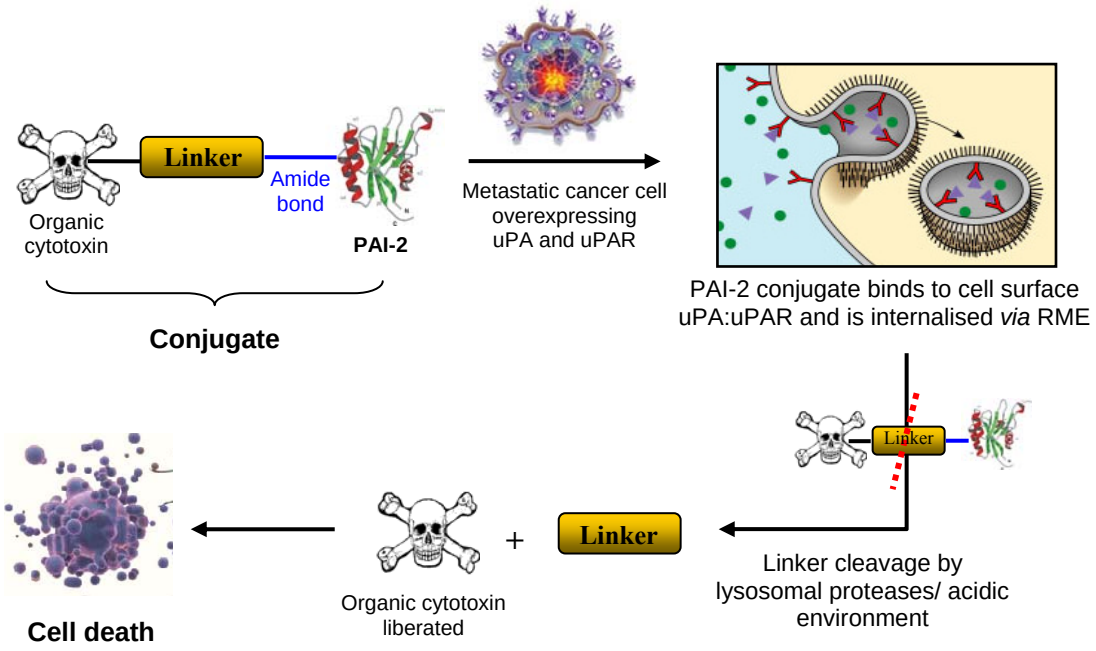

Scheme 6.1 Schematic representation of PAI-2-cytotoxin targeted delivery to uPA and uPAR positive metastatic cancer cells *via* receptor mediated endocytosis (RME).

3. Investigate the *in vitro* cytotoxic activity of the PAI-2-5-FUdr conjugate in comparison to the free drug and demonstrate its targeting ability by screening against two mammary gland adenocarcinoma cell lines with different uPA profiles.

In addition to designing prodrugs such as 5-FUdrsucc, with linkers that are to be cleaved by non-specific esterases, acid labile linkers have also proved effective when exploiting receptor mediated endocytosis (RME) delivery mechanisms. Considering the *N*-alkylisatins (**39**, **45**, **48** and **54**) have shown > 10 times more

activity *in vitro* than the conventional chemotherapeutic 5-FU (Appendix 2, Figure A2.1), yet show non target-organ uptake *in vivo*, further aims were to:

1. Derivatise an *N*-alkylisatin so as to contain an acid-labile linker for attachment to PAI-2 *via* amide bond formation with free lysine residues.
2. Assess the lability of the linker using varying pH conditions for subsequent *in vitro* studies.
3. Investigate the *in vitro* cytotoxicity of the PAI-2-*N*-alkylisatin conjugate and demonstrate its targeting ability by screening against cancer cell lines with different uPA profiles.

6.2 Materials and Methods

6.2.1 General

2′-Deoxy-5-fluoro-3′-*O*-(3-carbonylpropanoyl)uridine (5-FUdrsucc) (**70**) and 5,7-dibromo-3-[*m*-(2'-carboxymethyl)-phenylimino)-*N*-(*p*-trifluoromethyl)isatin (**72**) were supplied by Dr. Julie M. Locke, Postdoctoral Research Fellow, Department of Chemistry, University of Wollongong. BioRad® DC protein concentration assay kit was purchased from Bio-Rad Laboratories (CA, USA). Human recombinant PAI-2 (47 kDa) was provided by PAI-2 Pty Limited (N.S.W., Australia) and purified human uPA (50 kDa) was obtained from American Diagnostica (CT, USA). Anhydrous DMF, NHS and DCC were purchased from Sigma-Aldrich (MO, USA) and the 30 kDa cut-off microconcentrators were purchased from Millipore (MA, USA).

6.2.2 Chemical Synthesis

6.2.2.1 Conjugation of 2′-deoxy-5-fluoro-3′-*O*-(3-carbonylpropanoyl)uridine (5-FUdrsucc) to PAI-2

6.2.2.1a Activation of the ester

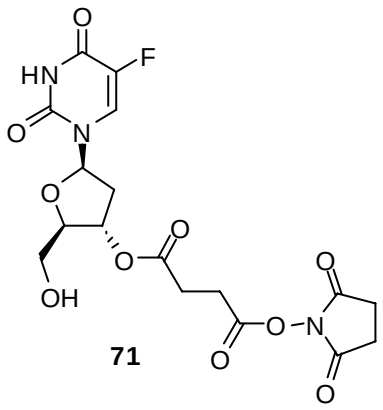

71

The active ester of 5-FUdrsucc (**71**) was prepared using a modification to the method described previously (Goerlach *et al.*, 1991). Briefly, 5-FUdrsucc (**70**, 1.73 mg, 5 μmol) was dissolved in dry DMF (70 μL). *N*-hydroxysuccinimide (NHS, 0.59 mg, 5.1 μmol) in DMF (17 μL) and dicyclohexylcarbodiimide (DCC, 6.18 mg, 30 μmol) in DMF (50 μL) were then added and the reaction mixture kept at RT for 3 h and then at 4 °C overnight. The crude colourless product (R_f 0.55, silica, 100% DCM) was used in future conjugation experiments without further purification.

6.2.2.1b Conjugation to PAI-2

In two separate experiments, a 20 and 50 fold molar excess of the activated ester (**71**) were incubated with PAI-2 (*ca* 2 mg/mL) in PBS (pH 7.4) at RT, with shaking. After 3 h the reaction mixture was centrifuged (maximum speed for 5 min) to remove any precipitate. The conjugate was then purified by gel filtration (PD-10 column), with PBS (pH 7.4) as eluant. Fractions corresponding to the protein peak (as determined by UV/Vis spectrophotometry, 280 nm) were pooled, sterile filtered (0.22 μM) and stored at 4 °C for future cytotoxicity studies. Protein concentration was determined using the standard Lowery protein determination assay and the amount of 5-FUdrsucc bound to

protein determined by electrospray ionisation mass spectrometry (ESI-MS) analysis. The protein yield was > 85%.

6.2.2.2 Conjugation of 5,7-dibromo-3-[*m*-(2'-carboxymethyl)-phenylimino)-*N*-(*p*-trifluoromethyl)isatin to PAI-2

6.2.2.2a Activation of the ester

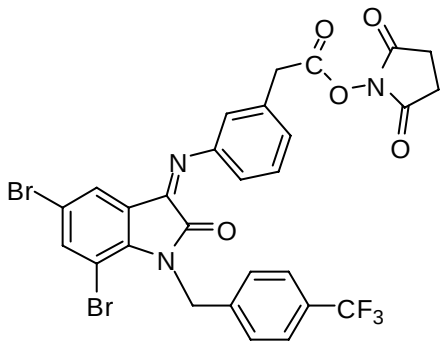

73

5,7-Dibromo-3-[*m*-(2'-carboxymethyl)-phenylimino)-*N*-(*p*-trifluoromethyl)isatin (**72**, 1.73 mg, 5 μmol) was dissolved in dry DMF (70 μL). *N*-hydroxysuccinimide (NHS, 0.59 mg, 5.1 μmol) in DMF (17 μL) and dicyclohexylcarbodiimide (DCC, 6.18 mg, 30 μmol) in DMF (50 μL) were then added and the reaction mixture shaken at RT between 15 min and 3 h and then 4 °C overnight. The crude orange product was then used in conjugation experiments without further purification; R_f 0.43 (100% DCM, silica).

6.2.2.2b Conjugation to PAI-2

A 20-fold molar excess of the activated ester (**73**) was incubated with PAI-2 (2.89 mg/mL) in PBS (pH 8.2) at RT, with shaking. After 1 h 15 min the reaction mixture was centrifuged (maximum speed for 5 min) to remove any precipitate. The conjugate was then purified by gel filtration (PD-10 column), eluting with PBS (pH 8.2). Fractions corresponding to the protein peak (as determined spectrophotometrically at 280 nm) were pooled, sterile filtered (0.22 μM) and stored at 4 °C for future cytotoxicity studies.

Protein concentration was determined using the standard Lowery protein determination assay and the amount of isatin bound to protein determined by UV/Vis spectrophotometry (ε_{432} = 2140 $M^{-1}cm^{-1}$) and electrospray ionisation mass spectrometry (ESI-MS) analysis. Protein yield was > 80%.

6.2.2.3 Characterisation of Protein-Cytotoxin Conjugates

6.2.2.3a Electrospray Ionisation Mass Spectrometry (ESI-MS)

The protein conjugate ratio was determined by ESI-MS. Samples were desalted by centrifugation using 30kDa cut-off microconcentrators for ESI-MS. Protein and protein conjugates were washed 5 times with milliQ water by centrifugation (~6000 × g, 5 min) before being made up to a final protein concentration of 1-10 μM. Samples were injected into the Micromass Q-TOF Ultima mass spectrometer (Waters, Wyntheshawe, UK) and run at 30 cone volts and a resolution power of 5000 Hz. The electrospray ion series was transformed to a mass scale using the MaxEnt deconvolution algorithm.

6.2.2.3b PAI-2: uPA Complex Formation

The ability of PAI-2 to retain activity and form stable complexes with uPA after modification by conjugation was compared to unmodified PAI-2 as previously described (Hang *et al*., 1998, Ranson *et al*., 2002). Briefly, conjugated and unconjugated PAI-2 were incubated with equimolar amounts of uPA in PBS (pH 7.4) for 30 min at 37 ºC and complex formation visualised by Coomassie blue staining of samples fractionated by SDS-PAGE under non-reducing conditions.

6.2.2.4 Hydrolysis Studies

Preliminary studies assessing the ability of 5,7-dibromo-3-[*m*-(2'-carboxymethyl)-phenylimino)-*N*-(*p*-trifluoromethyl)isatin (**72**) to cleave under different pH conditions was assessed *via* UV/Vis spectrophotometry. In addition, scanning spectra of compound **72** conjugated to transferrin (as an example ligand) was used to asses the acid lability of the imine linker when conjugated. Increasing concentrations of 1M HCl were added to a total volume of 100 µL of conjugate in PBS (pH 7.5) then incubated at RT for 20 h before measuring the absorbance over a range of 260-750 nm. A decrease in the absorbance at 303 and 440 nm was indicative of imine linker cleavage of the cytotoxin from the protein.

6.2.2.5 *In vitro* Cytotoxicity Evaluation

The cytotoxic activities of protein alone (PAI-2), protein-cytotoxin conjugates (PAI-2-5-FUdrsucc and PAI-2-CF_3imine) as well as unconjugated cytotoxins (5-FUdr, 5-FUdrsucc (**70**), 5,7-dibromo-*N*-(*p*-trifluoromethyl)isatin (**54**) and 5,7-dibromo-3-[*m*-(2'-carboxymethyl)-phenylimino)-*N*-(*p*-trifluoromethyl)isatin (**72**)) were determined against two human breast adenocarcinoma cell lines (MDA-MB-231 and MCF-7) which vary in their expression levels of uPA (Andronicos and Ranson, 2001; Ranson *et al.*, 2002). Cytotoxicity was determined using the CellTiter 96 Aqueous One Solution Cell Proliferation Assay (MTS), in 96-well microplates, as described in Chapter 2, Materials and Methods, Section 2.3.2.1. Test compounds were incubated with different cell lines, in triplicate, at increasing concentrations for 48 h (unless stated otherwise) prior to the addition of MTS reagent. Cytotoxic activity was then determined spectrophoto-

meterically at 490 nm. Results for each compound are reported as the concentration (μM) required to inhibit the metabolic activity of 50% of the cell population (IC_{50}) in comparison to PBS or DMSO treated cells. These values were calculated from logarithmic sigmoidal dose response curves using the variable slope parameter, generated from GraphPad Prism V 4.02 software (GraphPad Software Inc.).

6.2.2.5a Addition of Exogenous uPA

Assays were performed as described in Section 6.2.2.5, however, prior to the addition of PAI-2-5-FUdrsucc (4 μM protein equiv.), MCF-7 cells were pre-incubated with 18 nM exogenous uPA (+ uPA) or PBS (- uPA) for 10 min at RT. Cells were then washed 3 × with RPMI-1640 (containing 5% FCS).

6.2.2.6 Statistical Analyses

Statistical significance of treatment groups as compared to control groups were determined using an unpaired students T-test (GraphPad Prism V 4.02). *P* values < 0.05 were considered statistically significant.

6.3 Results and Discussion

6.3.1 Chemistry

A series of reactions were performed to prepare 2′-deoxy-5-fluoro-3′-*O*-(3-carbonylpropanoyl)uridine (5-FUdrsucc, **70**, Scheme 6.2) for chemical attachment to

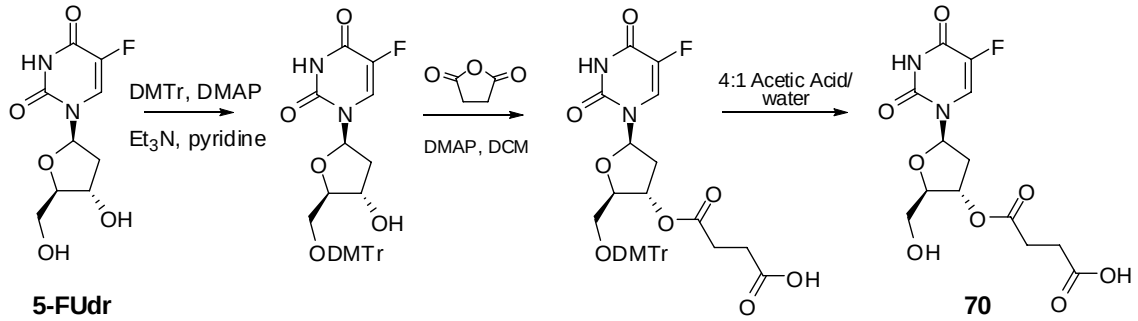

Scheme 6.2 Preparation of 2′-deoxy-5-fluoro-3′-*O*-(3-carbonylpropanoyl)uridine (5-FUdrsucc, **70**) from 2′-deoxy-5-fluorouridine (5-FUdr). Reactions were carried out by Dr Julie Locke (Postdoctoral Research Fellow) Department of Chemistry, UOW, using the method described by Goerlach *et al*., 1991.

PAI-2, which involved the introduction of a carboxyl group by succinylation of protected 5-FUdr (performed by Dr. Julie Locke, Postdoctoral Research Fellow, UOW). Yields obtained were > 65%. The carboxyl group of **70** was then activated by forming the ester (**71**) with 1.1 equiv. of NHS and 6 equiv. of DCC in dry DMF (Scheme 6.3). The molar equivalents used were based on those described previously for the activation of 5-FUdrsucc (Goerlach *et al*., 1991). However, it was noted that the active ester formed rapidly at RT as evidenced by TLC (R_f 0.55, silica 100% DCM) and longer reaction times, such as those described by Goerlach and colleagues (1991), were not necessary. Since the active ester was unable to be recrystallised, it was used in the proceeding conjugation experiments without further purification.

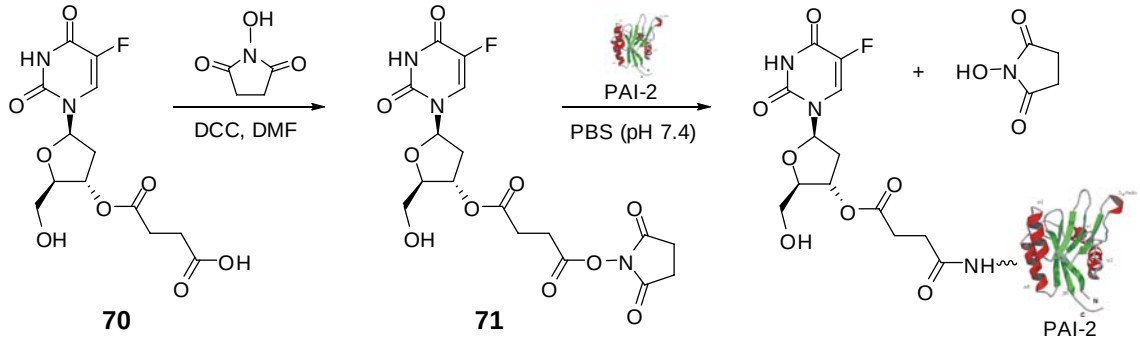

Scheme 6.3 Activation of 5-FUdrsucc (**70**) to form the active ester **71** and conjugation to PAI-2 *via* amide bond formation with free surface lysines.

To optimise coupling, different molar excesses of **71** were added to PAI-2 in order to obtain conjugates with the highest amount of substitution. The greatest 5-FUdruscc: PAI-2 ratio was obtained using a 50-fold molar excess of **71**, yielding up to 7 molecules of 5-FUdrsucc for every protein molecule (Figure 6.1). This was determined by ESI-MS analysis and corresponds well to previous reports on cDTPA incorporation into PAI-2 (Ranson *et al*., 2002; Allen *et al*., 2003). According to the 3D structure of PAI-2, at least 5 free lysine groups are accessible for chemical conjugation at the surface of the protein (Dr. Fares Al-Ejeh, per. com., Appendix 4, Figure A4.1). However, this was only determined for the amino nitrogens that were > 50% accessible and did not include the *N*-terminal amino acid, suggesting that incorporation of a larger number of cytotoxin molecules is possible. ESI-MS data also demonstrated that the PAI-2-5-FUdrsucc preparations contained a mixture of several PAI-2-5-FUdrsucc moieties with

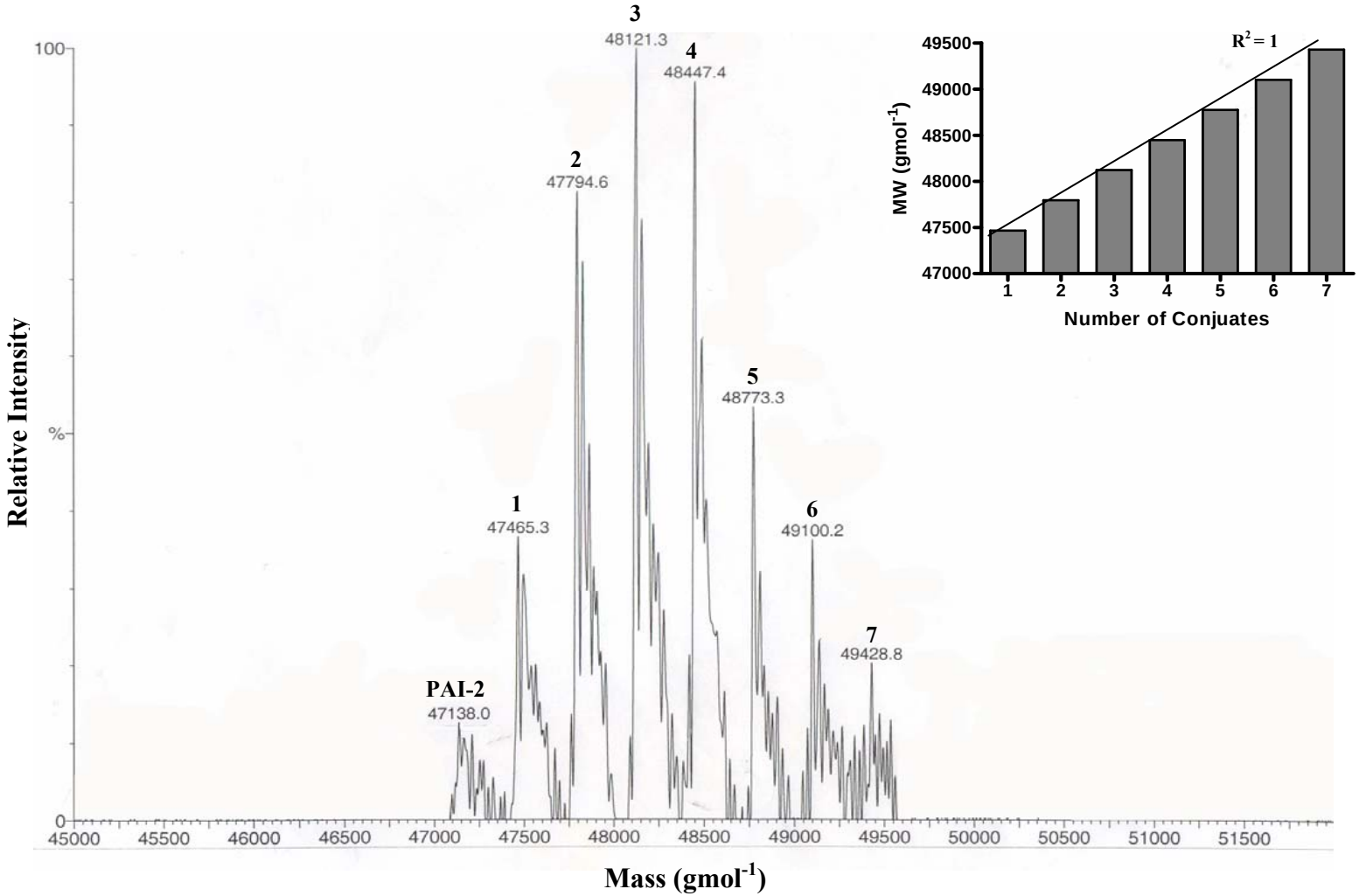

Figure 6.1 ESI-MS of PAI-2-5-FUdrsucc. Conjugates were prepared for electrospray ionisation mass spectrometry (ESI-MS) in Milli Q water and were made up fresh to a final concentration of 1-10 μM. Numbers displayed on the peaks represent the number of 5-FUdrsucc molecules incorporated into the PAI-2 targeting ligand. *Inset*: the number of PAI-2-5-Fudrsucc conjugates was plotted against molecular weight (mw). The difference in mass for each species represents the exact weight of 5-FUdrsucc (327 $gmol^{-1}$), giving a correlation coefficient (R^2) = 1.

an average of 3-4 cytotoxins incorporated per protein molecule (Figure 6.1). Although the relative abundance of free PAI-2 was < 10%, future studies may involve purifying the PAI-2 moiety with the highest number of 5-FUdrsucc molecules, by preparative HPLC for further *in vitro* and *in vivo* testing.

The ability of PAI-2-5-FUdrsucc to form stable complexes with uPA was next investigated in an effort to confirm that the uPA inhibitory activity was maintained by modified PAI-2 (Figure 6.2). After a 30 min incubation period with 1 molar equiv. of uPA, PAI-2-5-FUdrscucc was found to form stable complexes of 80 and 98 kDa with

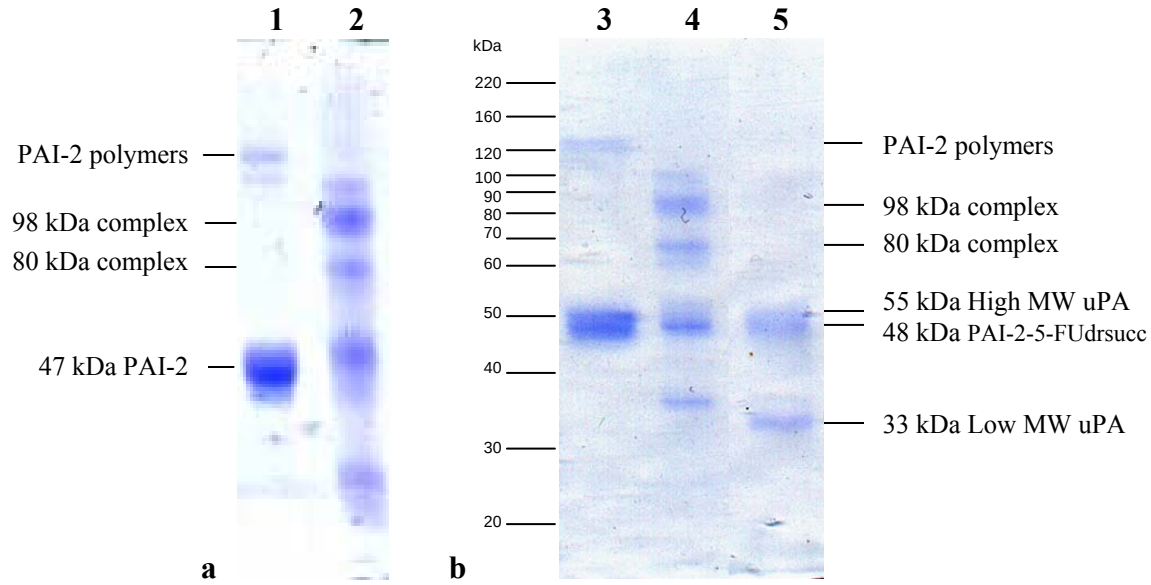

Figure 6.2 Samples fractioned by SDS PAGE showing the ability of a) unmodified and b) modified PAI-2 to form stable complexes with uPA. Briefly, PAI-2 and PAI-2-5-FUdrsucc were incubated with equimolar amounts of uPA at 37 °C for 30 min. Samples were then fractionated under non-reducing conditions using 12% acrylamide SDS PAGE and visualised by staining with Coomassie blue. Lane 1: PAI-2, Lane 2: PAI-2: uPA, Lane 3: PAI-2-5-FUdrsucc, Lane 4: PAI-2-5-FUdrsuc: uPA, Lane 5: uPA.

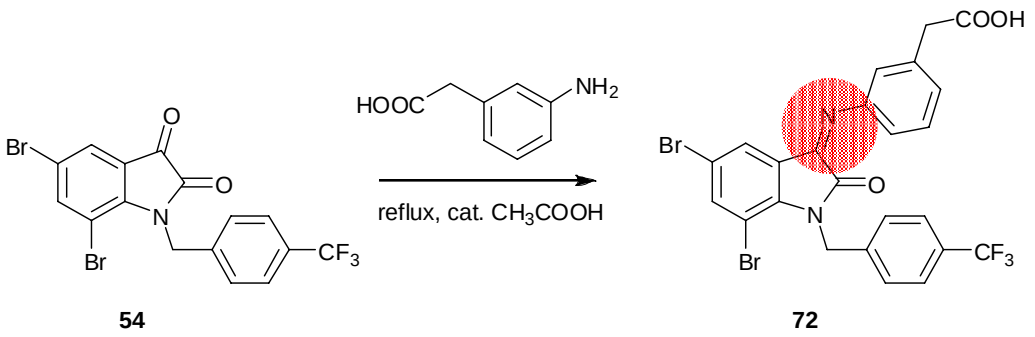

54 **72**

Scheme 6.4 Preparation of 5,7-dibromo-3-[*m*-(2'-carboxymethyl)-phenylimin-o)-*N*-(*p*-trifluoromethyl)isatin (**72**). The reaction was carried out by Dr Julie Locke (Postdoctoral Research Fellow) Department of Chemistry, UOW and the acid-labile imine linker is shown in red.

low and high molecular weight uPA subunits (33 and 55 kDa respectively, Figure 6.2b). This was similar to that observed for unmodified PAI-2 (Figure 6.2a), confirming that the modification of lysine functional groups leading to the incorporation of up to 7 molecules of 5-FUdrsucc does not compromise the inhibitory ability of the protein. Hence, one of the most active *N*-alkylisatins (**54**) was derivatised to produce the acid labile imine (**72**) for further conjugation experiments as outlined in Scheme 6.4.

The activation of 5,7-dibromo-3-[*m*-(2'-carboxymethyl)phenylimino)-*N*-(*p*-trifluoro-methyl)isatin (**72**) was then carried out using a modification to the method described for the activation of **70**. Reaction of **72** with NHS and either 2 or 6 molar equiv. of the coupling reagent DCC, found no difference in the rate of the formation of **73** (Scheme 6.5) as determined by TLC analysis (R_f 0.43, silica, 100% DCM). Like **70**, **72** was found to form the active ester (**73**) rapidly at RT and since it could not be recrystallised,

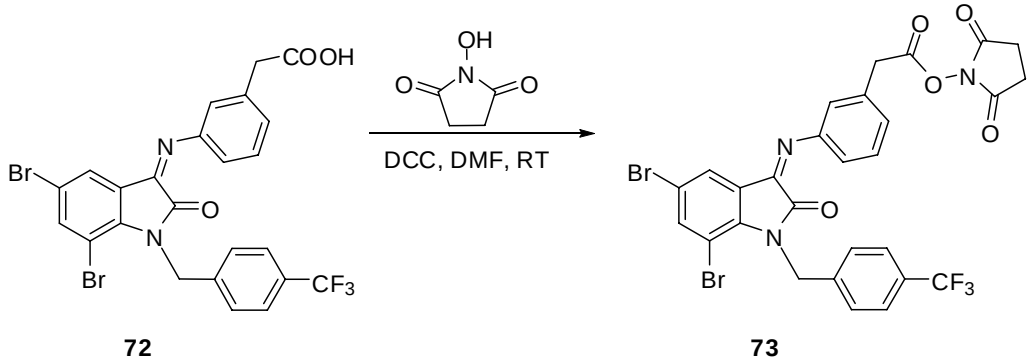

Scheme 6.5 Activation of 5,7-dibromo-3-[*m*-(2'-carboxymethyl)phenylimino)-*N*-(*p*-trifluoromethyl)isatin (**72**) to form the activated ester **73**.

was used in the further conjugation experiments without purification. A 20-fold molar excess of **73**, was then incubated with PAI-2 and the crude conjugate purified by size exclusion chromatography. In each case, the protein yield was always greater than 85%. Considering the acid-sensitive nature of the imine linker (see Figure 6.4), quantification of the number of cytotoxins incorporated (i.e. the conjugation ratio) was determined *via* UV/Vis spectrophotometry instead of ESI-MS (due to the need to acidify the samples to aid ionisation) and was found to be 4:1. After 0.22 μm filter sterilisation of the solution however, the number of molecules of **72** decreased to 1 per protein molecule (determined by UV/Vis spectrophotometry). Since the protein concentration remained the same after filtration, it is hypothesised that **72** interacts with the polyvinylidene fluoride (PVDF) membrane due to its high lipophilicity and is possibly cleaved through the sterilisation procedure. Future studies may investigate the use of different membranes such as nitrocellulose, PTFE-hydrophobic, cellulose acetate or nylon in an effort to further preserve the conjugate. Finally, like PAI-2-5FUdrsucc, PAI-2-CF_3imine

was also able to form stable complexes with uPA as determined by SDS-PAGE (Figure 6.3).

Analysis of linker hydrolysis by UV/Vis spectroscopy found compound **72** (when conjugated to transferrin as an example ligand) to be stable in the pH range of 5.5 - 7.5 after 20 h at RT (Figure 6.4). Analysis of spectra in the 260-750 nm range, found identical peaks at 303 nm (representing the linker) and 440 nm (representing the cytotoxin) for conjugates acidified with 1M HCl in PBS (pH 5.5 - 7.5). Imine cleavage was detected at pH 3.0 and showed a characteristic reduction in OD at 303 and

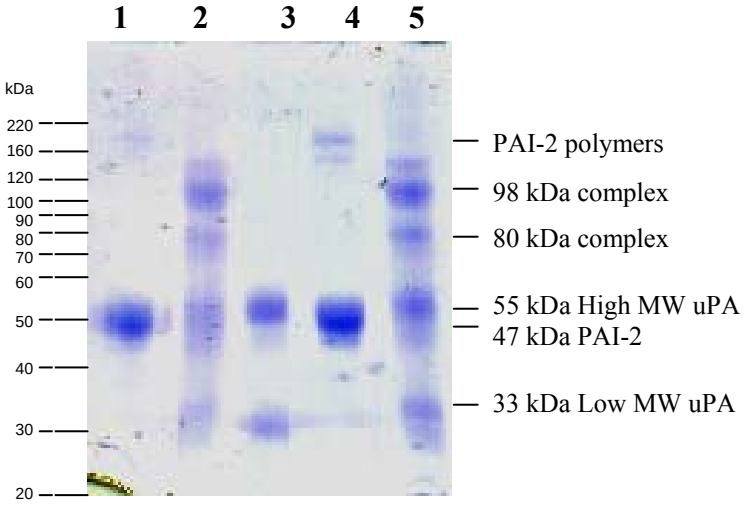

Figure 6.3 Samples fractioned by SDS PAGE showing the ability of modified and unmodified PAI-2 to form stable complexes with uPA. Briefly, PAI-2 or the PAI-2-CF_3imine conjugate were incubated with equimolar amounts of uPA at 37 °C for 30 min. Samples were then fractionated under non-reducing conditions using 12% acrylamide SDS PAGE and visualised by staining with Coomassie blue. Lane 1: PAI-2, Lane 2: PAI-2: uPA, Lane 3: uPA, Lane 4: PAI-2-CF_3imine and Lane 5: PAI-2-CF_3imine: uPA.

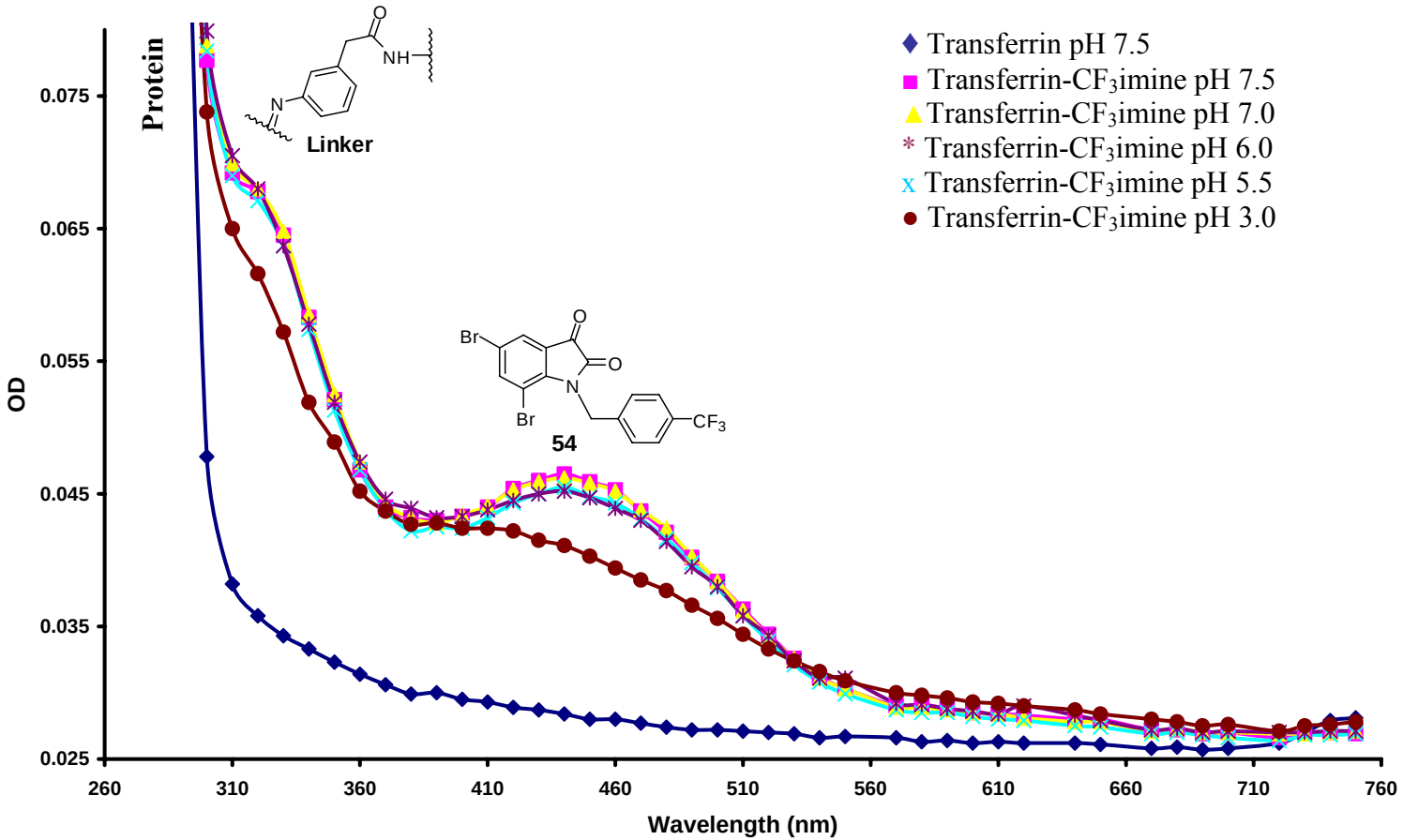

Figure 6.4 UV absorption spectrum of transferrin and transferrin-CF_3imine conjugates under different pH conditions. Comparison of unmodified transferrin with modified transferrin shows three distinct maxima corresponding to the protein (280 nm), the liker (303 nm) and the cytotoxin (440 nm) chromophores. Briefly, protein or protein conjugates were exposed to different volumes of 1 M HCl and incubated at RT for 20 h before analysis *via* scanning UV/Vis spectrophotometry between the wavelengths of 260 and 750 nm.

440 nm corresponding to linker hydrolysis and liberation of free **54**. This reduction in OD is representative of the loss of **54** as **54** is highly insoluble in an aqueous environment and precipitates out of solution when it is not associated with the protein (hence a reduction in OD at 440 nm). This suggests that the acid lability of the imine bond at C3 is altered after conjugation, as the unconjugated compound (**72**) was found to readily cleave at pH 5.5, exhibiting a $t_{½}$ of 2 h, but was stable for greater than 8 h at pH 7.4 (Appendix 4, Figure A4.2). Finally, both PAI-2 conjugates, PAI-2-5-FUdrsucc and PAI-2-CF_3imine were found to be stable in sterile PBS >12 months after preparation and activity was maintained as determined by the ability of modified PAI-2 to form stable SDS PAGE complexes with uPA (data not shown).

6.3.2 Biological Evaluation

6.3.2.1 PAI-2-5-FUdrsucc

To assess the targeting ability of PAI-2 *in vitro*, the newly synthesised PAI-2-5-FUdrsucc conjugate and corresponding free cytotoxins were evaluated for inhibitory activity in two breast adenocarcinoma cell lines (Table 6.1) varying in expression levels of uPA. The cytotoxicity of 5-FUdrsucc (IC_{50} 2.8 μM) against the metastatic MDA-MB-231 cell line (expressing high levels of uPA and uPAR), was 10-fold lower than that of 5-FUdr (IC_{50} 0.27 μM, Table 6.1), suggesting that succinylation of the 3′-group of 5-FUdr results in the loss of some activity. Similarly, Goerlach *et al*., (1991) reported a 10-fold decrease in activity for 5-FUdrsucc against the murine thymoma cell line E3, *in vitro* and hypothesise that it may be due to the inefficient uptake of the modified

Table 6.1 The effect of PAI-2-5-FUdrsucc and unconjuagted cytotoxins 5-FUdr and 5-FUdrsucc on two mammary adenocarcinoma cell lines varying in their expression levels of uPA.

		IC_{50} (μM)[a]			
Cell line	**uPA[b]**	**5-FUdr**	**5-FUdrsucc**	**PAI-2**	**PAI-2-5-FUdrsucc**
MCF-7	low	>203	>144	NA[c]	>3.2
MDA-MB-231	high	0.27	2.8	NA	1.0

[a] IC_{50} values were calculated based on moles of cytotoxin from sigmoidal dose response curves (variable slope), generated using GraphPad Prism V. 4.02 (GraphPad Software Inc.). Values are the mean of triplicate experiments.
[b] Relative expression levels of uPA (Andronicos and Ranson 2001; Ranson *et al.*, 2002).
[c] NA: Not active, even at the highest concentration tested (i.e. 1.1 μM).

compound into the cell by the nucleoside transport system. Despite this, the MDA-MB-231 cell line was still >50 times more sensitive to 5-FUdrsucc than the non-metastatic MCF-7 cell line (expressing low levels of uPA and uPAR). The IC_{50} of PAI-2-5-FUdrsucc, with an average of 3 molecules of 5-FUdrsucc incorporated per protein molecule was calculated to be 1 μM against the MDA-MB-231 cell line, which was 2.8 times lower than the free 5-FUdrsucc, suggesting that PAI-2 aids in the cellular uptake of the modified cytotoxin through RME. Of importance however, was that there was >3 times more activity observed towards the uPA positive cell line MDA-MB-231 (IC_{50} 1.0 μM), than the MCF-7 cell line (IC_{50} >3.2 μM, Table 6.1 and Figure 6.5A) after treatment with the cytotoxin conjugate. Furthermore, saturation of cell surface receptor (uPAR) on MCF-7 cells by pre-incubation with exogenous uPA (Stillfreid *et al*., 2007), followed by treatment with 3.8 μM PAI-2-5-FUdrsucc for 48 h showed a significant decrease in cell viability (P = 0.0002) compared to MCF-7 cells with endogenous

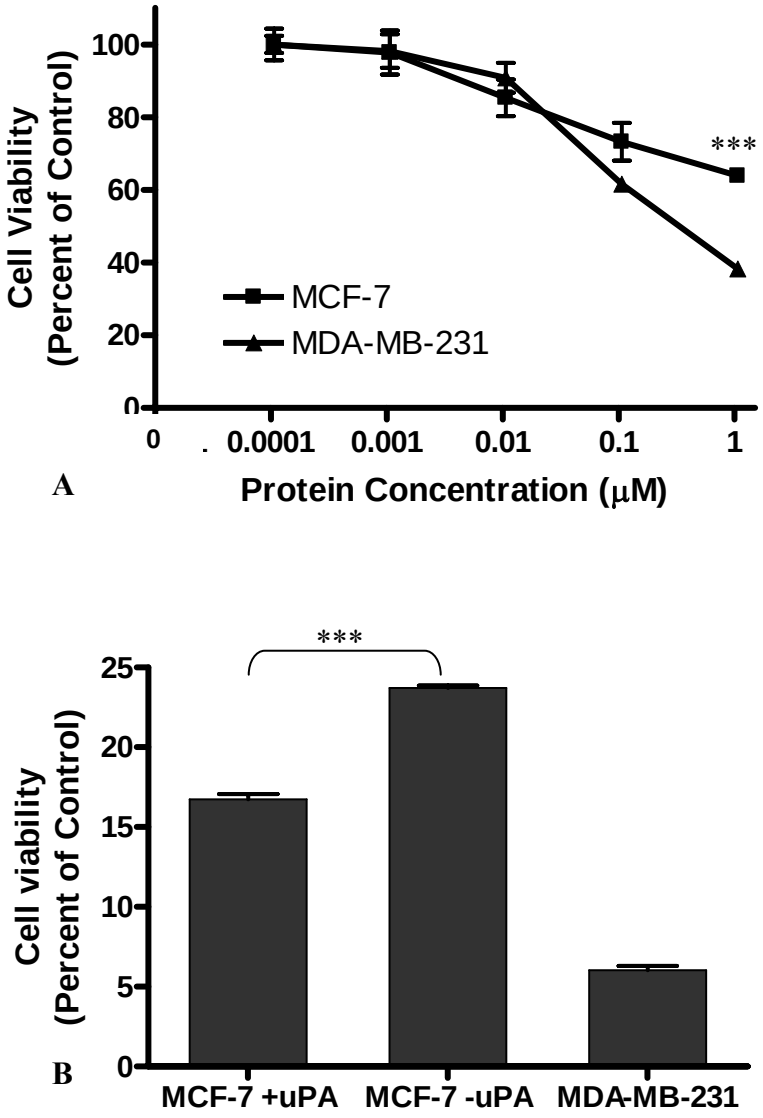

Figure 6.5 The *in vitro* cytotoxicity of PAI-2-5-FUdrsucc against the high and low uPA and uPAR expressing breast adenocarcinoma cell lines, MDA-MB-231 and MCF-7. A) Cells (1.0×10^4) were cultured for 48 h in the presence of increasing concentrations of the protein cytotoxin conjugate PAI-2-5-FUdrsucc and percent viability of the cells determined in reference to PBS vehicle controls. B) PAI-2-5-FUdrsucc at a single concentration of 3.8 μM was incubated with MDA-MB-231 cells or MCF-7 cells pretreated with (+) or without (-) exogenous uPA for 48 h. Percent viability was determined in reference to PBS controls. Data points are the means of triplicate experiments ±SE. *** P <0.001 extremely significant.

receptor bound uPA only (Figure 6.5B). MDA-MB-231 cells with high endogenous uPAR bound uPA were even more sensitive, showing a reduction in cell viability of between 3 and 4 times that of MCF-7 cells treated with (+) or without (–) uPA (Figure 6.5B). Considering cell surface uPA is essential for PAI-2: uPA/uPAR endocytosis (Al-Ejeh *et al*., 2004), this indicates that cytotoxicity is most likely mediated *via* a uPA-dependent mechanism. This has previously been reported for PAI-2 conjugated to the α–emitting radioisotope ^{213}Bi (Ranson *et al*., 2002), whereby PAI-2-^{213}Bi was found to be selectively toxic to uPA expressing breast cancer cells *in vitro*, but not to freshly isolated, normal human leukocytes on which cell-surface localised active uPA was not detectable (Ranson *et al*., 2002). Although the exact mechanism of action of the PAI-2-5-FUdrsucc is not known, it is anticipated that the conjugate is digested in the lysosomes after internalisation *via* RME. Non-specific esterases present in the lysosomes are predicted to hydrolyse the ester bond between 5-FUdr and the succinyl group to liberate free 5-FUdr, which is likely to be metabolised to produce the active components required for inhibition of thymidylate synthase and hence DNA synthesis. Future studies may involve the use of ^{3}H-labeled 5-FUdrsucc which will enable extensive stability and cellular processing studies of the PAI-2-5-FUdrsucc conjugate to be carried out.

Preliminary dose tolerance studies conducted on female Balb/c mice with PAI-2-5-FUdrsucc found no toxicity (as defined by acute weight loss and/or behavioural changes) after a single bolus i.p. administration of the highest possible concentration of

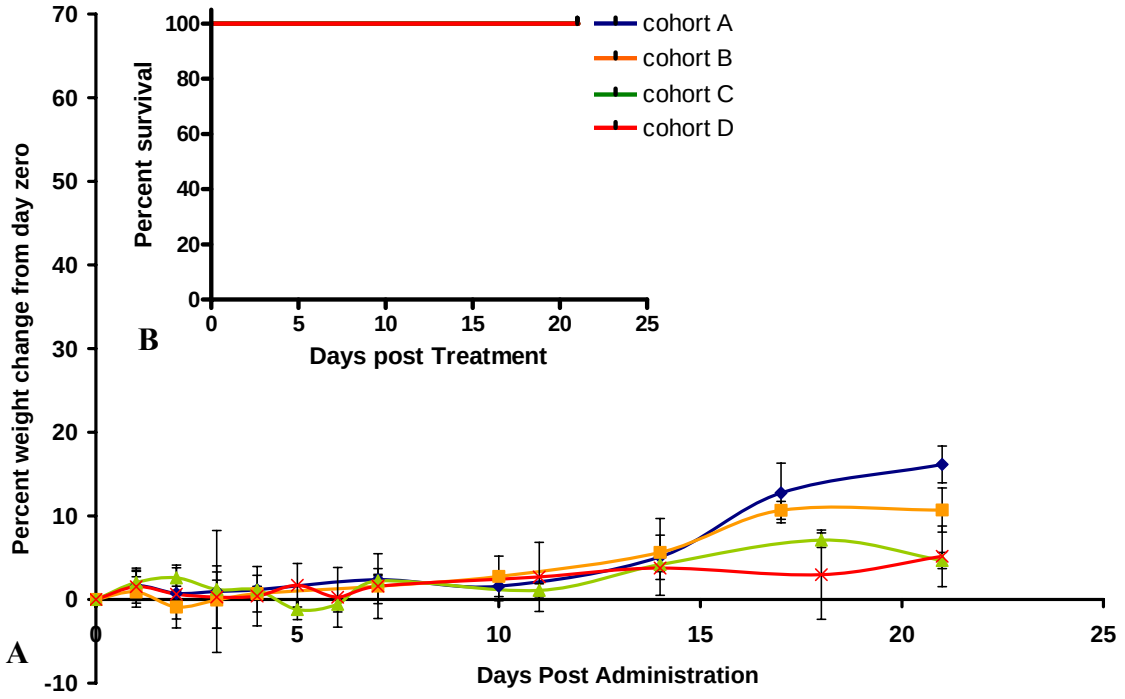

Figure 6.6 Average weight change from day zero and percent survival of mice treated with different concentrations of 5-FUdrsucc (**70**) and PAI-2-5-FUdrsucc. Female Balb/c mice were administered by i.p. injection, a single bolus dose of compound **70** at either ■ 5 mg/kg (Cohort B) or ▲ 15 mg/kg (Cohort C) or PAI-2-5-FUdrsucc conjugate at **x** 32 mg/kg (Cohort D) and A) weights recorded and compared to weight change from day zero or B) percent survival determined using the Kaplan-Meier log rank test (GraphPad Prism V 4.02). Treatments were compared to ♦ vehicle control treated mice (Cohort A). Data points are the means of $n = 3 \pm$ SD.

protein (i.e. 32 mg/kg PAI-2-5-FUdrsucc) after 21 days (Figure 6.6). However, this was only equivalent to 0.71 mg/kg of 5-FUdrsucc (**70**), which suggests toxicity may never be reached as no signs of toxicity were observed even after a single i.p. administration of up to 15 mg/kg 5-FUdrsucc (Figure 6.6). Despite this, PAI-2-5-FUdrsucc may still prove efficacious in mouse models bearing uPA positive human tumour xenografts as has been observed for the targeted radiotherapeutic PAI-^{213}Bi (Stutchbury *et al.*, 2007).

6.3.2.2 PAI-2-CF_3imine

Considering the potent activity displayed by 5,7-dibromo-*N*-(*p*-trifluoromethylbenz-yl)isatin (**54**) against MDA-MB-231 cells *in vitro* (Chapter 4, Table 4.3), the cytotoxic activity of the derivatised compound **72**, after conjugation to PAI-2 was compared to that of the free cytotoxins **54** and **72**, in an effort to further demonstrate the targeting ability of PAI-2. Firstly, the *in vitro* cytotoxicity of compound **72** (IC_{50} 4.70 μM) against the MDA-MB-231 cells was 9-fold lower than that of compound **54** (IC_{50} 0.54 μM), suggesting that the lower cellular toxicity of **72** over **54** is likely due to poorer uptake of the carboxylate. This is interesting as a decrease in the biological activity of other C3 substituted isatins (i.e. **20**, **21**, **22**, **24**, **25** and **26**), was also observed against a range of cell lines, including MDA-MB-231 and MCF-7 cells (Chapter 3, Table 3.1, Section 3.3.2, Vine *et al*., 2007). This is despite reports that many C3 substituted isatins are active against PTK's at sub-micromolar concentrations in cell- based assays (Sun *et al*., 1998; Fong *et al*., 1999).

Table 6.2 The effect of PAI-2-CF_3imine and unconjugated cytotoxins **54** and **72** on two mammary adenocarcinoma cell lines varying in their expression levels of uPA.

		IC_{50} (μM)[a]			
Cell line	**uPA** [b]	**54**	**72**	**PAI-2**	**PAI-2-CF_3imine**
MCF-7	low	7.13	9.56	NA[c]	NA
MDA-MB-231	high	0.54	4.70	NA	NA

[a] IC_{50} values were calculated based on moles of cytotoxin from sigmoidal dose response curves (variable slope), generated using GraphPad Prism V. 4.02 (GraphPad Software Inc.). Values are the mean of triplicate experiments.
[b] Relative expression levels of uPA (Andronicos and Ranson 2001; Ranson *et al.*, 2002).
[c] NA: Not active, even at the highest concentration tested (i.e. 1.1 μM protein).

Like 5-FUdrsucc, compound **72** also showed enhanced activity against the metastatic MDA-MB-231 cell line over the non-metastatic MCF-7 cell line (Table 6.2), which may be attributed to the difference in the rates of cellular proliferation (Appendix 4, Figure A4.3) and therefore compound uptake. Conversely, both MDA-MB- 231 and MCF-7 cell lines treated with PAI-2-CF_3imine showed no signs of toxicity even at the highest concentration tested (i.e. 1.1 μM of protein, Figure 6.7). This was unexpected considering the activity displayed by PAI-2-5-FUdrsucc and may be attributed to a combination of two factors. Firstly, recalculation of the cytotoxin: protein ratio (after sterile filtration) found a reduction in the number of **72** molecules bound to protein, decreasing from 4 molecules to 1 as evidenced by UV/Vis spectrophotometry. This indicated that the concentration of **72** and hence **54** delivered to cells was ultimately

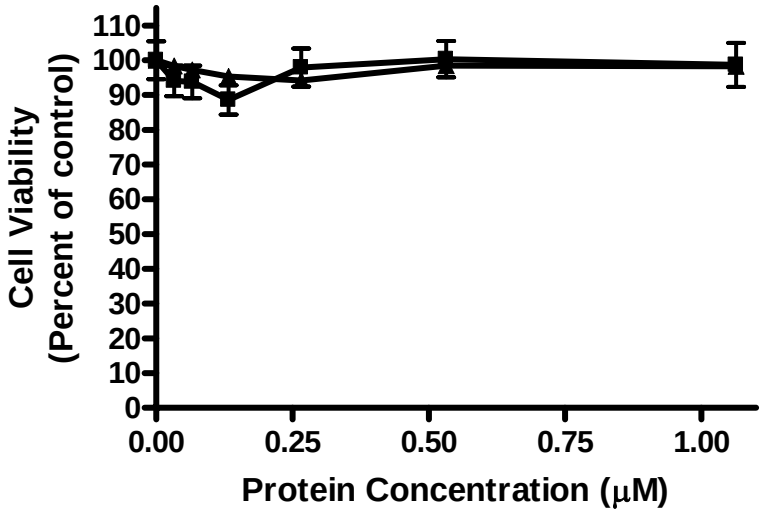

Figure 6.7 The *in vitro* cytotoxicity of PAI-2-CF_3imine against the uPA and non-uPA expressing breast adenocarcinoma cell lines, ▲ MDA-MB-231 and ■ MCF-7. Briefly, cells (1.0×10^4) were cultured for 24 h in the presence of increasing concentrations of protein conjugate (PAI-2-CF_3imine) and percent viability of the cells determined in reference to PBS controls. Data points are the means of triplicate experiments ±SE.

much less than anticipated. Secondly, hydrolysis of the imine linker was only found to occur at a pH lower that that found in the lysosomes (i.e. pH 3, Figure 6.4), suggesting that cleavage may not be occurring after internalisation *via* RME. Furthermore, if cleavage did occur due to lysosomal enzymes such as proteases, this would only liberate compound **72** and not **54**, of which the IC_{50} is greater than the highest concentration tested in this assay (i.e. 1.1 μM of **72** would be liberated from the highest concentration of PAI-2, whereas the IC_{50} of **72** is 4.70 and 9.56 μM against MDA-MB-231 and MCF-7 cells respectively). Recent work by Rodrigues *et al*., (2006) has demonstrated that the chemical bond between the ligand and cytotoxin for pH controlled activation is critical for drug release, whereby, a consistent correlation between the antiproliferative activity of PEG-daunorubicin conjugates was observed with increasing pH lability. Furthermore, transferrin conjugates in which chlorambucil was bound through non-acid sensitive linkers were not active, while the two acid sensitive hydrazone bonds were as active, or more active than chlorambucil alone (Beyer *et al*., 1998). Future studies may therefore look at derivatising the most active *N*-alkylisatins and developing a range of acid labile linkers that cleave in the range of pH-5-6, such as that found in late lysosomes (Ohkuma and Poole, 1978).

6.4 Conclusions

In summary two cytotoxins, namely 5-FUdrsucc (**70**) and 5,7-dibromo-3-[*m*-(2'-carboxymethyl)phenylimino)-*N*-(*p*-trifluoromethyl)isatin (**72**) were successfully derivatised and conjugated to PAI-2 after synthesis of the activated esters **71** and **73**. An average of 4 molecules of **70** and **72** were incorporated into PAI-2 *via* amide bond formation with

free lysine residues without altering the inhibitory capacity of the protein. This was determined by the ability of modified PAI-2 to form stable SDS PAGE complexes with active uPA. The *in vitro* cytotoxicity of PAI-2-5-FUdrsucc on breast cancer cells was shown to be specific, indicating that the cell killing ability of the conjugate almost certainly depends on the targeting of cells in a receptor-bound, active uPA-dependent manner. Furthermore, preliminary dose tolerance studies in mice show that PAI-2-5-FUdrsucc is not toxic even at the highest concentration of protein administered (i.e. 32 mg/kg). Conversely, the PAI-2-CF_3imine conjugate did not inhibit the metabolic activity of either MDA-MB-231 or MCF-7 cells, even at 1.1 μM, which was most likely due to the stability of the imine linker at pH 5.0. Despite this, this is the first study to demonstrate the ability of cytotoxins to be chemically conjugated to PAI-2. Considering the advantages of using PAI-2 as a targeting molecule over other ligands such as PAI-1 or mAbs, this study implies that PAI-2-cytotoxin based therapies have potential as new therapeutic agents for targeted therapy of breast, prostate and colorectal cancers in the future.

CHAPTER 7

Conclusions and Future Directions

In this study, the cytotoxic properties, SARs and modes of action of a range of isatin-based compounds were investigated in an effort to identify lead compounds for the development of a new class of cancer therapeutics. Natural products have made enormous contributions to many of the anticancer agents used clinically today, and in this study, the cytotoxic molluscan metabolite tyrindoleninone (**1**), present in the egg masses of the muricid *Dicathais orbita*, was initially used as a template for drug design. This was primarily because the cytotoxic activity of synthetically pure **1** and derivatives thereof had not previously been reported. However, despite various synthetic approaches, analogues of **1** could not be obtained for biological testing due to the reactive nature of the indoleninone ring. As a result, a range of stable isatin derivatives, based on 6-bromoisatin (**5**), a mildly cytotoxic oxidative artifact also present within *D.*

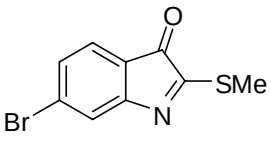

1

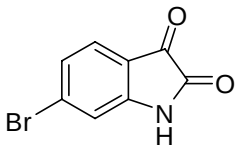

5

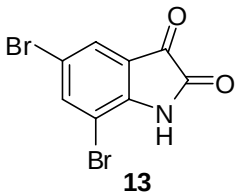

13

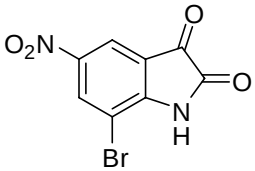

18

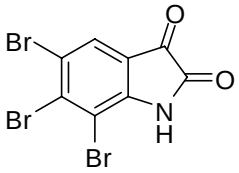

19

orbita egg masses, were synthesised (or obtained). This resulted in the generation of 23 isatin analogues, including two new compounds (**18** and **19**). Cytotoxicity screening of compounds **4**-**26** revealed the tri-bromoisatin **19**, to be the most active compound across all cancer cell lines, with activity against Jurkat cells (IC_{50} 5.8 μM) comparable to that of the extracted natural product (**1**). In addition, treatment of the lymphoma cell line with compound **19** resulted in the activation of the effector caspases 3 and 7 after 5 h, indicative of apoptotic cell death. Moreover, various isatins were also found to be selective for cancer cells over normal human PBLs. These results thus emphasise the ability of natural products to continue to provide molecular scaffolds, on which novel compounds of therapeutic interest can be built.

Considering the potent activity and selectivity displayed by the first generation of indolinone-based compounds, structural modification of di- and tri-substituted isatins at N1 *via* alkyl and arylalkylation was subsequently carried out in an effort to further enhance compound activity. This afforded a further 28 derivatives, 19 of which were new. Of particular interest were the novel compounds **39**, **45**, **49**, **51**, **52**, **53**, **54**, **58** and **60** (Chapter 4, Table 4.1), which exhibited potent cell-based cytotoxicity in the high nanomolar range against several different cancer cell types. A structure activity-based selection process was used to identify several crucial structural requirements needed to enhance activity, which are summarised in Figure 7.1. Of the 28 compounds screened, 5,7-dibromo-*N*-(*p*-methylbenzyl)isatin, (**39**) was the most active, exhibiting an IC_{50} value of 490 nM against two hematopoietic cell lines which was greater than 22 times

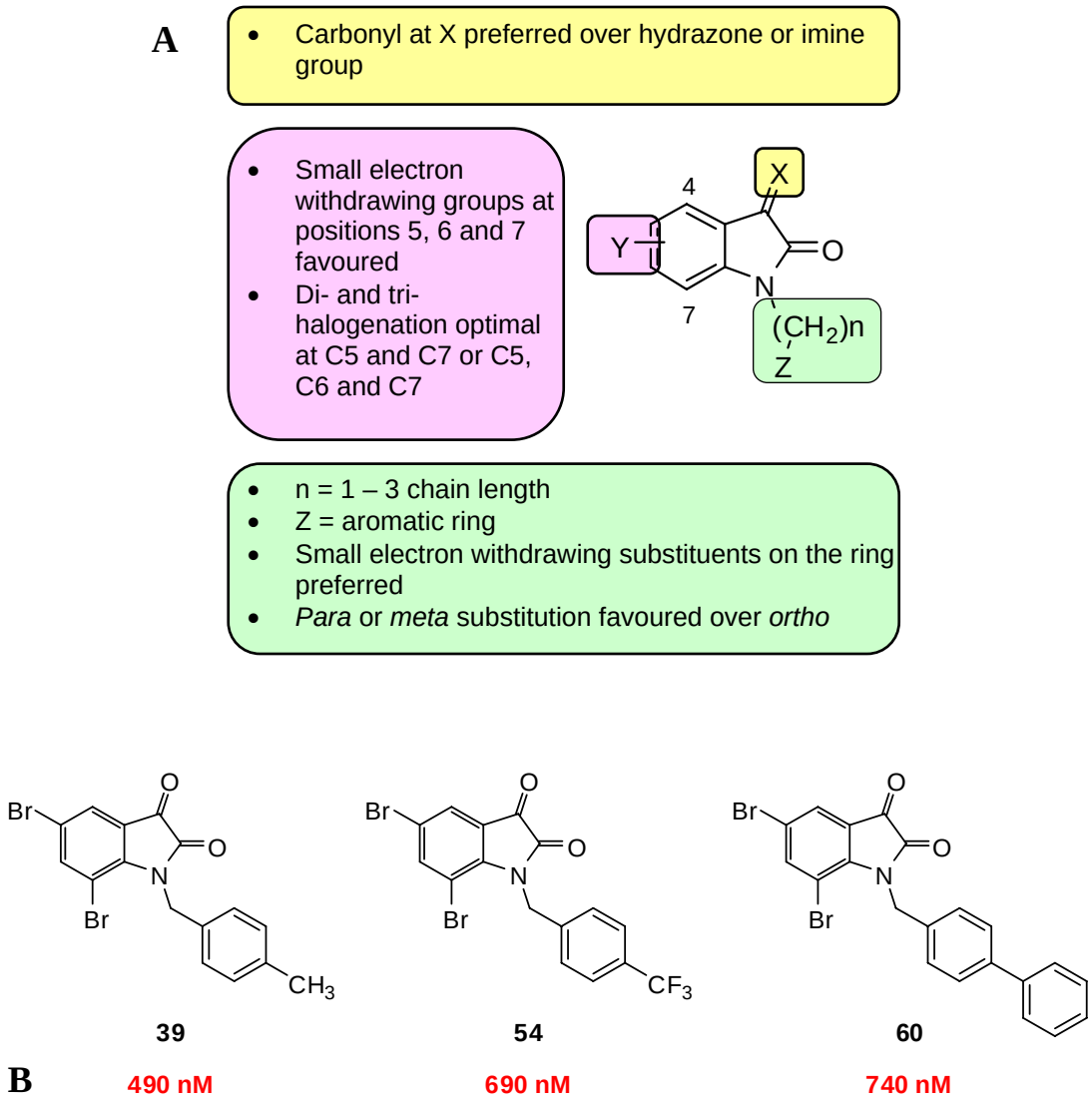

Figure 7.1 A) A cytotoxicity structure-activity summary for the *N*-alkylisatin derivatives. B) Examples of three potent, selective inhibitors of cellular proliferation against the human leukemic T-cell line (Jurkat). IC_{50} values are shown in red.

more active than the unsubstituted 5,7-dibromoisatin (**13**). This thus illustrates the importance of N1 substitution for cytotoxic activity. Also of interest was the *N*-alkylisatin **54**, which exerted potent anticancer activity on a broad range of cancer cell lines and was the most active compound (IC_{50} = 540 nM) against the MDA-MB-231

metastatic breast adenocarcinoma cell line. Investigation into the molecular mode of action of a range of *N*-alkylisatins found the *p*-trifluoromethybenzyl derivative (**54**), together with the representative compounds **35**, **39**, **45**, **59** and **60**, to destabilise microtubules *via* inhibition of tubulin polymerisation. This resulted in cell cycle arrest at G2/M and apoptotic cell death after activation of the effector caspases 3 and 7. Considering the potential of developing novel anti-tubulin binding agents for the treatment of tumours with resistance to current tubulin-targeting drugs, the efficacy of a representative *N*-alkylisatin was further investigated in an animal model.

Preliminary *in vivo* investigations into the pharmacological profile of compound **54**, found this substituted *N*-benzylisatin to be moderately efficacious in a human tumour xenograft mouse model bearing the mammary MDA-MB-231 adenocarcinoma. When administered at a total dose of 25 mg/kg, **54** showed a 43% reduction in tumour size compared to vehicle control treated mice by day 23, with no evidence of systemic toxicity. Histopathological analysis of the bone marrow *in situ* after acute dosing found only mild hematopoietic suppression, suggesting that the development of new antimitotic agents based on **54** may hold some benefit over treatment with conventional agents such as vinblastine. Furthermore, analysis of biodistribution *via* SPECT imaging found moderate tumour uptake of both ^{123}I radioiodinated compounds (**67** and **68**) in a rat mammary carcinoma model 48 h p.i., although large amounts of activity were also detected in the gut and liver. Future work involving modifications to the substituents on the N1-benzyl aromatic ring may lead to new compounds with enhanced tumour uptake and improved pharmacological profiles. Despite modification, it is projected that

normal cells that are largely dependent upon microtubule dynamics, such as those displaying increased rates of proliferation, may still be affected. To counter this, the *N*-benzylisatin **54** was derivatised in such a way that it could be chemically linked to a targeting moiety that would specifically deliver it to cancer cells. This strategy was aimed at reducing non-target organ uptake and should ultimately result in fewer side effects.

Conjugation of the derivatised *N*-benzylisatin **72** (containing a novel acid labile imine linker and a carboxylic acid for amide bond formation) to the protein PAI-2 and analysis by UV/Vis spectrophotometry found up to 4 molecules of **72** successfully incorporated. Of importance was that addition of the organic cytotoxin to the protein *via* lysine-based amide bond formation did not alter its inhibitory capacity. This was determined by the ability of the PAI-2-CF_3imine conjugate to form stable complexes with uPA. In this study, it was anticipated that once the PAI-2-CF_3imine had bound to

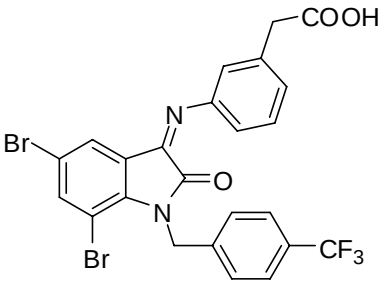

72

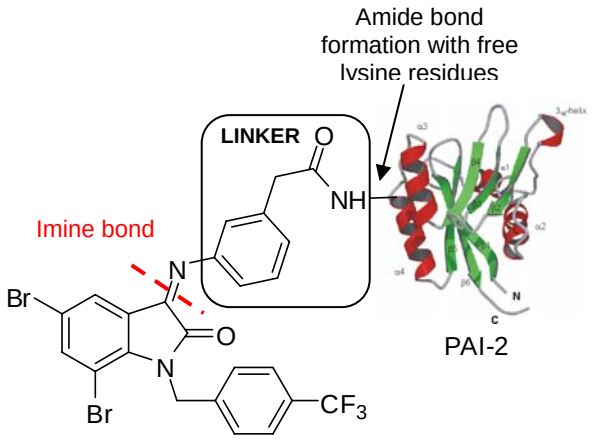

PAI-2-CF_3imine

uPA and uPAR on the cell surface of receptor positive breast cancer cells, the conjugate would be internalised and the imine bond cleaved, upon exposure to the acidic environment of the lysosomes and liberate free **54**. Investigation into the cytotoxicity of the PAI-2-CF_3imine conjugate in two breast cancer cell lines, which vary in their expression levels of uPA and uPAR, found no activity even at the highest concentration tested. This was unexpected considering the activity displayed by **54** against both cell lines *in vitro* was in the low micromolar range (See Chapter 4, Table 4.3). Such a lack of activity is most likely due to the stability of the imine linker at pH 5.0., whereby cleavage was observed to occur at a much lower pH than that reported in the lysosomal compartments of cells. Future studies may therefore endeavor to investigate the acid lability of a range of different linker systems, for example those based on hydrazones, with the aim of increasing target-specific cytotoxicity profiles. Alternatively, derivatising compound **54** so as to contain an ester or peptide linkage allowing cleavage by lysosomal esterases/ peptidases after internalisation *via* RME by cancer cells would also be of interest, considering the impressive targeting ability displayed the PAI-2-5-FUdrsucc conjugate in a proof of concept study (see Chapter 6, Section 6.3.2.1). Moreover, other targeting ligands that are internalised *via* RME may also be used. For example, HER-2 is over-expressed in 20-25% of invasive breast cancers (Slamon *et al.,* 1989; Gusterson *et al.,* 1992; Witters *et al.,* 2002) and is associated with an aggressive tumour phenotype and overall reduced survival rates (Slamon *et al.*, 1989). It may therefore be of interest to conduct future studies utilising an anti-HER-2 mAb as the targeting ligand.

Finally, PAI-2-cytotoxin based therapies hold potential as new therapeutic agents for targeted therapy of uPA positive malignancies, with limited side effects and therefore should be further investigated.

REFERENCES

Abadi, A. H., Abou-Seri, S. M., Abdel-Rahman, D. E., Klein, C., Lozach, O. and Meijer, L. (2006) Synthesis of 3-substituted-2-oxoindole analogues and their evaluation as kinase inhibitors, anticancer and antiangiogenic agents. *Eur. J. Med. Chem.* **41**, *3*, 296-305.

Abeloff, M. D. and Armitage, J. O. 2004 Clinical Oncology. Churchill Livingstone. 3205

Adachi, J., Mori, Y., Matsui, S., Takigami, H., Fujino, J., Kitagawa, H., Miller, C. A., 3rd, Kato, T., Saeki, K. and Matsuda, T. (2001) Indirubin and indigo are potent aryl hydrocarbon receptor ligands present in human urine. *J. Biol. Chem.* **276**, *34*, 31475-8.

Alam, M. and Thomson, R. H. (1998) Handbook of Natural Products from Marine Invertebrates, Part 1: Phylum Mollusca. Amsterdam, Hardwood Academic Publishers.

Alberts, B., Bray, D., Lewis, J., Raff, M., Roberts, K. and Watson, J. D. (2002) *Molecular Biology of the cell*. M. Robertson. USA, Garland Publishing, Taylor & Francis Group 1-1294.

Al-Ejeh, F., Croucher, D. and Ranson, M. (2004) Kinetic analysis of plasminogen activator inhibitor type-2: urokinase complex formation and subsequent internalisation by carcinoma cell lines. *Exp. Cell Res.* **297**, *1*, 259-71.

Allen, B. J., Tian, Z., Rizvi, S. M., Li, Y. and Ranson, M. (2003) Preclinical studies of targeted alpha therapy for breast cancer using 213Bi-labelled-plasminogen activator inhibitor type 2. *Br. J. Cancer* **88**, *6*, 944-50.

Allen, T. M. (2002) Ligand-targeted therapeutics in anticancer therapy. *Nat. Rev. Cancer* **2**, *10*, 750-63.

Andreani, A., Granaiola, M., Leoni, A., Locatelli, A., Morigi, R., Rambaldi, M., Garaliene, V., Welsh, W., Arora, S., Farruggia, G. and Masotti, L. (2005) Antitumor activity of new substituted 3-(5-imidazo[2,1-b]thiazolylmethylene)-2-indolinones and study of their effect on the cell cycle. *J. Med. Chem.* **48**, *17*, 5604-7.

Andreasen, P. A., Egelund, R. and Petersen, H. H. (2000) The plasminogen activation system in tumor growth, invasion, and metastasis. *Cell Mol. Life Sci.* **57**, *1*, 25-40.

Andreasen, P. A., Kjoller, L., Christensen, L. and Duffy, M. J. (1997) The urokinase-type plasminogen activator system in cancer metastasis: a review. *Int. J. Cancer* **72**, *1*, 1-22.

Argiris, A., Hensing, T., Yeldandi, A., Patel, S., Raji, A., Sturgis, C., Masters, G., Gooding, W., Pins, M. and Kolesar, J. (2006) Combined analysis of molecular and clinical predictors of gefitinib activity in advanced non-small cell lung cancer: epidermal growth factor receptor mutations do not tell the whole story. *J Thorac Oncol* **1**, *1*, 52-60.

Argraves, K. M., Battey, F. D., MacCalman, C. D., McCrae, K. R., Gafvels, M., Kozarsky, K. F., Chappell, D. A., Strauss, J. F., 3rd and Strickland, D. K. (1995) The very low density lipoprotein receptor mediates the cellular catabolism of lipoprotein lipase and urokinase-plasminogen activator inhibitor type I complexes. *J. Biol. Chem.* **270**, *44*, 26550-7.

Arora, A. and Scholar, E. M. (2005) Role of tyrosine kinase inhibitors in cancer therapy. *J. Pharmacol. Exp. Ther.* **315**, *3*, 971-9.

Ashkenazi, A. and Dixit, V. M. (1999) Apoptosis control by death and decoy receptors. *Curr. Opin. Cell Biol.* **11**, *2*, 255-60.

Askew, D. S., Ashmun, R. A., Simmons, B. C. and Cleveland, J. L. (1991) Constitutive c-myc expression in an IL-3-dependent myeloid cell line suppresses cell cycle arrest and accelerates apoptosis. *Oncogene* **6**, *10*, 1915-22.

Astedt, B., Lindoff, C. and Lecander, I. (1998) Significance of the plasminogen activator inhibitor of placental type (PAI-2) in pregnancy. *Semin. Thromb. Hemost.* **24**, *5*, 431-5.

Aszalos, A. A. (1981) Antitumor compounds of natural origin : chemistry and biochemistry. Boca Raton, Fla, CRC Press.

Authier, F., Metioui, M., Fabrega, S., Kouach, M. and Briand, G. (2002) Endosomal proteolysis of internalized insulin at the C-terminal region of the B chain by cathepsin D. *J. Biol. Chem.* **277**, *11*, 9437-46.

Bach, G., Chen, C. S. and Pagano, R. E. (1999) Elevated lysosomal pH in Mucolipidosis type IV cells. *Clin. Chim. Acta.* **280**, *1-2*, 173-9.

Bacher, G., Nickel, B., Emig, P., Vanhoefer, U., Seeber, S., Shandra, A., Klenner, T. and Beckers, T. (2001) D-24851, a novel synthetic microtubule inhibitor, exerts curative antitumoral activity in vivo, shows efficacy toward multidrug-resistant tumor cells, and lacks neurotoxicity. *Cancer Res.* **61**, *1*, 392-9.

Baguley, B. C. and Finlay, G. J. (1995) Pharmacokinetic/cytokinetic principles in the chemotherapy of solid tumours. *Clin. Exp. Pharmacol. Physiol.* **22**, *11*, 825-8.

Baker, T. J. and Duke, C. C. (1972) Chemistry of the indoleninones I. *Aust. J. Chem.* **25**, 2467-2473.

Baker, T. J. and Duke, C. C. (1973) Chemistry of the indoleninones II. *Aust. J. Chem.* **26**, 2153-2157.

Banker, D. E., Pastan, I., Gottesman, M. M. and Herschman, H. R. (1989) An epidermal growth factor-ricin A chain (EGF-RTA)-resistant mutant and an epidermal growth factor-Pseudomonas endotoxin (EGF-PE)-resistant mutant have distinct phenotypes. *J. Cell Physiol.* **139**, *1*, 51-7.

Bartek, J., Falck, J. and Lukas, J. (2001) CHK2 kinase--a busy messenger. *Nat. Rev. Mol. Cell Biol.* **2**, *12*, 877-86.

Baselga, J. (2006) Targeting tyrosine kinases in cancer: the second wave. *Science* **312**, *5777*, 1175-8.

Bass, R. J. (1971) Iodination of Isatins. *Tetrahedron Lett.* **16**, 1087.

Beckers, T. and Mahboobi, S. (2003) Natural, semisynthetic and synthetic microtubule inhibitors for cancer therapy. *Drugs Future* **28**, 767-785.

Beckers, T., Reissmann, T., Schmidt, M., Burger, A. M., Fiebig, H. H., Vanhoefer, U., Pongratz, H., Hufsky, H., Hockemeyer, J., Frieser, M. and Mahboobi, S. (2002) 2-aroylindoles, a novel class of potent, orally active small molecule tubulin inhibitors. *Cancer Res.* **62**, *11*, 3113-9.

Bellamy, W. T. (1996) P-glycoproteins and multidrug resistance. *Annu. Rev. Pharmacol. Toxicol.* **36**, 161-83.

Benkendorff, K. 1999 Bioactive molluscan resources and their conservation: Biological and chemical studies on the egg masses of marine molluscs. Departement of Biological Sciences. University of Wollongong.

Benkendorff, K., Bremner, J. B. and Davis, A. R. (2000) A putative role for the precursors of Tyrian Purple in the egg masses of the Austrailan Muricid, *Dicathais orbita*. *J. Chem. Ecol.* **26**, *1037-1050*.

Benkendorff, K., Bremner, J. B. and Davis, A. R. (2001a) Indole derivatives from the egg masses of muricid molluscs. *Molecules* **6**, 70-8.

Benkendorff, K., Davis, A. R. and Bremner, J. B. (2001b) Chemical defense in the egg masses of benthic invertebrates: an assessment of antibacterial activity in 39 mollusks and 4 polychaetes. *J. Invertebr. Pathol.* **78**, *2*, 109-18.

Berchem, G. J., Bosseler, M., Mine, N. and Avalosse, B. (1999) Nanomolar range docetaxel treatment sensitizes MCF-7 cells to chemotherapy induced apoptosis, induces G2M arrest and phosphorylates bcl-2. *Anticancer Res.* **19**, *1A*, 535-40.

Berger, D. H. (2002) Plasmin/plasminogen system in colorectal cancer. *World J. Surg.* **26**, *7*, 767-71.

Bertram, J. S. (2000) The molecular biology of cancer. *Mol. Aspects Med.* **21**, *6*, 167-223.

Beyer, U., Roth, T., Schumacher, P., Maier, G., Unold, A., Frahm, A. W., Fiebig, H. H., Unger, C. and Kratz, F. (1998) Synthesis and in vitro efficacy of transferrin conjugates of the anticancer drug chlorambucil. *J. Med. Chem.* **41**, *15*, 2701-8.

Bhattacharya, S. K. and Chakraborti, A. (1998) Dose related proconvulsant and anticonvulsant activity of isatin, a putative biological factor in rats. *Indian. J. Exp. Biol.* **36**, 118–121.

Bhattacharya, S. K., Glover, V., McIntyre, I., Oxenkrug, G. and Sandler, M. (1988) Stress causes an increase in endogenous monoamine oxidase inhibitor (tribulin) in rat brain. *Neurosci. Lett.* **92**, *2*, 218-21.

Bold, R. J., Termuhlen, P. M. and McConkey, D. J. (1997) Apoptosis, cancer and cancer therapy. *Surg. Oncol.* **6**, *3*, 133-42.

Bolton, R. (2002) Radiohalogen incorporation into organic systems. *J. Label Compd. Radiopharm.* **45**, 485–528.

Bonne, D., Heusele, C., Simon, C. and Pantaloni, D. (1985) 4',6-Diamidino-2-phenylindole, a fluorescent probe for tubulin and microtubules. *J. Biol. Chem.* **260**, *5*, 2819-25.

Bonneau, D. and Longy, M. (2000) Mutations of the human PTEN gene. *Hum. Mutat.* **16**, *2*, 109-22.

Bramson, H. N., Corona, J., Davis, S. T., Dickerson, S. H., Edelstein, M., Frye, S. V., Gampe, R. T., Jr., Harris, P. A., Hassell, A., Holmes, W. D., Hunter, R. N., Lackey, K. E., Lovejoy, B., Luzzio, M. J., Montana, V., Rocque, W. J., Rusnak, D., Shewchuk, L., Veal, J. M., Walker, D. H. and Kuyper, L. F. (2001) Oxindole-based inhibitors of cyclin-dependent kinase 2 (CDK2): design, synthesis, enzymatic activities, and X-ray crystallographic analysis. *J. Med. Chem.* **44**, *25*, 4339-58.

Brancale, A. and Silvestri, R. (2007) Indole, a core nucleus for potent inhibitors of tubulin polymerization. *Med. Res. Rev.* **27**, *2*, 209-38.

Brock, J. H. (1985) Transferrins. London, Macmillan.

Buchdunger, E., O'Reilly, T. and Wood, J. (2002) Pharmacology of imatinib (STI571). *Eur. J. Cancer* **38 Suppl 5**, S28-36.

Cai, W. and Chen, X. (2006) Anti-angiogenic cancer therapy based on integrin alphavbeta3 antagonism. *Anticancer Agents Med. Chem.* **6**, *5*, 407-28.

Calvary, H. O., Noller, C. R. and Adams, R. J. (1925) *Am. Chem. Soc* **47**, 3058.

Campos, L., Rouault, J. P., Sabido, O., Oriol, P., Roubi, N., Vasselon, C., Archimbaud, E., Magaud, J. P. and Guyotat, D. (1993) High expression of bcl-2 protein in acute myeloid leukemia cells is associated with poor response to chemotherapy. *Blood* **81**, *11*, 3091-6.

Cane, A., Tournaire, M. C., Barritault, D. and Crumeyrolle-Arias, M. (2000) The endogenous oxindoles 5-hydroxyoxindole and isatin are antiproliferative and proapoptotic. *Biochem. Biophys. Res. Commun.* **276**, *1*, 379-84.

Carlomagno, F. and Santoro, M. (2005) Receptor tyrosine kinases as targets for anticancer therapeutics. *Curr. Med. Chem.* **12**, *15*, 1773-81.

Carrasco, R. A., Stamm, N. B. and Patel, B. K. (2003) One-step cellular caspase-3/7 assay. *Biotechniques* **34**, *5*, 1064-7.

Carte, B. K. (1996) Biomedical potential of marine natural products. *Bioscience* **46**, *4*, 271-286.

Carter, P., Presta, L., Gorman, C. M., Ridgway, J. B., Henner, D., Wong, W. L., Rowland, A. M., Kotts, C., Carver, M. E. and Shepard, H. M. (1992) Humanization of an anti-p185HER2 antibody for human cancer therapy. *Proc. Natl. Acad. Sci. U S A* **89**, *10*, 4285-9.

Chabner, B. A. and Roberts, T. G., Jr. (2005) Timeline: Chemotherapy and the war on cancer. *Nat. Rev. Cancer* **5**, *1*, 65-72.

Chabner, B. A., Wittes, R., Hoth, D. and Hubbard, S. (1984) Investigational trials of anticancer drugs: establishing safeguards for experimentation. *Public Health Rep.* **99**, *4*, 355-60.

Chadwick, D. E., Jean, L. F., Jamal, N., Messner, H. A., Murphy, J. R. and Minden, M. D. (1993) Differential sensitivity of human myeloma cell lines and normal bone marrow colony forming cells to a recombinant diphtheria toxin-interleukin 6 fusion protein. *Br. J. Haematol.* **85**, *1*, 25-36.

Chandler, L. A., Sosnowski, B. A., McDonald, J. R., Price, J. E., Aukerman, S. L., Baird, A., Pierce, G. F. and Houston, L. L. (1998) Targeting tumor cells via EGF receptors: selective toxicity of an HBEGF-toxin fusion protein. *Int. J. Cancer* **78**, *1*, 106-11.

Chari, R. V. (1998) Targeted delivery of chemotherapeutics: tumor-activated prodrug therapy. *Adv. Drug Deliv. Rev.* **31**, *1-2*, 89-104.

Chen, W. Z. and Xie, Y. Y. (1984) [Studies on uranium mobilization drugs: synthesis of two new types of phosphonic acid chelating agents]. *Yao Xue Xue Bao* **19**, *11*, 865-8.

Chen, Z., Merta, P. J., Lin, N. H., Tahir, S. K., Kovar, P., Sham, H. L. and Zhang, H. (2005) A-432411, a novel indolinone compound that disrupts spindle pole formation and inhibits human cancer cell growth. *Mol. Cancer Ther.* **4**, *4*, 562-8.

Chen, Z., Xiao, Z., Chen, J., Ng, S. C., Sowin, T., Sham, H., Rosenberg, S., Fesik, S. and Zhang, H. (2003) Human Chk1 expression is dispensable for somatic cell death and critical for sustaining G2 DNA damage checkpoint. *Mol. Cancer Ther.* **2**, *6*, 543-8.

Cooksey, C. J. (2001) Tyrian purple: 6,6'-dibromoindigo and related compounds. *Molecules* **6**, 736-69.

Cornforth, J., Hitchcock, P. B. and Rozos, P. (1996) Isatin chloride: a phantom. Reactions of 2-(2,2-dichloro-2,3-dihydro-3-oxoindol-1-yl)-3H-indol-3-one. *J. Chem. Soc., Perkin Trans.* **1**, 2787-2792.

Cory, A. H., Owen, T. C., Barltrop, J. A. and Cory, J. G. (1991) Use of an aqueous soluble tetrazolium/formazan assay for cell growth assays in culture. *Cancer Commun.* **3**, *7*, 207-12.

Cragg, M. S. and Glennie, M. J. (2004) Antibody specificity controls in vivo effector mechanisms of anti-CD20 reagents. *Blood* **103**, *7*, 2738-43.

Croucher, D., Saunders, D. N. and Ranson, M. (2006) The urokinase/PAI-2 complex: a new high affinity ligand for the endocytosis receptor low density lipoprotein receptor-related protein. *J. Biol. Chem.* **281**, *15*, 10206-13.

Crumeyrolle-Arias, M., Medvedev, A., Cardona, A., Barritault, D. and Glover, V. (2003) In situ imaging of specific binding of [3H]isatin in rat brain. *J. Neurochem.* **84**, *3*, 618-20.

da Silva, J. F. M., Garden, S. J. and Pinto, A. C. (2001) The Chemistry of Isatins: a Review from 1975 to 1999. *J. Braz. Chem. Soc.* **12**, *3*, 273-324.

Damle, N. K. and Frost, P. (2003) Antibody-targeted chemotherapy with immunoconjugates of calicheamicin. *Curr. Opin. Pharmacol.* **3**, *4*, 386-90.

Datta, S. R., Brunet, A. and Greenberg, M. E. (1999) Cellular survival: a play in three Akts. *Genes Dev.* **13**, *22*, 2905-27.

de Carcer, G., de Castro, I. P. and Malumbres, M. (2007) Targeting cell cycle kinases for cancer therapy. *Curr. Med. Chem.* **14**, *9*, 969-85.

De Martino, G., Edler, M. C., La Regina, G., Coluccia, A., Barbera, M. C., Barrow, D., Nicholson, R. I., Chiosis, G., Brancale, A., Hamel, E., Artico, M. and Silvestri, R. (2006) New arylthioindoles: potent inhibitors of tubulin polymerization. 2. Structure-activity relationships and molecular modeling studies. *J. Med. Chem.* **49**, *3*, 947-54.

De Martino, G., La Regina, G., Coluccia, A., Edler, M. C., Barbera, M. C., Brancale, A., Wilcox, E., Hamel, E., Artico, M. and Silvestri, R. (2004) Arylthioindoles, potent inhibitors of tubulin polymerization. *J. Med. Chem.* **47**, *25*, 6120-3.

de Vries, D. J. and Hall, M. R. (1994) Marine biodiversity as a source of chemical diversity. *Drug Dev. Res.* **33**, *2*, 161-173.

Dear, A. E. and Medcalf, R. L. (1995) The cellular and molecular biology of plasminogen activator inhibitor type-2. *Fibrinolysis* **9**, 321–330.

Demain, A. L. and Zhang, L. (2005) *Natural products and drug discovery*. Natural Products: Drug discovery and therapeutic medicine. L. Zhang and A. L. Demain. Totowa, Humana Press Inc. 3-29.

DeVita, V. T. J. (1997) Principles of cancer management: chemotherapy. Philadelphia, Lippincott-Raven.

Di Massimo, A. M., Di Loreto, M., Pacilli, A., Raucci, G., D'Alatri, L., Mele, A., Bolognesi, A., Polito, L., Stirpe, F. and De Santis, R. (1997) Immunoconjugates made of an anti-EGF receptor monoclonal antibody and type 1 ribosome-inactivating proteins from Saponaria ocymoides or Vaccaria pyramidata. *Br. J. Cancer* **75**, *6*, 822-8.

Doble, B. W. and Woodgett, J. R. (2003) GSK-3: tricks of the trade for a multi-tasking kinase. *J. Cell Sci.* **116**, *Pt 7*, 1175-86.

Drenou, B., Lamy, T., Amiot, L., Fardel, O., Caulet-Maugendre, S., Sasportes, M., Diebold, J., Le Prise, P. Y. and Fauchet, R. (1997) CD3- CD56+ non-Hodgkin's lymphomas with an aggressive behavior related to multidrug resistance. *Blood* **89**, *8*, 2966-74.

Druker, B. J. (2002) Inhibition of the Bcr-Abl tyrosine kinase as a therapeutic strategy for CML. *Oncogene* **21**, *56*, 8541-6.

Druker, B. J. (2004) Imatinib as a paradigm of targeted therapies. *Adv. Cancer Res.* **91**, 1-30.

Drukman, S. and Kavallaris, M. (2002) Microtubule alterations and resistance to tubulin-binding agents (review). *Int. J. Oncol.* **21**, *3*, 621-8.

Duffy, M. J. (2004) The urokinase plasminogen activator system: role in malignancy. *Curr. Pharm. Des.* **10**, *1*, 39-49.

Duffy, M. J. and Duggan, C. (2004) The urokinase plasminogen activator system: a rich source of tumour markers for the individualised management of patients with cancer. *Clin. Biochem.* **37**, *7*, 541-8.

Duke, C. C. 1974 A study of the precursors to purple dyes from the Australian Gastropod Molluscs and of analogous synthetic compounds. James Cook University of North Queensland. 1-124

Duncan, R. and Spreafico, F. (1994) Polymer conjugates. Pharmacokinetic considerations for design and development. *Clin. Pharmacokinet.* **27**, *4*, 290-306.

Dyba, M., Tarasova, N. I. and Michejda, C. J. (2004) Small molecule toxins targeting tumor receptors. *Curr. Pharm. Des.* **10**, *19*, 2311-34.

Easton, J., Wei, T., Lahti, J. M. and Kidd, V. J. (1998) Disruption of the cyclin D/cyclin-dependent kinase/INK4/retinoblastoma protein regulatory pathway in human neuroblastoma. *Cancer Res.* **58**, *12*, 2624-32.

Ellis, V., Wun, T. C., Behrendt, N., Ronne, E. and Dano, K. (1990) Inhibition of receptor-bound urokinase by plasminogen-activator inhibitors. *J. Biol. Chem.* **265**, *17*, 9904-8.

Epenetos, A. A., Carr, D., Johnson, P. M., Bodmer, W. F. and Lavender, J. P. (1986) Antibody-guided radiolocalisation of tumours in patients with testicular or ovarian cancer using two radioiodinated monoclonal antibodies to placental alkaline phosphatase. *Br. J. Radiol.* **59**, *698*, 117-25.

Eshba, N. H. and Salama, H. M. (1985) 5-(2-Oxo-3-indolinylidene)thiazolidine-2,4-dione-1,3-di-Mannich base derivatives: synthesis and evaluation for antileukemic activity. *Pharmazie* **40**, *5*, 320-2.

Evan, G. I. and Vousden, K. H. (2001) Proliferation, cell cycle and apoptosis in cancer. *Nature* **411**, *6835*, 342-8.

Faulkner, D. J. (2000) Marine natural products. *Nat. Prod. Rep.* **17**, *1*, 7-55.

Faulkner, D. J. (2001) Marine natural products. *Nat. Prod. Rep.* **18**, *1*, 1-49.

Fenical, W. (1997) New pharmaceuticals from marine organisms. *Trends. Biotechnol.* **15**, *9*, 339-41.

Ferguson, R. E., Jackson, S. M., Stanley, A. J., Joyce, A. D., Harnden, P., Morrison, E. E., Patel, P. M., Phillips, R. M., Selby, P. J. and Banks, R. E. (2005) Intrinsic chemotherapy resistance to the tubulin-binding antimitotic agents in renal cell carcinoma. *Int. J. Cancer* **115**, *1*, 155-63.

Fiebig, H. and Schuler, J. B. (2006) *In vivo antitumor activity of 5-methyl-indirubin.* Indirubin, the red shade of indigo. L. Meijer, N. Guyard, A. L. Skaltsounis and G. Eisenbrand. Roscoff, France, Editions "Life in Progress 209-213.

Foekens, J. A., Buessecker, F., Peters, H. A., Krainick, U., van Putten, W. L., Look, M. P., Klijn, J. G. and Kramer, M. D. (1995a) Plasminogen activator inhibitor-2: prognostic relevance in 1012 patients with primary breast cancer. *Cancer Res.* **55**, *7*, 1423-7.

Foekens, J. A., Look, M. P., Peters, H. A., van Putten, W. L., Portengen, H. and Klijn, J. G. (1995b) Urokinase-type plasminogen activator and its inhibitor PAI-1: predictors of poor response to tamoxifen therapy in recurrent breast cancer. *J. Natl. Cancer Inst.* **87**, *10*, 751-6.

Fong, T. A., Shawver, L. K., Sun, L., Tang, C., App, H., Powell, T. J., Kim, Y. H., Schreck, R., Wang, X., Risau, W., Ullrich, A., Hirth, K. P. and McMahon, G. (1999) SU5416 is a potent and selective inhibitor of the vascular endothelial growth factor receptor (Flk-1/KDR) that inhibits tyrosine kinase catalysis, tumor vascularization, and growth of multiple tumor types. *Cancer Res.* **59**, *1*, 99-106.

Foote, M. (1998) The Importance of Planned Dose of Chemotherapy on Time: Do We Need to Change Our Clinical Practice? *Oncologist* **3**, *5*, 365-368.

Fracasso, G., Bellisola, G., Castelletti, D., Tridente, G. and Colombatti, M. (2004) Immunotoxins and other conjugates: preparation and general characteristics. *Mini Rev. Med. Chem.* **4**, *5*, 545-62.

Frankel, A. E., Fleming, D. R., Hall, P. D., Powell, B. L., Black, J. H., Leftwich, C. and Gartenhaus, R. (2003) A phase II study of DT fusion protein denileukin diftitox in patients with fludarabine-refractory chronic lymphocytic leukemia. *Clin Cancer Res* **9**, *10 Pt 1*, 3555-61.

Frenette, G., Tremblay, R. R., Lazure, C. and Dube, J. Y. (1997) Prostatic kallikrein hK2, but not prostate-specific antigen (hK3), activates single-chain urokinase-type plasminogen activator. *Int. J. Cancer* **71**, *5*, 897-9.

Gale, T. (2002) "Maximum Tolerated Dose." Encyclopedia of Public Health.

Garden, S. J., Torres, J. C., da Silva, L. E. and Pinto, A. C. (1998) A convenient methodology for the N-alkylation of isatin compounds. *Synth. Commun.* **28**, 1679-1689.

Gastpar, R., Goldbrunner, M., Marko, D. and von Angerer, E. (1998) Methoxy-substituted 3-formyl-2-phenylindoles inhibit tubulin polymerization. *J. Med. Chem.* **41**, *25*, 4965-72.

Geldof, A. A., Minneboo, A. and Heimans, J. J. (1998) Vinca-alkaloid neurotoxicity measured using an in vitro model. *J. Neurooncol.* **37**, *2*, 109-13.

Ghobrial, I. M., Witzig, T. E. and Adjei, A. A. (2005) Targeting apoptosis pathways in cancer therapy. *CA Cancer J. Clin.* **55**, *3*, 178-94.

Gibson, L. F., Fortney, J., Magro, G., Ericson, S. G., Lynch, J. P. and Landreth, K. S. (1999) Regulation of BAX and BCL-2 expression in breast cancer cells by chemotherapy. *Breast Cancer Res. Treat.* **55**, *2*, 107-17.

Glover, V. (1998) Function of endogenous monoamine oxidase inhibitors (tribulin). *J. Neural. Transm. Suppl.* **52**, 307-13.

Goerlach, A., Krauer, K. G., McKenzie, I. F. and Pietersz, G. A. (1991) In vitro antitumor activity of 2'-deoxy-5-fluorouridine-monoclonal antibody conjugates. *Bioconjug. Chem.* **2**, *2*, 96-101.

Goold, R. G. and Gordon-Weeks, P. R. (2001) Microtubule-associated protein 1B phosphorylation by glycogen synthase kinase 3beta is induced during PC12 cell differentiation. *J. Cell. Sci.* **114**, *Pt 23*, 4273-84.

Gottesman, M. M. (2002) Mechanisms of cancer drug resistance. *Annu. Rev. Med.* **53**, 615-27.

Gottesman, M. M., Fojo, T. and Bates, S. E. (2002) Multidrug resistance in cancer: role of ATP-dependent transporters. *Nat. Rev. Cancer* **2**, *1*, 48-58.

Gottesman, M. M. and Pastan, I. (1993) Biochemistry of multidrug resistance mediated by the multidrug transporter. *Annu. Rev. Biochem.* **62**, 385-427.

Gould, D. J., Foxwell, B. M., Feldmann, M. and Chernajovsky, Y. (1998) Potentiation of TNF-alpha toxicity by conjugation with ricin A-chain. *Cytokine* **10**, *12*, 931-9.

Grabley, S. and Thiericke, R. (1999) *The impact of natural products on drug discovery*. Drug Discovery from Nature. S. Grabley and R. Thiericke. Berlin Heidelberg, Springer-Verlag 3-37.

Greenfield, R. S., Kaneko, T., Daues, A., Edson, M. A., Fitzgerald, K. A., Olech, L. J., Grattan, J. A., Spitalny, G. L. and Braslawsky, G. R. (1990) Evaluation in vitro of adriamycin immunoconjugates synthesized using an acid-sensitive hydrazone linker. *Cancer Res.* **50**, *20*, 6600-7.

Grimshaw, J. and Begley, W. (1974) Synthesis of 2-Anilino-3H-indol-3-one derivatives. *Synthesis*, 496-498.

Gschwind, A., Fischer, O. M. and Ullrich, A. (2004) The discovery of receptor tyrosine kinases: targets for cancer therapy. *Nat. Rev. Cancer* **4**, *5*, 361-70.

Guo, P., Ma, J., Li, S., Guo, Z., Adams, A. L. and Gallo, J. M. (2001) Targeted delivery of a peripheral benzodiazepine receptor ligand-gemcitabine conjugate to brain tumors in a xenograft model. *Cancer Chemother. Pharmacol.* **48**, *2*, 169-76.

Gusterson, B. A., Gelber, R. D., Goldhirsch, A., Price, K. N., Save-Soderborgh, J., Anbazhagan, R., Styles, J., Rudenstam, C. M., Golouh, R. and Reed, R. (1992) Prognostic importance of c-erbB-2 expression in breast cancer. International (Ludwig) Breast Cancer Study Group. *J. Clin. Oncol.* **10**, *7*, 1049-56.

Hagemann, E. (1950) [Oversized ureteral calculus with perforation into the bladder.]. *Z. Urol.* **43**, *3-4*, 160-6.

Hamann, P. R., Hinman, L. M., Beyer, C. F., Lindh, D., Upeslacis, J., Flowers, D. A. and Bernstein, I. (2002) An anti-CD33 antibody-calicheamicin conjugate for treatment of acute myeloid leukemia. Choice of linker. *Bioconjug. Chem.* **13**, *1*, 40-6.

Hanahan, D. and Weinberg, R. A. (2000) The hallmarks of cancer. *Cell* **100**, *1*, 57-70.

Hansch, C. and Leo, A. (1979) Substituent Constants for Correlation Analysis in Chemistry and Biology. New York, Wiley.

Harada, M., Murata, J., Sakamura, Y., Sakakibara, H., Okuno, S. and Suzuki, T. (2001) Carrier and dose effects on the pharmacokinetics of T-0128, a camptothecin analogue-carboxymethyl dextran conjugate, in non-tumor- and tumor-bearing rats. *J. Control Release* **71**, *1*, 71-86.

Harada, M., Sakakibara, H., Yano, T., Suzuki, T. and Okuno, S. (2000) Determinants for the drug release from T-0128, camptothecin analogue-carboxymethyl dextran conjugate. *J. Control Release* **69**, *3*, 399-412.

Harbour, J. W. and Dean, D. C. (2000) The Rb/E2F pathway: expanding roles and emerging paradigms. *Genes Dev.* **14**, *19*, 2393-409.

Hartwell, L. H. and Weinert, T. A. (1989) Checkpoints: controls that ensure the order of cell cycle events. *Science* **246**, *4930*, 629-34.

Havlicek, L., Hanus, J., Vesely, J., Leclerc, S., Meijer, L., Shaw, G. and Strnad, M. (1997) Cytokinin-derived cyclin-dependent kinase inhibitors: synthesis and cdc2 inhibitory activity of olomoucine and related compounds. *J. Med. Chem.* **40**, *4*, 408-12.

Hayflick, L. (1997) Mortality and immortality at the cellular level. A review. *Biochemistry (Mosc)* **62**, *11*, 1180-90.

Hermanson, G. T. (1996) Bioconjugate Techniques. San Diego, California, Acedemic Press, Inc.

Herz, J., Clouthier, D. E. and Hammer, R. E. (1992) LDL receptor-related protein internalizes and degrades uPA-PAI-1 complexes and is essential for embryo implantation. *Cell* **71**, *3*, 411-21.

Hingorani, S. R. and Tuveson, D. A. (2003) Targeting oncogene dependence and resistance. *Cancer Cell* **3**, *5*, 414-7.

Hirai, H., Kawanishi, N. and Iwasawa, Y. (2005) Recent advances in the development of selective small molecule inhibitors for cyclin-dependent kinases. *Curr. Top. Med. Chem.* **5**, *2*, 167-79.

Hirota, N., Ueda, M., Ozawa, S., Abe, O. and Shimizu, N. (1989) Suppression of an epidermal growth factor receptor-hyperproducing tumor by an immunotoxin conjugate of gelonin and a monoclonal anti-epidermal growth factor receptor antibody. *Cancer Res.* **49**, *24 Pt 1*, 7106-9.

Hoessel, R., Leclerc, S., Endicott, J. A., Nobel, M. E., Lawrie, A., Tunnah, P., Leost, M., Damiens, E., Marie, D., Marko, D., Niederberger, E., Tang, W., Eisenbrand, G. and Meijer, L. (1999) Indirubin, the active constituent of a Chinese antileukaemia medicine, inhibits cyclin-dependent kinases. *Nat. Cell. Biol.* **1**, *1*, 60-7.

Hoogenboom, H. R., Volckaert, G. and Raus, J. C. (1991) Construction and expression of antibody-tumor necrosis factor fusion proteins. *Mol. Immunol.* **28**, *9*, 1027-37.

Hopewel, J. W., Duncan, R., Wilding, D. and Chakrabarti, K. (2001) Preclinical evaluation of the cardiotoxicity of PK2: a novel HPMA copolymer-doxorubicin-galactosamine conjugate antitumour agent. *Hum. Exp. Toxicol.* **20**, *9*, 461-70.

Horak, E. R., Leek, R., Klenk, N., LeJeune, S., Smith, K., Stuart, N., Greenall, M., Stepniewska, K. and Harris, A. L. (1992) Angiogenesis, assessed by platelet/endothelial cell adhesion molecule antibodies, as indicator of node metastases and survival in breast cancer. *Lancet* **340**, *8828*, 1120-4.

Hurwitz, E., Kashi, R., Arnon, R., Wilchek, M. and Sela, M. (1985) The covalent linking of two nucleotide analogues to antibodies. *J. Med. Chem.* **28**, *1*, 137-40.

Igosheva, N., Lorz, C., O'Conner, E., Glover, V. and Mehmet, H. (2005) Isatin, an endogenous monoamine oxidase inhibitor, triggers a dose- and time-dependent switch from apoptosis to necrosis in human neuroblastoma cells. *Neurochem. Int.* **47**, *3*, 216-24.

Imahori, K. and Uchida, T. (1997) Physiology and pathology of tau protein kinases in relation to Alzheimer's disease. *J. Biochem. (Tokyo)* **121**, *2*, 179-88.

Imai, K. and Takaoka, A. (2006) Comparing antibody and small-molecule therapies for cancer. *Nat. Rev. Cancer* **6**, *9*, 714-27.

Jackson, J. R., Patrick, D. R., Dar, M. M. and Huang, P. S. (2007) Targeted anti-mitotic therapies: can we improve on tubulin agents? *Nat. Rev. Cancer* **7**, *2*, 107-17.

Jankun, J. (1992) Antitumor activity of the type 1 plasminogen activator inhibitor and cytotoxic conjugate in vitro. *Cancer Res.* **52**, *20*, 5829-32.

Jaspers, M. (1998) *Pharmacy of the deep- marine organisms as sources of anticancer agents*. Advances in drug discovery techniques. A. L. Harvey, John Wiley and Sons Ltd.

Jordan, A., Hadfield, J. A., Lawrence, N. J. and McGown, A. T. (1998) Tubulin as a target for anticancer drugs: agents which interact with the mitotic spindle. *Med. Res. Rev.* **18**, *4*, 259-96.

Jordan, M. A. and Wilson, L. (1998) Microtubules and actin filaments: dynamic targets for cancer chemotherapy. *Curr. Opin. Cell Biol.* **10**, *1*, 123-30.

Jordan, M. A. and Wilson, L. (2004) Microtubules as a target for anticancer drugs. *Nat. Rev. Cancer* **4**, *4*, 253-65.

Juranic, Z., Anastasova, F., Juranic, I., Stanojkovic, T., Radulovic, S. and Vuletic, N. (1999) Antiproliferative action of isatine-beta-thiocarbohydrazone and N-ethylisatine-beta-thiocarbohydrazone on human PBMC and on two neoplastic cell lines. *J. Exp. Clin. Cancer Res.* **18**, *3*, 317-24.

Kaelin, W. G., Jr. (2005) The concept of synthetic lethality in the context of anticancer therapy. *Nat. Rev. Cancer* **5**, *9*, 689-98.

Kamiya, H., Muramoto, K. and Yamazaki, M. (1986) Aplysianin-A, an antibacterial and antineoplastic glycoprotein in the albumen gland of a sea hare, Aplysia kurodai. *Experientia* **42**, *9*, 1065-7.

Karp, J. E. and Broder, S. (1995) Molecular foundations of cancer: new targets for intervention. *Nat. Med.* **1**, *4*, 309-20.

Kavallaris, M., Verrills, N. M. and Hill, B. T. (2001) Anticancer therapy with novel tubulin-interacting drugs. *Drug Resist. Updat.* **4**, *6*, 392-401.

Kelland, L. R. (2004) Of mice and men: values and liabilities of the athymic nude mouse model in anticancer drug development. *Eur. J. Cancer* **40**, *6*, 827-36.

Kelloff, G. J., Fay, J. R., Steele, V. E., Lubet, R. A., Boone, C. W., Crowell, J. A. and Sigman, C. C. (1996) Epidermal growth factor receptor tyrosine kinase inhibitors as potential cancer chemopreventives. *Cancer Epidemiol. Biomarkers Prev.* **5**, *8*, 657-66.

Kerbel, R. S. (2003) Human tumor xenografts as predictive preclinical models for anticancer drug activity in humans: better than commonly perceived-but they can be improved. *Cancer Biol. Ther.* **2**, *4 Suppl 1*, S134-9.

King, K. L. and Boder, G. B. (1979) Correlation of the clinical neurotoxicity of the vinca alkaloids vincristine, vinblastine, and vindesine with their effects on cultured rat midbrain cells. *Cancer Chemother. Pharmacol.* **2**, *4*, 239-42.

King, P. D. and Perry, M. C. (2001) Hepatotoxicity of chemotherapy. *Oncologist* **6**, *2*, 162-76.

Kircheis, R., Wightman, L., Kursa, M., Ostermann, E. and Wagner, E. (2002) Tumor-targeted gene delivery: an attractive strategy to use highly active effector molecules in cancer treatment. *Gene Ther.* **9**, *11*, 731-5.

Kirschberg, T. A., VanDeusen, C. L., Rothbard, J. B., Yang, M. and Wender, P. A. (2003) Arginine-based molecular transporters: the synthesis and chemical evaluation of releasable taxol-transporter conjugates. *Org. Lett.* **5**, *19*, 3459-62.

Koehn, F. E. and Carter, G. T. (2005) The evolving role of natural products in drug discovery. *Nat. Rev. Drug Discov.* **4**, *3*, 206-20.

Kopka, K., Faust, A., Keul, P., Wagner, S., Breyholz, H. J., Holtke, C., Schober, O., Schafers, M. and Levkau, B. (2006) 5-pyrrolidinylsulfonyl isatins as a potential tool for the molecular imaging of caspases in apoptosis. *J. Med. Chem.* **49**, *23*, 6704-15.

Kounnas, M. Z., Henkin, J., Argraves, W. S. and Strickland, D. K. (1993) Low density lipoprotein receptor-related protein/alpha 2-macroglobulin receptor mediates cellular uptake of pro-urokinase. *J. Biol. Chem.* **268**, *29*, 21862-7.

Koyanagi, N., Nagasu, T., Fujita, F., Watanabe, T., Tsukahara, K., Funahashi, Y., Fujita, M., Taguchi, T., Yoshino, H. and Kitoh, K. (1994) In vivo tumor growth inhibition produced by a novel sulfonamide, E7010, against rodent and human tumors. *Cancer Res.* **54**, *7*, 1702-6.

Kratz, F. and Beyer, U. (1998) Serum proteins as drug carriers of anticancer agents: A review. *Drug Delivery* **5**, 281-299.

Kratz, F., Beyer, U. and Schutte, M. T. (1999) Drug-polymer conjugates containing acid-cleavable bonds. *Crit. Rev. Ther. Drug Carrier Syst.* **16**, *3*, 245-88.

Kroemer, G., Dallaporta, B. and Resche-Rigon, M. (1998) The mitochondrial death/life regulator in apoptosis and necrosis. *Annu. Rev. Physiol.* **60**, 619-42.

Kruithof, E. K., Baker, M. S. and Bunn, C. L. (1995) Biological and clinical aspects of plasminogen activator inhibitor type 2. *Blood* **86**, *11*, 4007-24.

Kung, M. P. and Kung, H. F. (1989) Peracetic acid as a superior oxidant for preparation of [123I]IBZM: A potential dopamine D-2 receptor imaging agent. *J. Label. Compd. Radiopharm.* **27**, 691–700.

Kuo, C. C., Hsieh, H. P., Pan, W. Y., Chen, C. P., Liou, J. P., Lee, S. J., Chang, Y. L., Chen, L. T., Chen, C. T. and Chang, J. Y. (2004) BPR0L075, a novel synthetic indole compound with antimitotic activity in human cancer cells, exerts effective antitumoral activity in vivo. *Cancer Res.* **64**, *13*, 4621-8.

Laemmli, U. K. (1970) Cleavage of structural proteins during the assembly of the head of bacteriophage T4. *Nature* **227**, *5259*, 680-5.

Laguzza, B. C., Nichols, C. L., Briggs, S. L., Cullinan, G. J., Johnson, D. A., Starling, J. J., Baker, A. L., Bumol, T. F. and Corvalan, J. R. (1989) New antitumor monoclonal antibody-vinca conjugates LY203725 and related compounds: design, preparation, and representative in vivo activity. *J. Med. Chem.* **32**, *3*, 548-55.

Laird, A. D., Vajkoczy, P., Shawver, L. K., Thurnher, A., Liang, C., Mohammadi, M., Schlessinger, J., Ullrich, A., Hubbard, S. R., Blake, R. A., Fong, T. A., Strawn, L. M., Sun, L., Tang, C., Hawtin, R., Tang, F., Shenoy, N., Hirth, K. P., McMahon, G. and Cherrington (2000) SU6668 is a potent antiangiogenic and antitumor agent that induces regression of established tumors. *Cancer Res.* **60**, *15*, 4152-60.

Langer, M., Kratz, F., Rothen-Rutishauser, B., Wunderli-Allenspach, H. and Beck-Sickinger, A. G. (2001) Novel peptide conjugates for tumor-specific chemotherapy. *J. Med. Chem.* **44**, *9*, 1341-8.

Leclerc, S., Garnier, M., Hoessel, R., Marko, D., Bibb, J. A., Snyder, G. L., Greengard, P., Biernat, J., Wu, Y. Z., Mandelkow, E. M., Eisenbrand, G. and Meijer, L. (2001) Indirubins inhibit glycogen synthase kinase-3 beta and CDK5/p25, two protein kinases involved in abnormal tau phosphorylation in Alzheimer's disease. A property common to most cyclin-dependent kinase inhibitors? *J. Biol. Chem.* **276**, *1*, 251-60.

Lee, D., Long, S. A., Murray, J. H., Adams, J. L., Nuttall, M. E., Nadeau, D. P., Kikly, K., Winkler, J. D., Sung, C. M., Ryan, M. D., Levy, M. A., Keller, P. M. and DeWolf, W. E., Jr. (2001) Potent and selective nonpeptide inhibitors of caspases 3 and 7. *J. Med. Chem.* **44**, *12*, 2015-26.

Lee, J. W., Moon, M. J., Min, H. Y., Chung, H. J., Park, E. J., Park, H. J., Hong, J. Y., Kim, Y. C. and Lee, S. K. (2005) Induction of apoptosis by a novel indirubin-5-nitro-3'-monoxime, a CDK inhibitor, in human lung cancer cells. *Bioorg. Med. Chem. Lett.* **15**, *17*, 3948-52.

Lee, M. D., Durr, F. E., Hinman, L. M., Hanmann, P. R. and Ellestad, G. A. (1993) The calicheamicins. *Adv. Med. Chem.* **2**, 31-66.

Leung, L. K. and Wang, T. T. (1999) Differential effects of chemotherapeutic agents on the Bcl-2/Bax apoptosis pathway in human breast cancer cell line MCF-7. *Breast Cancer Res. Treat.* **55**, *1*, 73-83.

Levin, V. A. (1980) Relationship of octanol/water partition coefficient and molecular weight to rat brain capillary permeability. *J. Med. Chem.* **23**, *6*, 682-4.

Li, Y., Rizvi, S. M., Ranson, M. and Allen, B. J. (2002) 213Bi-PAI2 conjugate selectively induces apoptosis in PC3 metastatic prostate cancer cell line and shows anti-cancer activity in a xenograft animal model. *Br. J. Cancer* **86**, *7*, 1197-203.

Ling, V. (1997) Multidrug resistance: molecular mechanisms and clinical relevance. *Cancer Chemother. Pharmacol.* **40 Suppl**, S3-8.

List, K., Jensen, O. N., Bugge, T. H., Lund, L. R., Ploug, M., Dano, K. and Behrendt, N. (2000) Plasminogen-independent initiation of the pro-urokinase activation cascade in vivo. Activation of pro-urokinase by glandular kallikrein (mGK-6) in plasminogen-deficient mice. *Biochemistry* **39**, *3*, 508-15.

Liu, Y., Lashuel, H. A., Choi, S., Xing, X., Case, A., Ni, J., Yeh, L. A., Cuny, G. D., Stein, R. L. and Lansbury, P. T., Jr. (2003) Discovery of inhibitors that elucidate the role of UCH-L1 activity in the H1299 lung cancer cell line. *Chem. Biol.* **10**, *9*, 837-46.

Luo, Y. and Prestwich, G. D. (2002) Cancer-targeted polymeric drugs. *Curr. Cancer Drug Targets* **2**, *3*, 209-26.

MacNeil, I. A., Tiong, C. L., Minor, C., August, P. R., Grossman, T. H., Loiacono, K. A., Lynch, B. A., Phillips, T., Narula, S., Sundaramoorthi, R., Tyler, A., Aldredge, T., Long, H., Gilman, M., Holt, D. and Osburne, M. S. (2001) Expression and isolation of antimicrobial small molecules from soil DNA libraries. *J. Mol. Microbiol. Biotechnol.* **3**, *2*, 301-8.

Maloney, D. G., Grillo-Lopez, A. J., White, C. A., Bodkin, D., Schilder, R. J., Neidhart, J. A., Janakiraman, N., Foon, K. A., Liles, T. M., Dallaire, B. K., Wey, K., Royston, I., Davis, T. and Levy, R. (1997) IDEC-C2B8 (Rituximab) anti-CD20 monoclonal antibody therapy in patients with relapsed low-grade non-Hodgkin's lymphoma. *Blood* **90**, *6*, 2188-95.

Malumbres, M. and Barbacid, M. (2001) To cycle or not to cycle: a critical decision in cancer. *Nat. Rev. Cancer* **1**, *3*, 222-31.

Malumbres, M. and Pellicer, A. (1998) RAS pathways to cell cycle control and cell transformation. *Front. Biosci.* **3**, d887-912.

Mandelkow, E. M. and Mandelkow, E. (1998) Tau in Alzheimer's disease. *Trends Cell Biol.* **8**, *11*, 425-7.

Mann, J. (2002) Natural products in cancer chemotherapy: past, present and future. *Nat. Rev. Cancer* **2**, *2*, 143-8.

Marchetti, P., Urien, S., Cappellini, G. A., Ronzino, G. and Ficorella, C. (2002) Weekly administration of paclitaxel: theoretical and clinical basis. *Crit. Rev. Oncol. Hematol.* **44 Suppl**, S3-13.

Marsh, M. (2001) Endocytosis. UK, Oxford University Press.

Marsters, S. A., Pitti, R. A., Sheridan, J. P. and Ashkenazi, A. (1999) Control of apoptosis signaling by Apo2 ligand. *Recent. Prog. Horm. Res.* **54**, 225-34.

Marx, J. (2005) Cancer. Encouraging results for second-generation antiangiogenesis drugs. *Science* **308**, *5726*, 1248-9.

Massague, J. (2004) G1 cell-cycle control and cancer. *Nature* **432**, *7015*, 298-306.

Masui, H., Kamrath, H., Apell, G., Houston, L. L. and Mendelsohn, J. (1989) Cytotoxicity against human tumor cells mediated by the conjugate of anti-epidermal growth factor receptor monoclonal antibody to recombinant ricin A chain. *Cancer Res.* **49**, *13*, 3482-8.

Maugard, T., Enaud, E., Choisy, P. and Legoy, M. D. (2001) Identification of an indigo precursor from leaves of Isatis tinctoria (Woad). *Phytochemistry* **58**, *6*, 897-904.

McDonald, E. R., 3rd and El-Deiry, W. S. (2000) Cell cycle control as a basis for cancer drug development (Review). *Int. J. Oncol.* **16**, *5*, 871-86.

McIntyre, I. M. and Norman, T. R. (1990) Serotonergic effects of isatin: an endogenous MAO inhibitor related to tribulin. *J. Neural. Transm. Gen. Sect.* **79**, *1-2*, 35-40.

Medarde, M., Ramos, A., Caballero, E., Pelaz-Lamamie de Clairac, R., Lopez, J., Garcia Gravalos, D. and San Feliciano, A. (1998) Synthesis and antineoplastic activity of combretastatin analogues: heterocombretastatins. *Eur. J. Med. Chem.* **33**, 71-77.

Meijer, L., Skaltsounis, A. L., Magiatis, P., Polychronopoulos, P., Knockaert, M., Leost, M., Ryan, X. P., Vonica, C. A., Brivanlou, A., Dajani, R., Crovace, C.,

Tarricone, C., Musacchio, A., Roe, S. M., Pearl, L. and Greengard, P. (2003) GSK-3-selective inhibitors derived from Tyrian purple indirubins. *Chem. Biol.* **10**, *12*, 1255-66.

Mendel, D. B., Laird, A. D., Smolich, B. D., Blake, R. A., Liang, C., Hannah, A. L., Shaheen, R. M., Ellis, L. M., Weitman, S., Shawver, L. K. and Cherrington, J. M. (2000) Development of SU5416, a selective small molecule inhibitor of VEGF receptor tyrosine kinase activity, as an anti-angiogenesis agent. *Anticancer Drug Des.* **15**, *1*, 29-41.

Meyerhardt, J. A. and Mayer, R. J. (2005) Systemic therapy for colorectal cancer. *N. Engl. J. Med.* **352**, *5*, 476-87.

Minna, J. D. and Dowell, J. (2005) Erlotinib hydrochloride. *Nat. Rev. Drug Discov.* **Suppl**, S14-5.

Moon, E. Y. and Lerner, A. (2002) Benzylamide sulindac analogues induce changes in cell shape, loss of microtubules and G(2)-M arrest in a chronic lymphocytic leukemia (CLL) cell line and apoptosis in primary CLL cells. *Cancer Res.* **62**, *20*, 5711-9.

Moriconi, E. J. and Murray, J. J. (1964) Pyrolysis and Photolysis of 1-Methyl-3-diazooxindole. Base Decomposition of Isatin 2-Tosylhydrazone. *J. Org. Chem.* **29**, 3577.

Morse, B. S. and Stohlman, F., Jr. (1966) Regulation of erythropoiesis. 18. The effect of vincristine and erythropoietin on bone marrow. *J. Clin. Invest.* **45**, *8*, 1241-50.

Motzer, R. J., Michaelson, M. D., Redman, B. G., Hudes, G. R., Wilding, G., Figlin, R. A., Ginsberg, M. S., Kim, S. T., Baum, C. M., DePrimo, S. E., Li, J. Z., Bello, C. L., Theuer, C. P., George, D. J. and Rini, B. I. (2006) Activity of SU11248, a multitargeted inhibitor of vascular endothelial growth factor receptor and platelet-derived growth factor receptor, in patients with metastatic renal cell carcinoma. *J. Clin. Oncol.* **24**, *1*, 16-24.

Mueller, B. M., Wrasidlo, W. A. and Reisfeld, R. A. (1990) Antibody conjugates with morpholinodoxorubicin and acid-cleavable linkers. *Bioconjug. Chem.* **1**, *5*, 325-30.

Naegel, L. C. A. and Cooksey, C. J. (2002) Tyrian purple from marine muricids, especially from *Plicopurpura pansa* (Gould, 1853). *J. Shellfish Res.* **21**, 193-200.

Nagle, D. G., Zhou, Y. D., Mora, F. D., Mohammed, K. A. and Kim, Y. P. (2004) Mechanism targeted discovery of antitumor marine natural products. *Curr. Med. Chem.* **11**, *13*, 1725-56.

Natarajan, A., Fan, Y. H., Chen, H., Guo, Y., Iyasere, J., Harbinski, F., Christ, W. J., Aktas, H. and Halperin, J. A. (2004) 3,3-diaryl-1,3-dihydroindol-2-ones as antiproliferatives mediated by translation initiation inhibition. *J. Med. Chem.* **47**, *8*, 1882-5.

Nesbit, C. E., Tersak, J. M. and Prochownik, E. V. (1999) MYC oncogenes and human neoplastic disease. *Oncogene* **18**, *19*, 3004-16.

Newcomb, E. W. (1995) P53 gene mutations in lymphoid diseases and their possible relevance to drug resistance. *Leuk. Lymphoma* **17**, *3-4*, 211-21.

Newman, D. J. and Cragg, G. M. (2005) *Developments and future trends in anticancer natural products drug discovery*. Anticancer Agents from Natural Products. G. M. Cragg, D. G. I. Kingston and D. J. Newman, CRC 553-571.

Newman, D. J., Cragg, G. M. and Snader, K. M. (2003) Natural products as sources of new drugs over the period 1981-2002. *J. Nat. Prod.* **66**, *7*, 1022-37.

Nguyen, J. T. and Wells, J. A. (2003) Direct activation of the apoptosis machinery as a mechanism to target cancer cells. *Proc. Natl. Acad. Sci. U S A* **100**, *13*, 7533-8.

Nielsen, L. S., Hansen, J. G., Skriver, L., Wilson, E. L., Kaltoft, K., Zeuthen, J. and Dano, K. (1982) Purification of zymogen to plasminogen activator from human glioblastoma cells by affinity chromatography with monoclonal antibody. *Biochemistry* **21**, *25*, 6410-5.

Nigg, E. A. (2001) Mitotic kinases as regulators of cell division and its checkpoints. *Nat. Rev. Mol. Cell Biol.* **2**, *1*, 21-32.

Nobes, C. D. and Hall, A. (1995) Rho, rac and cdc42 GTPases: regulators of actin structures, cell adhesion and motility. *Biochem. Soc. Trans.* **23**, *3*, 456-9.

Nooter, K. and Sonneveld, P. (1993) Multidrug resistance (MDR) genes in haematological malignancies. *Cytotechnology* **12**, *1-3*, 213-30.

Nooter, K. and Stoter, G. (1996) Molecular mechanisms of multidrug resistance in cancer chemotherapy. *Pathol. Res. Pract.* **192**, *7*, 768-80.

Norbury, C. and Nurse, P. (1992) Animal cell cycles and their control. *Annu. Rev. Biochem.* **61**, 441-70.

Nuijen, B., Bouma, M., Manada, C., Jimeno, J. M., Schellens, J. H., Bult, A. and Beijnen, J. H. (2000) Pharmaceutical development of anticancer agents derived from marine sources. *Anticancer Drugs* **11**, *10*, 793-811.

Nurse, P. (1975) Genetic control of cell size at cell division in yeast. *Nature* **256**, *5518*, 547-51.

Nykjaer, A., Kjoller, L., Cohen, R. L., Lawrence, D. A., Garni-Wagner, B. A., Todd, R. F., 3rd, van Zonneveld, A. J., Gliemann, J. and Andreasen, P. A. (1994) Regions involved in binding of urokinase-type-1 inhibitor complex and pro-urokinase to the endocytic alpha 2-macroglobulin receptor/low density lipoprotein receptor-related protein. Evidence that the urokinase receptor protects pro-urokinase against binding to the endocytic receptor. *J. Biol. Chem.* **269**, *41*, 25668-76.

O'Dwyer, M. E., Gatter, K. M., Loriaux, M., Druker, B. J., Olson, S. B., Magenis, R. E., Lawce, H., Mauro, M. J., Maziarz, R. T. and Braziel, R. M. (2003) Demonstration of Philadelphia chromosome negative abnormal clones in patients with chronic myelogenous leukemia during major cytogenetic responses induced by imatinib mesylate. *Leukemia* **17**, *3*, 481-7.

Ogata, M., Chaudhary, V. K., FitzGerald, D. J. and Pastan, I. (1989) Cytotoxic activity of a recombinant fusion protein between interleukin 4 and Pseudomonas exotoxin. *Proc. Natl. Acad. Sci. U S A* **86**, *11*, 4215-9.

Ohkuma, S. and Poole, B. (1978) Fluorescence probe measurement of the intralysosomal pH in living cells and the perturbation of pH by various agents. *Proc. Natl. Acad. Sci. U S A* **75**, *7*, 3327-31.

Okuno, S., Harada, M., Yano, T., Yano, S., Kiuchi, S., Tsuda, N., Sakamura, Y., Imai, J., Kawaguchi, T. and Tsujihara, K. (2000) Complete regression of xenografted human carcinomas by camptothecin analogue-carboxymethyl dextran conjugate (T-0128). *Cancer Res.* **60**, *11*, 2988-95.

Oldendorf, W. H. (1974) Lipid solubility and drug penetration of the blood brain barrier. *Proc. Soc. Exp. Biol. Med.* **147**, *3*, 813-5.

O'Loughlin, E., Winter, M., Shun, A., Hardin, J. A. and Gall, D. G. (1994) Structural and functional adaptation following jejunal resection in rabbits: effect of epidermal growth factor. *Gastroenterology* **107**, *1*, 87-93.

Owen-Schaub, L., Chan, H., Cusack, J. C., Roth, J. and Hill, L. L. (2000) Fas and Fas ligand interactions in malignant disease. *Int. J. Oncol.* **17**, *1*, 5-12.

Pace, A., Bove, L., Aloe, A., Nardi, M., Pietrangeli, A., Calabresi, F., Innocenti, P. and Jandolo, B. (1997) Paclitaxel neurotoxicity: clinical and neurophysiological study of 23 patients. *Ital. J. Neurol. Sci.* **18**, *2*, 73-9.

Pajouhesh, H., Parson, R. and Popp, F. D. (1983) Potential anticonvulsants VI: condensation of isatins with cyclohexanone and other cyclic ketones. *J. Pharm. Sci.* **72**, *3*, 318-21.

Pandeya, S. N., Smitha, S., Jyoti, M. and Sridhar, S. K. (2005) Biological activities of isatin and its derivatives. *Acta. Pharm.* **55**, *1*, 27-46.

Parums, D. V., Cordell, J. L., Micklem, K., Heryet, A. R., Gatter, K. C. and Mason, D. Y. (1990) JC70: a new monoclonal antibody that detects vascular endothelium associated antigen on routinely processed tissue sections. *J. Clin. Pathol.* **43**, *9*, 752-7.

Pataki, I., Mezei, Z., Adamik, A., Glover, V., Gecse, A. and Telegdy, G. (2005) In vivo effects of isatin on rat platelet eicosanoids. *Platelets* **16**, *1*, 39-43.

Patel, N. H. and Rothenberg, M. L. (1994) Multidrug resistance in cancer chemotherapy. *Invest. New Drugs* **12**, *1*, 1-13.

Pattabhiraman, S. 2003 Transcriptional regulation of 12/15-lipoxygenase expression and the implication of the enzyme in hepoxilin biosynthesis and apoptosis. Humboldt-Universität zu Berlin, Medizinische Fakultät Universitätsklinikum Charité. 1-122

Petersen, L. C., Lund, L. R., Nielsen, L. S., Dano, K. and Skriver, L. (1988) One-chain urokinase-type plasminogen activator from human sarcoma cells is a proenzyme with little or no intrinsic activity. *J. Biol. Chem.* **263**, *23*, 11189-95.

Piche, A., Grim, J., Rancourt, C., Gomez-Navarro, J., Reed, J. C. and Curiel, D. T. (1998) Modulation of Bcl-2 protein levels by an intracellular anti-Bcl-2 single-chain antibody increases drug-induced cytotoxicity in the breast cancer cell line MCF-7. *Cancer Res.* **58**, *10*, 2134-40.

Pietersz, G. A. (1990) The linkage of cytotoxic drugs to monoclonal antibodies for the treatment of cancer. *Bioconjug Chem.* **1**, *2*, 89-95.

Pietersz, G. A. and Krauer, K. (1994) Antibody-targeted drugs for the therapy of cancer. *J. Drug Target* **2**, *3*, 183-215.

Pietra, F. (1997) Secondary metabolites from marine microorganisms: bacteria, protozoa, algae and fungi. Achievements and prospects. *Nat. Prod. Rep.* **14**, *5*, 453-64.

Pitti, R. M., Marsters, S. A., Lawrence, D. A., Roy, M., Kischkel, F. C., Dowd, P., Huang, A., Donahue, C. J., Sherwood, S. W., Baldwin, D. T., Godowski, P. J., Wood, W. I., Gurney, A. L., Hillan, K. J., Cohen, R. L., Goddard, A. D., Botstein, D. and Ashkenazi, A. (1998) Genomic amplification of a decoy receptor for Fas ligand in lung and colon cancer. *Nature* **396**, *6712*, 699-703.

Podolsky, D. K. (1993) Regulation of intestinal epithelial proliferation: a few answers, many questions. *Am. J. Physiol.* **264**, *2 Pt 1*, G179-86.

Polk, D. B. and Tong, W. (1999) Epidermal and hepatocyte growth factors stimulate chemotaxis in an intestinal epithelial cell line. *Am. J. Physiol.* **277**, *6 Pt 1*, C1149-59.

Polychronopoulos, P., Magiatis, P., Skaltsounis, A. L., Myrianthopoulos, V., Mikros, E., Tarricone, A., Musacchio, A., Roe, S. M., Pearl, L., Leost, M., Greengard, P. and Meijer, L. (2004) Structural basis for the synthesis of indirubins as potent and selective inhibitors of glycogen synthase kinase-3 and cyclin-dependent kinases. *J. Med. Chem.* **47**, *4*, 935-46.

Prenen, H., Cools, J., Mentens, N., Folens, C., Sciot, R., Schoffski, P., Van Oosterom, A., Marynen, P. and Debiec-Rychter, M. (2006) Efficacy of the kinase inhibitor SU11248 against gastrointestinal stromal tumor mutants refractory to imatinib mesylate. *Clin. Cancer. Res.* **12**, *8*, 2622-7.

Quesada, A. R., Barbacid, M. M., Mira, E., Aracil, M. and Marquez, G. (1996) Chemosensitization and drug accumulation assays as complementary methods for the screening of multidrug resistance reversal agents. *Cancer Lett.* **99**, *1*, 109-14.

Rai, S. S. and Wolff, J. (1996) Localization of the vinblastine-binding site on beta-tubulin. *J. Biol. Chem.* **271**, *25*, 14707-11.

Rajopadhye, M. and Popp, F. D. (1988) Potential anticonvulsants. 11. Synthesis and anticonvulsant activity of spiro[1,3-dioxolane-2,3'-indolin]-2'-ones and structural analogues. *J. Med. Chem.* **31**, *5*, 1001-5.

Rang, H. P., Dale, M. M. and Ritter, J. M. (1999) *Cancer chemotherapy*. Pharmacology. B. Simmons. Edinburgh, Churchill Livingstone 663-684.

Ranson, M. and Andronicos, N. M. (2003) Plasminogen binding and cancer: promises and pitfalls. *Front. Biosci.* **8**, s294-304.

Ranson, M., Tian, Z., Andronicos, N. M., Rizvi, S. and Allen, B. J. (2002) In vitro cytotoxicity of bismuth-213 (213Bi)-labeled-plasminogen activator inhibitor type 2 (alpha-PAI-2) on human breast cancer cells. *Breast Cancer Res. Treat.* **71**, *2*, 149-59.

Rao, S., Orr, G. A., Chaudhary, A. G., Kingston, D. G. and Horwitz, S. B. (1995) Characterization of the taxol binding site on the microtubule. 2-(m-Azidobenzoyl)taxol photolabels a peptide (amino acids 217-231) of beta-tubulin. *J. Biol. Chem.* **270**, *35*, 20235-8.

Ribas, J., Bettayeb, K., Ferandin, Y., Knockaert, M., Garrofe-Ochoa, X., Totzke, F., Schachtele, C., Mester, J., Polychronopoulos, P., Magiatis, P., Skaltsounis, A. L., Boix, J. and Meijer, L. (2006) 7-Bromoindirubin-3'-oxime induces caspase-independent cell death. *Oncogene* **25**, *47*, 6304-18.

Rinehart, K. L. (2000) Antitumor compounds from tunicates. *Med. Res. Rev.* **20**, *1*, 1-27.

Rodrigues, P., Scheuermann, K., Stockmar, C., Maier, G., Fiebig, H., Unger, C., Mulhaupt, R. and Kratz, F. (2003) Synthesis and in vitro efficacy of acid-sensitive poly(ethylene glycol) paclitaxel conjugates. *Bioorg. Med. Chem. Lett.* **13**, *3*, 355-60.

Rodrigues, P. C., Beyer, U., Schumacher, P., Roth, T., Fiebig, H. H., Unger, C., Messori, L., Orioli, P., Paper, D. H., Mulhaupt, R. and Kratz, F. (1999) Acid-sensitive polyethylene glycol conjugates of doxorubicin: preparation, in vitro efficacy and intracellular distribution. *Bioorg. Med. Chem.* **7**, *11*, 2517-24.

Roesener, J. A. and Scheuer, P. J. (1986) Ulapualide A and B, extrordinary antitumor macrolides from nudibrnch eggmasses. *J. Am. Chem. Soc.* **108**, 846-47.

Romer, J., Nielsen, B. S. and Ploug, M. (2004) The urokinase receptor as a potential target in cancer therapy. *Curr. Pharm. Des.* **10**, *19*, 2359-76.

Rothenberg, M. L., Carbone, D. P. and Johnson, D. H. (2003) Improving the evaluation of new cancer treatments: challenges and opportunities. *Nat. Rev. Cancer* **3**, *4*, 303-9.

Rowinsky, E. and Donehower, R. C. (1997) Antimicrotubule agents. Philadelphia, Lippincott-Raven.

Rowinsky, E. K. (1997) The development and clinical utility of the taxane class of antimicrotubule chemotherapy agents. *Annu. Rev. Med.* **48**, 353-74.

Rydberg, B. (2001) Radiation-induced DNA damage and chromatin structure. *Acta. Oncol.* **40**, *6*, 682-5.

Sakakura, C., Sweeney, E. A., Shirahama, T., Hakomori, S. and Igarashi, Y. (1996) Suppression of bcl-2 gene expression by sphingosine in the apoptosis of human leukemic HL-60 cells during phorbol ester-induced terminal differentiation. *FEBS Lett.* **379**, *2*, 177-80.

Sausville, E. A. and Burger, A. M. (2006) Contributions of human tumor xenografts to anticancer drug development. *Cancer Res.* **66**, *7*, 3351-4, discussion 3354.

Sawicki, E., Stanley, T. W., Hauser, T. R. and Barry, R. (1959) *Anal. Chem.* **31**, 1664.

Sawyers, C. (2004) Targeted cancer therapy. *Nature* **432**, *7015*, 294-7.

Schatzlein, A. G., Rutherford, C., Corrihons, F. and Moore, B. D. (2001) Phage derived peptides for targeting of doxorubicin conjugates to solid tumours. *J. Control Release* **74**, *1-3*, 357-62.

Schiff, P. B., Fant, J. and Horwitz, S. B. (1979) Promotion of microtubule assembly in vitro by taxol. *Nature* **277**, *5698*, 665-7.

Schmitt, M., Harbeck, N., Thomssen, C., Wilhelm, O., Magdolen, V., Reuning, U., Ulm, K., Hofler, H., Janicke, F. and Graeff, H. (1997) Clinical impact of the plasminogen activation system in tumor invasion and metastasis: prognostic relevance and target for therapy. *Thromb. Haemost.* **78**, *1*, 285-96.

Schrama, D., Reisfeld, R. A. and Becker, J. C. (2006) Antibody targeted drugs as cancer therapeutics. *Nat. Rev. Drug. Discov.* **5**, *2*, 147-59.

Seymour, L. W., Ulbrich, K., Wedge, S. R., Hume, I. C., Strohalm, J. and Duncan, R. (1991) N-(2-hydroxypropyl)methacrylamide copolymers targeted to the hepatocyte galactose-receptor: pharmacokinetics in DBA2 mice. *Br. J. Cancer* **63**, *6*, 859-66.

Shen, W. C. and Ryser, H. J. (1981) cis-Aconityl spacer between daunomycin and macromolecular carriers: a model of pH-sensitive linkage releasing drug from a lysosomotropic conjugate. *Biochem. Biophys. Res. Commun.* **102**, *3*, 1048-54.

Sherr, C. J. (2000) Cell cycle control and cancer. *Harvey Lect.* **96**, 73-92.

Sherr, C. J. and Roberts, J. M. (1999) CDK inhibitors: positive and negative regulators of G1-phase progression. *Genes Dev.* **13**, *12*, 1501-12.

Sievers, E. L., Appelbaum, F. R., Spielberger, R. T., Forman, S. J., Flowers, D., Smith, F. O., Shannon-Dorcy, K., Berger, M. S. and Bernstein, I. D. (1999) Selective ablation of acute myeloid leukemia using antibody-targeted chemotherapy: a phase I study of an anti-CD33 calicheamicin immunoconjugate. *Blood* **93**, *11*, 3678-84.

Silverman, G. A., Bird, P. I., Carrell, R. W., Church, F. C., Coughlin, P. B., Gettins, P. G., Irving, J. A., Lomas, D. A., Luke, C. J., Moyer, R. W., Pemberton, P. A., Remold-O'Donnell, E., Salvesen, G. S., Travis, J. and Whisstock, J. C. (2001) The serpins are an expanding superfamily of structurally similar but functionally diverse proteins. Evolution, mechanism of inhibition, novel functions, and a revised nomenclature. *J. Biol. Chem.* **276**, *36*, 33293-6.

Simmons, T. L., Andrianasolo, E., McPhail, K., Flatt, P. and Gerwick, W. H. (2005) Marine natural products as anticancer drugs. *Mol Cancer Ther* **4**, *2*, 333-42.

Simon, R. and Norton, L. (2006) The Norton-Simon hypothesis: designing more effective and less toxic chemotherapeutic regimens. *Nat. Clin. Pract. Oncol.* **3**, *8*, 406-7.

Singh, M. (1999) Transferrin As A targeting ligand for liposomes and anticancer drugs. *Curr. Pharm. Des.* **5**, *6*, 443-51.

Skipper, R. and DeStephano, D. B. (1989) A rapid stain for Campylobacter pylori in gastrointestinal tissue sections using Diff-Quik. *J. Histotechnol.* **12**, 303–304.

Slamon, D. J., Clark, G. M., Wong, S. G., Levin, W. J., Ullrich, A. and McGuire, W. L. (1987) Human breast cancer: correlation of relapse and survival with amplification of the HER-2/neu oncogene. *Science* **235**, *4785*, 177-82.

Slamon, D. J., Godolphin, W., Jones, L. A., Holt, J. A., Wong, S. G., Keith, D. E., Levin, W. J., Stuart, S. G., Udove, J. and Ullrich, A. (1989) Studies of the HER-2/neu proto-oncogene in human breast and ovarian cancer. *Science* **244**, *4905*, 707-12.

Smith, R., Xue, A., Gill, A., Scarlett, C., Saxby, A., Clarkson, A. and Hugh, T. (2007) High Expression of Plasminogen Activator Inhibitor-2 (PAI-2) is a Predictor of Improved Survival in Patients with Pancreatic Adenocarcinoma. *World J. Surg.* **31**, *3*, 493-502.

Soengas, M. S., Capodieci, P., Polsky, D., Mora, J., Esteller, M., Opitz-Araya, X., McCombie, R., Herman, J. G., Gerald, W. L., Lazebnik, Y. A., Cordon-Cardo, C. and Lowe, S. W. (2001) Inactivation of the apoptosis effector Apaf-1 in malignant melanoma. *Nature* **409**, *6817*, 207-11.

Stambolic, V., Mak, T. W. and Woodgett, J. R. (1999) Modulation of cellular apoptotic potential: contributions to oncogenesis. *Oncogene* **18**, *45*, 6094-103.

Stern, L. E., Erwin, C. R., O'Brien, D. P., Huang, F. and Warner, B. W. (2000) Epidermal growth factor is critical for intestinal adaptation following small bowel resection. *Microsc. Res. Tech.* **51**, *2*, 138-48.

Still, W. C., Kahn, M. and Mitra, A. (1978) Rapid chromatographic technique for preparative separations with moderate resolution. *J. Org. Chem.* **43**, 2923-2925.

Stutchbury, T. K., Al-Ejeh, F., Stillfried, G. E., Croucher, D. R., Andrews, J., Irving, D., Links, M. and Ranson, M. (2007) Preclinical evaluation of 213Bi-labeled plasminogen activator inhibitor type 2 in an orthotopic murine xenogenic model of human breast carcinoma. *Mol. Cancer Ther.* **6**, *1*, 203-12.

Subr, V., Duncan, R. and Kopecek, J. (1990) Release of macromolecules and daunomycin from hydrophilic gels containing enzymatically degradable bonds. *J. Biomater. Sci. Polym. Ed.* **1**, *4*, 261-78.

Sumpter, W. C. and Amundsen, L. (1932) The preparation of 5,7-di-iodoisatin. *J. Am. Chem. Soc.* **54**, 1917-1918.

Sun, Q. Y., Luria, A., Rubinstein, S. and Breitbart, H. (1998) Protein kinase inhibitors induce the interphase transition by inactivating mitogen-activated protein kinase in mouse eggs. *Zygote* **6**, *3*, 277-84.

Szekeres, T. and Novotny, L. (2002) New targets and drugs in cancer chemotherapy. *Med. Princ. Pract.* **11**, *3*, 117-25.

Tahir, S. K., Nukkala, M. A., Zielinski Mozny, N. A., Credo, R. B., Warner, R. B., Li, Q., Woods, K. W., Claiborne, A., Gwaltney, S. L., 2nd, Frost, D. J., Sham, H. L., Rosenberg, S. H. and Ng, S. C. (2003) Biological activity of A-289099: an orally active tubulin-binding indolyloxazoline derivative. *Mol. Cancer Ther.* **2**, *3*, 227-33.

Tamaoki, T. (1991) Use and specificity of staurosporine, UCN-01, and calphostin C as protein kinase inhibitors. *Methods Enzymol.* **201**, 340-7.

Teeyapant, R., Woerdenbag, H. J., Kreis, P., Hacker, J., Wray, V., Witte, L. and Proksch, P. (1993) Antibiotic and cytotoxic activity of brominated compounds from the marine sponge Verongia aerophoba. *Z. Naturforsch [C]* **48**, *11-12*, 939-45.

Todd, G. C., Gibson, W. R. and Morton, D. M. (1976) Toxicology of vindesine (desacetyl vinblastine amide) in mice, rats, and dogs. *J Toxicol Environ Health* **1**, *5*, 843-50.

Tozer, G. M., Kanthou, C., Parkins, C. S. and Hill, S. A. (2002) The biology of the combretastatins as tumour vascular targeting agents. *Int. J. Exp. Pathol.* **83**, *1*, 21-38.

Uppuluri, S., Knipling, L., Sackett, D. L. and Wolff, J. (1993) Localization of the colchicine-binding site of tubulin. *Proc. Natl. Acad. Sci. U S A* **90**, *24*, 11598-602.

van Stolk, R., Stoner, G., Hayton, W. L., Chan, K., DeYoung, B., Kresty, L., Kemmenoe, B. H., Elson, P., Rybicki, L., Church, J., Provencher, K., McLain, D., Hawk, E., Fryer, B., Kelloff, G., Ganapathi, R. and Budd, G. T. (2000) Phase I trial of exisulind (sulindac sulfone, FGN-1) as a chemopreventive agent in patients with familial adenomatous polyposis. *Clin. Cancer Res.* **6**, *1*, 78-89.

Vincent, E., Saxton, J., Baker-Glenn, C., Moal, I., Hirst, J. D., Pattenden, G. and Shaw, P. E. (2007) Effects of ulapualide A and synthetic macrolide analogues on actin dynamics and gene regulation. *Cell Mol. Life Sci.* **64**, *4*, 487-97.

Vine, K. L. 2002 Cytotoxicity of Marine Molluscs. Department of Biological Sciences. Univesity of Wollongong.

Vine, K. L., Locke, J. M., Ranson, M., Pyne, S. G. and Bremner, J. B. (2007) In vitro cytotoxicity evaluation of some substituted isatin derivatives. *Bioorg. Med. Chem.* **15**, *2*, 931-8.

Vitale, M., Zamai, L., Mazzotti, G., Cataldi, A. and Falcieri, E. (1993) Differential kinetics of propidium iodide uptake in apoptotic and necrotic thymocytes. *Histochemistry* **100**, *3*, 223-9.

Vitols, S. (1991) Uptake of low-density lipoprotein by malignant cells--possible therapeutic applications. *Cancer Cells* **3**, *12*, 488-95.

Voisin, E. M., Ruthsatz, M., Collins, J. M. and Hoyle, P. C. (1990) Extrapolation of animal toxicity to humans: interspecies comparisons in drug development. *Regul. Toxicol. Pharmacol.* **12**, *2*, 107-16.

Voorzanger-Rousselot, N. and Garnero, P. (2007) Biochemical markers in oncology. Part I: Molecular basis. Part II: Clinical uses. *Cancer Treat. Rev.* **33**, *3*, 230-283.

Vyas, S. P. and Sihorkar, V. (2000) Endogenous carriers and ligands in non-immunogenic site-specific drug delivery. *Adv. Drug. Deliv. Rev.* **43**, *2-3*, 101-64.

Vyas, S. P., Singh, A. and Sihorkar, V. (2001) Ligand-receptor-mediated drug delivery: an emerging paradigm in cellular drug targeting. *Crit. Rev. Ther. Drug Carrier Syst.* **18**, *1*, 1-76.

Wakefield, J. G., Stephens, D. J. and Tavare, J. M. (2003) A role for glycogen synthase kinase-3 in mitotic spindle dynamics and chromosome alignment. *J. Cell Sci.* **116**, *Pt 4*, 637-46.

Walz, G., Zanker, B., Brand, K., Waters, C., Genbauffe, F., Zeldis, J. B., Murphy, J. R. and Strom, T. B. (1989) Sequential effects of interleukin 2-diphtheria toxin fusion protein on T-cell activation. *Proc. Natl. Acad. Sci. U S A* **86**, *23*, 9485-8.

Wang, L. G. and Mencher, S. K. (2006) *Multiple faces of indirubin and its analogues in fighting cancer*. Indirubin, the red shade of indigo. L. Meijer, N. Guyard, A. L. Skaltsounis and G. Eisenbrand. Roscoff, France, Editions "Life in Progress" 247-58.

Wang, T. S., Malaspina, D. and Van Heertum, R. L. (1998) A simple method of preparation for [123I]-(S)-(-)-IBZM. *Appl. Radiat. Isot.* **49**, *4*, 369-72.

Weigelt, B., Peterse, J. L. and van 't Veer, L. J. (2005) Breast cancer metastasis: markers and models. *Nat. Rev. Cancer* **5**, *8*, 591-602.

Wender, P. A., DeBrabander, J., Harran, P. G., Jimenez, J. M., Koehler, M. F., Lippa, B., Park, C. M., Siedenbiedel, C. and Pettit, G. R. (1998) The design, computer modeling, solution structure, and biological evaluation of synthetic analogs of bryostatin 1. *Proc. Natl. Acad. Sci. U S A* **95**, *12*, 6624-9.

Wender, P. A. and Lippa, B. (2000) Synthesis and biological evaluation of bryostatin anaologues. *Tet. Lett.* **41**, 1007–1011.

Westley, C. B., Vine, K. L. and Benkendorff, K. (2006) *A proposed functional role for indole derivatives in reproduction and defence of the Muricidae*

(Neogastropoda: Mollusca). Indirubin, the red shade of indigo. L. Meijer, N. Guyard, L. Skaltsounis and G. Eisenbrand. Roscoff, France, Editions "Life in Progress" 23-44.

Witters, L., Engle, L. and Lipton, A. (2002) Restoration of estrogen responsiveness by blocking the HER-2/neu pathway. *Oncol. Rep.* **9**, *6*, 1163-6.

Wolfel, T., Hauer, M., Schneider, J., Serrano, M., Wolfel, C., Klehmann-Hieb, E., De Plaen, E., Hankeln, T., Meyer zum Buschenfelde, K. H. and Beach, D. (1995) A p16INK4a-insensitive CDK4 mutant targeted by cytolytic T lymphocytes in a human melanoma. *Science* **269**, *5228*, 1281-4.

Wu, C. L., Kirley, S. D., Xiao, H., Chuang, Y., Chung, D. C. and Zukerberg, L. R. (2001) Cables enhances cdk2 tyrosine 15 phosphorylation by Wee1, inhibits cell growth, and is lost in many human colon and squamous cancers. *Cancer Res.* **61**, *19*, 7325-32.

Xiao, Z., Hao, Y., Liu, B. and Qian, L. (2002) Indirubin and meisoindigo in the treatment of chronic myelogenous leukemia in China. *Leuk. Lymphoma* **43**, *9*, 1763-8.

Yamada, F. (2000) [Development of synthetic methods for 4-substituted indoles and their applications for the syntheses of natural products]. *Yakugaku Zasshi* **120**, *4*, 363-73.

Yu, H. and Rohan, T. (2000) Role of the insulin-like growth factor family in cancer development and progression. *J. Natl. Cancer Inst.* **92**, *18*, 1472-89.

Zang, M., Waelde, C. A., Xiang, X., Rana, A., Wen, R. and Luo, Z. (2001) Microtubule integrity regulates Pak leading to Ras-independent activation of Raf-1. insights into mechanisms of Raf-1 activation. *J. Biol. Chem.* **276**, *27*, 25157-65.

Zetter, B. R. (1998) Angiogenesis and tumor metastasis. *Annu. Rev. Med.* **49**, 407-24.

Zhang, B., Zhang, D. and Ren, H. (2000) [Resistance of Bcl-2 adenovirus vector to HepG(2) cell apoptosis induced by ethanol]. *Zhonghua Gan Zang Bing Za Zhi* **8**, *4*, 215-7.

Zhang, J. Y. (2002) Apoptosis-based anticancer drugs. *Nat. Rev. Drug Discov.* **1**, *2*, 101-2.

APPENDICES

Appendix 1

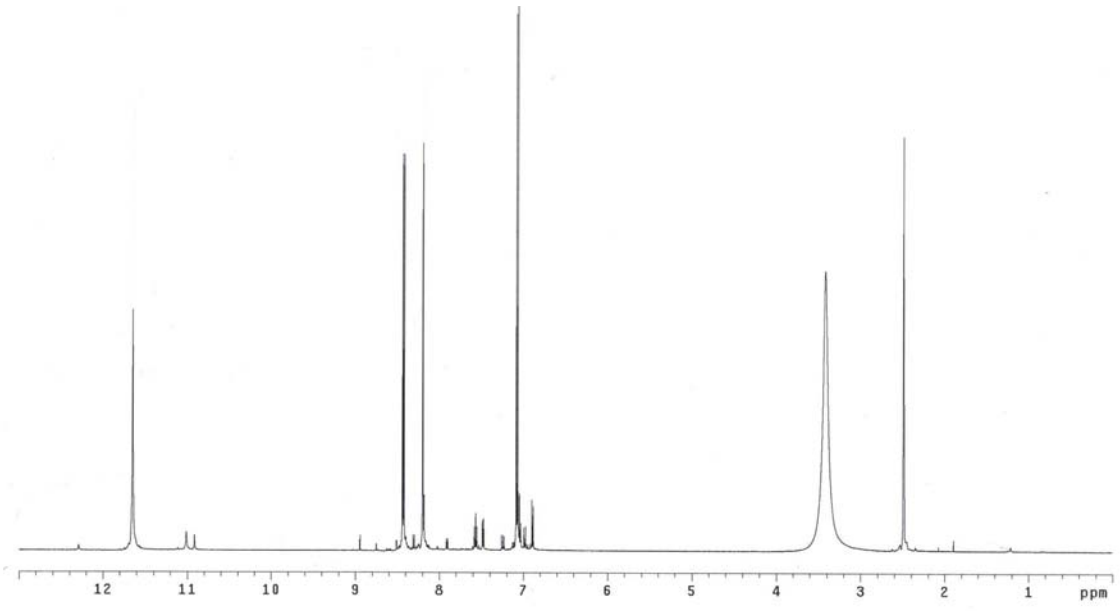

Figure A1.1 ^{1}H NMR spectrum of 5-nitroisatin (**11**)

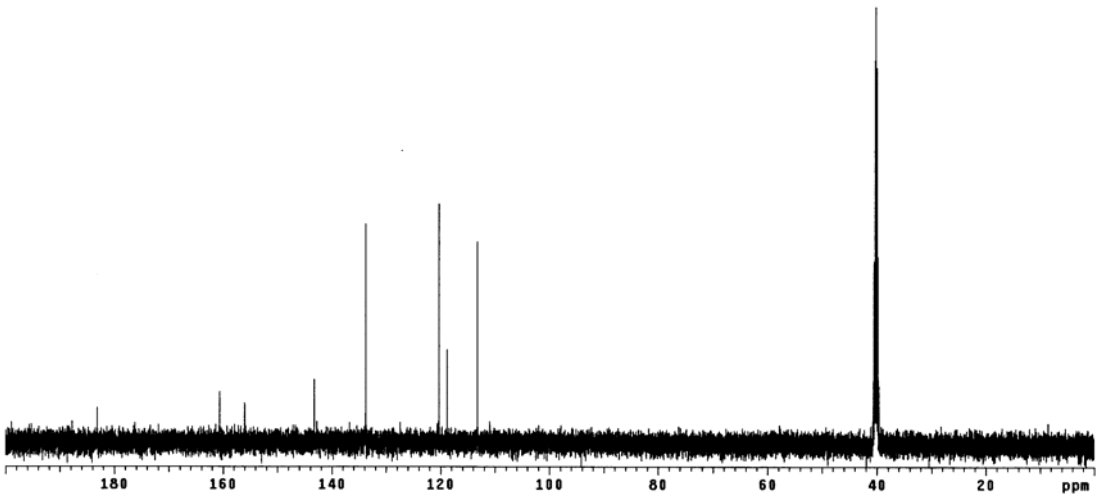

Figure A1.2 ^{13}C NMR spectrum of 5-nitroisatin (**11**)

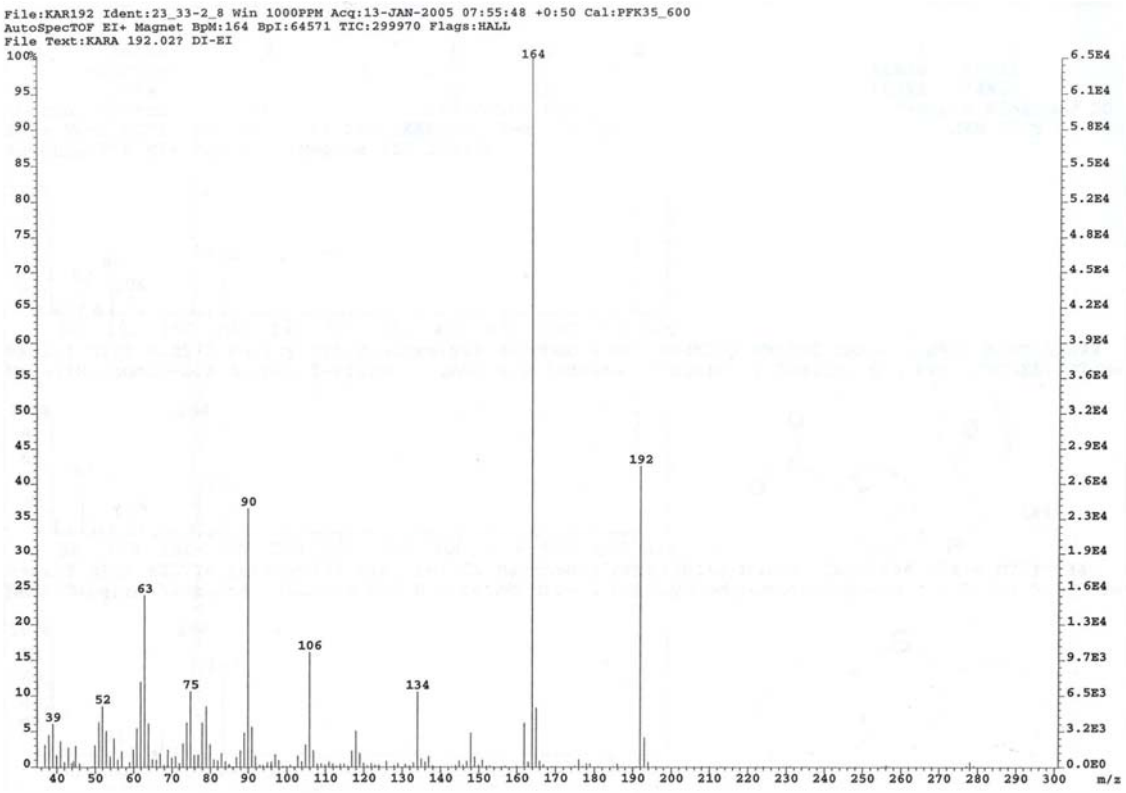

Figure A1.3 LREI-MS spectrum of 5-nitroisatin (**11**)

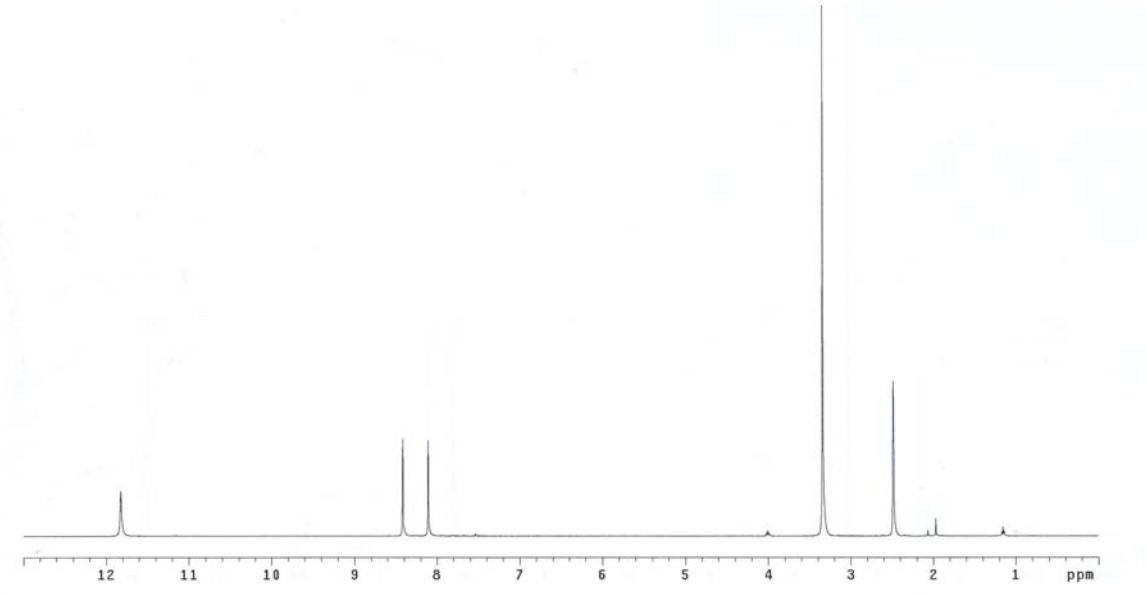

Figure A1.4 ^{1}H NMR spectrum of 5-Bromo-7-nitroisatin (**16**)

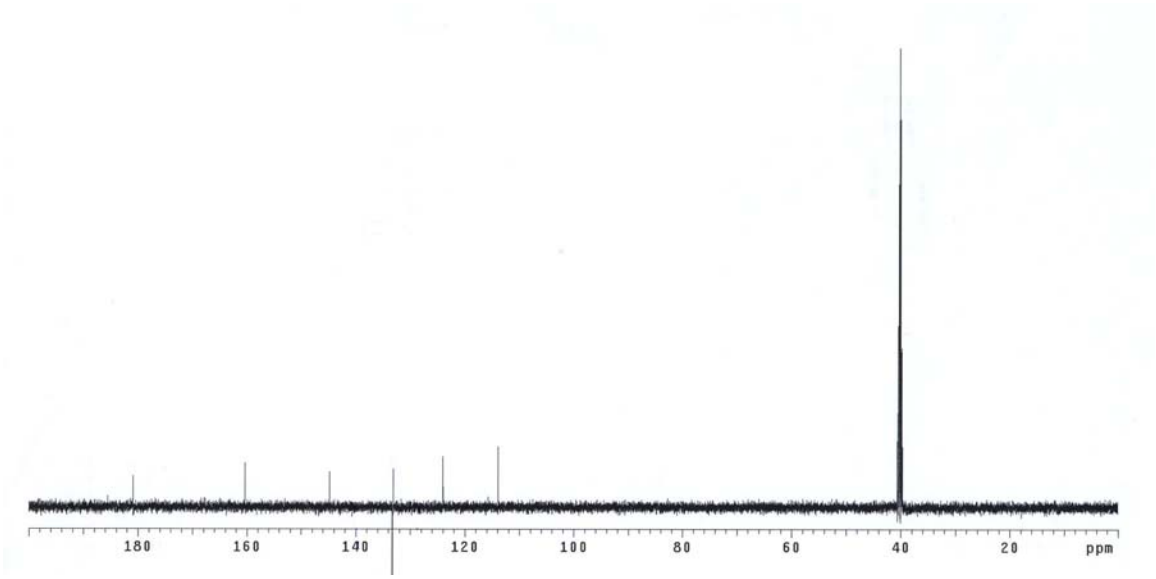

Figure A1.5 ^{13}C NMR spectrum of 5-bromo-7-nitroisatin (**16**)

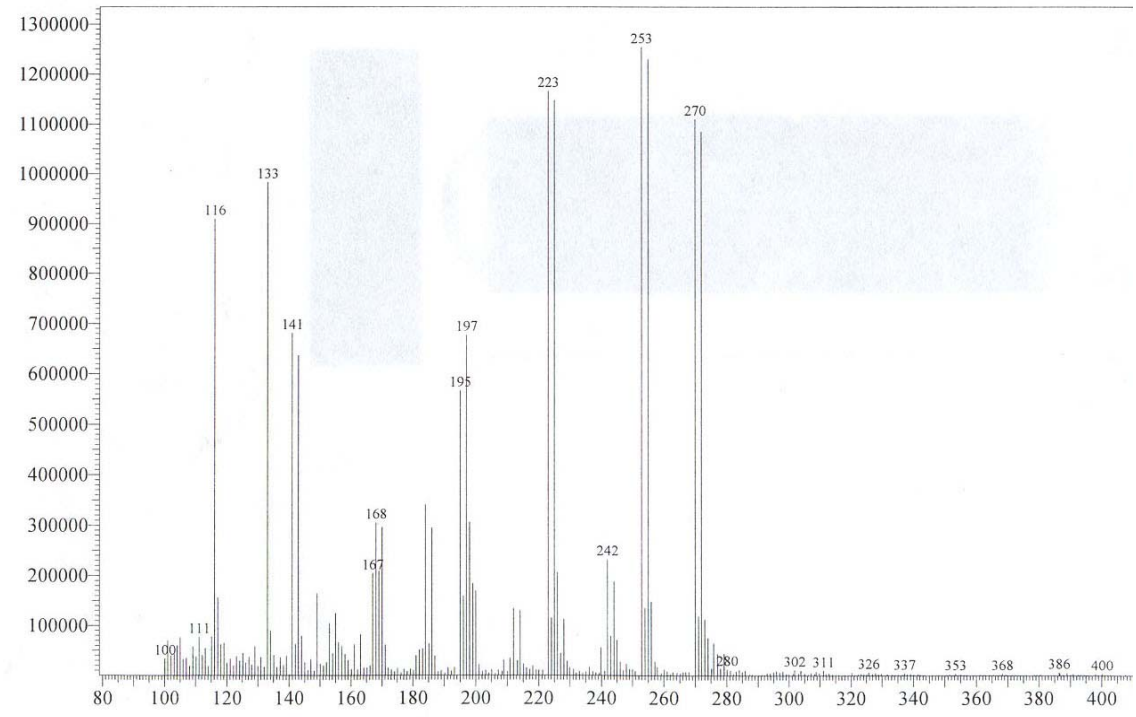

Figure A1.6 LREI-MS spectrum of 5-bromo-7-nitroisatin (**16**)

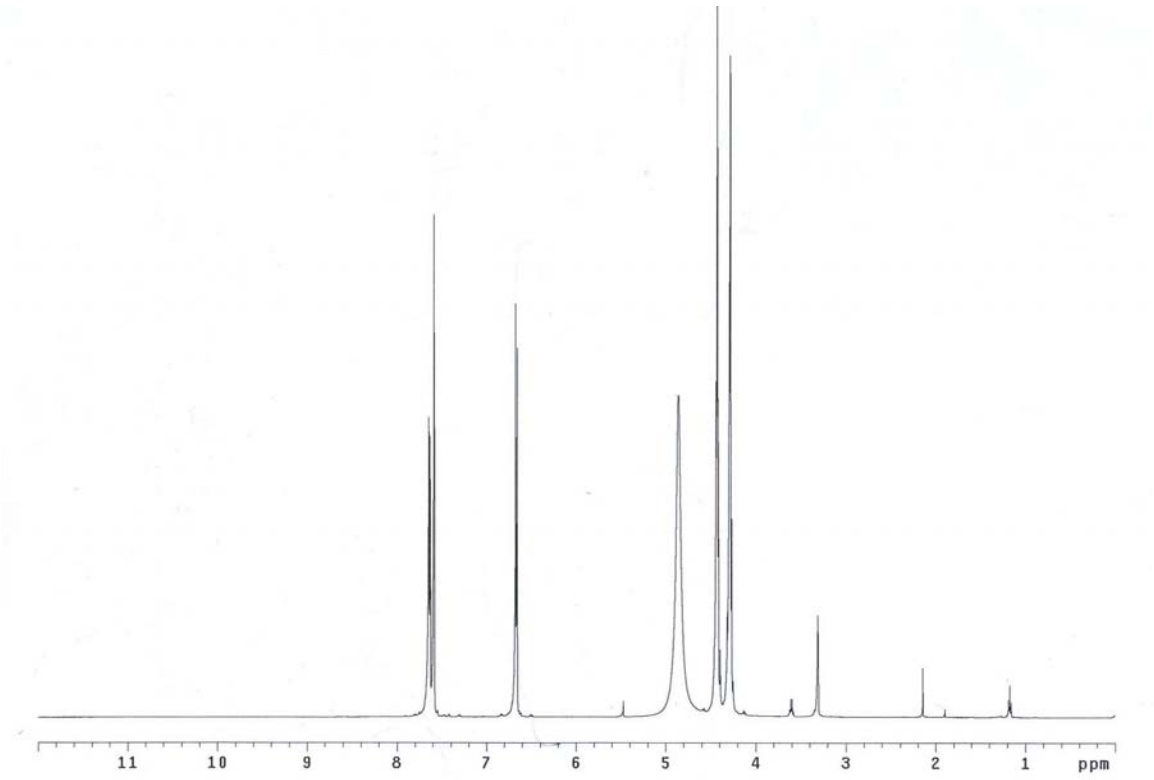

Figure A1.7 ^{1}H NMR spectrum of 5'-iodo-spiro[1,3-dioxolane-2,3'-[3*H*]indol]-2'(1'*H*)-one (**15a**)

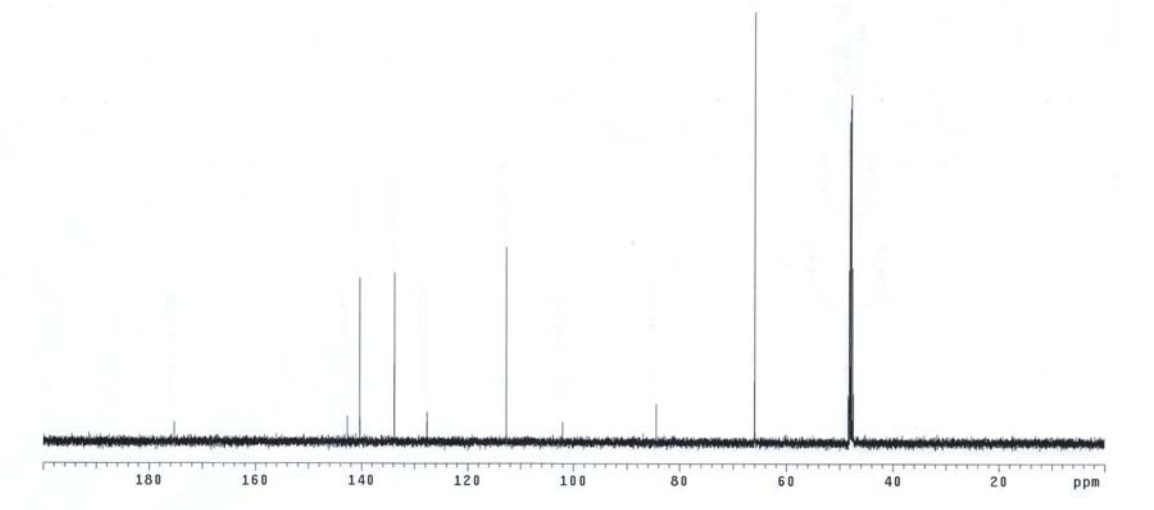

Figure A1.8 ^{13}C NMR spectrum of 5'-iodo-spiro[1,3-dioxolane-2,3'-[3*H*]indol]-2'(1'*H*)-one (**15a**)

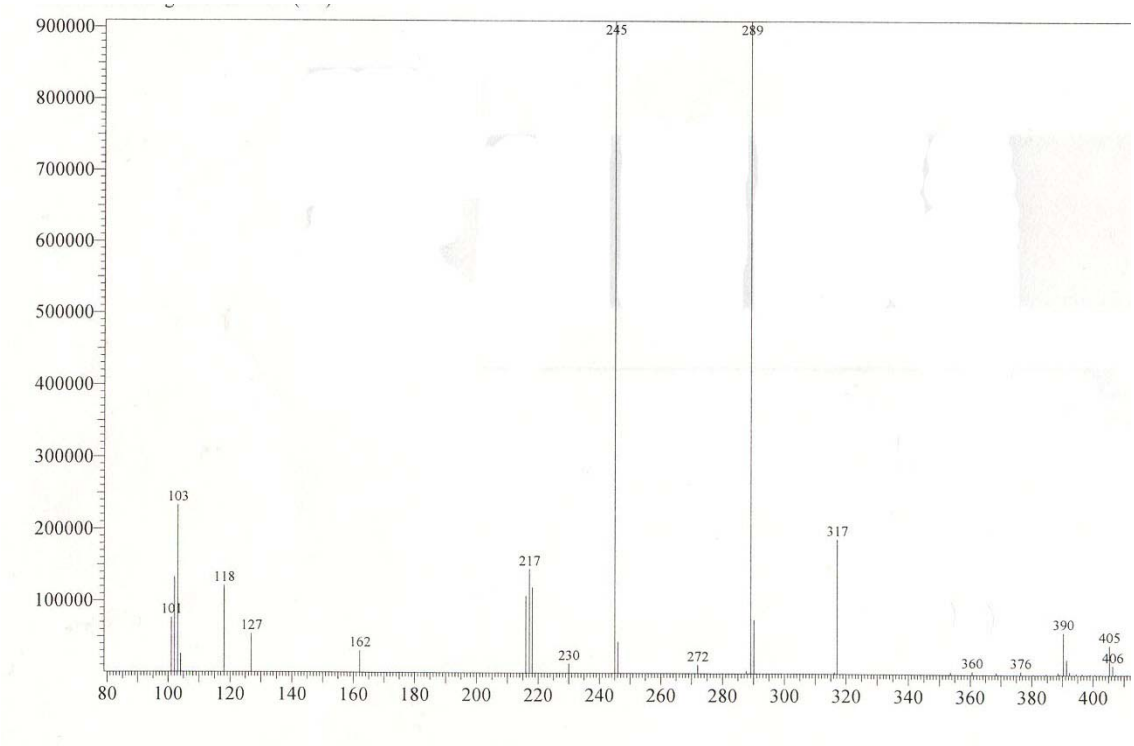

Figure A1.9 LREI-MS spectrum of 5'-iodo-spiro[1,3-dioxolane-2,3'-[3*H*]indol]-2'(1'*H*)-one (**15a**)

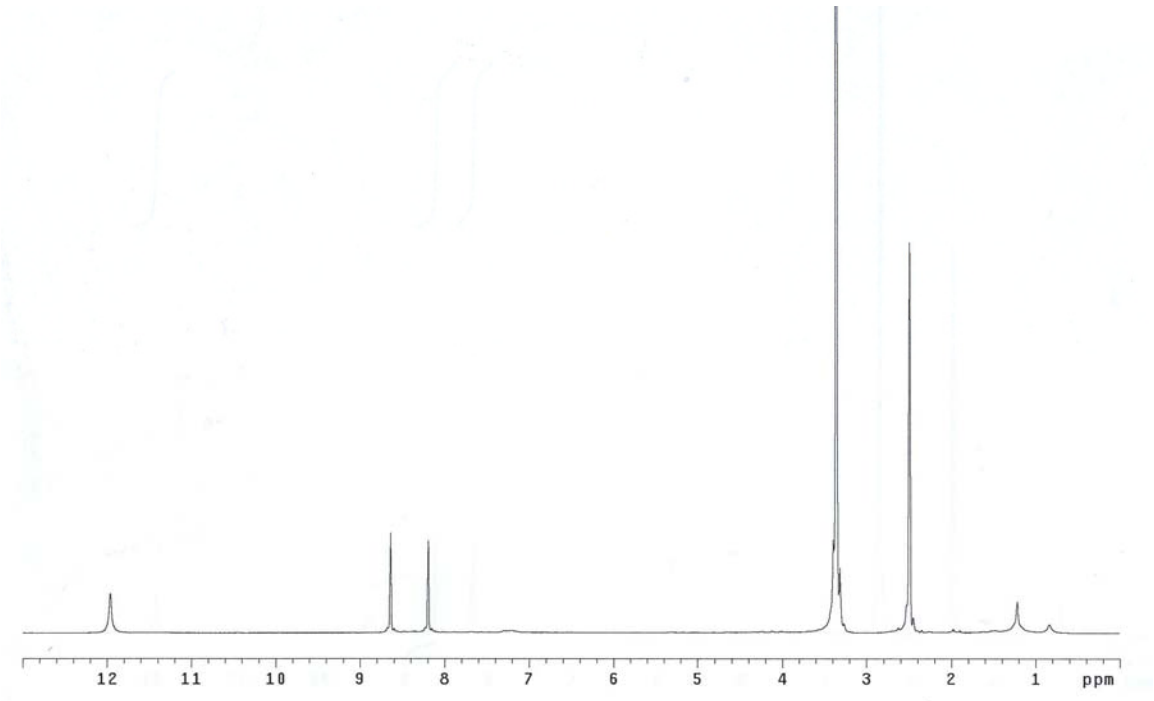

Figure A1.10 ^{1}H NMR spectrum of 7-bromo-5-nitroisatin (**18**)

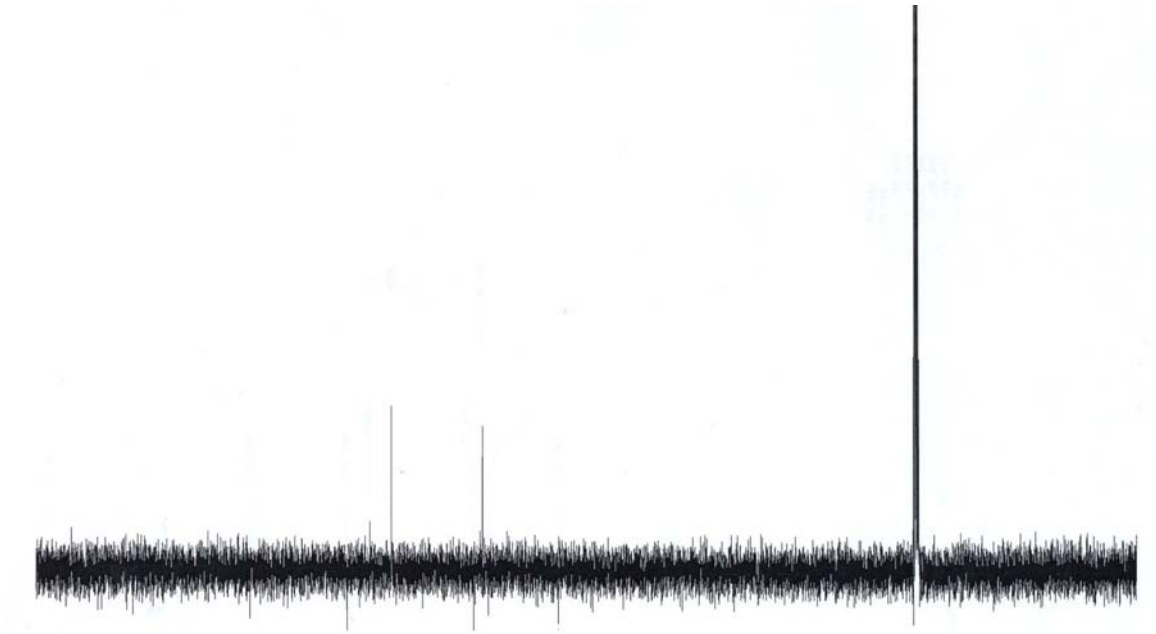

Figure A1.11 ^{13}C NMR spectrum of 7-bromo-5-nitroisatin (**18**)

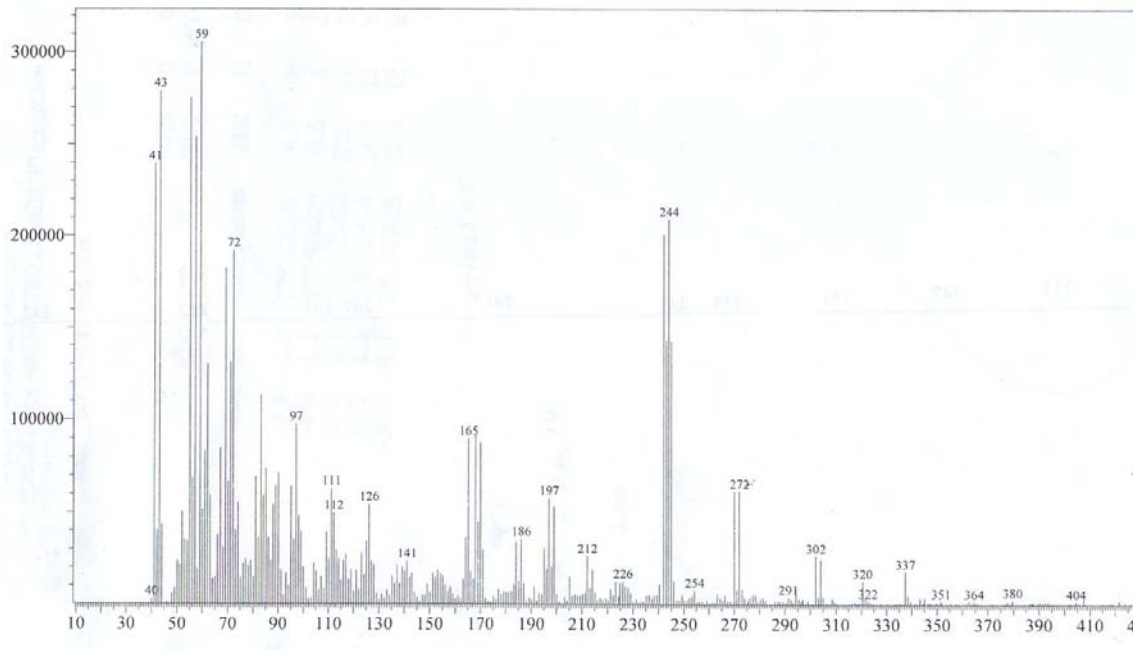

Figure A1.12 LREI-MS spectrum of 7-bromo-5-nitroisatin (**18**)

Appendix 2

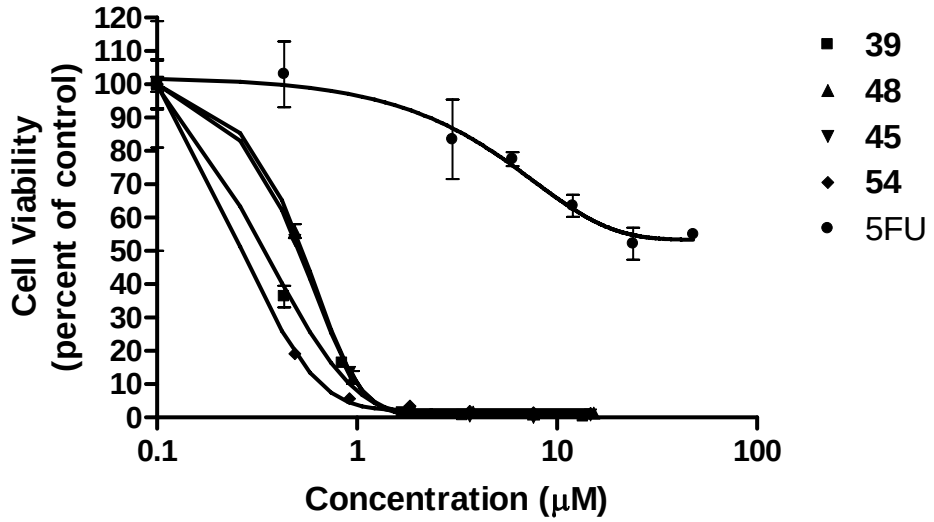

Figure A2.1 Viability of U937 cells after treatment with different concentrations of ●) 5,7-dibromo-*N*-(*p*-methylbenzyl)isatin (**39**), ▲) 5,7-dibromo-*N*-(*m*-methoxybenzyl)-isatin (**48**), ▼) 5,7-dibromo-*N*-(*p*-methoxybenzyl)isatin (**45**), ♦) 5,7-dibromo-*N*-(*p*-trifluoromethylbenzyl)isatin (**54**) and ■) 5-fluorouracil (5-FU). Briefly, cells were incubated for 24 h at 37 °C (95% humidity, 5% CO_2) with increasing concentrations of test compounds, then analysed for a change in metabolic activity and expressed as percent viability in reference to the DMSO control. Each data point is a mean of triplicates ± SE.

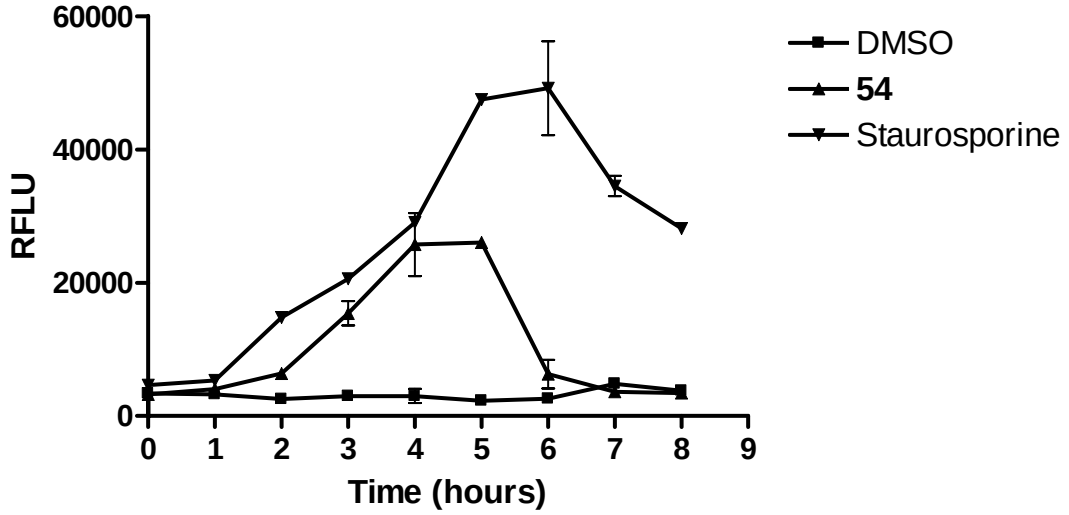

Figure A2.2 Activation of the effector Caspases 3 and 7 in Jurkat cells. Cells (2.0×10^4) were exposed to either ■ 2.5% DMSO vehicle control, ▲ 7 μM 5,7-dibromo-*N*-(*p*-trifluoromethylbenzyl)isatin (**54**) or ▼ 2 μM staurosporine for up to 8 h at 37°C. Cells were then incubated with the Caspase-3/7 reagent for 1 h at room temperature and fluorescence measured at an excitation wavelength of 485 nm and 520 nm emission. Data are means ± SE of one representative experiment performed in triplicate.

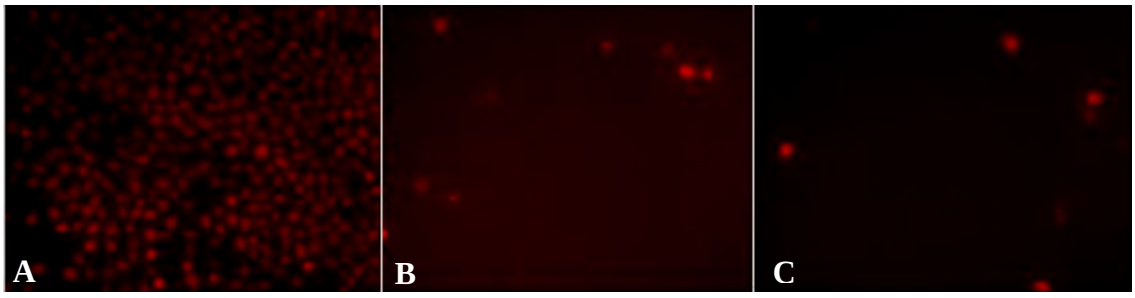

Figure A2.3 Cell associated fluorescence of U937 cells after treatment with the representative *N*-alkylisatin 5,7-dibromo-*N*-(*p*-methylbenzyl)isatin (**39**). Cells were treated with either A) a high concentration of **39** 30 μM (12.5 μg/mL), or B) a low concentration of **39** 1 μM (0.39 μg/mL) or C) 2.5% DMSO vehicle control for 24 h. Cells were then stained with 1 mg/mL PI (final concentration 10 μg/mL) and assessed for fluorescence with a 488nm excitation laser viewed at 40 × magnification on a Leica DM IL inverted contrasting fluorescence microscope.

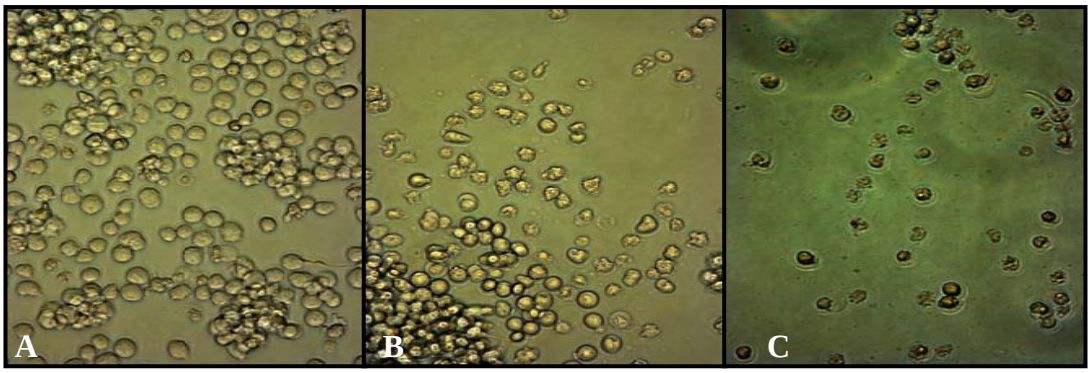

Figure A2.4 Morphological effects of staurosporine on human leukemic (Jurkat) T-cells. Briefly cells (1.0×10^4) were prepared as described in Chapter 4, Section 4.3.2.1 and incubated with either A) DMSO vehicle control for 24 h, B) staurosporine 2 μM for 5 h, or C) staurosporine 2 μM for 24 h. Images were obtained by brightfield microscopy on an inverted light microscope using a Leica DC500 12-megapixel high-performance FireWire camera system. Images were viewed at 1000 × magnification.

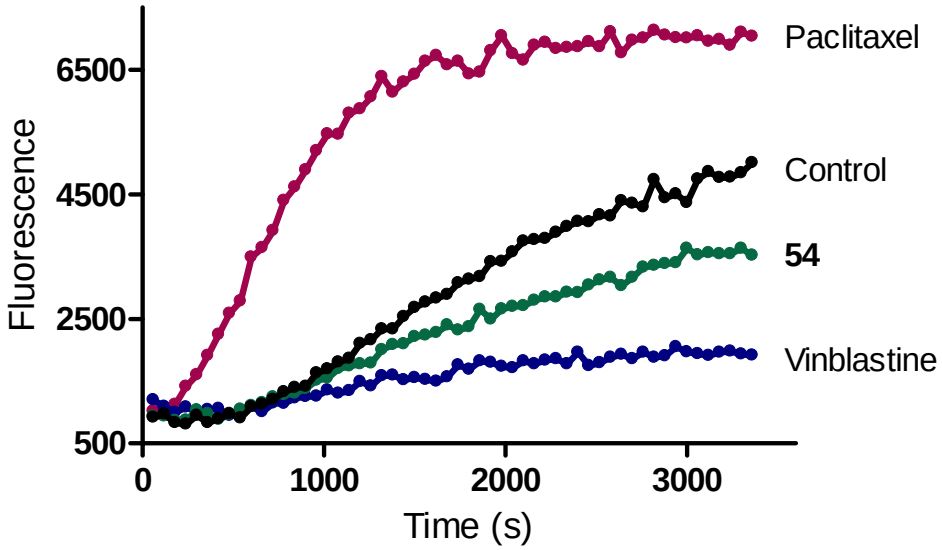

Figure A2.5 The effect of compound **54** and commercial anticancer agents on tubulin polymerization as determined in the *in vitro* microtubule polymerization assay. Purified bovine neuronal tubulin was used to assay for microtubule formation in the presence of either: ●) vehicle control, ●) paclitaxel 3 μM, ●) vinblastine sulfate 3 μM or ●) 5,7-dibromo-*N*-(*p*-trifluoromethylbenzyl) isatin (**54**) 3 μM at 37°C. A shift of the curve to the left or right of the control is indicative of either an increase or decrease, respectively, in the rate of tubulin polymerization. Changes in fluorescence were measured at an excitation wavelength of 360 ±10 nm and the fluorescence was collected at 440 ±10 nm. Data points are the means of duplicate experiments. SD values were omitted for clarity and were always less than 10% of the mean.

Appendix 3

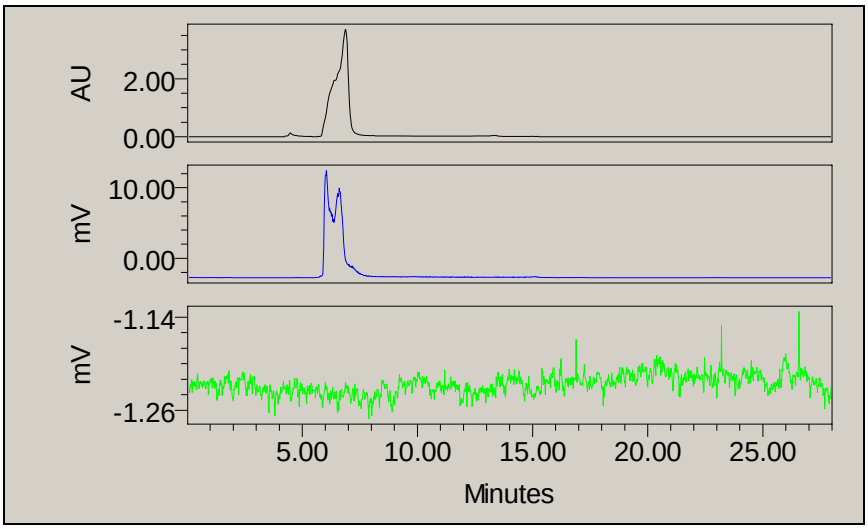

Figure A3.1 HPLC chromatogram of compound **67** after preparation with Chloramine-T as the oxidizing agent (method described in Chapter 5, Section 5.2.2.4, Method 1). Compound **67** was dissolved in mobile phase (ACN/H_2O 65/35 + 0.01% TFA and injected into a HPLC (Phenomenex Bondclone C18 300 × 7.8 mm, 2 mL/min). No activity was associated with the UV trace of the cold material (compound **65**, data not shown) at 13.2 min. AU = UV/Vis detector, mV = radioactivity detector.

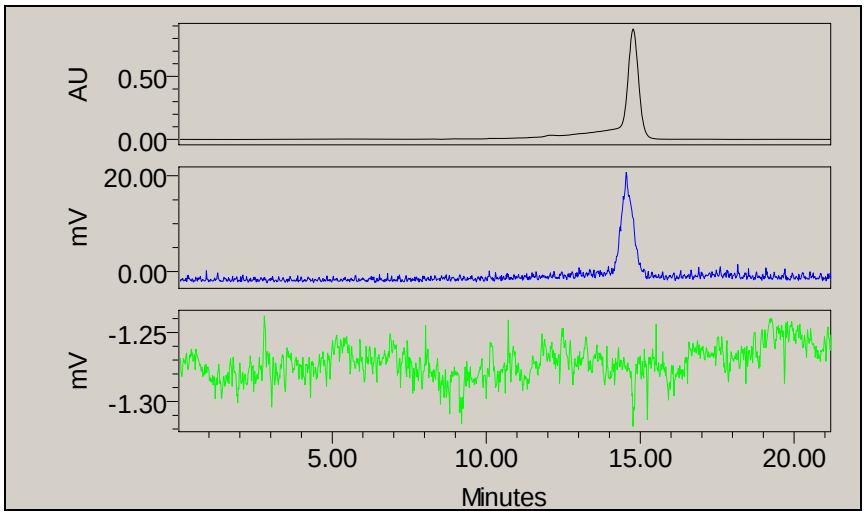

Figure A3.2 HPLC chromatogram of compound **67** after preparation with peracetic acid solution (37%) as the oxidizing agent (method described in Chapter 5, Section 5.2.2.4, Method 2). Compound **67** was dissolved in mobile phase (ACN/H_2O 65/35 + 0.01% TFA and injected into a HPLC (Phenomenex Bondclone C18 300 × 7.8 mm, 2 mL/min). Activity was associated with the UV trace of the cold material (compound **65**) at 14.8 min. AU = UV/Vis detector, mV = radioactivity detector.

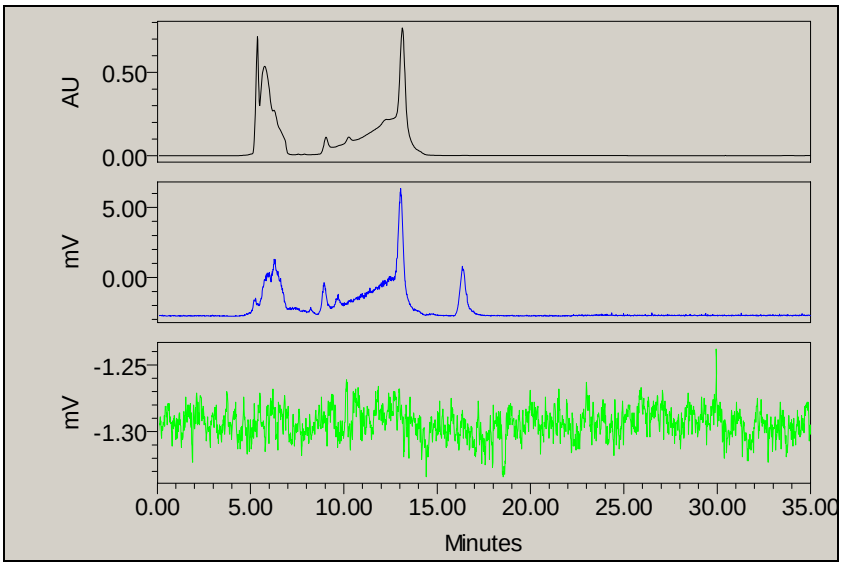

Figure A3.3 HPLC chromatogram of compound **68** after preparation with a peracetic acid: acetic acid solution (1:10 v/v) as the oxidizing agent (method described in Chapter 5, Section 5.2.2.5, Method 1). Compound **68** was dissolved in mobile phase (ACN/H_2O 80/20 + 0.1% TFA) and injected into a HPLC (Phenomenex Bondclone C18 300 × 7.8 mm, 2 mL/min). Activity was associated with the UV trace of the cold material (compound **66**) at 13.3 min. AU = UV/Vis detector, mV = radioactivity detector.

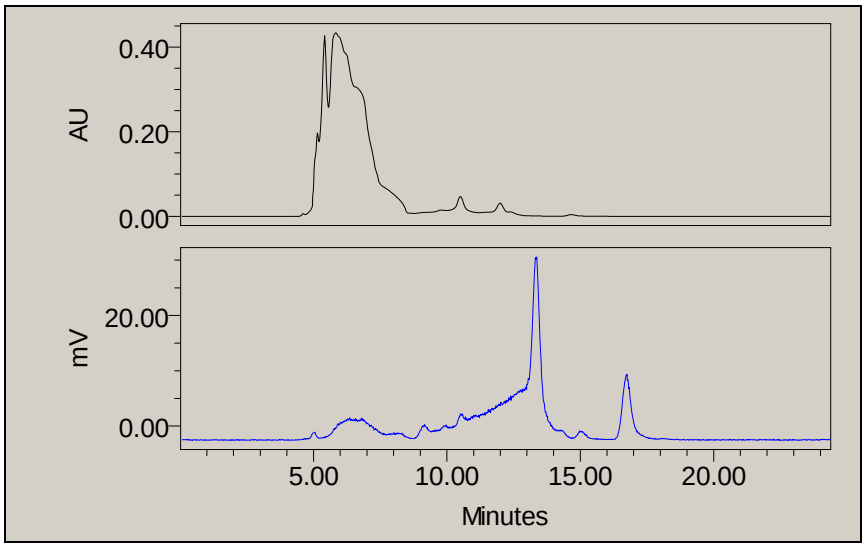

Figure A3.4 HPLC chromatogram of compound **68** after preparation with a peracetic acid: acetic acid solution (1:1 v/v) as the oxidizing agent (method described in Chapter 5, Section 5.2.2.5, Method 2). Compound **68** was dissolved in mobile phase (ACN/H_2O 80/20 + 0.1% TFA) and injected into a HPLC (Phenomenex Bondclone C18 300 × 7.8 mm, 2 mL/min). Activity was associated with the UV trace of the cold material (compound **66**) at 13.3 min (Figure A3.3). AU = UV/Vis detector, mV = radioactivity detector.

A3.1 Human Amelanotic Melanoma (A375) Xenograft in Nude Mice

A3.1.1 Preparation of A375 Cells for Injection into Balb/c Nu/Nu Mice

In a biohazard cabinet, media was aseptically removed from cells in a 175 cm^2 flask by pipetting out and disposing. To the flask of cells, trypsin (~2 mL) was added, to wash the bottom of the flask and immediately removed. Fresh trypsin (~2 mL) was then added to the flask and placed into a 37°C, 5% CO_2 incubator until all cells had detached from the base of the flask. To the flask, 25 mL of phosphate buffered saline (PBS) without Ca^{2+} and Mg^{2+} was added aseptically and pipetted to mix. The entire contents of the flask was then transferred to a sterile 50 mL centrifuge tube, and centrifuged at 500 ×*g* for 5 min. After centrifugation the supernatant was removed and the pellet resuspended by gentle flicking of the tube. To the pellet, PBS (~2 mL) was added and mixed well, noting the entire volume. A small amount (< 500 µL) of the cell suspension was then aliquoted into an eppendorf tube. From the eppendorf a 10 × dilution with trypan blue was prepared (20 µL of cells suspension and 180 µL of trypan blue) and counted using a haemocytometer at 10 × magnification. The 4 outer squares of the grid were counted for live (clear) and dead (blue) cells. From the haemocytometer results the cell concentration was determined, as well as the cell viability. From the calculated cell concentration, appropriate dilutions were undertaken to achieve a viable cell injection concentration of 1×10^7 cells/mL (1×10^6 cells/ 0.1 mL injection). The cells were aliquoted into 2 mL sterile tubes and kept on ice during the injections, ensuring that the cell suspension was shaken and dispersed adequately before charging each syringe.

A3.1.2 Injection of A375 cells into Balb/c Nu/Nu Mice for Imaging

Mice were restrained by the scruff of the neck by one operator, whilst the other operator held onto the tail, laying the mouse on its right side. Each syringe (29 g 0.33 mm × 12.7 mm insulin syringe) was charged to 0.1 mL with prepared cell suspension by first filling up and down 3 times and ensuring there were no air bubbles. The syringe was held parallel to the hind flank and inserted so that half the needle was under the skin. The syringe was then gently lifted to ensure that the needle has not entered into the muscle of the flank and ejected, delivering the cell suspension subcutaneously (s.c.).The needle was then withdrawn and any cell suspension that may have leaked out from the point of injection was removed with wiping. All mice were given coloured markings on their tails for identification and had their weights recorded along with their monitoring checklist.

A3.2 Rat 13762 MAT B III Mammary Adenocarcinoma in F344 Fisher Rats

A3.2.1 Preparation of Rat 13762 MAT B III Cells for Injection into F344 Fisher Rats

In a biohazard cabinet, cells were aseptically removed from the flask by pipetting and placed into sterile 50 mL centrifuge tubes. Cells were then centrifuged for 5 min at 500 rpm. After centrifugation the supernatant was removed and the pellet resuspended by gentle flicking of the tube. To the pellet, PBS (~10 mL) without Ca^{2+} and Mg^{2+} was added and mixed, noting the entire volume. A small amount (< 500 μL) of the cell suspension was aliquoted into an eppendorf tube. From the eppendorf tube a 10 × dilution with trypan blue was prepared (20 μL of cell suspension and 180 μL of trypan blue) and counted using a haemocytometer at 10 × magnification. The 4 outer squares

of the grid were counted for live (clear) and dead (blue) cells. From the haemocytometer results the cell concentration was determined, as well as the cell viability. The cells were then centrifuged at 500 rpm for 5 min and the supernatant removed The appropriate amount of PBS without $Ca^{2+}$and Mg^{2+} was added aseptically to produce 1×10^7 cells/mL (1×10^6 cells/ 0.1 mL injection) and pipetted to mix. The cells were aliquoted into 2 mL sterile tubes and kept on ice during the injections, ensuring that the cell suspension was shaken and dispersed adequately before charging each syringe.

A3.2.1 Injection of Rat 13762 MAT B III Cells into F344 Fisher Rats for Imaging

Inhalant isoflurane anesthetic mixed with 200 cc/min oxygen through an anesthetic diffuser was administered to the rat *via* a nose cone. Once the rat's tail had become flaccid, hair from the left flank of the animal was removed by shaving in preparation for injection. Each syringe (29 g 0.33 mm × 12.7 mm insulin syringe) was charged to 0.1 mL with prepared cell suspension by first filling up and down 3 times and ensuring there were no air bubbles. A small amount of the shaved skin was gathered by gentle pinching and was lifted away from the body. The needle was inserted completely into this gathered skin with the syringe being held horizontal to the animal as the cell suspension was ejected (s.c.). Light pressure was applied to the injection site as the syringe was removed to minimise cell leakage. The animal was then removed from anesthetic, was identified by colouring with markers on the tail and had its weight and monitoring checklist recorded. Animals were monitored until complete recovery from anesthetic.

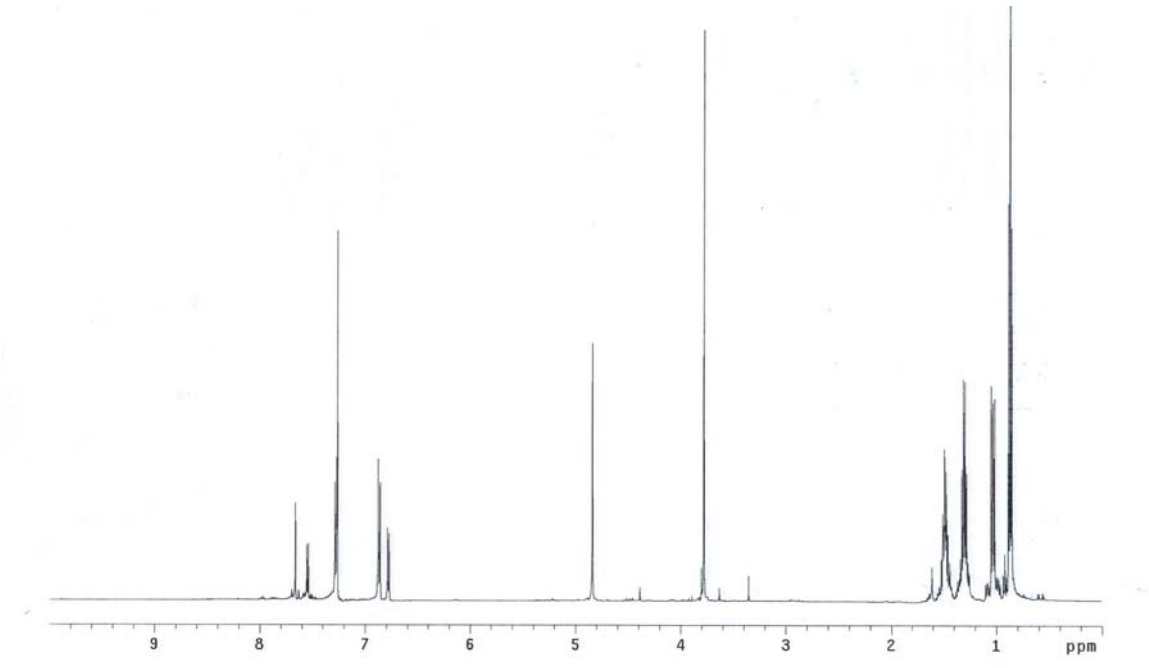

Figure A3.5 ^{1}H NMR spectrum of *N*-(*p*-methoxybenzyl)-5-(tributylstannyl)isatin (**65**)

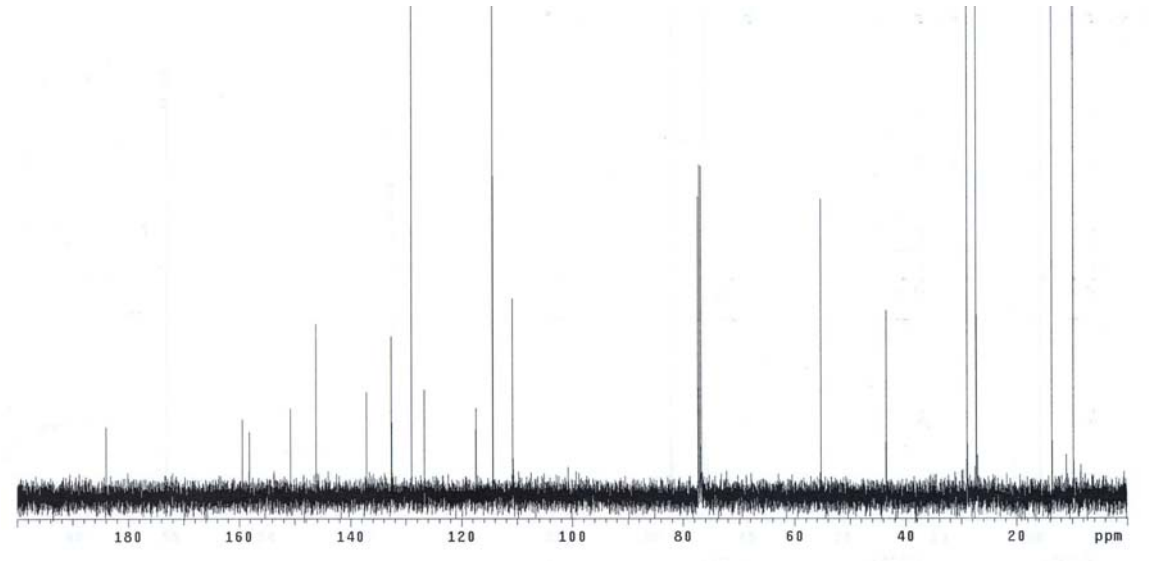

Figure A3.6 ^{13}C NMR spectrum of *N*-(*p*-methoxybenzyl)-5-(tributylstannyl)isatin (**65**)

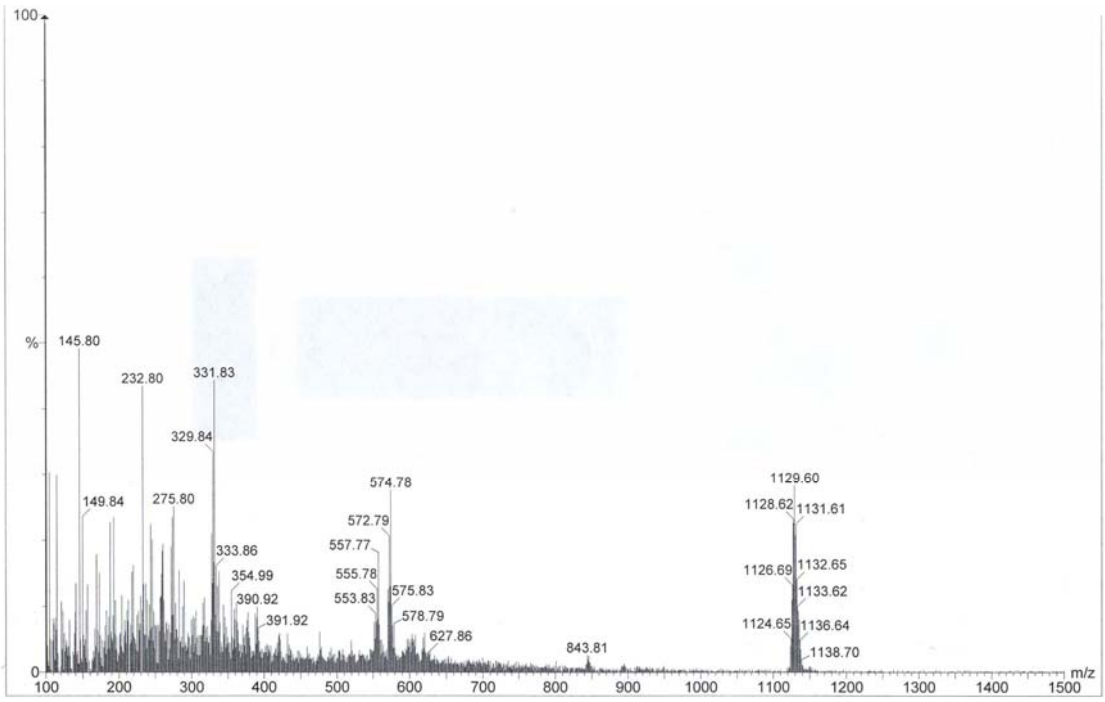

Figure A3.7 HREI-MS spectrum of *N*-(*p*-methoxybenzyl)-5-(tributylstannyl)isatin (**65**)

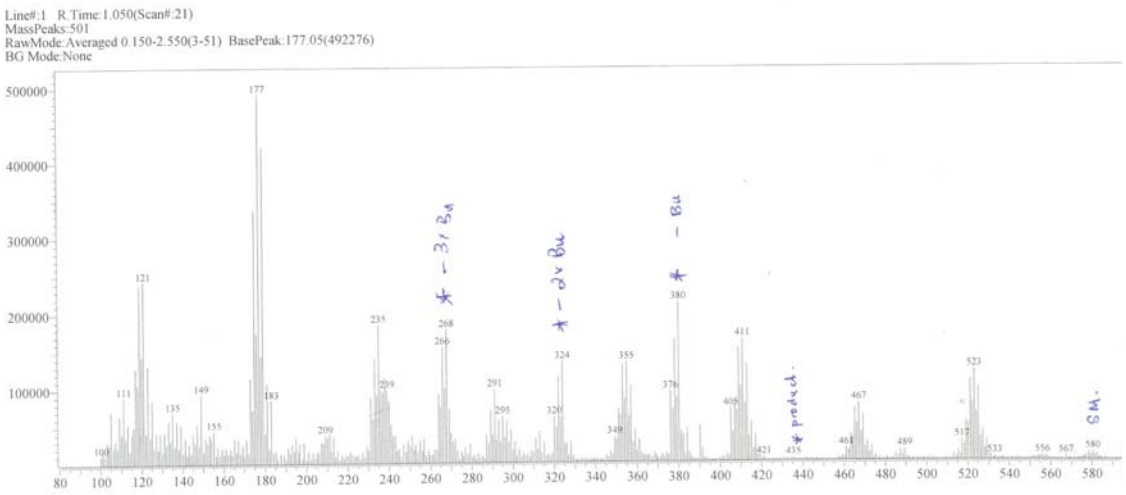

Figure A3.8 LREI-MS spectrum of 5-(tributylstannyl)isatin (**64**)

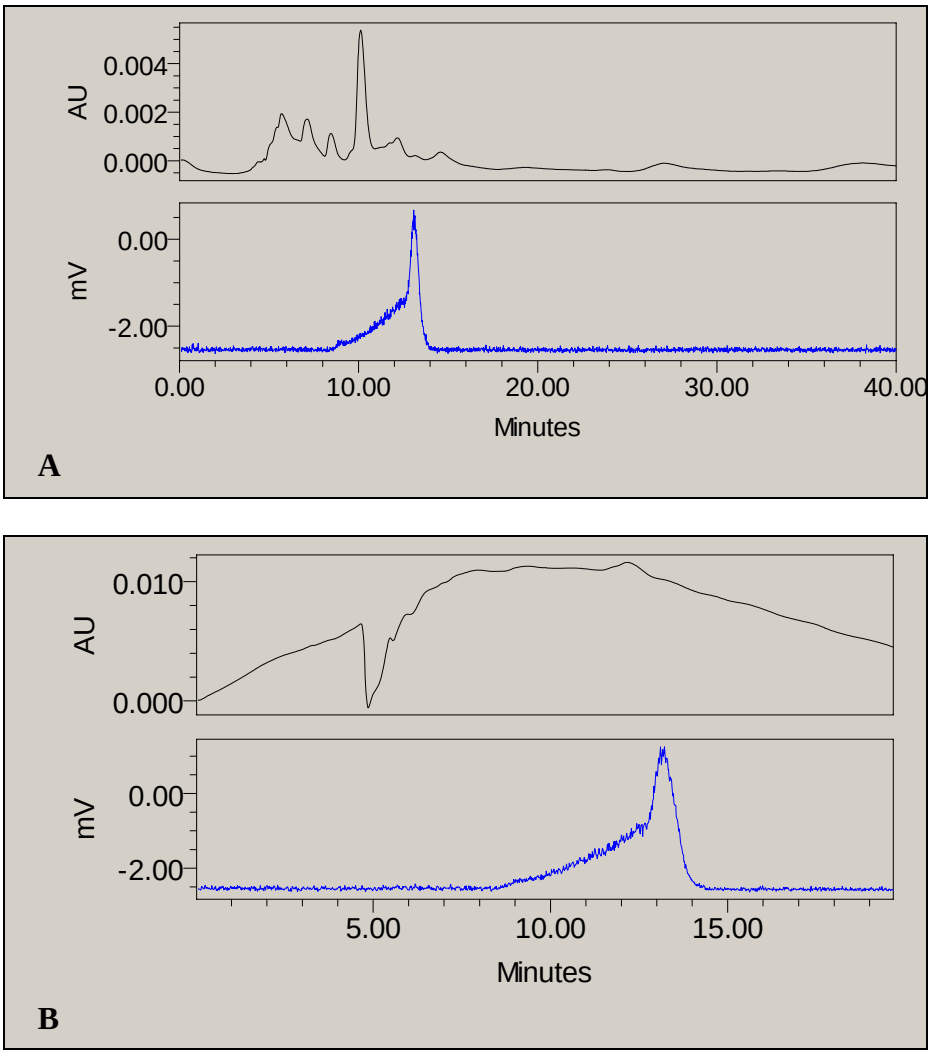

Figure A3.9 HPLC chromatogram of **68** showing compound integrity over time. Compound **68** was dissolved in mobile phase (ACN/H_2O 80/20 + 0.1% TFA) and injected into a HPLC (Phenomenex Bondclone C18 300 × 7.8 mm, 2 mL/min) A) 70 min or B) 120 min post synthesis. No compound breakdown was detected at either time point, with activity peaks at 13.3 min corresponding to those of freshly prepared material (Figure A3.3). AU = UV/Vis detector, mV = radioactivity detector.

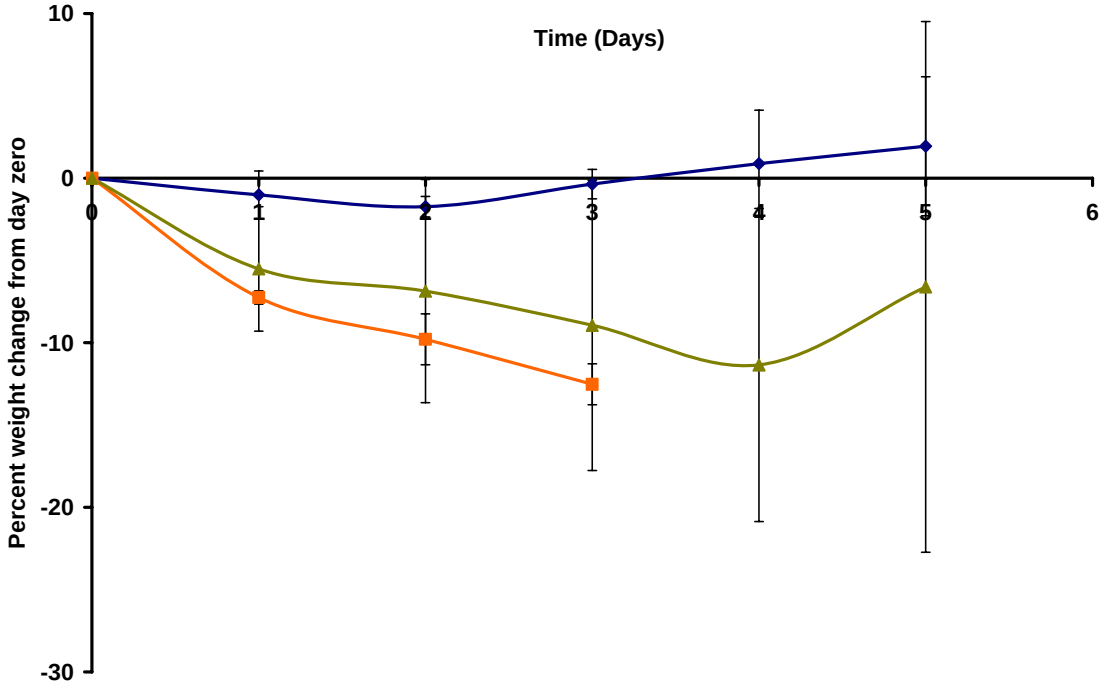

Figure A3.10 Average weight change from day zero of mice treated with 5,7-dibromo-*N*-(*p*-trifluoromethylbenzyl)isatin (**54**). Breifly, Balb/c mice were administered either ● DMSO vehicle control or 40 mg/kg of compound **54** and sacrificed ▲ 3 days or ■ 5 days post administration and organs assessed histopathologically for toxicity. Animal weights were recorded and compared to weight change from day zero. Data points are the means of $n = 4 \pm$ SD.

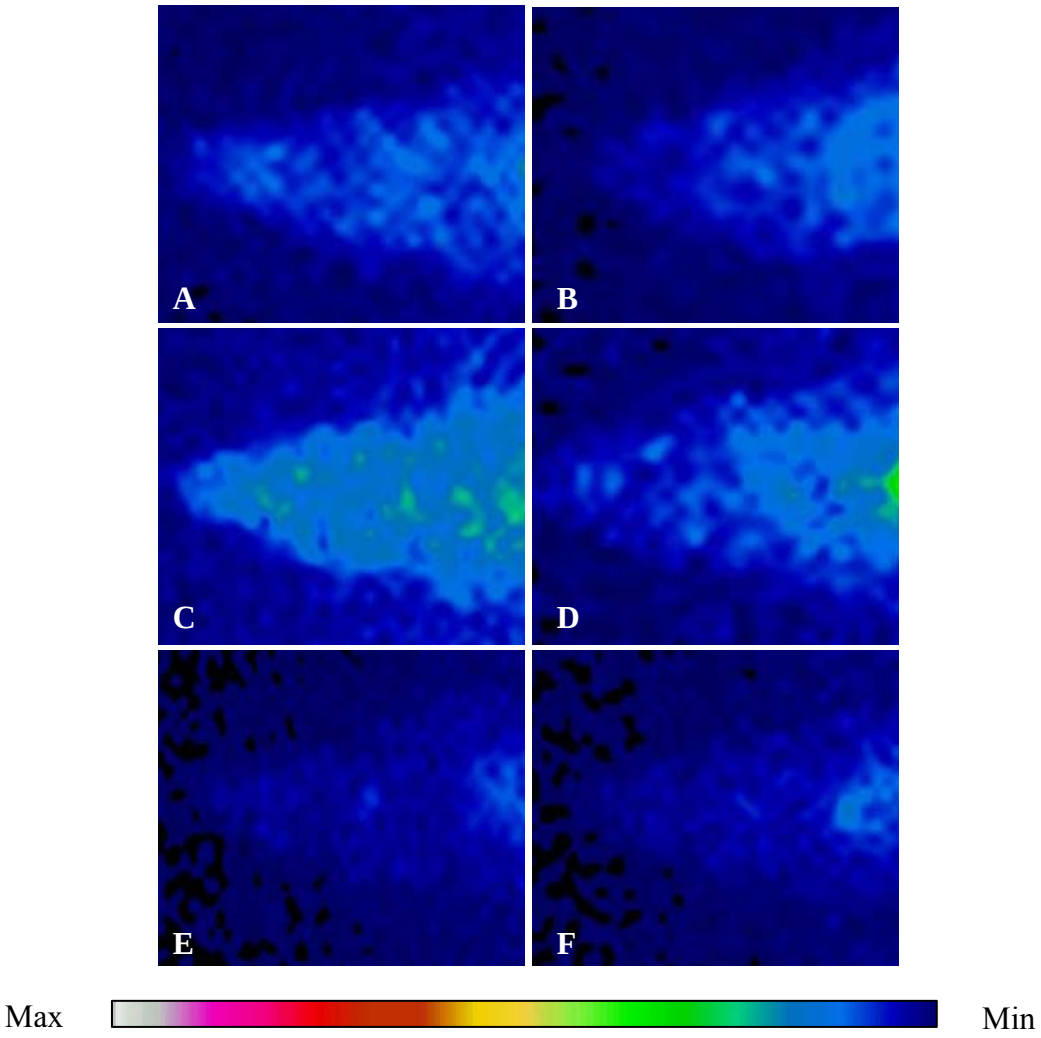

Figure A3.11 SPECT imaging of ^{123}I labeled compounds **67** (left panels) and **68** (right panels) in the heads of F344 Fisher rats bearing 13762 MAT B III mammary adenocarcinoma. Images were obtained at A and B) 1 h min, C and D) 3 h 20 min, E and F) 6 h 15 min post injection. Rats were injected *via* the tail vein with 100 µL of 5 µCi/µL radiotracer in 0.9% saline and 5% EtOH. Images are one representative animal from experiments performed in duplicate.

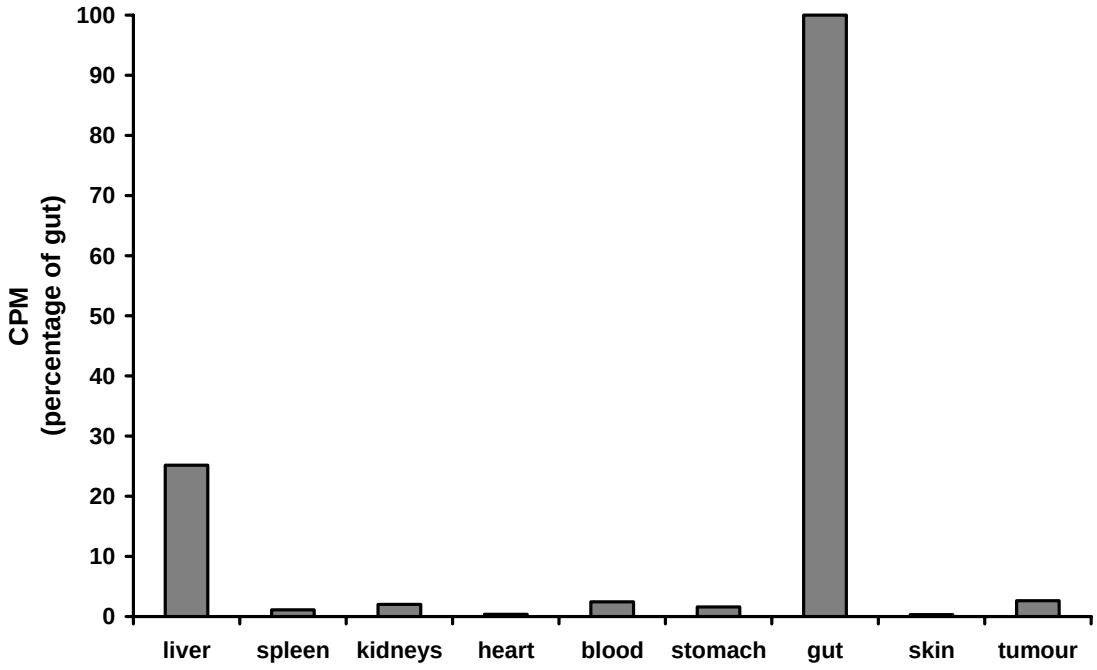

Figure A3.12 Crude biodistribution of the ^{123}I labeled compound **68** in a F344 Fisher rat bearing 13762 MAT B III mammary adenocarcinoma. Briefly, after the 72 h imaging time point, the liver, spleen, kidneys, heart, blood (2 mL), stomach, gut, skin and tumour were collected from one representative rat and the activity counted. Activity is expressed as the percentage of the maximum activity detected in the gut.

Appendix 4

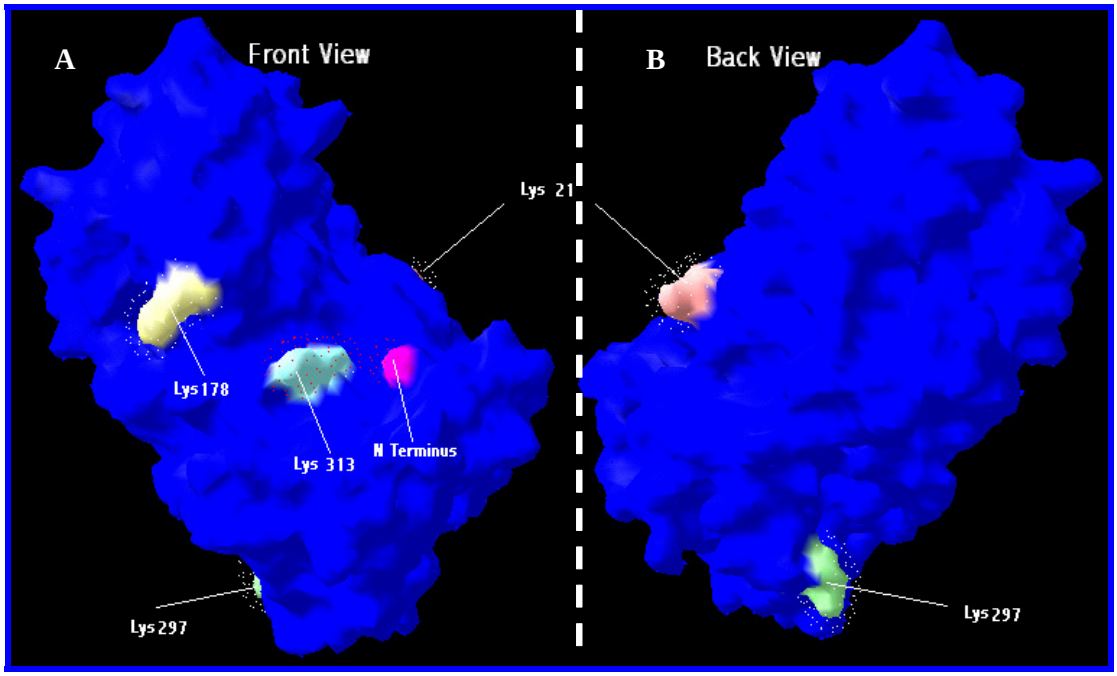

Figure A4.1 Lysine sites available for amide bond formation with compound **70** and **72**. The 3D models were prepared using SwissModel® program from ExPaSy server by Fares Al-Ejeh (PhD candidate, School of Biological Sciences, UOW). PAI-2 coordinates were obtained from Protein Data Bank (PDB). Modelling of PAI-2 was performed using these coordinates and surface modelling was performed using OpenGL settings marking residues that fit the criteria of having free amino groups with > 50% accessibility.

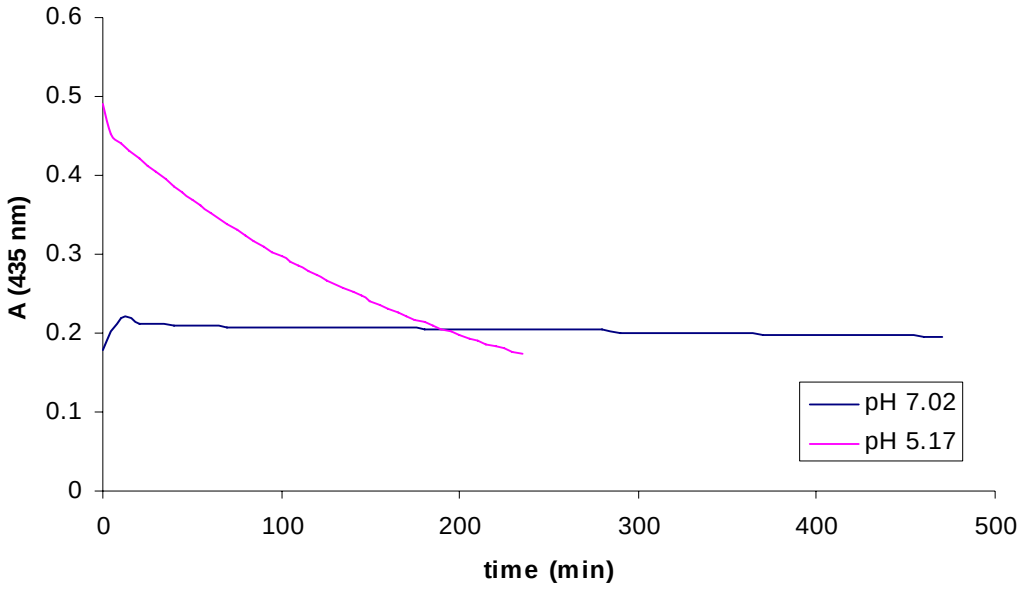

Figure A4.2 The stability of compound **72** in sodium acetate buffer at pH 7.02 and 5.17. Hydrolysis of the imine bond was monitored by measuring the absorbance at 435 nm for a period of up to 8 h, by Dr Julie Locke (Postdoctoral Research Fellow, Department of Chemistry, UOW). At pH 5.17 T½ = 120 min.

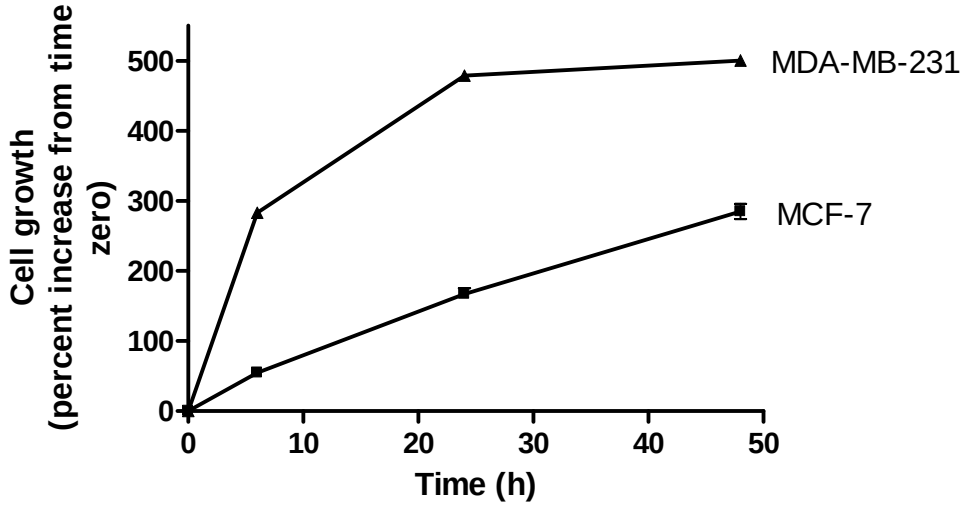

Figure A5.3 Cell growth of the two breast adenocarcinoma cell lines MDA-MB-231 and MCF-7 *in vitro*. Briefly, harvested cells (1.0×10^4) were seeded into the wells of a 96-well microtitre plate and incubated in RPMI-1640 supplemented with 5% FCS. At various time points, 20 μL of MTS reagent was added and the cells incubated for a further 4 h. Absorbance was determined at 490 nm and was directly proportional to the number of viable cells in culture. Data is expressed as the percent increase in absorbance from time zero and is the mean of triplicate experiments ± SE.